UNIVERSITY OF LEICESTER

Simulating river runoff and terrestrial water storage variability in data-scarce semi-arid catchments using remote sensing

Thesis submitted for the degree of

Doctor of Philosophy

at the University of Leicester

by

Peshawa Mustafa Najmaddin (MSc)

School of Geography, Geology, and the Environment

University of Leicester

2017

[This page is left intentionally blank]

Abstract

Simulating river runoff and terrestrial water storage variability in data-scarce semi-arid catchments using remote sensing.

Peshawa M Najmaddin

Remotely sensed data can be used as an alternative to ground based observations to predict river discharge and water storage variability. The latter dataset used consists of meteorological records from four stations (2003-2014) and daily river discharge records from one stations (2010-2014). A model was developed named 'Leicester Model for Semi-Arid Region' (LEMSAR). It was applied in the semi-arid Kurdistan region of Northern Iraq.

TRMM Multi-satellite Precipitation Analysis (TMPA) data products (TMPA 3B42 and 3B42RT) were used with and without a bias correction. The uncorrected TMPA underestimated observed mean catchment rainfall by 10% compared to corrected data with 0.7%.

Four methods of computing reference evapotranspiration (ET_o) were applied which include Hargreaves-Samani (HS), Jensen-Haise (JH), McGuinness-Bordne(MB) and FAO Penman Monteith(PM). The variables utilised are air temperature, relative humidity and cloud cover fraction from the Atmospheric Infrared Sounder / Advanced Microwave Sounding (AIRS/AMSU), and wind speed at 10 m height from MERRA (Modern-Era Retrospective Analysis for Research and Application). Compared to $ET_{o\text{-}G}$ (PM), $ET_{o\text{-}RS}$ (HS) underestimated $ET_{o\text{-}G}$ (PM) by 3% while JH and MB overestimated by 8% to 40% at different stations.

Nash-Sutcliffe Efficiency (NSE) for the LEMSAR fit with the observed hydrograph was 0.75, for a calibration period (2010-2011) using gauged rainfall data with $ET_{o\text{-}G}$ (PM). Model validation performance (2012–2014) was best (NSE =0.61) using the corrected 3B42 data with $ET_{o\text{-}RS}$ HS and poorest when driven by uncorrected 3B42RT data with $ET_{o\text{-}RS}$ JH (NSE =0.07).

Data from the Gravity Recovery and Climate Experiment (GRACE: 2003-2014) were used to evaluate total water storage variability and compared with that of well observations data and LEMSAR. Trends in GRACE_TWSA were approximately -33.72 mm y-1 for the Lesser Zab catchment and -35.4 mm y-1 for the Hawler well monitoring zone while LEMSAR predicted 15 mm y-1 for the Lesser Zab Catchment. This suggest that reduction in recharge (modelled by LEMSAR) may only be responsible for about 50% of the reduction in groundwater storage. The rest could be the result of increased abstraction in response to the drought.

Overall, results suggest that RS data can be usefully employed to simulate river discharge and to evaluate terrestrial water storage variability in semi-arid areas. It has the potential to help decision-makers improve water resources management.

Dedication

This thesis is dedicated to my parents and my parents-in-law, my lovely wife (Sana), my lovely sons (Baran, Meer and Zheer), sisters, brother, brothers-in-law and sister-in-law. I am grateful to all of you.

Acknowledgments

First of all, I would like thank my supervisors Heiko Balzter and Mick Whelan. To Heiko, for your excellent guidance, supervision and support and to Mick, for your enthusiasm for the subject, constant flow of ideas, and patience in teaching me how to code, without either of you I would never have got this far.

I gratefully acknowledge the Higher Committee for Education Development in Iraq (HCED) for funding my PhD project. With particular grateful to the Ministry of Agriculture and Water Resources in the Kurdistan Regional Government for providing well level data, Hydrology Department of the Dukan and Darbandekhan Dam Directorate for providing river discharge data and to the Directorate of Meteorology in Sulaimanyiah for providing meteorological data.

Much gratitude goes to; NASA Goddard Space Flight Center for providing access to TMPA data; to NASA's Jet Propulsion Laboratory, Pasadena, Calif., under contract to NASA for providing AIRA/AUSU data and to NASA MEaSUREs Program for providing GRACE monthly mass grid-land data which are available at http://grace.jpl.nasa.gov. I would moreover like to acknowledge the R Development Core Team who continuously improve and support this liberate available software.

I very much appreciate technical ideas and knowledge we have shared with all CLCR colleagues. And also very much appreciate to all friends who help me during the early stage of my scholarship. And last, but my no means least, to my lovely wife "Sana" and my lovely sons "Baran, Meer and Zheer" for all patience and support throughout the duration of my research without your continued unwavering support I would not be where I am today and for that I will be eternally grateful.

Table of contents

List of Figures

List of Tables

List of acronyms and abbreviations

LEMSA	Leicester Model for Semi-Arid Regions
RS	Remote Sensing
TRMM	Tropical Rainfall Measuring Mission
TMPA	TRMM Multi-satellite Precipitation Analysis
AIRS	Atmospheric Infrared Sounder
AMSU	Advanced Microwave Sounding
MERRA	Modern-Era Retrospective Analysis for Research and Application
HS	Hargreaves and Samani
JH	Jensen- Haise
MB	McGuinness – Bordne
PM	Penman Monteith
GRACE	The Gravity Recovery and Climate Experiment
HOF	Hortonian Overland Flow
θ	Soil water content
ψ	soil water potential
mm d^{-1}	Millimetre per day
%	Percentage
NSE	Nash-Sutcliffe Efficiency
r	Pearsons Correlation Coefficient
TWSA	Total Water Storage Anomalies
GLDAS	Global Land Data Assimilation System
JPL	the Jet Propulsion Laboratory
CSR	the Center for Space Research at University of Texas, Austin
GFZ	the GeoForschnungsZentrum
$GRACE\_{TWSA}$	Average value of the three different GRACE processing centres products

U_{TWSA}	uncertainty for $GRACE\_{TWSA}$
cm y^{-1}	Centimetres per year
km^3 y^{-1}	Cubic kilometres per year
IPCC	The Intergovernmental Panel on Climate Change
E	Evaporation
T	Transpiration
ET	Evapotranspiration
ET_p	Potential evapotranspiration
ET_a	Actual evapotranspiration
ET_o	Reference evapotranspiration
$ET_{o\text{-}RS}$	Reference evapotranspiration estimated from remote sensing data
$ET_{o\text{-}G}$	Reference evapotranspiration estimated from ground-based stations
LC	Land cover
LU	Land use
i.e.	Example
ARIMA	Autoregressive Integrated Moving Average
DBM	Data Based Mechanistic
ANN	Artificial Neural Networks
SWM	Stanford Watershed Model
HBV	Hydrologiska Byråns Vattenbalansavdelning model
PRMS	Precipitation Runoff Modeling System
HRU	Hydrologic Response Unit
PESERA	The Pan-European Soil Erosion Risk Assessment model
SWAT	Soil and Water Assessment Tool
WG	Walnut Gulch experimental watershed
RUSLE	Revised Universal Soil Loss Equation
WEPP	Water Erosion Prediction Project
CERAMS	Chemical, Runoff, and Erosion from Agricultural Management system
NALC	North American Landscape Characterisation classification

GCM	Global Climate Model
GIUH	Geomorphologic Instantaneous Unit Hydrograph
SFB	Surface infiltration Baseflow
GIS	Geographic Information System
NASA	National Aeronautical and Space Administration
JAXA	Japan Aerospace Exploratory Agency
GPM	Global Precipitation Measurement
HEC	Hydrologic Engineering Center
HMS	Hydrologic Modelling System
FCR	Fractional cover of rainfall
IMERG	Integrated Multi-satellite Retrievals for GPM
CERES	Clouds and Earth's Radiant Energy System
VIC	Variable Infiltration Capacity
HSB	Humidity Sounder Brazil
TWS	Terrestrial Total Water Storage
°C	Degree Celsius
m	Meter
SRTM	Shuttle Radar Topography Mission
DEM	Digital Elevation Model
BSH	Subtropical semi-arid
RH	Relative Humidity
FAO	Food and Agriculture Organisation
PBIAS	Percentage Bias
SOMA	Self Organizing Migrating Algorithm
RMSE	Root-Mean-Square Error
GLUE	Generalised Likelihood Uncertinty Estimation
MCS	Monte Carlo Simulation
FAR	False Alarm Ratio
POD	Probability of Detection
HSS	Heidke Skill Score
FDC	Flow duration curves

DLR	the German Deutsche Forschungsanstalt für Luft und Raumfahrt
$GRACE\_{GWRA}$	GRACE groundwater residual anomalies
U_{GWRA}	Uncertainty in GRACE groundwater residual anomalies
Sy	Specific yield

Chapter 1: Introduction and thesis overview

1 Introduction

This chapter presents an overview of the existing knowledge of the water resources issues in semi-arid areas. It also gives a brief review of hydrological processes, rainfall-runoff modelling and the application of such models in semi-arid regions. Finally it explore the role of remote sensing in hydrological modelling. It concludes with summary, an assessment of important gaps in the literature, aim, objectives and the thesis structure.

1.1 General context

1.1.1 Water resources issues in semi-arid regions

Water is one of the most important natural resources. It is an essential component in the climate system and has an environmental, economic and social value. Globally, human demands for water have increased and are predicted to grow further in the coming decades (Kundzewicz et al., 2007). This is driving, for example, groundwater over-pumping for irrigation and domestic supply which is being exacerbated by global climate change (Abdulla, 2008; Al-Ansari and Knutsson, 2011; Ibraimo and Munguambe, 2007; Zakaria et al., 2013). The Intergovernmental Panel on Climate Change IPCC (2013) stated that the global temperature is predicted to increase by 1.5 ˚C by the end of the twenty-first century. Such changes to the climate will be associated with changes in a number of components of the hydrological cycle such as: patterns in precipitation, atmospheric water vapour content, soil moisture, snow cover and snow pack depth, widespread melting of ice (Bates et al., 2008). As a result, surface-groundwater availability are projected to increase in some wet areas (Bates et al. 2008) but decrease in arid and semi-arid areas particularly in southern Europe, western Russia, North Africa and the Middle East (Arnell, 2003; Kundzewicz, 2008). Allan (2001); Chenoweth et al. (2011); Al-Ansari (2013) and Joodaki et al. (2014) have also stated that water scarcity will drive the Middle East region to be even more unstable politically and socio-economically.

The catchments of many major rivers in the Middle East (e.g. the Tigris and the Euphrates) are shared by more than one country and the construction of dams has significantly contributed to reduced downstream river flows (Abdulla and Al-Badranih, 2000; Al-Ansari and Knutsson, 2011; Bozkurt and Sen, 2013; Issa et al., 2014; Abdul Hameed et al., 2010). For instance, the Grate Anatolia Project ‘GAP’ in Turkey, is constructing 22 dams and 19 hydropower stations on the headwater of the Euphrates and Tigris rivers (Unver, 1997). Undoubtedly this project

will have a great impact on water resources in the downstream countries (e.g. Iraq). Al-Ansari & Knutsson (2011) analysed data from several sources to identify the effects of the GAP and its consequences for water resources in Iraq. The results showed that the discharge from the Tigris River could be depleted by up to 47% after the completion of the GAP.

The severe water crises faced by many semi-arid catchments require a solid understanding of hydrological process in order to develop sound mitigation strategies to limited available water resources which are insufficient for the meeting demands of agriculture and domestic/ industrial supply. However, a significant issue with many semi-arid zones outside of Europe and North America is that meteorological and hydrological data availability is often scarce. This has been recognised as a major challenge in hydrological modelling in arid and semi-arid regions (Pilgrim et al., 1988; Wilby and Yu, 2013). Data-Scarce can be defined as a short length of historical observations and spatially insufficient observations which have undergone some quality control procedures recommended by the World Meteorological Organization (WMO, 2007). For instance, for certain parameters such as precipitation, a separation of 10 km between stations may be required in same areas for purposes such as climatology and hydrological forecasting (WMO, 2006). In this study data-scarce means a lack of hydro-meteorological data to drive a rainfall-runoff model.In this thesis an attempt is made to gain a better understand of the hydrological processes in a data poor semi-arid regions and quantify spatiotemporal variations in water resources for better water resource planning and management. Catchments in Northern-Iraq, for conducting this study are used to illustrate the general ideas which are developed.

1.2 Hydrological processes in semi-arid regions

Hydrology is the study of the distribution and circulation of water (Davie, 2008). It provides an understanding of how water moves around the planet and which factors influence it (Chow et al., 1988). Arid to semi-arid areas have been recognised as having higher temporal and spatial variability of all hydrological processes (i.e. rainfall, evapotranspiration, infiltration and runoff generation) than in humid regions (Food and Agriculture Organization (FAO), 1981; Pilgrim et al., 1988; Wheater et al., 2007).

1.2.1 Rainfall

Rainfall is an important component of the hydrological cycle and is the primary input for hydrological modelling. Rainfall in arid and semi-arid regions has several unique characteristics compared to rainfall in humid regions. For instance, storm events in arid and semi-arid areas are often by random, short duration and high intensity, with greater spatial variation than in humid regions (Pilgrim et al., 1988; Chahine, 1992; Wheater, 2002). The extreme temporal variability of rainfall and long, dry periods may have far-reaching effects on the hydrological processes and the production of runoff in semi-arid regions (Pilgrim et al., 1988; Reaney, 2008; Buytaert and Beven, 2011). There are several studies regarding the temporal variability of rainfall such as (White et al., 1997; Gutiérrez et al., 1998) and spatial variability such as (Goodrich et al., 1997; White et al., 1997; Goodrich et al., 2008; Babu et al., 2016). Consequently, rainfall measurement is crucially important in order to understanding and modelling of hydrological processes within arid and a semi- arid areas. However, this is compounded by the fact that there is a significant issue with many semi-arid zones outside of Europe and North America is that meteorological and hydrological data availability is often scarce.

1.2.2 Interception and evapotranspiration

Interception loss and evapotranspiration are two main elements of the hydrological cycle. Interception refers to rainfall that is intercepted by surface elements such as trees, shrubs and grass before it hits the ground (Savenije, 2004) and is returned to the atmosphere by direct evaporation from plant surfaces (Pilgrim et al., 1988). Interception can be a very significant part of the total water loss to the atmosphere in some environments (e.g. forest) (Návar, 2017). However, it often can be neglected in arid areas with sparse vegetation based on the argument that it is a very small proportion of total water loss in these areas (Savenije, 2004).

Evapotranspiration (*ET*) is one of the main components of the hydrological cycle. Its quantification is essential for water resource management (Zhao et al., 2013). However, it is arguably the most difficult process to measure directly, especially in arid and semi-arid areas where losses of water tend to be temporally highly variable (Nikam et al., 2014; Pilgrim et al., 1988).

Evapotranspiration *(ET)* consists of two main component processes: evaporation and transpiration (Chahine, 1992; Shaw, 1994). Evaporation (*E*), is the loss of water from open water surfaces such as oceans, lakes, reservoirs, rivers and from soil pores directly to the atmosphere. In the evaporation process, energy is required to convert liquid water to the vapour state. Most of this energy comes from absorbed radiation which depends (*inter alia*) on latitude, season, cloud cover, air temperature and surface albedo (the fraction of solar shortwave radiation reflected from the earth back into space, which is affected by surface conditions and soil moisture: Chahine, 1992; Strugnell et al., 2001). Transpiration (*T*), occurs when water absorbed by plant roots is returned to the atmosphere through their stomata (López-Urrea et al., 2006). It is noteworthy to highlight that evaporation and transpiration occur simultaneously and it is complex to differentiate them. There are three different expressions for *ET*: potential evapotranspiration (ET_p), reference evapotranspiration (ET_o) and actual evapotranspiration (ET_a). ET_p is the water loss which would occur from a vegetated surface when sufficient moisture is available in the soil such that stomata are fully open and resistance to water vapour transport from bare soil to the atmosphere is minimal (Beaumont et al., 2016). ET_o is defined as the evapotranspiration rate from a hypothetical reference surface with unlimited soil moisture availability (Allen et al., 1998). The reference surface is assumed to be a grass sward with a height of 0.12 m, a fixed surface resistance (representing the ease with which water vapour is transferred between the surface layer and the atmosphere) of 70 s m^{-1} and an albedo of 0.23 (Allen et al., 1998). ET_a is the loss of water from a vegetated surface under ambient soil moisture conditions (i.e. soil moisture may be limiting to the evapotranspiration rate). ET_o can vary significantly on a daily time scale (which is the most commonly applied input data time step for hydrological modelling). In contrast to precipitation (which is notoriously variable) several studies have reported that variation of ET_o is likely to be relatively uniform spatially at the basin scale, except where there are topographic complexities or strong gradients in relief (Tabari et al., 2012a; Herath et al., 2017; Alemayehu et al., 2017).

1.2.3 Runoff generation process

The runoff generation is one of the most complex and non-linear process in hydrology. Rainfall-runoff transformation involves many hydrological processes (e.g. interception, *ET*, soil drainage, through flow, overland flow and base flow). For many years, hydrologists have attempted to understand runoff generation in order to predict river discharge and flood risk assessment. There is a large volume of published studies describing runoff generation in humid

regions (i.e. Betson, 1964; Weyman, 1975; Pearce et al., 1986; Allan and Roulet, 1994; Dohnal et al., 2016; van Meerveld et al., 2016) and in arid and semi-arid regions (i.e. Yair and Lavee, 1976; Yair and Lavee, 1985; Abrahams et al., 1995; Lange et al., 2003; Ries et al., 2016).

In humid regions, four different processes: Hortonian Overland Flow (HOF), shallow subsurface flow, saturation overland flow and groundwater flow may be involved at different times and magnitudes in excess runoff generation (Betson, 1964; Weyman, 1975; Pearce et al., 1986; Allan and Roulet, 1994; Dohnal et al., 2016; van Meerveld et al., 2016). In the arid and semi-arid regions, the dominant mechanism of runoff generation is generally assumed to be Hortonian Overland Flow (HOF) which occurs when the rate of (unsaturated) infiltration is less than the rainfall rate (Pilgrim et al., 1988; Lange, 1999).

Runoff response to a rainfall event is controlled by different factors including rainfall characteristics (Yair and Lavee, 1985; Castillo et al., 2003) and catchment characteristics such as, relief, soil composition, initial soil water content, land cover and land use and the underlying (hydro) geology (Hernandez et al., 2000; Ohana-Levi et al., 2015; van Meerveld et al., 2016; Pilgrim et al., 1988; Hendrickx, 1990). Rainfall characteristics include rainfall intensity and duration. For instance, when rainfall intensity is greater than the soil infiltration rate and rainfall duration is longer than ponding time (the time required to saturate the uppermost layer of soil for a given initial soil moisture profile: Assouline et al., 2007), this results in the accumulation of excess water at the ground and the generation of HOF.

Initial water content has a great influence on infiltration. In principle, water movement in the soil profile occurs as a result of gradients in potential energy (the hydraulic potential) (Hendrickx, 1990). When the soil is dry potential energy is low and water will infiltrate quickly. As the soil wets up, the potential energy gradient decrease and infiltration rate decreases. Infiltration and water movement are also strongly affected by hydraulic soil properties, particularly hydraulic conductivity and the water retention characteristics (Hendrickx, 1990). The hydraulic conductivity determines soils capacity to move water through the porous space and fractures. The water retention characteristics describe the relationship between the water content (θ) and soil water potential (ψ) or matrix potential which is affected by capillary forces which are, in turn, a function of pore size for empty pores (Niemela, 2011). Non-linear relationships between water content and matric potential can be described mathematically

using a number of analytical functions such as those of Brooks and Corey (1966) and van Genuchten (1980) equations which are commonly used for water flow in soil profiles.

Yair and Lavee (1985) in Israel and Wallace and Lane (1976) in southeastern Arizona studied Hortonian Overland Flow in semi-arid contexts. In both cases, the infiltration rate was found to be the main driver of HOF. Casenave and Valentin (1992) analysed some factors including antecedent soil water content and soil surface characteristics such as soil crusting which have a huge impact on infiltration and runoff processes in the semi-arid area of west Africa. Other studies have also shown that soil infiltration rate reduces at higher in soil moisture contents (Cerdà et al., 1997).

Land cover (LC) and land use (LU) also represent crucial factors influencing runoff. Ohana-Levi et al. (2015) stated that decreasing LC is one of the main causes of increased runoff rate and high peak flow due to reduced infiltration of rainfall on bare ground. This which confirms a strong negative relationship between vegetation cover and the relative volume of runoff. Similarly, van Meerveld et al. (2016) studied the effects of LU on runoff generation in upland, eastern Madagascar. Their results show that the runoff coefficient (RC) depend on soil type, rainfall intensity and land cover. Runoff coefficient varied with different land cover (e.g. RC for a deforestation site, young forest site and mature forest site were 22%, 3.5% and 2.7% respectively.

1.2.4 Groundwater

Groundwater is simply the subsurface water in fully saturated soil pore spaces and in the fractures of rock formations. Groundwater is replenished naturally by precipitation via soil drainage. It can be one of the most important sources of water for river flow, crucial to sustain flow in rain-free periods by returning water to the river (McCallum et al., 2013; Candela et al., 2014; Abo and Merkel, 2015; Shaw, 1994). Groundwater recharge depends on the local climate, soil properties, vegetation characteristics and geology (Shaw, 1994; Scanlon et al., 2006).

In both humid and semi-arid regions, groundwater recharge occurs based on the time factor (Simmers, 1988) via short term recharge (Sharma and Hughes, 1985), seasonal recharge (Rushton and Ward, 1979), perennial recharge (Morel and Wright, 1978) and historical recharge (Campana and Simpson, 1984). Recharge estimation is very a challenging element to

predict in hydrology, due to the difficulty in direct subsurface observation. This is particularly true for the arid and semi-arid areas because of a high temporal and spatial variability of all water balance components, in addition to the lack of observation data including meteorological, soil characteristics, geomorphology and vegetation cover (Koeniger et al., 2016; Pilgrim et al., 1988; Candela et al., 2014). There are a variety of techniques that can be used to estimate groundwater recharge rate indirectly, including rainfall-runoff modelling, (Scanlon et al., 2006). These techniques have been described and reviewed by several studies (Lerner et al., 1990; Hendrickx and Walker, 1997; Kinzelbach et al., 2002; Banimahd et al., 2015; Izady et al., 2014; Acworth et al., 2016; Koeniger et al., 2016).

1.2.5 River flow regimes

Understanding the hydrological behavior of rivers is crucial to assessing water resource management. Lerner et al. (1990) classified river flow into three flow categories: perennial, seasonal and ephemeral. Perennial rivers flow throughout the year, seasonal rivers only flow during part of the year, and ephemeral rivers have extremely high flow variability: from no flow to flash floods during storms. The variation in river discharge over a long period constitutes its regime which is the direct consequence of climatic factors (precipitation and temperature) in the catchment area and the catchment characteristics including soils, rock structure, basin morphometry and hydraulic geometry (Haines et al., 1988; Harris and Gurnell, 2000; Zhu et al., 2012) .

A catchment is the area where precipitation is collected and redistributed to the drainage network and translated to river discharge at the catchment outlet. Catchment hydrology takes into account the integration of hydrological processes at the catchment scale and determines the catchment response to rainfall. River discharge can be measured directly at a gauging station or can be predicted by rainfall-runoff modelling. There are some factors that affect the accuracy of the river flow measurements such as the integrity of the gauging structure and the choice of rating equation. Simulation accuracy can be affected by artificial influences such as large abstractions upstream of the gauging station, controlling river flow through regulated reservoir releases (Shaw, 1994).

Understanding of these processes, particularly within semi-arid catchments, can provide better options for water resources management. However, experience has shown that quantifying hydrological variables (i.e. river discharge) is often difficult and subject to uncertainties (Wilby

et al., 2017). In addition, hydrological data and field observation may not be available. Therefore, rainfall-runoff models can be help to estimate rainfall runoff relationships, can significantly contribute to scientific understanding and support decision making in water resources management (Beven, 2012).

1.3 Rainfall-runoff modelling

Rainfall-runoff models are powerful tools which can be used in many aspects of catchment hydrology. There are mathematical representation(s) of the hydrological cycle which renders an approximate description of the system under study via set of equations linking the inputs and outputs (Chow et al., 1988). They contain various quantities (i.e. parameters, initial and boundary conditions) which are incompletely known (Janssen and Heuberger, 1995). The characteristics of a watershed are represented by parameters (Dent et al., 2004). These artificial representations of the physical world always incorporate some level of simplification of physics over the spatial and temporal domains (Dent et al., 2004). Most rainfall-runoff models have parameters that cannot be measured directly, either because they represent several physical processes or because the scale at which they are applied in the model does not correspond to the scale at which they can be measured (i.e. parameters that define groundwater flow), as well as parameters that can be measured or observed directly such as the area of the catchment (Dent et al., 2004; Beven, 2012). Those parameters that are not directly observable need to be determined by indirect techniques of matching the model output to historical observed data. This is called calibration (Gupta et al., 1998). It means the searching for the parameter values that give the best predictions (Janssen and Heuberger, 1995). Most hydrological models are calibrated and so this becomes a critical phase in the modelling process (Beven, 2012).

This adjustment may be done by several strategies including (i) manual trial-and-error where the modeler manually changes the values of the parameters until they are satisfied with the model results against observations. This method can be successful in applications where the model has a small number of parameters (e.g. <3). However, it can suffer from low objectivity and reproducibility (Janssen and Heuberger, 1995); (ii) Automatic calibrations which are useful in calibrating complex models with a large number of parameters (Dent et al., 2004). Example include , (a) inverse modelling method where a search algorithm is applied to minimise an objective function reflecting the distance between simulations and observations and (b)

parameter space methods where parameter values are selected from a population of values (i.e. Monte Carlo Markov Chain) and usually need a large number of model runs (Šimůnek and De Vos, 1999; Dent et al., 2004; Arnold and Moriasi, 2012; Tada and Beven, 2012; Beven, 2012). The advantages in applying automatic calibration are (usually) a closer fit between model output and observations as well as increased objectivity and reproducibility in the process (Doherty and Johnston, 2003; Dent et al., 2004).

Hydrologists commonly apply different models to meet particular requirements when they intend to deal with issues such as (i) leaching of pollutants to water resources (Seibert, 1999; Whelan and Gandolfi, 2002; Pullan et al., 2014), predict flooding (Lundin et al., 1998), (ii) manage water resources (Buytaert and Beven, 2011; Pechlivanidis and Jackson, 2011), and (iii) predict the potential impacts of climate change on water resources (Bergström et al., 2001; Ragab and Prudhomme, 2002; Shepherd et al., 2010; Jung and Chang, 2011; Milman et al., 2013; Hatcher and Jones, 2013; Bozkurt and Sen, 2013; Gosling and Arnell, 2013; Li et al., 2015; Sarhadi et al., 2016).

1.3.1 Rainfall-runoff modelling processes

The modelling process has two components: the model building process and the modelling protocol (i.e. the way to use the model for either operational managment or research: Solomatine and Wagener, 2011). In model building, four different stages exist (Beven, 2012): The first stage, the perceptual model, involves the collection of background information on the physical system uner consideration based on previous research, data analysis and field site experience which may help to develop a good model. The perceptual model stage is not formalised or constrained by mathematical theory. A mathematical description is then required in order to formulate a model. This is the starting point for the evaluation of a practical model and is the basis of the next stage which is called the conceptual model. This may use mathematical equations for components represented in the catchment and for the definition of the boundary conditions for the real system. The next stage is the development of a procedural model which requires techniques of numerical analysis to transform the equations of the conceptual model into code that will run on computes-. It is then necessary to calibrate the parameters, as described in previous section. After the model parameter values have been specified, a simulation can be performed and the model can be validated, (on an independent data set which has not used in calibration) to evaluate model performance (Beven, 2012).

1.3.2 Classification of rainfall-runoff models

Rainfall-runoff models have been classified in many ways. Examples of the classifications are given by Clarke (1973); Todini (1988); O'Connell (1991); Wheater et al. (1993);Singh (1995); and Refsgaard and Knudsen (1996). There are two criteria: (i), the extent to which physical principles are applied in the model structure and (ii) the treatment of the model inputs and parameters as a function of space and time. As well as the physical process description, a hydrological model can also be defined as either stochastic or deterministic (Dzubakova, 2010; Pechlivanidis and Jackson, 2011; Solomatine and Wagener, 2011). Stochastic models use random variables to link a single set of inputs, for instance rainfall, to produce different outputs such as runoff (Dzubakova, 2010; Pechlivanidis and Jackson, 2011; Solomatine and Wagener, 2011). Deterministic models, on the other hand, represent the physical processes observed to give the same output for a given set of input variables (Dzubakova, 2010; Solomatine and Wagener, 2011).

Models can also be classified according to whether the model has a lumped or distributed description of the catchment area. Lumped models treat the catchment as a homogenous unit with the output representing an average over the catchment area, while distributed models discretise a catchment into different units and the output represents the weighted average of the response of the different discrete unite (which may also be time-dependent). Distributed models usually need more detailed input data than is usually available (Beven, 2012).

Furthermore, model descriptions of hydrological processes can be empirical, conceptual or physical based. Three classes of deterministic model can be distinguished: (i) metric or 'black box' models which are entirely empirical, (ii) conceptual or 'gray box' models which include some physical process representation-often in conceptual way, and (iii) physical or 'white box' models which attempt to describe conditions and process using mechanistic, physical-based concepts (Wheater, 2002; Dzubakova, 2010; Solomatine and Wagener, 2011).

Metric or black box models are essentially empirical and statistical tools which attempt to reproduce the catchment scale relationship between inputs and outputs using mathematical equations that have been derived from an analysis of the simultaneous climatic input data (i.e. rainfall and evapotranspiration) and output time series (Pechlivanidis and Jackson, 2011). The unit hydrograph method, which was originally developed by Sherman (1932), is used widely as an example of empirical methods. It is a simple linear model that can be used to produce

hydrographs based on an excess rainfall (Chow et al., 1988). This type of model represents stream response to individual storm events, either by non-linear loss functions or linear transfer functions. Other examples of statistical model include those based on regression and correlation (Chow et al., 1988). A good examples of a recent approach to in statistical modeling is the Autoregressive Integrated Moving Average (ARIMA) model (Box and Jenkins, 1970). Other interesting black box modelling approaches include Data Based Mechanistic models (DBM: Young et al., 1997; Young, 1998; Young, 2001; Young, 2003; Ratto et al., 2007) and Artificial Neural Networks (ANN: Lange, 1999; Dawson and Wilby, 2001; Jain et al., 2004; Dawson et al., 2007).

Conceptual models are characterised by two criteria: firstly, model parameters have no direct physical measurement and secondly the structure is specified prior to any modelling being undertaken (Wheater, 2002; Solomatine and Wagener, 2011). Conceptual models vary considerably in complexity and an extensive number of interconnected schematic storages are used to represent important physical hydrological features in a catchment. Rainfall, snowmelt, infiltration and percolation recharge the stores depleted through evapotranspiration and runoff. Parameters and fluxes are represented by average values over the entire catchment and parameter values are usually obtained through calibration against observed time series data (Seibert, 1999; Wagener et al., 2001; Wagener et al., 2003). These models can be used to obtain both a short term and long term prediction of runoff (Seibert 1999). Pechlivanidis and Jackson (2011) argue that a balance between model complexity and available input data is crucial for a successful prediction. Model complexity can be controlled by sensitivity analysis which is a technique used to determine how different values of an independent parameter impact a particular dependent parameter under a given set of assumption (Fenicia et al., 2008; Jiang et al., 2015). Parameter can be held constant to which the model is insensitive (Li et al., 2009; McIntyre and Al-Qurashi, 2009). Examples include the Stanford Watershed Model (SWM: Crawford and Linsley, 1966), the Hydrologiska Byråns Vattenbalansavdelning model (HBV: Bergström and Forsman, 1973), theSacramento Soil Moisture Accounting model (Burnash et al., 1973); (Wheater, 2002), TOPMODEL (Beven and Kirkby, 1979) and the ARNO model (Todini, 1996). These models describe hydrological processes in relatively simple ways in terms of catchment scale input-output relationships (Pechlivanidis & Jackson, 2011; Solomatine & Wagener, 2011). A brief description of several conceptual models are

given by Fleming (1972); Todini (1988); Franchini and Pacciani (1991); Singh (1995); Dzubakova (2010); and Beven (2012).

Physical models are based on the basic physical principles such as the law of conservation mass, energy and momentum (Solomatine & Wagener, 2011). Hydrological processes are modelled by different equations of mass, momentum and conservation or by empirical equations derived from an independent experimental study (Abbott et al., 1986). Hydrological processes such as evapotranspiration, infiltration, and saturated and unsaturated zone flow can all be represented by physical models (Pechlivanidis & Jackson, 2011). These variables are measureable in laboratory and field experiments (Pechlivanidis & Jackson, 2011). Beven and Freer (2001) stated that, in theory, the physics-based model can provide a continuous simulation of the rainfall-runoff relationship without calibration but, in practice, such a model has a number of important issues. For instance, the parameter measurements of these models are essentially made at the point scale, but, the models themselves use average parameters at the grid scale, which is basically greater than the scale of variation of the process, thus raising uncertainty about their applicability (Beven, 2004). In addition, this does not adequately represent heterogeneity at the grid or catchment scale (Pechlivanidis and Jackson, 2011). Examples of physically based models include, SHE/ MIKE SHE (Abbott et al., 1986); Precipitation Runoff Modeling System (PRMS: Leavesley et al., 1983) and the Penn State Integrated Hydrologic Model devised by Qu and Duffy in 2007 (Solomatine & Wagener, 2011).

1.3.3 Selection of rainfall-runoff model

Choosing the best model depends on the specific problems considered. In most cases several different models could be applied. For data scarce catchments, models with many parameters are not suitable because evaluation and estimation of parameters from a knowledge of the physical characteristics of the catchment is very difficult. . Beven (2012) argued that main criteria that can be used in choosing a models can be categorized as follows:

1. Study objectives.

2. The availability of rainfall and runoff data and other input data required by the model.

3. The variables predicted by each model and the model's ability to offer the output needed to meet the aims.

4. Model ability to address the problem of parameter calibration.

5. The characteristics of the hydrological system considered.

Although it is often possible to represent the physical processes more closely using physically-based distributed models, this will involve greater complexity, an increase in the number of parameters and require more data and information (i.e. readings at more frequent time intervals and on a denser spatial network). However, if the input data (or information) are not available, these models are of little use. Thus, data availability and the need for practical usefulness of the results often restrict the choice of a model. A conceptual model would be the model of choice for this study due to; (i) low data requirements; (ii) ability to describe all hydrological processes and (iii) the use of semi empirical equations with a physical basis. Other types of model not considered here include ; (i) empirical models (i.e. unit hydrograph method : Chow et al., 1988) which cannot easily be applied to other catchment; and (ii) physically based models (i.e. SHE/MIKE SHE model : Abbott et al., 1986) which have high data requirements.

1.3.4 Examples of rainfall-runoff models

Some commonly used rainfall-runoff models are described below.

The Precipitation Runoff Model System (PRMS) model (Leavesley et al. 1983) is a conceptual, continuous simulation with physical and fitted Hydrologic Response Unit (HRU) parameters models used for evaluation of the impact of precipitation, climate and land use on stream flow. HBV is a conceptual lumped model but is sometimes referred as a distributed model and is based on the theory of linear reservoirs (Bergström and Singh, 1995).

TOPMODEL is a rainfall-runoff model that was originally developed at the University of Leeds (United Kingdom) to predict different types of hydrological response (Beven and Kirkby, 1979; Ambroise et al., 1996). It is a topography-based model designed to estimate runoff from hillslopes. According to Beven (2012), TOPMODEL uses two fundamental assumptions to relate down-slope flow from a point to discharge at the catchment outlet. Firstly, the dynamics of the saturated zone are approximated by successive steady state representation with the recharge rate (mm hr^{-1}) entering the water table over the area (a). Secondly, the effective hydraulic gradient of the saturated zone is approximated by the local surface slope (S or tan β). The strengths of this model include its simplicity and the possibility of visualising predictions of near-surface saturation spatially (Beven, 1997). TOPMODEL also has some

weaknesses. For example, Beven (2012) argued that the model cannot provide a good simulation of stream discharge in drier catchment areas because the dynamics of the saturated contributed area may not respond under very dry conditions, for example in Mediterranean regions (see Beven (2012: for more details) .

The HEC-HMS model (Lundin et al., 1998; Feldman, 2000) is a conceptual hydrological model with lumped parameters, which was developed by the US Army Crop of Engineers Hydrologic Engineering Center. It uses different methods of hydrological analysis, including the unit hydrograph, to conceptually describe catchment responses to precipitation (Lundin et al., 1998).

Like TOPMODEL, the Pan-European Soil Erosion Risk Assessment model (PESERA) uses simple lumped soil water balance calculations but with a focus on the prediction of overland flow. It was developed specifically to predict soil erosion in large catchments using a simple (but physically-based) description of the processes controlling sheet and rill erosion via Hortonian and saturation-excess overland flow (Kirkby et al. 2003). It has the ability to combine the influence of climate, vegetation cover, soil properties and topography in the prediction of runoff and erosion (Kirkby et al. 2003).

The Soil and Water Assessment Tool (SWAT) is another rainfall-runoff model based on a conceptual representation of physical processes. It is comprehensive in the scope of processes represented and semi-distributed (in that it can represent different behaviours in a number of hydrologically similar zones – so-called hydrologic response units or HRUs). One disadvantage of SWAT is that it has high input parameter requirements so model set-up (paramaterisation and calibration) can be difficult and time consuming (Arnold & Moriasi 2012).

1.3.5 Applications of rainfall-runoff models in semi-arid regions

Although data are often scarce in arid and semi-arid catchments, some rainfall-runoff models have been developed and employed for a variety of purposes in these areas, particularly where ground data are available (e.g. in the south-western USA but also Africa, Australia, India, Saudi Arabia and Israel).

The semi-arid experimental catchment of Walnut Gulch (WG-USA), has a long history of hydrological investigation and a wealth of data have been collected including detailed

topographic data, drainage density, geomorphological characteristics of the stream, meteorological and runoff data. This has facilitated the successful application of different models. Wallace and Lane (1976), for example, applied the kinematic cascade model to investigate the effects of landform evolution on drainage systems; Grayson et al. (1992) presented and applied the THALES model, which is a simple distributed parameter rainfall-runoff model, to simulate surface runoff; Renard et al. (1993) applied four simulation models [KINEROS, the Revised Universal Soil Loss Equation (RUSLE), Water Erosion Prediction Project (WEPP) and Chemical, Runoff, and Erosion from Agricultural Management system (CREAMS)], to explore the effect of land management on runoff and erosion; Karnieli et al. (1994) applied the CELMOD5 model which is a parametric, semi-distributed linear rainfall-runoff model to study larger rainfall-runoff events; Wheater et al. (1997) outlined the structure of an integrated model of arid areas to evaluate the groundwater recharge management options; Hernandez et al. (2000) applied two hydrological models, (KINEROS and SWAT) to evaluate the land cover change and the effect of the spatial variability of rainfall on catchment responses; Nichols et al. (2016) applied the distributed rainfall-runoff model KINEROS2 to simulate event runoff discharge and gully erosion processes. The authors conclude that the rich and reliable data at WG watershed have contributed to enhance our understanding of hydrological processes in semi-arid environments but there is still a need for studies in different semi-arid areas where data is scarce.

Hydrological models that have been developed specifically for arid and semi-arid regions of South Africa have been reviewed by Hughes (2008). The Pitman monthly time-step model was developed in the 1970s (Pitman, 1973). It went through different numbers of revisions since then and now exists in several forms. The model consists of different stores including interception, soil moisture and groundwater. The Pitman Model has been more widely applied within the southern African region than any other hydrological model (Gan et al., 1997; Hughes et al., 2006; Hughes, 2008; Rojas-Serna et al., 2016).The authors concluded that uncertainties and limitations of meteorological data and observed river flow were the most significant challenges for model calibration and validation.

Models developed, applied and tested in Australia include the conceptual lumped rainfall-runoff model RORB3 (Kotwicki, 1987) which was used to estimate unrecorded past river inflows to the 450,000 km^2 arid Lake Eyre; Ye et al. (1997) applied three different rainfall-runoff models: (1) a simple conceptual model (the Generalised Surface infiltration Baseflow:

GSFB (Boughton, 1984), (2) the : IHACRES model (Identification of Hydrographs and Components from Rainfall Evapotranspiration and Streamflow data: Jakeman et al., 1990) and (3) a complex conceptual model (the Large Scale Catchment Model (LASCAM : Sivapalan and Viney, 1994) to assess their prediction capability to predict runoff in ephemeral river. An important conclusion from this study was that a much denser hydro-meteorological data network is required in order to make good hydrological predictions.

Few studies of rainfall runoff modelling have been focused on the semi-arid regions of Middle East. The Geomorphologic Instantaneous Unit Hydrograph (GIUH) model, introduced by (Rodríguez-Iturbe and Valdes, 1979) has been applied in the region by serval authors including (Allam, 1990; Al-Turbak, 1996; Shadeed et al., 2007). A single event watershed model was developed and applied by Abdulla et al. (2002) in the western Iraqi desert region. This model is based on the water balance equation and performed well with respect to observed data. However, the authors concluded that a more complete dataset for the spatial distribution of rainfall, evapotranspiration, and soil properties is required to obtain improved estimates of hydrological processes in the catchment considered.

1.4 Alternative ways of estimating the meteorological forcing data for hydrological models.

Despite significant progress made during the last few decades, rainfall-runoff modelling continues to face some fundamental issues. These include the continued need for calibration, issues connected with equifinality (the fact that several different combinations of of parameters make similarly good or bad simulations: Beven, 2012) and validation (Beven and Binley, 1992; Beven and Freer, 2001; Beven and Alcock, 2012; Brazier et al., 2000; Franks et al., 1997). Some of these issues are linked to the limited availability of data for driving the models at an appropriate scale (e.g. meteorological data), the spatial density and accuracy of river discharge measurements and characterization of catchment characteristics (especially in the subsurface). The spatial and temporal resolution of key driving variables (i.e. rainfall and evapotranspiration) remain particularly challenging, regardless of the climate (Shaw, 1994; Beven, 2012; Tada and Beven, 2012). However, the installation and maintenance of new meteorological stations is expensive and unlikely to represent a significant investment target in most countries in the near to medium term. Therefore, establishing alternative ways of

estimating (accurately, cheaply and at appropriate spatial and temporal resolutions) the meteorological forcing data for hydrological models and their applications is a major need.

1.4.1 Application of weather generators and downscaling methods in hydrological modelling.

Weather generators and downscaling techniques can be used as alternative ways to simulate hydro- meteorological data at higher temporal and spatial resolutions (Vezzoli, 2013). Downscaling techniques can be divided into two main categories: dynamic (Global Climate Model GCM) and statistical (Vezzoli, 2013). In dynamic downscaling, the GCM provides boundary and initial conditions to Regional Climate Model (RCM) simulations over the region of interest with a finer spatial resolution than the original one. Statistical downscaling techniques are based on statistical models applied to historical data (e.g. regression models). Statistical downscaling can reach a finer resolution than dynamic downscaling, depending on the availability of observations, and it is generally less demanding from a computational point of view (Vezzoli, 2013). Weather generators were statistical tools able to simulate, from observed statistics, atmospheric variables like rainfall, temperature, relative humidity, solar radiation, etc., in one or more sites. The simulated variables reflect the statistical behaviour of the observed ones. Wilby and Yu (2013) applied weather generator techniques to produce gridded maps of annual mean precipitation and temperature, as well as parameters for site-specific, daily weather generation in Yemen. Their results show that the weather generator reproduced daily and annual diagnostics when run with parameters from observed meteorological series for a test site at Taiz. However, when run with interpolated parameters, the frequency of wet days, mean wet-day amount, annual totals and variability were underestimated. Downscaling techniques have been widely used in different studies to generate daily precipitation scenarios to simulate winter flooding and for filling in missing values (Wilby et al., 2014). Although this study does not take these techniques into account, future extension of this work may consider them.

1.4.2 Application of remote sensing (RS) data into hydrological models.

Remote sensing (RS) is the science of obtaining information about an object using data acquired by a device ("sensor") that is not in contact with the object. It is typically used to refer to the observation of the earth's surface and atmosphere via the measurement of the reflection, absorption and emission of electromagnetic waves (from gamma rays to microwaves), either

passively (using natural electromagnetic radiation from the sun) or actively (generating a signal and observing its transmission and reflection) (Lillesand et al., 2014). Measurements are often taken using sensors mounted on satellites but sensors can also be mounted on aircraft, including UAVs. This can yield important (and previously unobtainable) information about the objects under consideration (Lillesand et al., 2014). The data generated by remote sensing is often processed spatially into pixels which represent single points or aggregations displayed in a graphic image. The pixels contain the raw data collected by the sensor on the electromagnetic signals received or may contain processed data which have been transformed to yield variables of environmental significance (such as temperature or the characteristics of the vegetation). There are currently many satellites in earth orbit including polar orbiting and geostationary (Lillesand et al., 2014). Polar orbiting satellites have an orbit close to both North and South poles. Satellites of this type have the advantage that they are sun-synchronous (i.e. the time of overpass is roughly the same for every point on the South to North ascending leg of the orbit and changes by 12 hours for the North to South descending leg (Cao et al., 2004). Geostationary satellites are positioned approximately 3600 km above the Earth's surface (Lillesand et al., 2014). They move in the same sense as the Earth's rotation and remain vertically above a particular point on the Earth's surface. Thus, a geostationary satellite sees the same view of the full Earth disc all the time (Lillesand et al., 2014).

Remote Sensing (RS) has been increasingly used to obtain the spatial and temporal information pertaining to the global water cycle and is now routinely used to help generate hydrological model-drivers as the acquisition of data has become easier and more cost–effective. Limitations of remote sensing include: (1) reliability - because many of the environmental factors are sensed indirectly, estimates may not always be usable in all circumstances and may require the interpretation of a skilled operator (Lillesand et al., 2014) and (2) calibrations and validation against ground-based data - the variables of interest need to be derived via transformation of the raw signals which may require some empirical model fitting (calibration). The resulting transformed data products subsequently need to be checked against empirical observations of the variable of interest (validation) so the use of satellite imagery does not do away with need for field measurements entirely. However, despite of these limitations, in some cases (e.g., in data-scarce areas) remote sensing data may be the only viable source for obtaining data needed for rainfall-runoff modelling (Katara et al., 2013).

Wavelength bands in the electromagnetic spectrum (Lillesand et al., 2014) which can yield useful hydrological information include: (i) the visible wavelength band between 0.4 and 0.7 μm (e.g. for cloud and vegetation monitoring); (ii) near and shortwave infra-red wavelengths between 0.7 and 3 μm (e.g. for vegetation indices such as NDVI); (iii) thermal infra-red wavelengths between 8 and 15 μm (e.g. for temperature of the surface observed); (iv) microwave sensor wavelengths between 1 and 300 μm (e.g. for rainfall detection).

There is a considerable amount of research regarding the application of RS data in hydrology. This includes runoff-erosion studies (King et al., 2005), the effects of impervious surface cover on the prediction of peak flow (Chormanski and Voorde, 2008), identifying suitable sites for rainwater harvesting (Bakir and Xingnan, 2008), land cover change effects on runoff (Santillan et al., 2011) and obtaining catchment properties (i.e. drainage area, slope, flow length, stream network density: Merwade, 2012).

1.4.2.1 Remotely-derived rainfall data

Unfortunately, no satellite yet exists which can reliably identify and accurately quantify rainfall rates in all circumstances. However, some sensors can make indirect estimates of rainfall by measuring things such as the thickness of clouds or the temperature of cloud tops but these images are not much use for giving a precise estimates of rainfall for particular points on the ground, at a particular time. In recent years, advances in remote sensing have established the potential to significantly improve rainfall estimates from space (Huffman et al., 2001). If the spatial and temporal resolution of such data are adequate, then such data may provide alternative inputs for rainfall-runoff modelling as long as they have sufficient accuracy compared with observed data. For example, the Tropical Rainfall Measuring Mission (TRMM), which was a joint mission between the National Aeronautical and Space Administration (NASA) Earth Science Enterprise and the Japan Aerospace Exploratory Agency (JAXA), was successfully launched in 1997 and ended in 2015. It initially operated at an altitude of 350 km (changed in 2001 to 402.5 km to increase mission life), with an orbital inclination of 35° and made approximately 16 orbits a day. The TRMM complement comprises the first rain radar to be flown in space and its rain sensor package consist of (i) a conical-precipitation radar (PR); (ii) a multi-channel passive microwave sensor (TMI); and (iii) an infrared and visible scanner (VIRS). Details of TRMM rain sensor can be found in Simpson et al. (1996).

TRMM has now been replaced by the Global Precipitation Measurement (GPM) mission (Prakash et al., 2016). The initial objective of TRMM was to monitor monthly and seasonal rainfall over the tropics and subtropics using a combination of passive microwave radiometry and radar (Huffman et al., 2007) in order to improve understanding of the hydrological cycle. One issue with obtaining spatially-distributed rainfall estimates from satellite-based sensors is that calibration and validation of these estimates may be challenging especially in the absence of a dense network of rain gauges (McCollum et al., 2000; Huffman et al., 2001; New et al., 2002; Collischonn et al., 2008).

Recent examples of applications of satellite-based precipitation estimates include Zulkafli et al. (2014), Nerini et al. (2015), Zubieta et al. (2015) and Zubieta et al. (2016). Harris et al. (2007) used satellite-derived rainfall data (TRMM and Multi-satellite Precipitation Analysis: TMPA) for flood prediction in the Upper Cumberland River basin Kentucky, using the HEC-HMS model and TOPMODEL (Beven and Kirkby, 1979). Their results showed that satellite data could be used successfully for flood prediction. Similarly, Tarnavsky et al. (2013) evaluated a dynamic hydrological model in dry lands using TRMM rainfall intensity at a spatial resolution of 1 km. TRMM data were corrected based on the fractional cover of rainfall (FCR) method in order to predict high enough rainfall intensities to generate realistic rates of predicted surface runoff.

Although recent studies of TRMM data showed that it can be used successfully in different applications, others highlight its limitations. For example, Cai et al. (2015) have evaluated TRMM data in Mid-High Latitude China and Mourre et al. (2016) over a mountainous watershed of approximately 10,000 km^2 in Peru . Their results show that; (i) TRMM may have poor performance over ice-covered areas because ice on the ground or in the atmosphere scatters the microwave energy in a similar way to rain; (ii) TRMM underestimates precipitation in mountainous regions possibly due to difficulty in detecting shallow, orographic rainfall (Dixon and Wilby, 2015).

1.4.2.2 Evapotranspiration derived from remote sensing

ET has a crucial role in the long term terrestrial water balance. Its estimation is essential for water resources management, particularly in semi-arid regions where resource availability is often low and variable (Pilgrim et al., 1988). However, as with rainfall, this can be a problem when observed data are sparse or unavailable, as is often the case in low and middle income

countries (Wilby and Dawson, 2013). Fortunately, remote sensing (RS) has the potential to provide estimates of the meteorological variables required to calculate *ET* at different scales. Over the last decade, significant improvements in dynamic atmospheric retrieval techniques from RS have been made for several relevant variables with different spatial and temporal resolutions. Examples include the Atmospheric Infrared Sounder (AIRS) / Advanced Microwave Sounding (AMSU) and the MODerate resolution Imaging Spectroradiometer (MODIS) which are mounted on NASA's Earth Observing System (EOS) Aqua satellite (Lee et al., 2013).

AIRS is a passive sensing system which uses infrared hyperspectral sensing to measure temperature and humidity (AIRS Science Team/Joao Texeira, 2013). The density profile of constituent atmospheric gases responsible for infrared absorption is used to define a weighting function for each of the 2378 AIRS channels, with wavelengths between 3.7 and 15.4 μm (AIRS Science Team/Joao Texeira, 2013). By measuring the infrared radiance (IR) in each of the AIRS channels, atmospheric temperature can be calculated using the Planck equation (Meier and Fiorino, 2016). When cloud cover prevents accurate IR temperature retrieval from the lower atmosphere, measurements can be made by its partner AMSU. This is a passive multi-channel microwave radiometer measuring atmospheric temperature with a 15-channel microwave sounder with a frequency range of 15-90 GHz (Meier and Fiorino, 2016). AMSU can provide atmospheric temperature measurements from the land surface up to an altitude of 40 km, as well as cloud filtering for the AIRS infrared channel at altitude to increase the accuracy of measurements (AIRS Science Team/Joao Texeira, 2013). This allows NASA to provide an integrated dataset (AIRS/AMSU, hereafter AIRS). AIRS has contributed to studies of the atmospheric temperature profile, sea-surface temperature, relative humidity, land surface temperature and emissivity and fractional cloud cover (AIRS Science Team/Joao Texeira, 2013).

Zhang et al. (2008) used remotely-sensed leaf area indices from MODIS with the Penman-Monteith equation, gridded meteorology and a two -parameter biophysical model for surface conductance (G_s) to estimate 8-day average evaporation (E_{RS}) at a 1 km spatial resolution. A steady-state water balance (precipitation – runoff) approach was used to calibrate E_{RS} which was then applied to estimate mean annual runoff, for 120 gauged sub-catchment in the Murray-Darling Basin of Australia. The results suggest that the evaporation model can be applied to

estimate steady-state evaporation and E_{RS} could be used with a hydrological model to generate runoff with an RMSE as low as 79 mm yr^{-1}.

Mu et al. (2009) developed an algorithm to estimate *ET* using the Penman-Monteith method driven by MODIS-derived vegetation data and daily surface meteorological inputs. They also applied the model with different meteorological inputs from ground-based stations and vapour pressure deficit and air temperature from the Advanced Microwave Scanning Radiometer (AMSR-E) and Global Modelling and Assimilation Office (GMAO) meteorological reanalysis-based humidity, solar radiation and near-surface air temperature data. Their results were validated using data from six flux towers across the northern USA. Simulated ET_{RS} derived from MODIS, AMSR-E and GMAO agreed well with tower-observed fluxes ($r > 0.7$ and RMSE of latent heat flux< 30 Wm^{-2} (i.e. $ET_o < 1.05$ mm d^{-1}).

Rahimi et al. (2014) compared the Surface Energy Balance Algorithm for Land (SEBAL) with the Penman-Monteith equation to investigate the accuracy of actual evapotranspiration (ET_a) estimation using MODIS data. The results showed that there was no significant difference between the SEBAL and PM methods for estimating hourly and daily ET_a (RMSE ranged from 0.091 mm d^{-1} to 1.49 mm d^{-1}). Peng et al. (2016) compared six existing RS-derived *ET* products at different spatial and temporal resolutions over the Tibetan Plateau. They used one product (LandFlux-EVAL) as a benchmark due to the lack of availability of *in situ* measurements. Their results showed that although existing *ET* products capture the seasonal variability well, validation against *in situ* measurements are still needed in order to confirm the accuracy of calculated *ET,* at least in this region and probably in general.

1.4.2.3 Total water storage changes derived from remote sensing

In addition to helping to estimate precipitation and evapotranspiration, satellite-derived sensors have significant potential for informing water storage terms in the terrestrial water balance. For example, the Gravity Recovery and Climate Experiment (GRACE) can be used to estimate changes in the strength of Earth's gravitational field from space. These estimates can be used to predict changes in terrestrial water storage (TWS) at various spatial and temporal scales (Tiwari et al., 2009; Famiglietti et al., 2011; Swenson and Wahr, 2002), which can be used to track changes in groundwater levels and to validate or improve predictions made by land surface models (Rodell et al., 2006). GRACE was launched in 2002 and has been used for various hydrological applications, including attempts to quantify the effects of climate change

on water resources at different scales (Rodell et al., 2004; Syed et al., 2005; Frappart et al., 2006; Lombard et al., 2007; Andersen et al., 2005; Yeh et al., 2006; Rodell et al., 2009; Castellazzi et al., 2016; Bhanja et al., 2016). Voss et al. (2013) reported GRACE-derived monthly anomalies in groundwater storage in the Tigris-Euphrates river basin (753,963 km^2) using the averaging kernel method developed by Swenson and Wahr (2002). This work suggested that TWS decreased by 27.2 mm y^{-1} between January 2003 and December 2009. Mulder et al. (2015) also estimated groundwater depletion in this region using the Mascon method (Mulder et al., 2015). They suggested that groundwater levels decreased by 39 ± 8 mm y^{-1} between 2007 and 2009. Unfortunately, both these studies were unsupported by ground-based observations of water table levels.

1.5 Summary

Generally water resources in the Middle East and particularly in Iraq are facing several issues including climate change, increased demands and reductions in cross border water transfers due to dam construction. In order to mitigate these threats, an understanding and modelling of hydrological processes is required. However, a significant issue with many semi-arid zones outside of Europe and North America is that meteorological and hydrological data availability is often scarce. Some of the problems associated with obtaining reliable long-term hydrological data in semi-arid regions include limited economic resources for monitoring and harsh climates. This is compounded by the fact that spatial and temporal variability in hydrological activity can be much higher in arid zones than in humid areas, requiring (in principle) denser monitoring networks (e.g. rain gauges and gauging stations) to capture the nature of system behaviour. Over last few decades, rainfall-runoff models have been widely built and used for a variety of purposes, but the majority of all modelling tools have been originally developed for data-rich areas. In addition, despite the increasing availability of remotely-sensed data at different spatial and temporal resolutions, they are scarcely used in hydrological modelling and only a small number of studies have been carried out (i.e. satellite data as input for hydrological modelling in data-scarce areas). Reasons may be related to: 1) the large errors (particularly) bias which often characterises satellite data. This can be modified by calibration and validation of the satellite derived products using ground estimates to quantify the direct usability of the products and 2) the spatial/temporal resolutions of the satellite data.

1.6 Gaps in the literature

The following gaps in the literature have been identified which require more study and focus:

- To date, the majority of all hydrological modelling tools have been originally developed for humid environments and for data rich semi-arid areas. Data-poor semi-arid regions have particular challenges and have consequently received little attention. Thus, a gap still exists for a parsimonious conceptual rainfall-runoff model that represents the main hydrological processes operating and which is able to generate time series of runoff and groundwater flow in such areas using readily available data at a daily time step.
- One issue with obtaining spatially-distributed rainfall estimates from satellite-based sensors is that calibration and validation of these estimates may be challenging especially in the absence of a dense network of rain gauges and the majority of studies have focused on data rich areas (McCollum et al., 2000; Huffman et al., 2001; New et al., 2002; Collischonn et al., 2008). Thus, assessment of the potential value of satellite-derived rainfall data for water resources management in a data-scarce areas crucially required.
- Despite the fact that other studies have used RS data to estimate *ET*, few previous attempts have been made, to my knowledge, to use AIRS data to estimate *ET* in a data-scarce semi-arid area, such as northern Iraq. Existing ET-$_{RS}$ and reanalysis data products with global spatial coverage include the MODIS 1km Penman Monteith (PM) data (Mu et al., 2009; Mu et al., 2011) and reanalysis data such as MERRA-2 (Global Modeling and Assimilation Office (GMAO), 2015). However, these data have temporal resolutions of eight days and one month, respectively – which are too course for many hydrological applications. Whilst attempts have been made elsewhere to obtain accurate evapotranspiration estimates from RS (ET_{o-RS}) at higher temporal resolutions (e.g. daily), for example in South Africa (Amy McNally NASA/GSFC/HSL, 2016) and the USA (Michael Jasinski, 2016), this has not been performed for many areas of the world where resources are limited and where ground observations are often very scarce. Thus, more studies are required to estimate daily ET_{o-RS}.
- Several studies have investigated variations in water storage using satellite data (e.g. GRACE) in northern Iraq, but none of these have been validated against ground-based data (i.e. well level data). There are also no studies looked at changes in water abstraction rates in northern-Iraq particularly during the drought periods. Additional

work is therefore, required to quantify and validate GRACE-derived terrestrial water storage variability in northern Iraq.

1.7 Aim and Objectives

1.7.1 Aim of research

The aim of this thesis is to develop and test a conceptual catchment scale rainfall-runoff model framework which can be driven by remote sensing data, in order to predict river runoff and evaluate surface and ground water storage variability in data-scarce semi-arid regions. The development of a validated and usable tool will be invaluable for present and future water resource management. This thesis has the following objectives to achieve the aim:

1.7.2 Objectives of the research

1. To develop a conceptual rainfall-runoff model framework which is parsimonious (i.e. has a low number of easily identifiable parameters) and which can run using a minimum input data set of daily temperature and precipitation.
2. To evaluate the ability of this conceptual model to simulate river discharge at the catchment outlet in a semi-arid catchment.
3. To estimate precipitation (P) and reference evapotranspiration (ET_o) from remote sensing (RS) data and to compare these estimates with those generated using ground-based meteorological data (i.e. simulating reduced input data availability and quality).

4. To evaluate the utility of satellite-based precipitation data to drive the rainfall-runoff model and to compare the predictions of runoff which are generated with those generated using ground-based meteorological data (i.e. simulating reduced input data availability and quality).

5. To evaluate variations in total terrestrial water storage using a combination of remote sensing data (GRACE), observed well data and rainfall-runoff modelling.

1.8 Structure of the thesis

The thesis is divided into six chapters, grouped into four sections, as shown schematically in Figure 1.2.

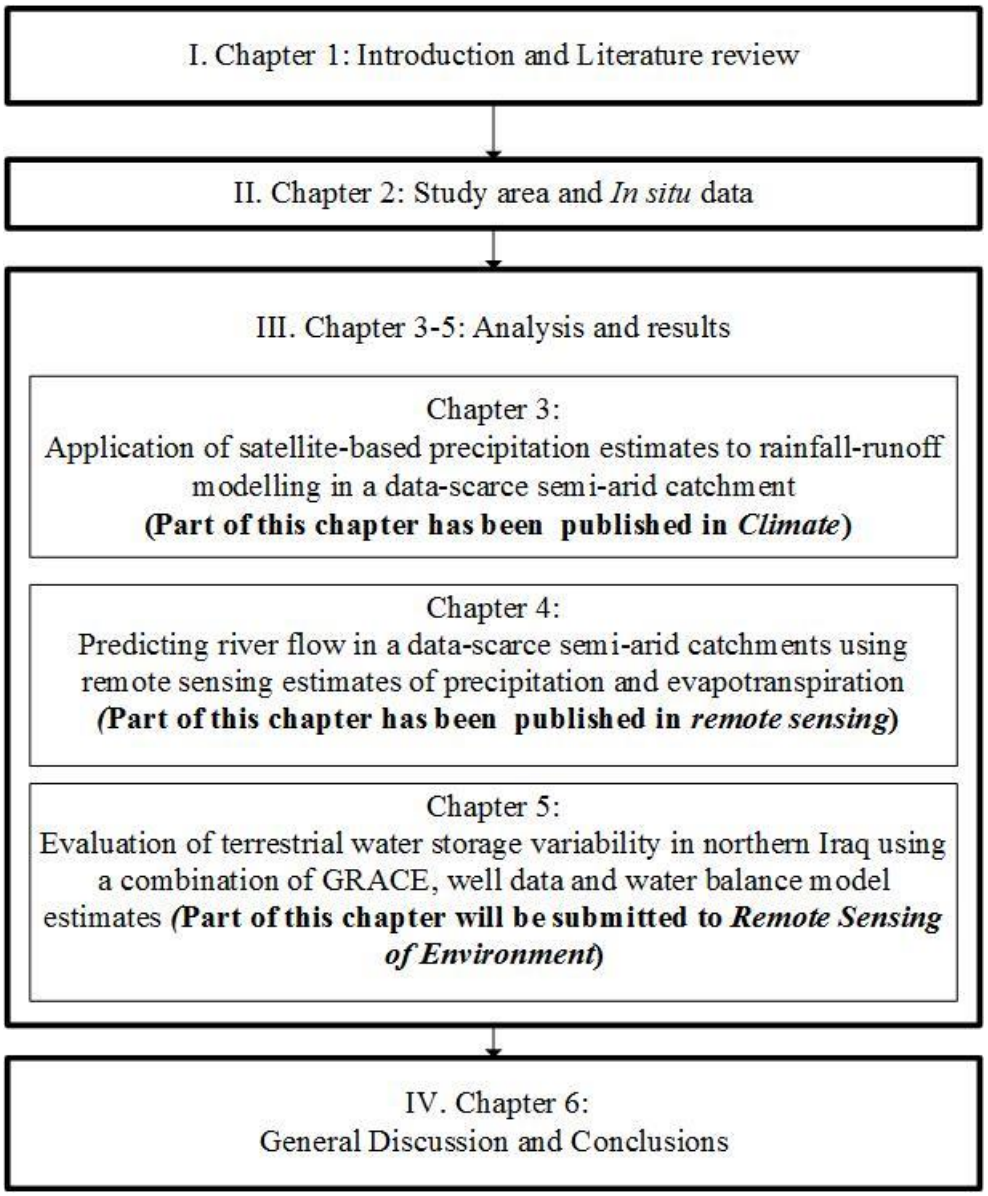

Figure 1. 1. Thesis structure.

The first chapter provides a general context and an overview of the problems facing water resources in semi-arid areas, a general review of hydrological processes in semi-arid regions and an outline of the rainfall-runoff modelling process including the limitations to developing and applying hydrological models in data-scarce semi-arid regions. It also discusses the potential role of remote sensing techniques for hydrological studies. The aim and objectives were developed based on identified knowledge gaps in the literature and problems identified for hydrological modelling in data-scarce catchments.

Chapter 2 describes the study area and the *in situ* data used in this research. The description of the study area includes topography, geology, soil type, land cover and land use, and climate including precipitation, temperature, wind speed and relative humidity. This was necessary in order to understand the nature of the environment needed for method selection etc.

Chapter 3 presents the developed conceptual rainfall-runoff model and provides an assessment of the application of remotely sensed rainfall estimates (TRMM) for driving this model. This chapter also contains a methodology to correct the TRMM data based on observed data from rain gauges and an insight into the analysis (calibration and validation) of the developed model.

Chapter 4 describes the estimation of daily reference evapotranspiration ET_o in a data-scarce semi-arid region using remotely-sensed meteorological data (e.g. net radiation flux density, surface temperature and relative humidity). It also evaluates the accuracy of the daily ET_o estimates derived from remote sensing ($ET_{o\text{-}RS}$) compared with those derived from four ground based stations ($ET_{o\text{-}G}$) using four different *ET* models. In addition this chapter evaluates the potential use of remote sensing *ET* data for simulating river discharge in the study area when the catchment is completely independent of ground-based observations.

Chapter 5 provides a quantitative assessment of temporal changes in terrestrial water storage in northeastern Iraq using the GRACE satellite data and, importantly, attempts a validation of the GRACE groundwater anomaly data using observed well data and a comparison with the simulated water balance using the model described in Chapter 3.

Chapter 6 provides a general discussion of the main body of research presented in the thesis and some conclusions. Recommendations for further work are also presented here.

Chapter 2: Study area and *In situ* data

2.1 Description of the study area

2.1.1 Location

The study area is situated in the Kurdistan region of north-eastern Iraq in the Middle East (33° 00’ 00” N, 42° 00’ 00” E to 37° 00’ 00” N, 47° 00’ 00” E). The study area boundary was delineated using 30m resolution digital elevation data from the Shuttle Radar Topography Mission (SRTM) (NASA Jet Propulsion Laboratory (JPL), 2013) (Figure 2.1).

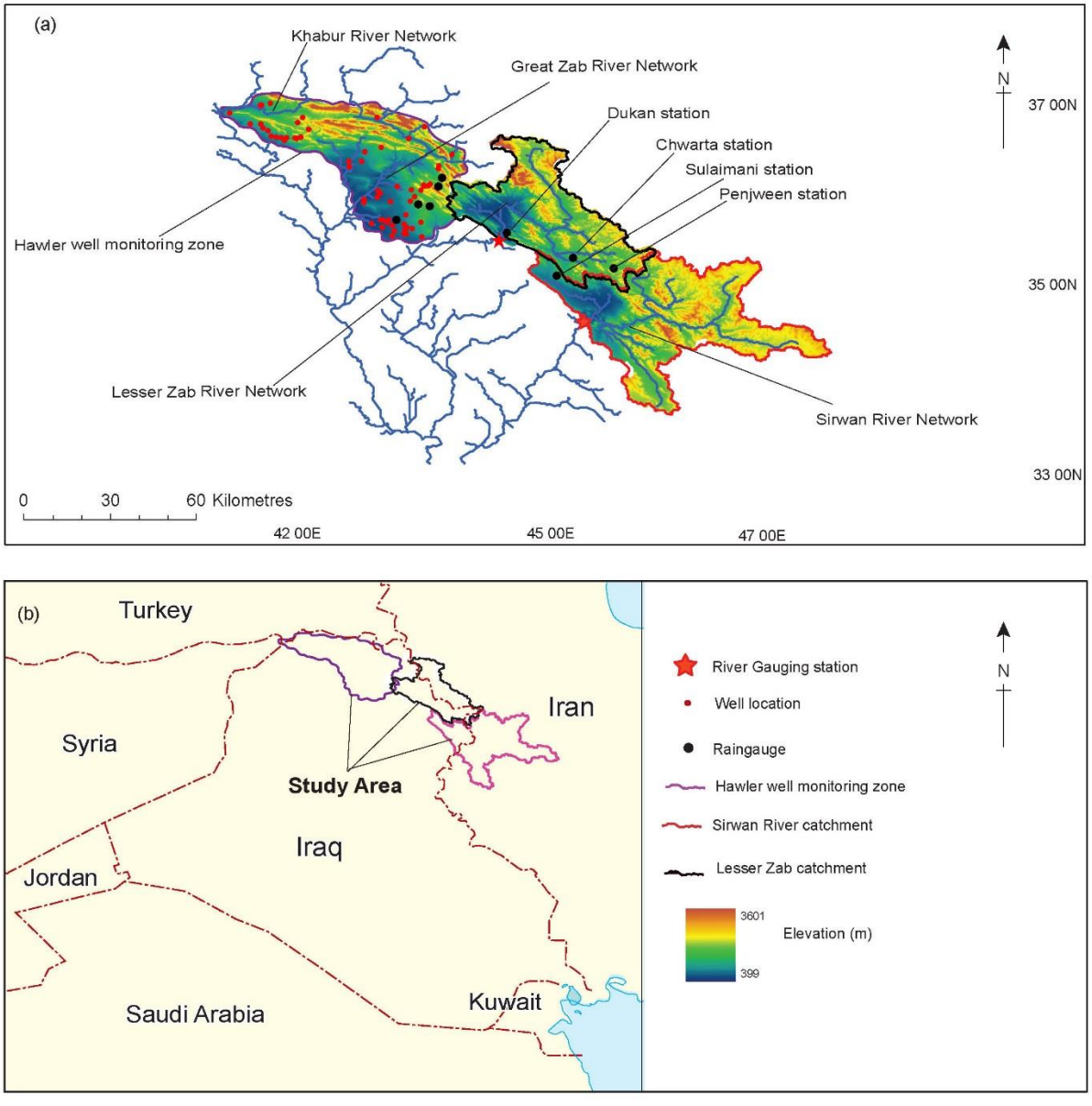

Figure 2. 1. (a) Elevation in the study area derived from the Shuttle Radar Topography Mission (SRTM) digital elevation model (DEM) (https://earthexplorer.usgs.gov/). (b) Regional location of the catchments.

It consists of three areas namely called the Lesser Zab River catchment (11,630 km^2), Sirwan River catchment (16,750 km^2) and Hawler well monitoring zone (15, 532 km^2).The latter comprises of part of the Greater Zab catchment and part of the Khabur catchment. Hawler well monitoring zone's boundary was defined arbitrarily to include all the monitoring wells for which data were available. The north eastern boundary of the study area is defined by the Zagros Mountains. The study area to the west is dominated by lower hills and lowland plains. Elevation ranges between 399 and 3601 m above sea level. The Lesser Zab and Sirwan River catchments were selected to evaluate Objective 2, 3 and 4. The Hawler well monitoring zone was selected to evaluate Objective 5 and Lesser Zab catchment was also used to evaluate Objective 5. These areas were selected for this research since they are equipped with a few hydro-meteorological stations and well monitoring system. These areas have also the capacity to represent similar river basins in the region due to similarity in some characteristics such as annual average temperature, annual precipitation, vegetation type, hydrographic pattern and geology. An overall description of the catchment and some summary information about the climatic inputs is given in the following section.

2.1.2 Climate

The climate of the study area is classified as subtropical semi-arid type (BSH: Rasul et al., 2016) which is hot and dry in summer (June to September) and cool and relatively wet in winter (October to May) (FAO, 2011). The transitions from winter to summer and vice versa are marked and often rapid (Beaumont et al., 2016). For the reason that the climate elements are crucial in this study, they are described in more detail.

2.1.2.1 Precipitation

The amount of precipitation depends on the two major factors in the study area; (i) the major moisture sources of the study area are the Mediterranean, Black and Caspian Seas, (ii) altitude, for instance the north and northeast parts receive a higher amount of precipitation than the south part. Average monthly rainfall during 2003-2014 is shown in Figure 2.2. Analysis of this record shows that the seasonal distribution of the precipitation in the study area varies and mostly falls as rain in winter and autumn with mean annual precipitation ranging from 350 and >1200 mm in the high mountain zone, but winter snowfall is common above 1000m above mean sea level (Zaitchik et al., 2007). The typical mean snow line in winter is 1270m ASL (Krásný et al., 2006). This means that highlands zone stores significant quantities of water as

snow pack during the winter period to be released, often as flood discharge or recharge groundwater, when temperatures begin to rise in spring. Whereas June, July and August are identified as drier months due to the absence of precipitation.

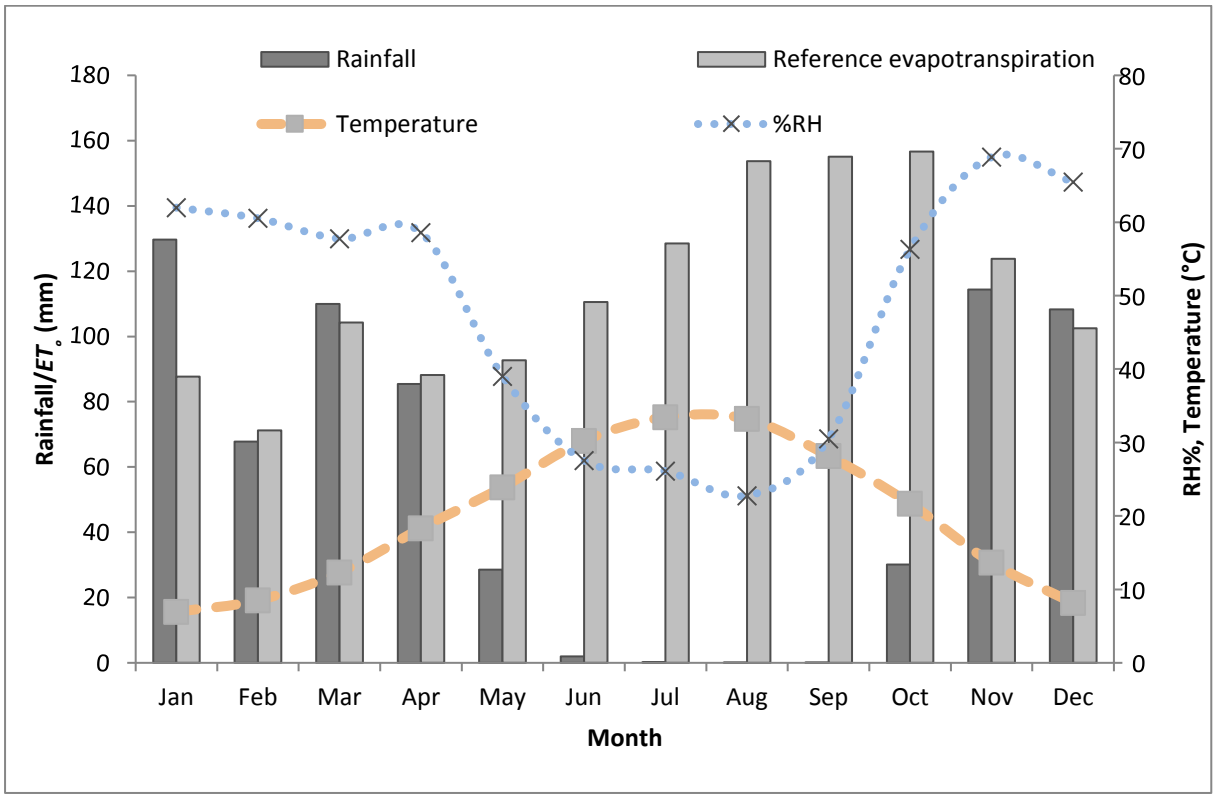

Figure 2. 2. Mean monthly spatially-averaged rainfall (Theisen polygons) for four stations, temperature, relative humidity and reference evapotranspiration (calculated using the Wasim-ET model: Hess et al., 2000) in the Lesser Zab catchment 2003-2014 (Sulaimani Meteorological Office, 2015).

2.1.2.2 Temperature

Throughout the regions temperature is characterised by warm and dry summers (June to September) and moderately cold and wet in winter (October to May). Summer temperatures are high almost everywhere. The highest mean daily summer temperatures exceed 40°C and have been recorded by meteorological stations in the study area (Figure 2.2). The lowest mean daily temperatures are recorded in the winter (Figure 2.2). In general, much stronger contrasts in temperature are noted between different regions in winter. This is due to the strong relationships between temperature and elevations. Therefore, the temperature in lower altitudes (Dukan and Sulaimani) is higher compared to high mountains (Penjween and Chwarta), as shown in Table 2.1.

Table 2. 1. Elevation, mean daily temperature, relative humidity and average annual rainfall of the four stations located in the study area from 2010 to 2014 (Sulaimani Meteorological Office, 2015).

Stations	Elevation (m)	Mean daily temperature (°C)	Relative humidity (%)	Rainfall (mm)
Dukan	650	23.1	44.2	586.3
Sulaimani	885	20.1	45.2	646.7
Chwarta	1128	19.6	46.1	693.2
Penjween	1300	14	57.1	951

2.1.2.3 Relative humidity, winds, evapotranspiration

The study area experiences extreme seasonal variations in relative humidity due to high variations in climate and altitude. The annual average RH is about 48% in the study area. It is high in winter and exceeds 70% but only 22% in August. RH also has higher values in the high mountains (Penjween and Chwarta) compared to lower altitudes (Dukan and Sulaimani). Wind is a very important variable of climate which moves moisture and temperature. Wind speed is one of the factors that influence the evapotranspiration (Allen et al., 1998). The mean speed of the wind at Sulaimani station during 2003-2014 was 1.8m sec^{-1}. Southerly winds from the lowlands bring increased temperatures and northerly winds tend to bring cooler air (Beaumont et al., 2016). Evapotranspiration is higher in summer where there is always a water deficit and lower rate in winter (Figure 2.2).

2.1.3 Hydrographic pattern and geology

The hydrographic pattern of the study area is dominated by the Khabur River, Greater Zab River, Lesser Zab, and Sirwan River (Figure 2.1). The Greater Zab and Khabur rivers originate in Turkey and the Lesser Zab River and Sirwan River rise in Iran. They join the river Tigris at the border between the Kurdistan region and the rest of Iraq. Each river catchment contains sparsely inhabited high mountains with high precipitation, groundwater storage and a seasonal snowpack (Buringh, 1960); a heterogeneous Karst zone characterised by fissured aquifers, canyons and dry valleys (Krásný et al., 2006) and lowland plains containing agricultural land (Figure 2.3) (FAO, 2011).

Figure 2. 3. Sample of hydrographic of Lesser Zab River flow, (a1) shows high mountain zone, (a2) represents karstified zone and (a3) is lowland plains area (Taken 2015).

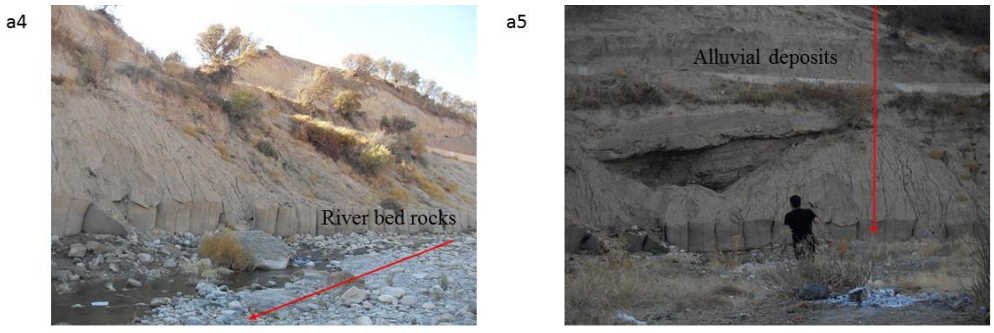

Figure 2. 4. (a4) shows Sample of alluvial deposit and (a5) shows layers of gravel, sand in Lesser Zab river bed (taken 2015).

The geology of the study area is very complex due to the interactions and movement of three major plates which are the African, Eurasian and Arabian plates (Beaumont et al., 2016). This motion led to the production of a crash zone, mountain ranges and different morphology forms during ancient geological periods (Beaumont et al., 2016). The study area land mass composed of different parents and older rocks is shown in Figure 2.3 which was delineated using 1:5000, 000 geological map of the world established by FAO (2011).

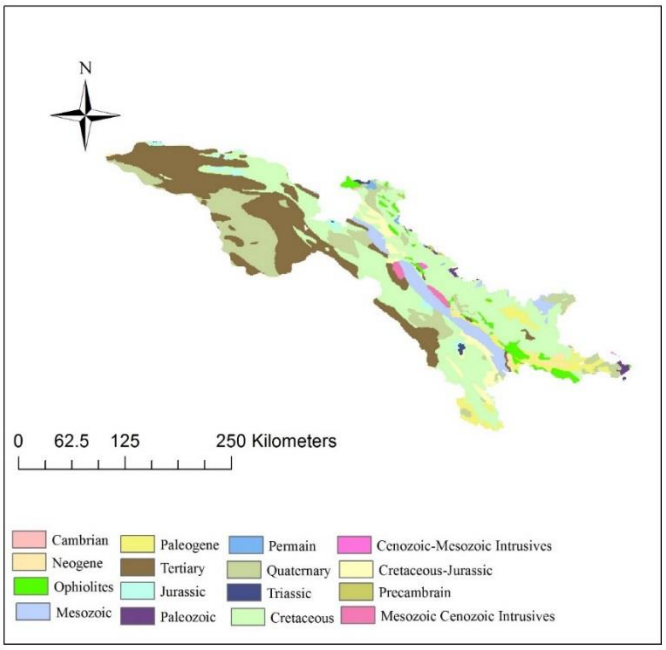

Figure 2. 5. Geology map of the study area derived from geological map of the world established by FAO (2011).

Generally, there are three major tectonic zones in the study area: (1) The Thrust Zone in the north (along the border with Turkey and Iran) which contains variable geological formations from the pre-Triassic to the late Tertiary; (2) the High Folded zone in the central part which is dominated by thick layers of karstified limestones and dolomitised limestones from the mid Jurassic to the mid Tertiary, which comprise important aquifers (i.e. Bekhma and Pilaspi; see next section) and (3) the Low Folded zone in the south. These formations are overlain by clastic sediments from the upper Miocene and Pliocene often with a thickness exceeding 1000m (Saad and Jeremy, 2006; Kamal, 2010) . These formations dominate the lowland plains and can act as aquifers. Fluvial terraces and recent alluvium are also presen (Figure 2.4) (Saad and Jeremy, 2006; Kamal, 2010).

Groundwater resources are significant but vary both in space and time. Generally, two main groups of significant aquifers were defined by Stevanovic and Markovic (2004), based on geological and hydrogeological similarities: The karstic and karstic-fissured aquifers of the extended carbonate formations (limestones and varieties) in the central, high-folded zones; and the intergranular aquifers of the lowlands. The main characteristics of karstic and karstic-fissured aquifers are that they are non-homogenous and anisotropic. Turbulent flow regimes exist and cavities exceeding 10 m in length may be encountered during drilling. Wells >150 m deep may have yields of up to 40-50 L s^{-1} with very limited drawdown (Stevanovic and Markovic, 2004). The groundwater flow direction is determined by the position of the erosion base and tectonics. The karst rock massifs are often drained by high-yield springs, 20 to 30 of which have a minimum discharge exceeding 100 L s^{-1}. In many cases very high transmissivity values of 6-9 x 10^{-2} m^2 s^{-1} have been observed (Stevanovic and Markovic, 2004).

Results of permeability tests in the intergranular aquifers also show a high degree of heterogeneity (Saad and Jeremy, 2006; Kamal, 2010) with calculated transmissivity values for the Bakhtiari aquifer ranging from 1 x 10^{-6} m^2 s^{-1} to1 x 10^{-1} m^2 s^{-1} while the hydraulic conductivity is on average 1 x 10^{-4} m s^{-1} (Stevanovic and Markovic, 2004). Locally, there are cemented layers obstructing aquifer recharge and groundwater circulation. Groundwater movement is slow and roughly follows the surface drainage pattern.

2.1.4 Land cover and Land use

The catchments area, which has an area of about 30,000 km^2, identifies 11 different type of land cover (Figure 2.6) which was delineated using a 1:5,000, 000 land cover map of the world established by FAO (2011). Land cover is the predominantly extensive grazing of sparsely vegetated areas but also includes some irrigated and rain-fed arable land, woodland, open water and some small urban areas (Figure 2.7). The percentage covers of each major land cover are shown in Table 2.2. The herbaceous vegetation, aquatic or regularly flooded land covers approximately 30% while, snow and glaciers covers 0.0033% of the all study area based on FAO (2011) .

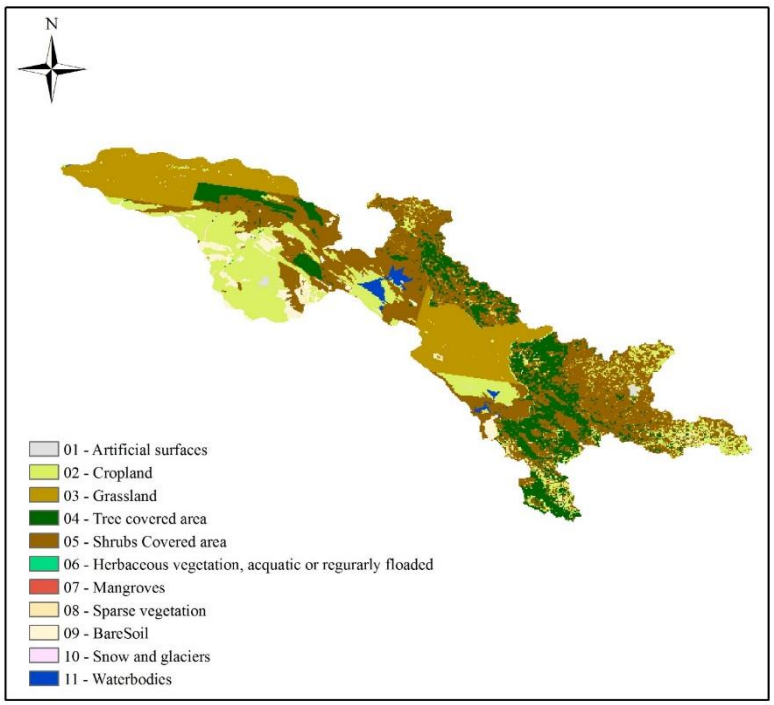

Figure 2. 6. Land cover map of the study area derived from land cover map of the world established by FAO (2011).

Table 2. 2. Land cover percentage in the study area (FAO, 2011)

Land cover taypes	Area %
Arificial Surafce	0.037
Cropland	0.32
Grassland	23.7
Trees	21.72
Shrubs	10.7
Herbaceous vegetation, acquatic or regurarly floaded	30.6
Mangroves	0.011
Sparse vegetation	0.67
Bare Soil	11.4
Snow and glaciers	0.0033
Waterbodies	0.91

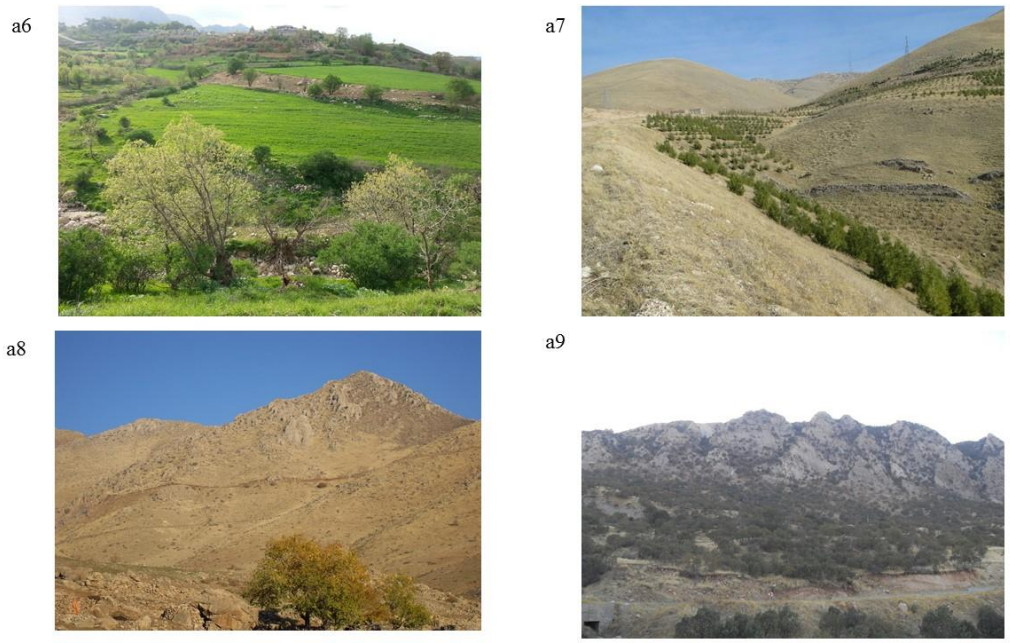

Figure 2. 7. Sample of different land cover type in the Study area, a6 shows natural grassed area, a7 illustrates artificial forest plantation, a8 displays sparsely vegetated hillslopes and a9 shows natural tree cover area (Taken 2015).

2.1.5 Soil of the study area

Different soil types can be found in the study area based on soil map classifications and descriptions (Figure 2.8) by the FAO (2011)). The dominant soil types are eutric lithosols, vertisols, xerosols, calcrtic and regosols and they vary in texture, structure, colour and composition. Texturally the Eutric lithosols chromic bertisols have a fine texture, which are mostly located at hill slopes and are related to the parent geological formation. Eutric lithosols is the shallow depths soil which were formed by the weathering of parent's rock and having 50% or more base saturation. Whereas calcaric regosols have deeper soil depths, at least between 20-50cm from the surface and whose formation was conditioned by climate, arid and semi-arid regions. Xerosols having a weak structure, aridic moisture regime and a calcic horizon within 125cm of the surface. According to the representative soil sample (Table A.1), all soil types of the watershed have a large percentage of silt to clay content that ranges from 30 to 57%. Besides these textural characteristics, soil bulk density, organic matter available water content and optimum moisture content also vary from place to place within the areas. They are highly linked to topography and are vulnerable to soil degradation by erosion, which is related to the land cover and soil conservation practice.

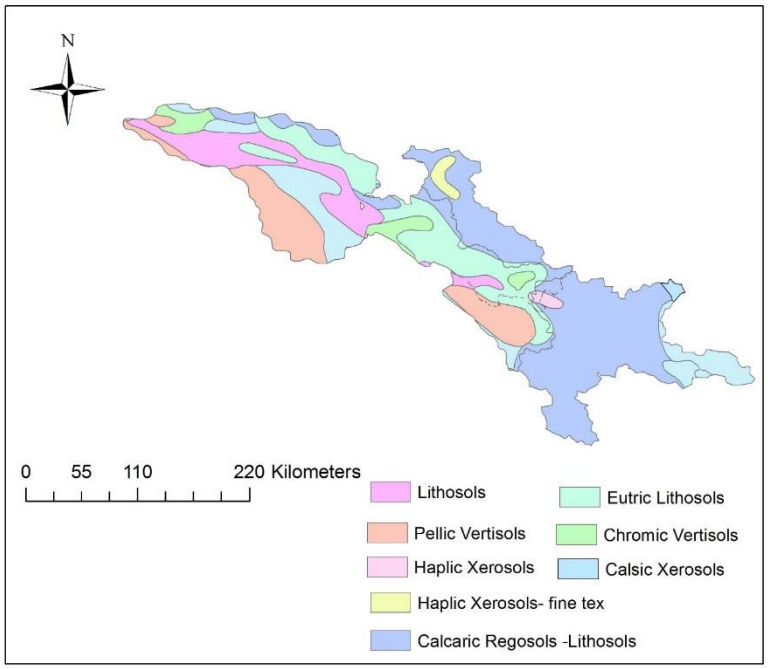

Figure 2. 8 Soil map of the study area derived from global soil map classifications by the FAO (2011).

2.2 *In situ* data

There are several challenges in obtaining ground-observed meteorological data in semi-arid areas of the Middle East., primarily the harsh situation of the study area (Figure 2.9). These include poor transport infrastructure (making access difficult), sparse population (restricting possible for regular manual observation) and harsh climate (e.g. very high day time temperatures which can make fieldwork challenging and potentially interfere with instrument performance. This is illustrated in Figure 2.9. Ground-observed meteorological data (minimum and maximum air temperature, relative humidity, sunshine hours, wind speed and rainfall) were obtained from the Sulaimani Meteorological office. In the Lesser Zab catchment meteorological data were obtained on a daily basis for four stations. In the Hawler well monitoring zone, meteorological data were obtained on monthly basis at five stations (Figure 2.1). Daily and monthly reference evapotranspiration (ET_o) was calculated based on the FAO Penman Monteith equation (Allen et al., 1998) using the Wasim-ET software (Hess et al., 2000). Mean daily river discharge data were obtained (for the Lesser Zab catchment only) for the station located upstream of the Dukan Dam reservoir (2010 - 2014) from the Hydrology Department of the Dukan Dam Directorate. Existing well information (Table 2.2) and observed

monthly well level data were obtained from the Ministry of Agriculture and Water Resources in the Kurdistan Regional Government for 65 monitoring wells distributed across the Hawler well monitoring zone for the period 2003-2009 (Figure 2.1).

Table 2. 3. Summary of the *In situ* data sets used in this study(Ministry of Agriculture and Water Resources in the Kurdistan Regional Government , Hydrology Department of the Dukan and Darbandikhan Dam Directorate and the Sulaimani Meteorological office).

Catchment_ name	**Variable**	**Resolution**		**Period**
		Spatial	**Temporal**	
Lesser Zab	Max and Min air temperature (°C)	-	daily	2003-2014
	Relative humidity (%)	-	daily	2003-2014
	Sunshine hours	-	daily	2003-2014
	Wind speed (m s^{-1})	-	daily	2003-2014
	Rainfall (mm)	-	daily	2003-2014
	River discharge (m^3 s^{-1})	-	daily	2010-2014
Sirwan River	River discharge(m^3 s^{-1})		daily	2010-2014
Hawler	Max and Min air temperature (°C)	-	monthly	2003-2014
	Relative humidity (%)	-	monthly	2003-2014
	Sunshine hours	-	monthly	2003-2014
	Wind speed (m s^{-1})	-	monthly	2003-2014
	Rainfall (mm)	-	monthly	2003-2014
	Well data (m)	-	monthly	2003-2009

Table 2. 4. Existing wells in Hawler and Lesser zab catchment, by well depth and status up to 2014 (Ministry of Agriculture and Water Resources in the Kurdistan Regional Government).

Catchment	**Number of Wells**	**Of which legal**	**well status**			**well depth (m)**				
			In use	**dry**	**others**	**<50**	**50-100**	**100-150**	**150-200**	**>200**
Hawler	6778	4093	5708	272	798	192	2200	405	2840	1141
Lesser zab	525	NA	330	48	147	26	174	12	201	4

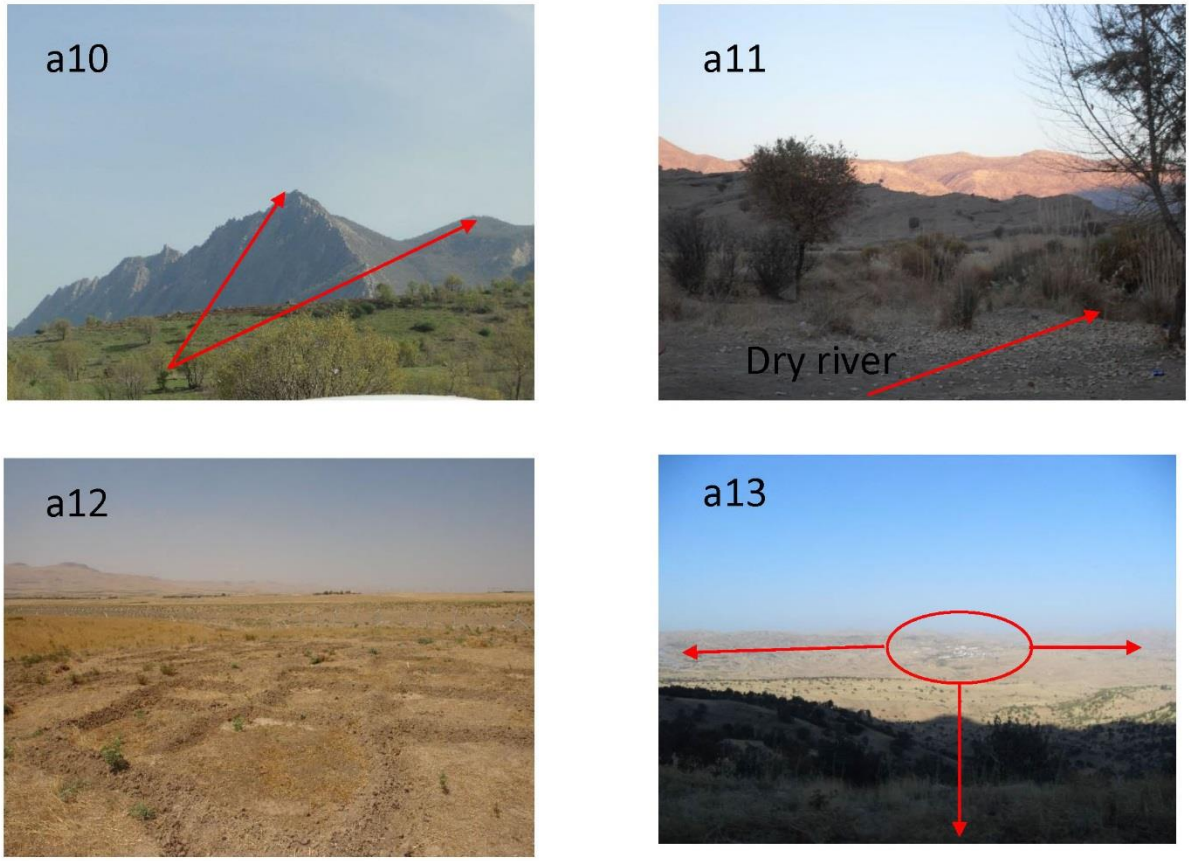

Figure 2. 9. Sample of different situations in the Study area, 10 shows a mountainous area, 11 illustrates a seasonality dry river, 12 displays a sparsely vegetated lowland area and 13 shows an urban area (Taken 2015).

2.3 Remote sensing data

2.3.1 TRMM data

The rainfall-runoff model employed here has a daily time step. The TMPA- 3B42 v7 and 3B42RT data products also have daily temporal resolution and 0.25° [approx. 27.83 km] spatial resolution, with global coverage from 50° N to 50° S (Huffman et al., 2007). They, therefore, represent suitable drivers for the model. These data were downloaded from the NASA data server (https://giovanni.gsfc.nasa.gov/giovanni/) for the period 2003–2014. For modelling 4383 daily precipitation layers of TMPAS were downloaded. To download data from the NASA data server, first, the area of interest is defined (Figure 2.10), and then with

the selection of time interval, the data are visualized. There are four format types: HDF, NetCDF, ASCLL and Google Earth KMZ. In this study, results were downloaded in NetCDF format for further operations. Files were processed to extract data for the catchment using R (R Core Team, 2014) and ArcGIS (ESRI, Redlands, CA, USA).

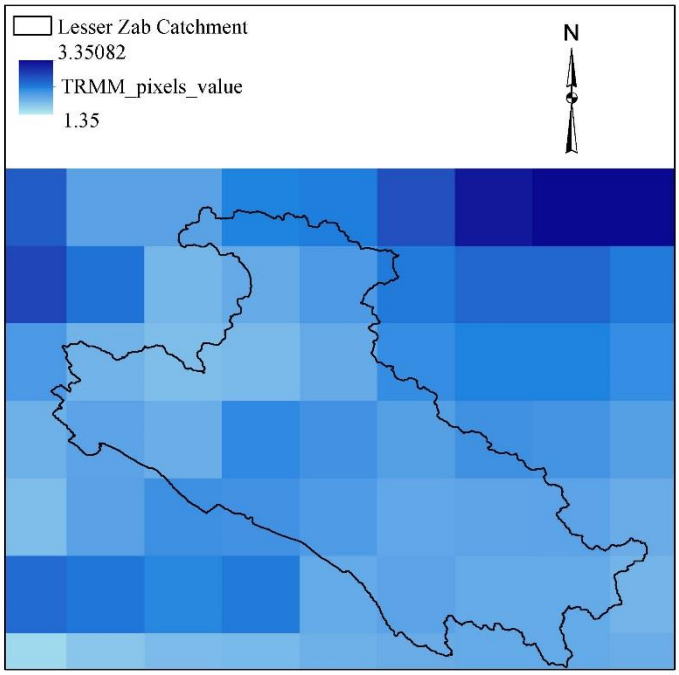

Figure 2. 10. Example of the TRMM pixel values for April 2003 in relation to the Lesser Zab catchment area.

2.3.2 AIRS data

Daily time series of near-surface air temperature (°C), RH (%) and cloud cover fraction were obtained from Aqua AIRS/AMSU Level 3 Daily Standard Physical Retrieval (AIRS + AMSU) 1 degree × 1 degree V006 (short name AIRX3STD) for 2010–2014 at 1° spatial resolution (Figure 2.11). These data were downloaded from the NASA data server (https://disc.gsfc.nasa.gov/SSW/#keywords=AIRX3STD%20006). Data gaps were filled using cubic spline interpolation (R Core Team, 2014). Although this can be problematic if temporal gaps in the data are wide, in this study AIRS data were available for 99% of the period of interest (2010–2014) and the maximum data gap was just four days. Cubic splines are considered to be a reasonable interpolation method at this resolution and have often been

reported to be better than simple linear interpolation for oscillating data, provided the temporal gaps are not too wide (McKinley and Levine, 1998).

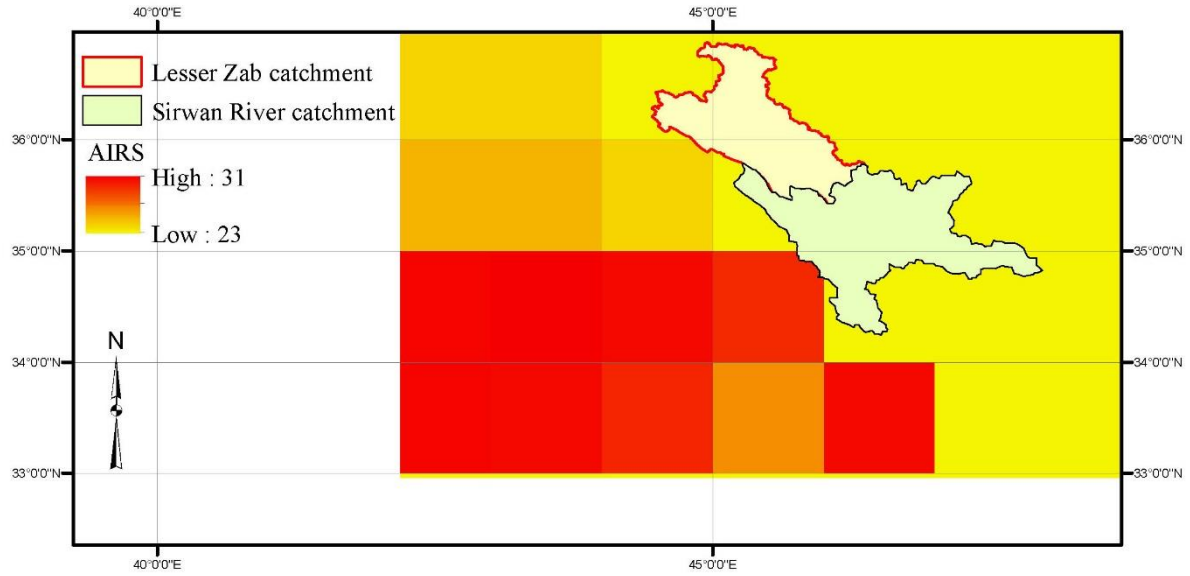

Figure 2. 11. Example of The AIRS pixel values for May 2012 in relation to the Lesser Zab and Sirwan River catchment area.

2.3.3 Reanalysis Data

MERRA is a reanalysis of daily meteorological datasets for the Era satellite which was built by NASA's GMAO. It assimilates atmospheric observations into a numerical model called the Goddard Earth Observation System Data Assimilation System Version 5 (GEOS-5). MERRA focuses on historical analysis of the hydrological cycle at a broad range of spatiotemporal scales. It offers a variety of reanalysis datasets including monthly surface pressure, relative humidity, air temperature and hourly wind speed. The output of interest for this study is wind speed due to its high temporal resolution. Daily estimates of wind speed at 10 m height were obtained from MERRA (GMAO: Global Modeling and Assimilation Office, 2008: http://giovanni.gsfc.nasa.gov/giovanni) at 0.5° x 0.6°. The spatial resolution of MERRA and AIRS is different. Bilinear interpolation was, therefore, applied to resample the MERRA data to a 1° spatial grid using the four orthogonal MERRA cells surrounding a given pixel.

2.3.4 GRACE data

GRACE is a joint mission by NASA and the German Deutsche Forschungsanstalt für Luft und Raumfahrt (DLR) (Swenson and Wahr, 2002). It consists of two identical satellites that fly about 220 km apart in polar orbit at an altitude of ~500 km (Tapley et al., 2004). A K/Ka-band microwave ranging system is used to make very accurate measurements of the relative speed and distance between the satellites caused by variations in their orbital motion resulting from differences in the Earth's gravitational field (Tregoning et al., 2012). Water storage can make a significant contribution to the gravitational field and temporal changes in water storage can, therefore, be detected at different locations on a monthly basis (Tregoning et al., 2012; Wahr et al., 1998). GRACE-derived Total Water Storage Anomalies (TWSA) (deviations from the 2004-2009 average: Landerer and Swenson, 2012) represent the vertically integrated water storage, including surface water, snow, soil moisture, biological water and groundwater. They are expressed in Equivalent Water Height (EWH, cm: Xie et al., 2016). Since its launch in 2002, the GRACE Science Data System has continuously released monthly gravity solutions from three different processing centres: (the Center for Space Research at University of Texas, Austin [CSR], the GeoForschnungsZentrum [GFZ] Potsdam and the Jet Propulsion Laboratory [JPL] (Wahr et al., 1998; Swenson et al., 2008; Scanlon et al., 2012; Jacob et al., 2012).

The first published results using data from the GRACE mission showed significant improvement in the accuracy with which the earth's gravity field could be measured (Tapley et al., 2004) and yielded the first estimates of the amplitude of annual variations in the global hydrological cycle. However, significant errors in a north–south striping pattern were evident in the solutions, completely masking the hydrological and oceanic signals that were being sought. The stripes were found to be related to unidentified errors in the reduction of the raw observations and filtering techniques were employed to reduce these errors (Tapley et al., 2004; Wahr et al., 2006). Rodell et al. (2004) found that the GRACE TWS estimates lay roughly between estimates derived from a water balance model and the Global Land Data Assimilation System (GLDAS) model. They also found that the spatial scaling applied to the GRACE data affected the amplitude of the variations in the GRACE estimates. They also conclude that a major source of uncertainty driving groundwater dynamics from GRACE is the need to subtract estimated soil moisture storage. Finally, the spatial resolution of GRACE (1 degree) is a too coarse for some hydrological studies.

Landerer and Swenson (2012) also suggested that due to the sampling and post-processing of GRACE observations, surface mass variations at small spatial scales tend to be attenuated. Users should, therefore, multiply GRACE data by a scaling grid in order to restore the signal removed by the destriping and filtering. For further detail, see (Landerer and Swenson, 2012). Total Water Storage Anomalies (TWSA) (deviations from the 2004-2009 average: Landerer and Swenson, 2012) of GRACE RL05 (1° x 1°)] from the three independent GRACE research centres (CSR, GFZ and JPL) were downloaded from the NASA data server (http://grace.jpl.nasa.gov) for the study period 2003 – 2014. First, the area of interest and time interval were defined (Figure 2.12), and then data are visualized. In this study, results were downloaded using NetCDF format for further operations. Files were processed to extract data for the catchment using R (R Core Team, 2014) and ArcGIS (ESRI, Redlands, CA, USA).

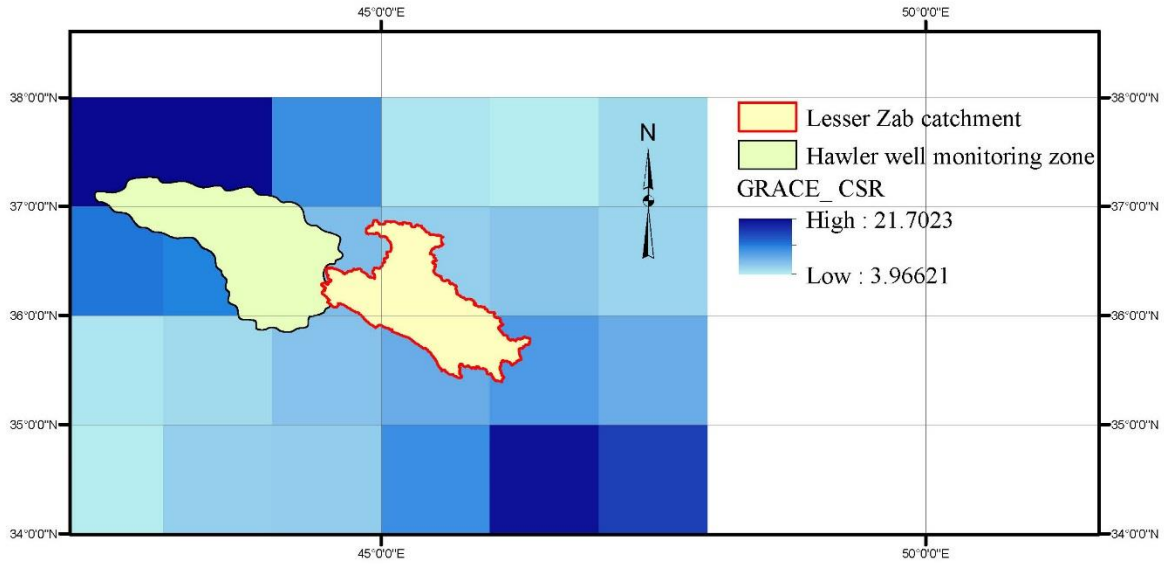

Figure 2. 12. Example of The GRACE pixel values for January 2003 in relation to the Lesser Zab catchment and the Hawler well monitoring zone.

2.3.5 GLDAS data

The Global Land Data Assimilation System (GLDAS) is a land surface modelling system that uses global satellite-based observations to drive climate and hydrological simulations (Rodell et al., 2004). It includes soil moisture and snow water equivalent and, importantly, does not include groundwater (Rodell et al., 2004). Zaitchik et al. (2010) stated that the main strength of GLDAS is the provision of information on land surface processes in data poor regions

although, it has considerable uncertainties in its runoff routing algorithm. This is a particular concern because of the nature of the "cell-to-cell" (CTC) algorithm, in which the runoff from each cell is routed to its downstream neighbour and is tracked along the river network on the basis of the continuity equation. This process does not consider within cell routing (Zaitchik et al., 2010). In contrast to CTC algorithms, in which all runoff must be routed explicitly through the conveyance and storage equations of every cell between a runoff source and the discharge point of interest, the "source-to-sink" approach (STS: Olivera et al., 2000) may solves for discharge at selected points on the landscape. However STS algorithms used as alternative to CTC, it does not improve the runoff routing in GLDAS runoff simulation which tend to underestimate observed runoff (Zaitchik et al., 2010).

Monthly GLDAS water storage prediction were obtained for the study period 2003-2014 from the NASA data server at http://grace.jpl.nasa.gov/data/get-data/land-water-content/. GLDAS has same spatial resolution (1° x 1°) as GRACE data (Figure 2.13).

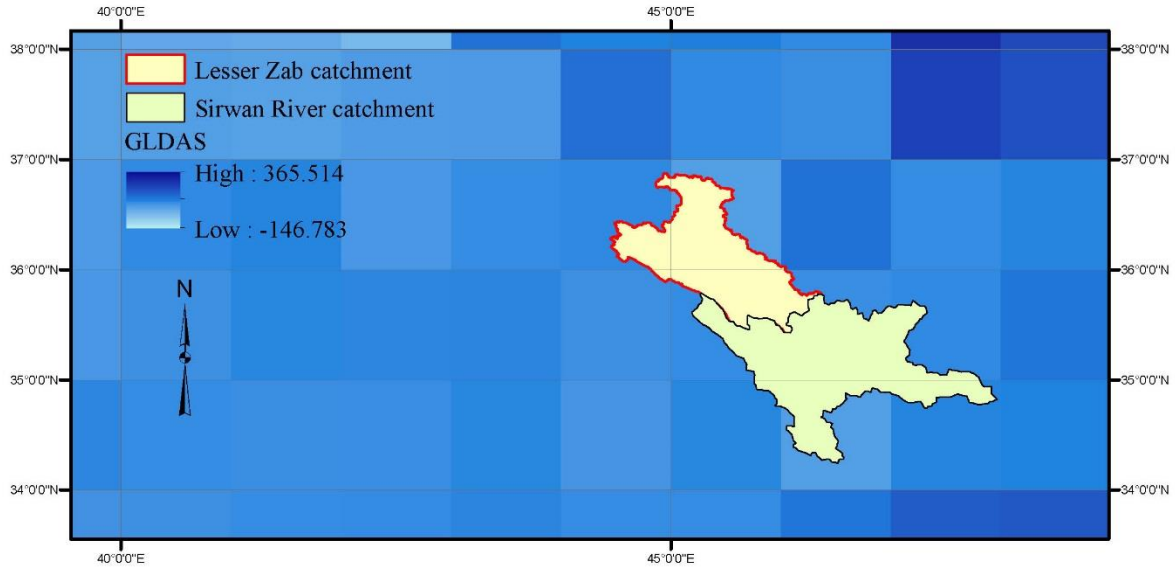

Figure 2. 13. Example of GRACE pixel values for January 2003 in relation to the Lesser Zab catchment and the Hawler well monitoring zone.

Chapter 3: Application of satellite-based precipitation estimates to rainfall-runoff modelling in a data-scarce semi-arid catchment

3.1 Introduction

Understanding and modelling hydrological processes is important for the management of water resources and for the analysis of extreme hydrological events, such as droughts or floods. However, a significant issue with many semi-arid zones outside of Europe and North America is that meteorological and hydrological data availability is often scarce. Some of the problems associated with obtaining reliable long-term hydrological data in semi-arid regions include limited economic resources for monitoring, sparse population and harsh climates (Wheater, 2002; Beaumont et al., 2016). This is compounded by the fact that spatial and temporal variability in hydrological activity can be much higher than in humid temperate areas, requiring (in principle) denser monitoring networks (e.g., rain gauges and streamflow gauging stations) to capture the nature of system behaviour (Sawunyama and Hughes, 2008; Collischonn et al., 2008; Draper et al., 2009). This issue is even more acute in mountainous areas where spatial and temporal variability in precipitation tends to be higher than in lowland areas. Unfortunately, the establishment and maintenance of such networks is often not a priority for many developing countries or is quite simply unaffordable. Even when monitoring data exist, they may be of variable quality, contain significant gaps or be unavailable to scientists without the necessary political contacts (Voss et al., 2013). These problems have brought about considerable uncertainty in the development, calibration and validation of hydrological models in data-poor semi-arid regions which may affect management decisions based on their simulations (Beven and Alcock, 2012). Alternatively, recent development in remote sensing (RS) based precipitation (i.e. TMPA) has the potential to cover these issues. In this chapter, a simple lumped hydrological model applied to the Lesser Zab River basin in the Kurdistan region of Iraq. The main purposes of the chapter were (a) to compare TMPA rainfall estimates to data from rain gauges installed at different locations in the catchment; (b) to evaluate the ability of a simple conceptual water balance model to simulate the hydrological response of a large and complex semi-arid catchment and (c) to compare model performance against

measured discharge data when driven by TMPA rainfall estimates and when driven by rain gauge data in order to assess the potential value of satellite-derived rainfall data for water resources management.

3.2 Materials and Methods

3.2.1 Study area

Study area of interest in this chapter is the Lesser Zab catchment which was described in (chapter 2, section 2.1).

3.2.1 *In situ* data

In situ data used in this chapter was described in (chapter 2, section 2.2).

3.2.2 Remote sensing data

The remote sensing data of interest in this chapter is TRMM products which described in (chapter 2, section 2.3.1)

3.2.3 TRMM correction

Comparisons between TRMM-derived rainfall estimates and ground-level gauge data suggest that TRMM data can sometimes be biased systematically (Arias-Hidalgo et al., 2013). Several attempts have been made to correct these estimates. Examples include mean bias correction (Seo et al., 1999), which uses the average bias for all stations to correct the satellite-derived rainfall, regression analysis (Immerzeel et al., 2009) based on historical time series and the spatial bias approach (Muhammad et al., 2012).

Here, a bias-correction approach (originally developed for downscaling climate model outputs) was used to adjust TRMM data, based on the assumption that the satellite and in situ data have similar statistical properties (Bouwer et al., 2004):

$$SRE_{c(t)} = \left(\frac{SRE_{0(t)} - \mu_{SRE}}{\sigma_{SRE}}\right) * \sigma_{OBS} + \mu_{OBS} \quad (3.1)$$

where $SRE_{c(t)}$ and $SRE_{0(t)}$ are the corrected and uncorrected satellite-derived rainfall estimates, respectively, μ_{OBS} is the average observed rainfall for all reporting stations, μ_{SRE} is the average satellite-derived rainfall, σ_{OBS} is the standard deviation of the observed data and σ_{SRE} is the standard deviation of satellite-derived rainfall.

This can be re-written as

$$SRE_{c(t)} = \left(SRE_{0(t)} - \mu_{SRE}\right) * \sigma_f + \mu_{SRE} * \mu_f \quad (3.2)$$

where

$$\mu_f = \frac{\mu_{OBS}}{\mu_{SRE}} \quad (3.3)$$

and

$$\sigma_f = \frac{\sigma_{OBS}}{\sigma_{SRE}} \quad (3.4)$$

Rainfall data were split into two periods: Period 1 from 2003 to 2009 (calendar years), in which we derived the two correction factors (μ_f and σ_f) and Period 2 from 2010 to 2014, in which the satellite-derived rainfall data were adjusted using the correction factors derived in Period 1 (μ_f = 1.05 and σ_f = 1.24). Period 2 represents an independent validation period for the rainfall correction method.

3.2.4 Rainfall-runoff model

LEMSAR (Leicester Model for Semi-Arid Regions) is a conceptual lumped rainfall-runoff model that simulates daily river discharge using daily rainfall and potential evapotranspiration data. It is based on the models described by Whelan and Gandolfi (2002) and Pullan et al. (2016), with added routines for snow melt and groundwater storage (Figure 3.1). LEMSAR has been coded with R programing language to assure minimum running times and an extended re-usability of the code (Figure A. 1).

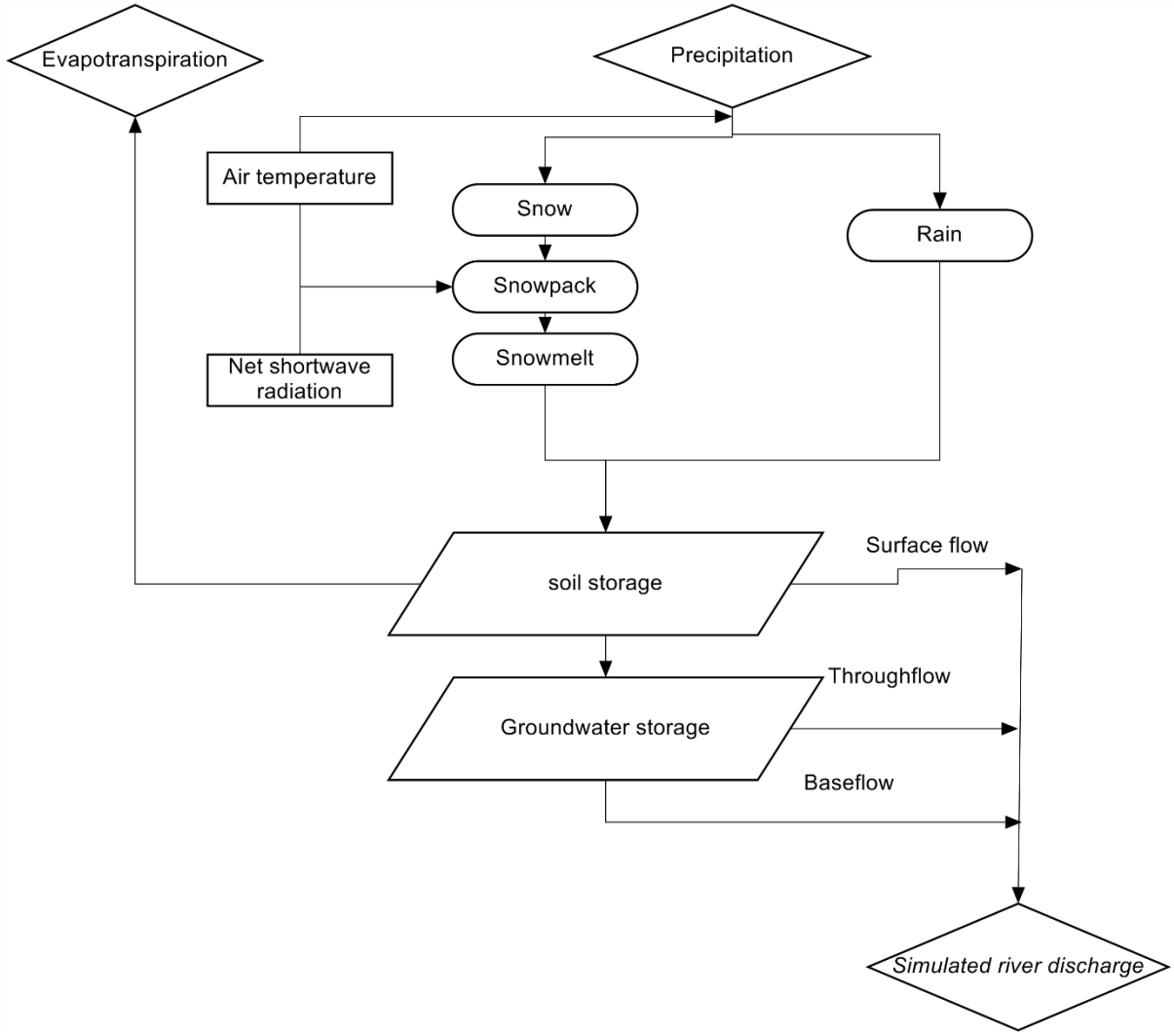

Figure 3. 1. Structure of the LEMSAR model

Briefly, the catchment is conceptualised using three moisture stores: (1) a single soil store, characterised by its depth (z), whole profile porosity ($\emptyset$) and by hydraulic parameters which describe the relationship between soil water content and unsaturated hydraulic conductivity; (2) a groundwater store which is augmented by recharge from the soil and depleted by baseflow to the river and (3) a time-variable snowpack.

A simple water balance is considered for the soil store:

$$\frac{dS}{dt} = P - ET - q - q_o + M_{tot} \tag{3.5}$$

where S is the whole profile soil water storage (mm), t is time (d), P is precipitation as rainfall (mm d^{-1}), ET is actual evapotranspiration (mm d^{-1}), q_o is overland flow (mm d^{-1}), q is vertical drainage out of the soil (mm d^{-1}) and M_{tot} is the area-weighted input from snowmelt (mm d^{-1}).

Actual evapotranspiration is calculated from reference evapotranspiration (ET_o) which can be either be imported or calculated from temperature using the Hargreaves equation (Hargreaves and Samani, 1985). It is assumed that ET is equal to ET_o when the soil moisture content exceeds a threshold value, θ_T, and that there is a linear decrease in ET as soil moisture content is depleted below θ_T down to zero at the permanent wilting point (θ_R). In the work described in this chapter ET_o was assumed to be equivalent to the reference ET rate which was imported from the Wasim-ET model (Hess et al., 2000) employing the FAO Penman-Monteith equation.

In the absence of a snow pack, Hortonian overland flow is described after Kirkby et al. (2008) using:

$$q_o = p(P - R_0) \tag{3.6}$$

where R_0 is a constant runoff threshold for precipitation (mm d^{-1}) and p is a dimensionless proportion of excess rainfall that flows over the land surface. Note that when $P < R_0$, q_o is zero.

Vertical drainage out of the soil is calculated using a simple gravity flow approximation under unit hydraulic gradient (Whelan and Gandolfi, 2002):

$$q = K(\theta) \tag{3.7}$$

where $K(\theta)$ is the unsaturated hydraulic conductivity (mm d^{-1}) at average profile volumetric water content (θ, cm^3 cm^{-3}). The daily value of q is partitioned between direct transfer to surface water (e.g., via shallow throughflow: q_{TF}) and groundwater recharge (q_{GW}) using an empirically-derived (calibrated) partition factor (f_g) ranging between 0 and 1:

$$q_{GW} = f_g . q \tag{3.8}$$

$$q_{TF} = (1 - f_g).q \tag{3.9}$$

$K(\theta)$ is calculated using the Mualem-van Genuchten equation (van Genuchten, 1980):

$$K(\theta) = K_{sat}\,.\,\theta_*^{0.5}.\left[1 - (1 - \theta_*^{\frac{1}{m}})^m\right]^2 \tag{3.10}$$

where K_{sat} is the saturated hydraulic conductivity (mm d^{-1}), m is an empirical shape factor parameter of the soil water retention curve and θ_* is the dimensionless water content (0 to 1):

$$\theta_* = \frac{\theta - \theta_r}{\emptyset - \theta_r} \tag{3.11}$$

where θ_r is the average profile residual water content (cm^3 cm^{-3}), assumed here to be the storage at the permanent wilting point—i.e., the water content at −1500 kPa tension). Note that in the Mualem-van Genuchten model θ_r is often lower than the wilting point but here the equations are employed with different physical significance for the parameters, which represent effective area responses rather than describing hydraulic properties at the Darcy scale (Pullan et al., 2016).

The shape parameter *m* is related to the van Genuchten parameter *n* via:

$$m = 1 - \frac{1}{n} \tag{3.12}$$

Snow accumulation and snow melt are assumed to occur in limited zones of the catchment delineated by altitude using the SRTM 30 m DEM. The daily air temperature in each zone is estimated from reference weather station data via:

$$T_i = T_a - \Omega\ (Z_i - Z_w) \tag{3.13}$$

where T_i is the temperature of zone i, Ω is the dry adiabatic lapse rate (0.0065 °C m^{-1}: (Miller, 1991), Z_i is the mean elevation of zone i (m) and Z_w is the elevation of the nearest reference station (m).

The treatment of the snowpack is based on a simple mass balance algorithm of water equivalent units similar to that employed in the HBV model (Bergström and Singh, 1995) which is augmented by snowfall and depleted by snowmelt. All precipitation in a zone is assumed to fall as snow when the daily average temperature (T_a) for the zone is below −0.5 °C (Fontaine et al., 2002). When the zonal temperature is above 1.5 °C all precipitation is assumed to be rainfall and between −0.5 and 1.5 °C the fraction of precipitation assumed to fall as snow is calculated by linear interpolation. Snow melt is assumed to be independent of the size of the snow store (except when the snow pack is exhausted) and is calculated from the difference between mean air temperate and 0 °C multiplied by a degree-day factor (Kustas et al., 1994). Although simplistic, this approach has been shown to produce reasonable results (Pipes and Quick, 1987; Cazorzi and Dalla Fontana, 1996). The daily rate of melting in each zone (M_i) is given by:

$$M_i = a\,[T_a - T_{melt}] + \beta\, R_n \tag{3.14}$$

where a is degree-day factor ranging between 2 and 2.5 (mm °$C^{-1}d^{-1}$), β is conversion factor for energy flux density to snowmelt depth (set to 0.26: Kustas et al., 1994), T_{melt} is a threshold temperature below which no melting occurs and R_n is the net radiation flux density in water equivalent units (mm d^{-1}). R_n is calculated from sunshine hours at the reference meteorological stations using the Angstrom formula and assuming a snow albedo of 0.7 (Allen et al., 1998). No adjustments for changes in cloud cover with altitude are made. Total snow melt M_{tot} is the area-weighted average of the daily snow melt in each zone which is added to the main soil store.

Baseflow is assumed to be proportional to water storage (S_G) in groundwater via a non-linear storage model (Moore, 2007):

$$q_b = k\, {S_G}^{\varepsilon} \tag{3.15}$$

where q_b is groundwater discharge (mm d^{-1}) and ε (>0) and k typically 0–1: (typically 0-1: Vogel and Kroll, 1996) are empirical coefficients. S_G is derived from mass balance as:

$$\frac{dS_G}{dt} = f_g . q - q_b \tag{3.16}$$

The predicted total daily river discharge (Q: mm d^{-1}) is calculated as

$$Q = q_o + q_b + q_{TF} \tag{3.17}$$

3.2.5 Calibration and validation of the LEMSAR model

The observed discharge data for the period 2010-2014 were divided into two subsets, one for calibration (2010-2011) and the another for validation (2012-2014). This is a "split record" validation. It is used in this study as it has been shown to be the most common method for a validation of rainfall runoff modelling (Arnold and Moriasi, 2012). Other validation methods include; (i) cross-validation (Dixon and Wilby, 2015; Biondi et al., 2012) in which inverting the group of data used for calibration and validation periods (Biondi et al., 2012) (ii) graphical techniques validation (i.e. stream flow duration curve: Biondi et al., 2012) in which allow a subjective and qualitative validation of the model.. Calibration was performed using the Self Organizing Migrating Algorithm (SOMA: Zelinka, 2004). The Nash-Sutcliffe Efficiency (NSE: Nash and Sutcliffe, 1970) was adopted as the objective function. Optimal parameter values are shown in Table 3.1 along with the range within which the parameters values were constrained in the SOMA procedure. The initial value for *S* was also optimised in the calibration routine but the initial value for S_G was arbitrarily set to 100 mm. Various configurations of the groundwater parameterization were attempted. Optimizing ε in the SOMA procedure (ε = 0.72) gave a NSE of 0.75 and Bias = 1.1% and a reasonable prediction of base flow. However, the slope of the 1:1 line in this calibration was closer to 1 when ε was arbitrarily set to 1 (i.e., when groundwater is represented by a linear reservoir), the NSE was unaffected although the Bias was higher (−12.6%). Furthermore, model performance in the validation period was superior when ε was fixed at 1 (Bias = 4%). Given the considerable uncertainty in the behaviour of the groundwater store in this catchment I, therefore, chose to

fix ε = 1 in all subsequent simulations. This issue is discussed further below. Four statistical measures were used to evaluate model performance in validation: the NSE; Pearson's Correlation Coefficient (r); the root-mean-square error (RMSE) and Percent bias (see Equations (3.18–3.21). The model was validated three times (using a different rainfall data set in each case) in order to evalute the value of satellite-derived rainfall as the driver for predicted runoff in this catchment and, potentially, in large semi-arid data-poor catchments.

$$NSE = 1 - \left[\frac{\sum_{i=1}^{m}(Q_i^{sim} - Q_i^{obs})^2}{\sum_{i=1}^{m}(Q_i^{obs} - \bar{Q}^{obs})^2}\right] \tag{3.18}$$

$$r = \frac{\sum_{i=1}^{n}(Q_i^{obs} - \bar{Q}^{obs})(Q_i^{sim} - \bar{Q}^{sim})}{\sqrt{\sum_{i=1}^{n}(Q_i^{obs} - \bar{Q}^{obs})^2}\sqrt{\sum_{i=1}^{n}(Q_i^{sim} - \bar{Q}^{sim})^2}} \tag{3.19}$$

$$RMSE = \sqrt{\frac{\sum_{i=1}^{n}(Q_i^{sim} - Q_i^{obs})^2}{N}} \tag{3.20}$$

$$Percent\ bias = \frac{\sum_{i=1}^{N}(Q_i^{sim} - Q_i^{obs})}{\sum_{i=1}^{N} Q_i^{obs}} * 100 \tag{3.21}$$

where Q_i^{obs} and Q_i^{sim} are the observed and simulated discharges, respectively, $\bar{Q}^{obs}$ is the average observed discharge, $\bar{Q}^{sim}$ is the average simulated discharge and N is the number of records.

Table 3. 1. Optimum parameter values generated by automatic calibration for LEMSAR in the Lesser Zab catchment (ε = 1).

Parameter	Description	Lower	Upper	Optimised Value
$\boldsymbol{n}$	Shape parameter in van Genuchten equation (-)	1	2.5	2.18
$\emptyset$	Saturated water content ($cm^3\ cm^{-3}$)	0.4	0.6	0.58
$\boldsymbol{\theta_R}$	Permanent wilting point ($cm^3\ cm^{-3}$)	0.03	0.22	0.10
$\boldsymbol{z}$	Soil depth (cm)	50	200	146
$\boldsymbol{\theta_T}$	Threshold water content when $ET < ET_o$ ($cm^3\ cm^{-3}$)	0.2	0.4	0.35
$\boldsymbol{\theta_r}$	Residual soil water content ($cm^3\ cm^{-3}$)	0.01	0.3	0.007
$\boldsymbol{K_{sat}}$	Soil saturated hydraulic conductivity ($mm\ d^{-1}$)	75	450	262
$\boldsymbol{R_0}$	Rainfall threshold for overland flow ($mm\ d^{-1}$)	5	50	42.9
$\boldsymbol{p}$	Fraction of excess rainfall which runs off (-)	0.05	0.1	0.06
$\boldsymbol{k}$	Empirical coefficient for groundwater flow (d^{-1})	0.1	0.99	0.6
$\boldsymbol{f_g}$	Empirical partition factor for groundwater recharge (-)	1	0.99	0.32
	Fixed parameters for snow pack sub-model			
Ω	Dry adiabatic lapse rate (0.0065 °C m^{-1})			
a	Degree-day factor (2.3 mm $°C^{-1}d^{-1}$)			
β	Conversion factor for energy flux density to snowmelt depth (0.26)			
T_{melt}	A threshold temperature below which no melting occurs (0 °C)			

3.2.6 Equifinality and sensitivity analysis in LEMSAR

Uncertainty analysis was conducted using the Generalised Likelihood Uncertinty Estimation (GLUE) methodology (Beven and Freer, 2001). R code for GLUE was obtained from a link in (Beven, 2010) and incorporated into the LEMSAR model. Briefly, a Monte Carlo Simulation (MCS) is performed in which model parameters are selected randomly from uniform distributions with pre-defined ranges in a large number of iterations. Model performance is estimated using a likelihood function (0–1) which is zero for parameter combinations which do not reflect system behaviour and unity for "optimal" parameter combinations. GLUE can

help to identify equifinality—the existence of different combinations of parameters which generate similarly "good" representations of system behaviour (Li et al., 2009). This often occurs when models are poorly constrained (e.g., they are evaluated solely on the basis of one predictor, such as stream discharge, with no check on model performance with respect to other predicted state variables, such as soil water content or groundwater storage). Here, 10,000 model iterations were performed and the NSE (Equation (3.18)) for Q (Equation (3.17)) was used as the likelihood function. An acceptability threshold of 0.5 was selected for NSE based on the model performance classification executed by Moriasi et al. (2007), (i.e., simulations were considered to be acceptable for NSE > 0.5).

3.3 Results

3.3.1 Comparison between gauged rainfall and TRMM data

Weighted-mean (Thiessen polygon) daily ground-observed rainfall is plotted against both uncorrected and corrected TMPA-3B42/3B42RT data for Periods 1 and 2 in Figure 3.2. Correlation coefficients (r) were highly significant in both cases ($p < 0.0001$) but there is a lot of scatter around the 1:1 line and, in general, the satellite-derived data tended to under-estimate the gauged data (negative bias). Figure 3.2 shows that for Period 1 the correction of the TMPA-3B42 and TMPA-3B42RT data resulted in a slight change to r (from 0.674 to 0.673 and from 0.545 to 0.546, respectively) but also a decrease in the magnitude of the bias (from −5.5% to −0.8% and −16.3% to −1.3%, respectively). For Period 2 (Figure 3.2c,d) the application of the correction factors derived with the Period 1 data also resulted in little change to r but reduced the bias from −10% to −0.7% for TMPA-3B42 and from −10.7% to −1.6% for TMPA-3B42RT.

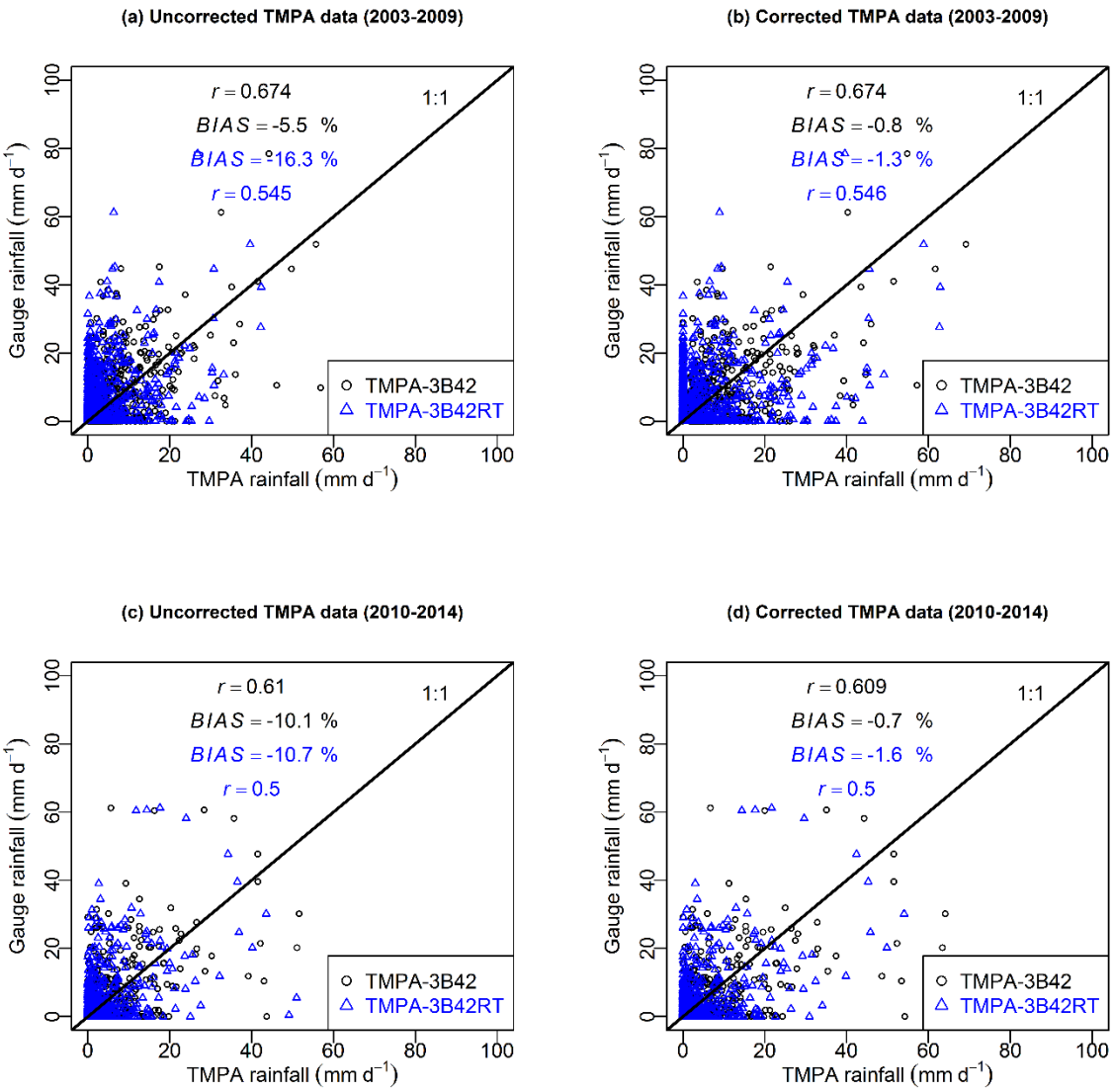

Figure 3. 2. Scatterplots of daily catchment-average gauged rainfall (Sulaimani, Dukan, Penjween and Chwarta stations) versus TRMM daily rainfall: (a,b) represent uncorrected and corrected TMPA-3B42/3B42RT data for Period 1 and (c,d) represent uncorrected and corrected TMPA-3B42/3B42RT data for Period 2.

To further investigate the correspondence between TMPA-3B42 / 3B42RT estimates and the rain gauge data, the following verification metrics were also employed, based on a contingency table (Table 3.2): (i) the False Alarm Ratio (FAR) i.e. the ratio of the number of times rainfall was forecast by the satellite data product but not observed in the gauged rainfall data to the

total number of times rain was forecasted successfully (Equation 3.22); (ii) the Probability of Detection (POD; see Equation 3.23) i.e. the ratio of the number of times rain days were successfully forecasted to the total number of rain days (Doswell et al., 1990; Tartaglione, 2010)) and (iii) the Heidke Skill Score (HSS; see Equation 3.24) i.e. a measure of the frequency of correct matches between satellite forecasts and gauged observations compared to the number of correct matches which would be expected by chance (Panofsky et al., 1958; Doswell et al., 1990). These verification statistics for Periods 1 and 2 are displayed in Figure 3.3. The FAR values for both the uncorrected and corrected TMPA-3B42RT were higher than those calculated for TMPA-3B42 for both Periods 1 and 2. The POD values were lower for the TMPA-3B42RT data than for the TMPA-3B42 for both periods. Overall, the 3B42 data performed better than the 3B42RT data. However, these statistics show that both TMPA products have serious problems in detecting the occurrence or not of rainfall. Values of HSS were about 0.4 for Period 1 and 0.3 for Period 2 for most rainfall intensities. Note that positive values of HSS indicate that the TMPA data products were better than chance. This is the case for the most common rainfall intensities (i.e. between 5 and 45 mm d^{-1}).

Table 3. 2. Contingency table comparing gauge area average and TMPA rainfall estimates.

TMPA-event forecast	**Gauge-event observed**		
	Yes	**No**	**Marginal total**
Yes	A	b	a + b
No	C	d	c + d
Marginal total	a + c	b + d	a + b + c +d

$$FAR = \frac{b}{a+b} \tag{3.22}$$

$$POD = \frac{a}{a+c} \tag{3.23}$$

$$HSS = \frac{2(ad - bc)}{(a + c)(c + d) + (a + b)(b + d)} \tag{3.24}$$

Where: a, b, c, d represent, respectively, hits, false alarms, missed and correct negatives

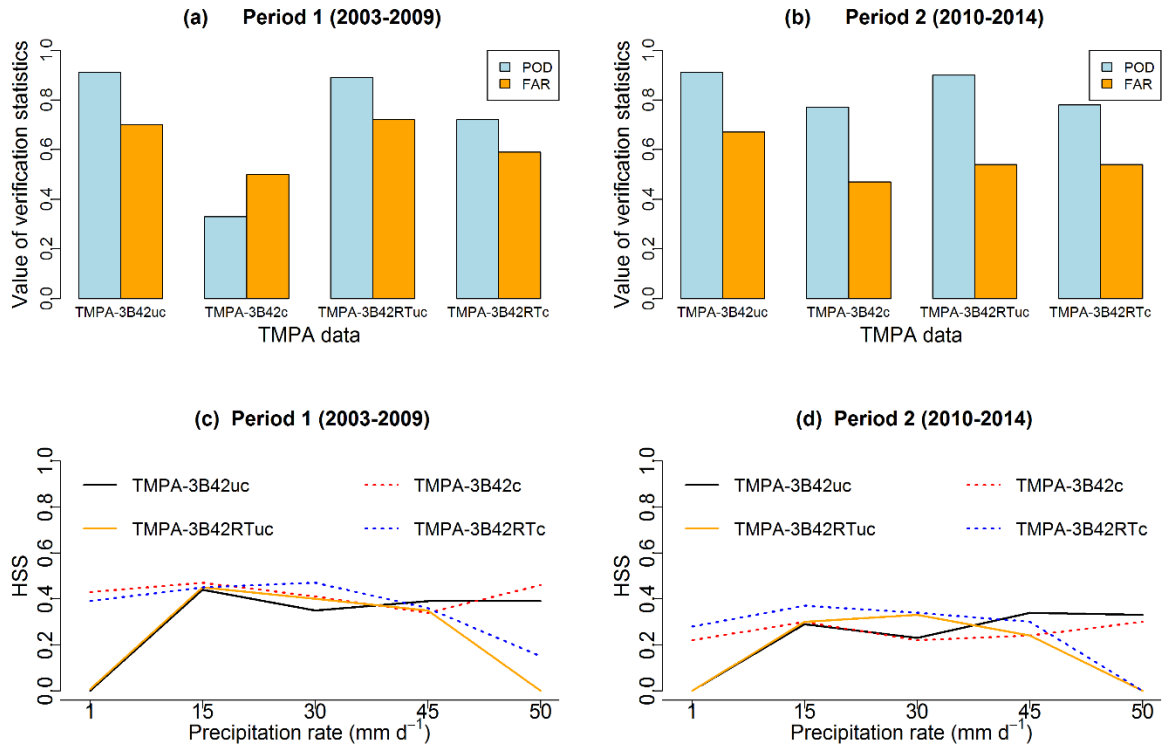

Figure 3. 3. Verification statistics between TMPA-3B42 / 3B42RT and observed (gauge) rainfall. Panels (a) and (b) show FAR and POD for Periods 1 and 2, respectively. Panels (c) and (d) show the HSS between TMPA-3B42 and TMPA-3B42RT and observed (gauge) rainfall for different rainfall intensities during Periods 1 and 2, respectively.

3.3.2 Comparing observed and simulated discharge

Observed and simulated discharge for the Lesser Zab River in different periods and driven by different rainfall data sets are shown in Figure 3.4. All hydrological model runs used weighted average values of daily ET_o calculated from ground-based meteorological observations. In all cases, the black line shows the observed discharge, the orange line represents predicted snowmelt and the red line is groundwater flow. In general, the seasonal agreement between

observed and simulated discharge is reasonable using both gauge-derived and corrected TMPA-3B42/3B42RT rainfall data. However, some hydrograph peaks appear to be noticeably under-predicted by the model, particularly when driven by the uncorrected TMPA-3B42/3B42RT rainfall data. In part, this reflects a general tendency for the TMPA data to under-estimate the gauge-derived rainfall data. Simulated flows are plotted against measured data in Figure 3.5, along with the best-fit linear regression and the 1:1 line. Most of the points are scattered around the 1:1 line when the model is driven by the area-weighted rain gauge data. However, there is considerable deviation at high flows (e.g., the model underestimates some measured discharge peaks >500 m^3s^{-1}) and for hydrograph recessions (in which predicted flows tend to reduce slightly faster than those observed). This results in a slope for the best-fit regression which is less than unity in the validation period. This systematic deviation was more pronounced when the model was driven by the uncorrected TMPA-3B42 and TMPA-3BRT rainfall data (Figure 3.5c and e). However, the TMPA correction procedure noticeably reduced (but did not eliminate) the systematic tendency for the model to under-estimate measured flow and resulted in tolerable discharge predictions overall. It is important to note that the factors (μ_f and σ_f) used for the correction of the TMPA data were derived from Period 1 (2003–2009) which does not overlap with either the calibration or the validation periods used for evaluating the hydrological model. The TMPA corrections are, therefore, independent of the rain gauge data used to drive the hydrological model over 2010–2014.

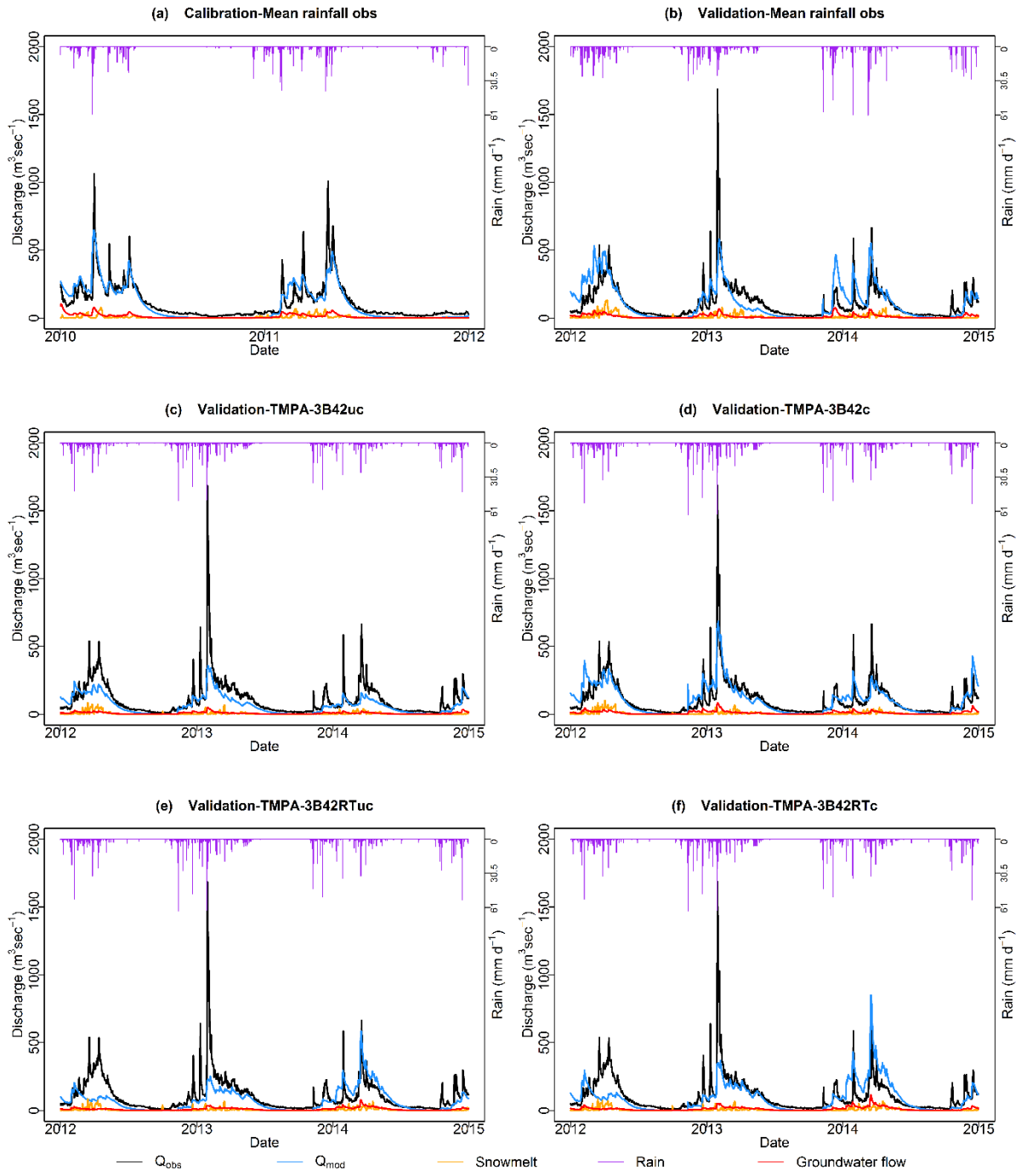

Figure 3. 4. Observed and simulated hydrographs for the Lesser Zab River above the Dukan reservoir. Data for the calibration period (2010-2011) are shown in (a). In all cases, hydrological model parameters were calibrated using the gauged rainfall data. Data for the validation period (2012-2014) are shown in (b), (c), (d), (e) and (f). The top right panel (b) shows validation when driven by the weighted-average gauge-derived rainfall. The middle panels (c and d) show validation driven by the uncorrected and corrected TMPA-3B42 rainfall data, respectively. The bottom panels (e and f) show validation driven by the uncorrected and corrected TMPA-3B42RT rainfall data, respectively. In all cases, the orange line shows modelled snowmelt and the red line is modelled groundwater flow.

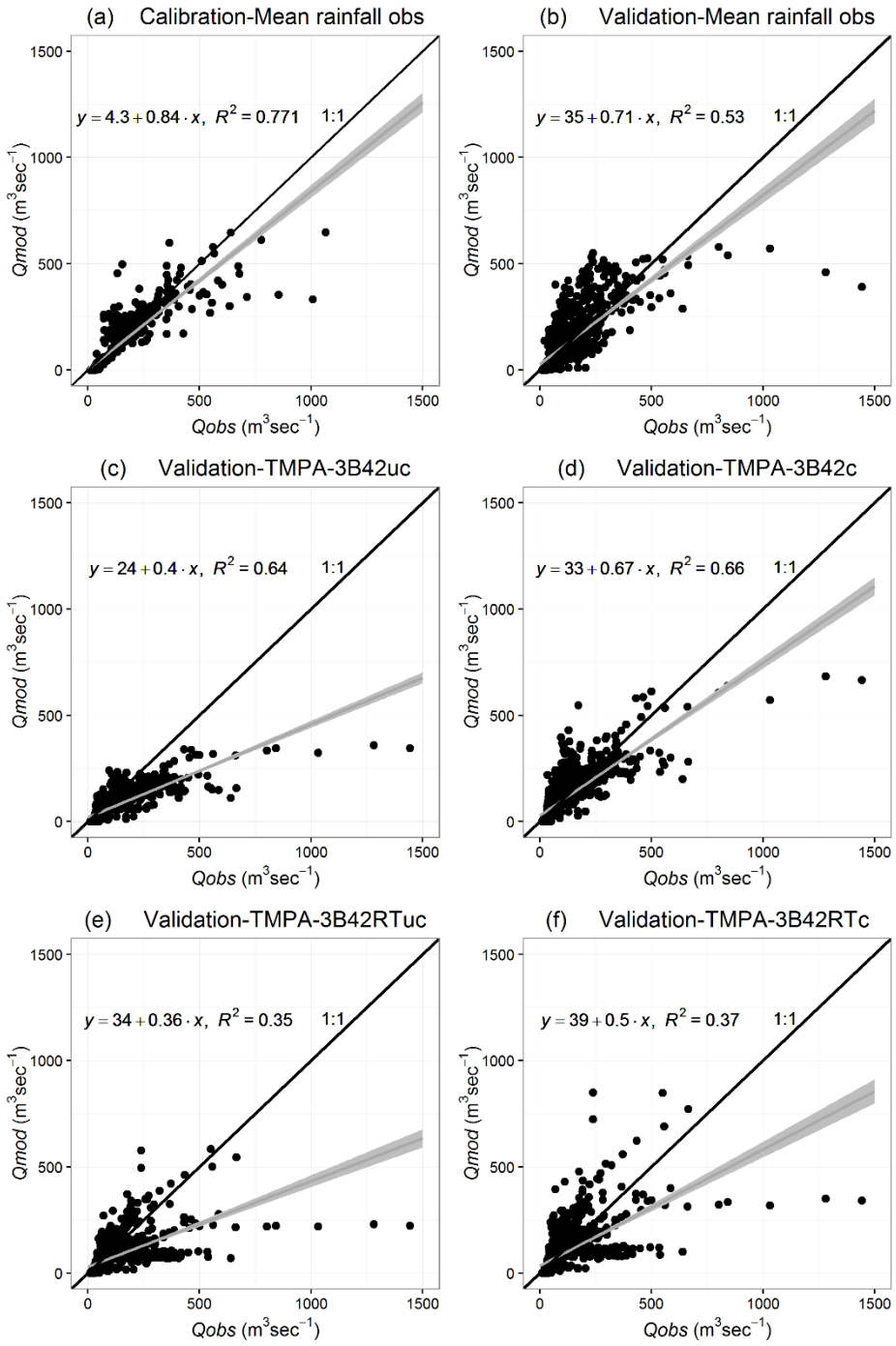

Figure 3. 5. Scatterplots of observed versus simulated discharge for (a) the calibration period (2010-2011) and (b) the validation period (2012-2014) when the model was driven by the weighted-average gauge-derived rainfall. The middle panels (c and d) show model performance for the validation period when driven by the uncorrected (c) and corrected (d) TMPA-3B42 rainfall data. The bottom panels (e and f) show validation simulations driven by the uncorrected (e) and the corrected (f) TMPA-3B42RT rainfall data, respectively. The solid line indicates the 1:1 relationship. The grey line shows the best fit regression with 95% confidence intervals.

Goodness-of-fit statistics are presented in Table 3.3. These statistics reinforce the message derived from the graphs that the model tends to under-estimate the measured river discharge in both the calibration and validation periods regardless of the rainfall data used. The bias was lowest when the measured rainfall data were used to drive the model and highest when the uncorrected TMPA-3B42/3B42RT rainfall data were used. However, the best NSE value for the validation period was obtained using the corrected TMPA-3B42 data. As expected, model performance was poorest when it was driven by the uncorrected TMPA-3B42/3B42RT data (lowest NSE, highest BIAS and highest RMSE). Overall, using the TMPA-3B42 product resulted in better model performance compared to usingTMPA-3B42RT product.

Table 3. 3. Summary of goodness of fit criteria for simulated discharge in the Lesser Zab catchment using different rainfall data sets to drive the model. * Significant at p≤0.01.

Statistical measures	**Calibration**	**Validation**				
	Mean rainfall obs	**Mean rainfall obs**	**TMPA-3B42uc**	**TMPA-3B42c**	**TMPA-3B42RTuc**	**TMPA-3B42RTc**
BIAS (%)	-12.6	4	-37.6	-2.6	-32	-14.2
RMSE ($m^3 s^{-1}$)	65	96	97	**77**	112	109
NSE	0.75	0.48	0.45	**0.66**	0.28	0.31
r	0.87*	0.72*	0.80*	**0.81***	0.59*	0.61*

Statistical comparisons between simulated and measured flows are also plotted on Taylor Diagrams in Figure 3.6. This diagram summarises the overall performance of LEMSAR during the calibration and validation periods when driven by different precipitation data. The position of each point appearing on the plot quantifies how closely simulated river discharge matches observations. In the case of the calibration period, when the model is driven by the area-weighted rain gauge data, the blue point lies closer to the dashed arc (line of standard deviation). Its correlation coefficient is about 0.89, the RMS error is about 65$m^3 s^{-1}$ and the standard deviation is about 148 $m^3 s^{-1}$. The relative merits of various validations of the model can be inferred from Figure 3.7. The black point represents validation when the model was driven by the area-weighted rain gauge data. This lies on the black arc line which means that the standard deviation of the simulated discharge is similar to that of the observed data (i.e. the

mean amplitude of discharge variations is similar). The green point represents simulated river discharge in the validation period when the model was driven by the corrected TMPA-3B42. This model run generally produced the best agreement with the observations and has the highest correlation (r = 0.81) and lowest RMSE (77 m^3 s^{-1}).

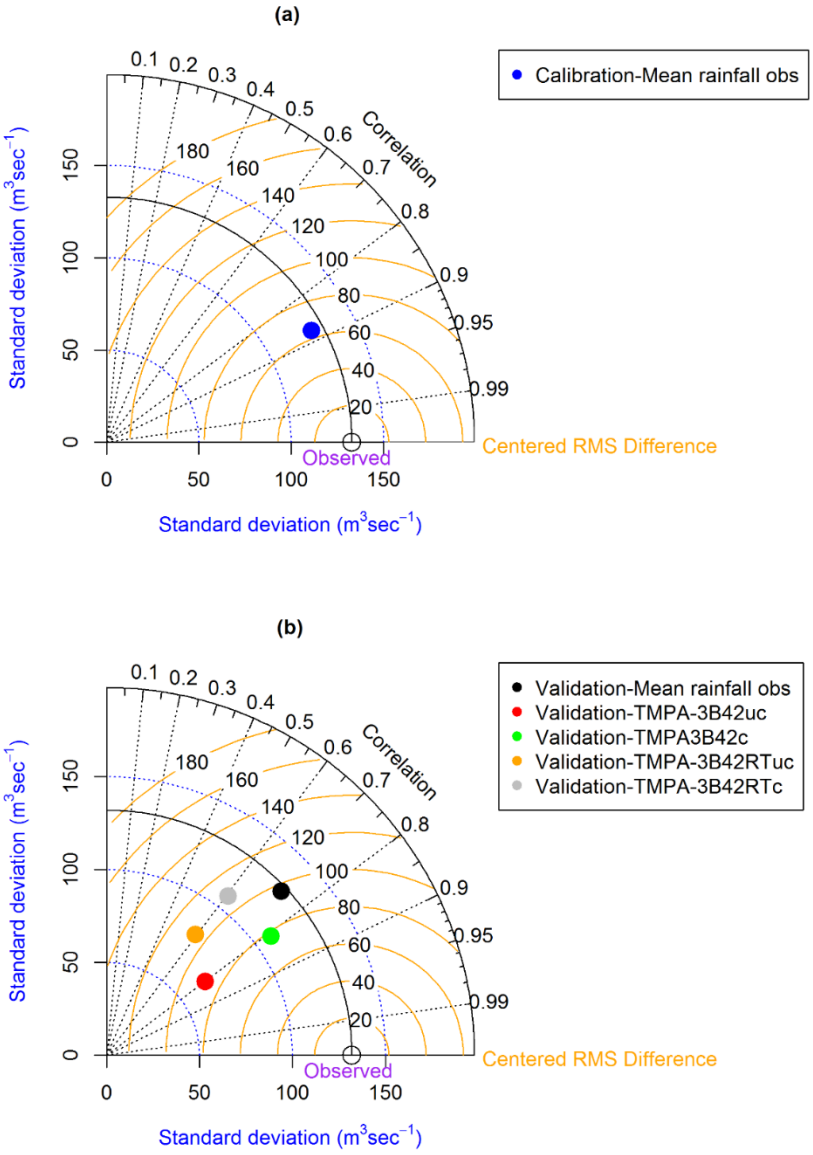

Figure 3. 6. Taylor diagram summarising the statistical performance of simulated versus observed river discharge for (a) the calibration period (2010-2011) and (b) the validation period (2012-2014) when the model was driven by the weighted-average gauge-derived rainfall, uncorrected and corrected TMPA-3B42 / 3B42RT rainfall data. The orange contours indicate the centred Root Mean Square (RMS) values which is proportional to the distance from the

point on the X-axis identified as “observed”. The blue dashed line shows standard deviations which are proportional to the radial distance from the origin.

3.3.3 Contribution of snowmelt and groundwater flow to simulated river discharge

The daily predicted contributions of snowmelt and groundwater in the Lesser Zab catchment are shown in (Figure 3.7). Although predicted daily snow melt contributions to total flow tended to be low (annual percentage contribution 4%–13.5%), predicted melt-derived flows can be substantial in spring and may contribute to occasional flood events (Figure 3.5). Monthly snowmelt contributions were highest when the model was driven by gauged rainfall data, principally due to a higher winter precipitation rate observed compared to both the uncorrected and corrected TMPA products, and hence a deeper simulated snowpack accumulation. The snowmelt contributions were also higher when LEMSAR was driven by both uncorrected and corrected TMPA-3B42RT data than it was driven by the TMPA-3B42 data.

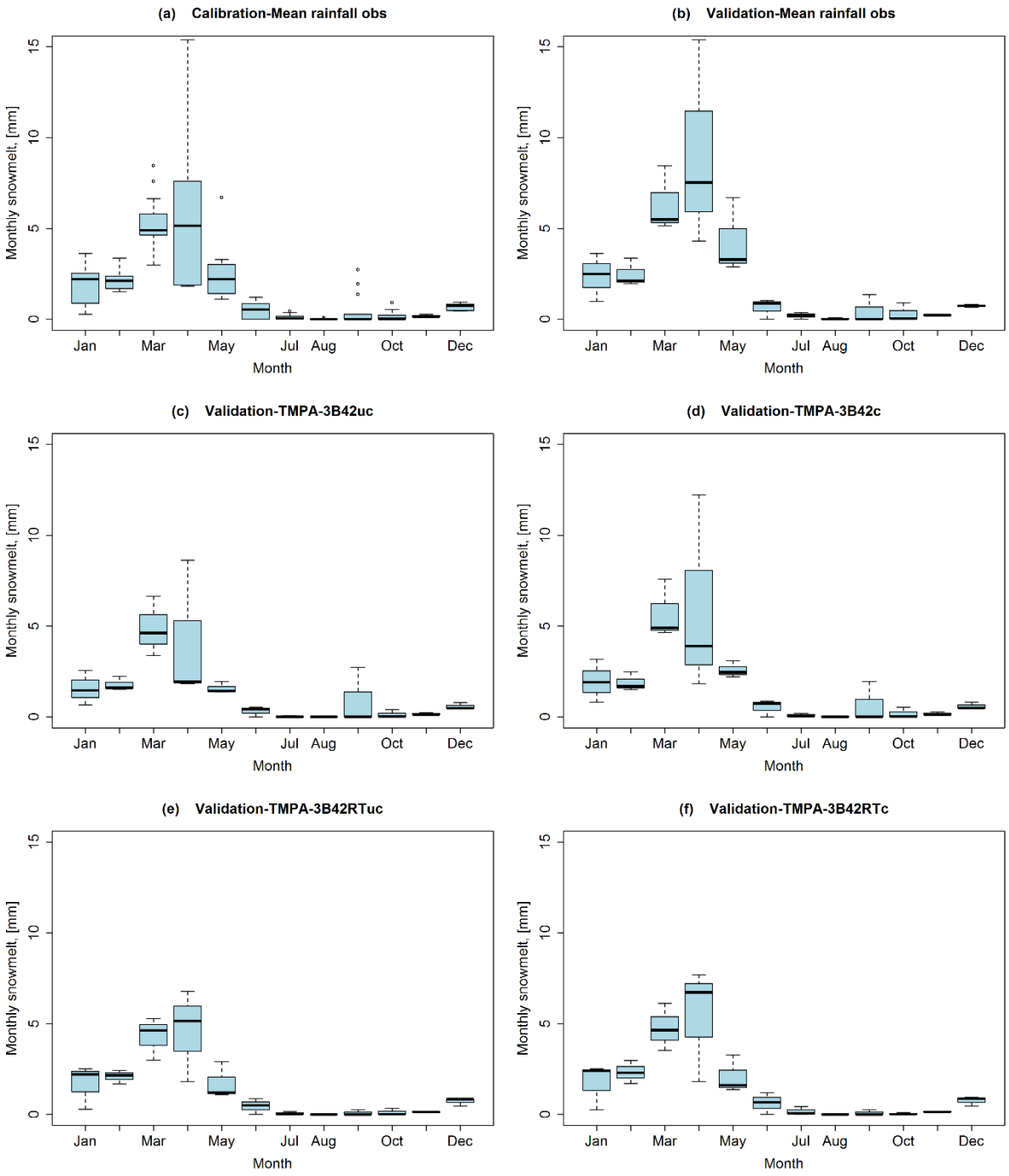

Figure 3. 7. Boxplots of predicted monthly snowmelt contributions to river discharge in the Lesser Zab catchment. The calibration period (2010–2011) is shown in the top left panel (a). Panels (b–f) show contributions during the validation period (2012–2014) using rain gauge data and uncorrected and corrected TMPA-3B42/3B42RT data. The horizontal line within each box represents the median, the box boundaries represent upper and lower quartiles and the dashed whiskers show the maximum and minimum values.

The predicted contribution of groundwater flow to river discharge is low and significantly underestimates baseflow. This is, in part, due to the simplistic representation of the complex and highly uncertain hydrogeological system underlying this catchment but it is also a result of the model parameterisation (including our arbitrary decision to set $\varepsilon = 1$). Overall model performance tended to be better with a high value of k (implying very steep groundwater recession and a perenially low groundwater storage). Many of the underlying strata in the catchment are karstic (i.e., they contain a highly conductive network of cracks and fissures) which respond rapidly during storm events but which have baseflow behaviours which are difficult to model (Doummar et al., 2012). A high value of k is consistent with the rapid behaviour of karstic systems, although I recognise that it penalises model performance at low flows in order to get a better simulation of the hydrograph during storm events.

3.3.4 Flow Duration Curves

Flow duration curves (FDC) for both observed and simulated river discharge are shown in Figure 3.8. The match between the curves is generally good, although there is some under-prediction of discharge at high exceedance percentiles (i.e., low flows tend to be under predicted) and some over-prediction of flows in the 5–25 exceedance percentile range. Again, the under-prediction of low flows is due in part to the simple nature of the baseflow model adopted here and its parameterisation. The source of rainfall data used to drive the model had a significant effect on the shape of the FDC. Flows were under predicted over most of the range when the model was driven by the uncorrected TMPA-3B42 and 3B42RT data but this noticeably improved for a significant percentile range when the TMPA-3B42/3B42RT data were corrected. Overall, reproduction of the FDC was slightly better when the model was driven by the corrected TMPA-3B42RT data than when it was driven by the TMPA-3B42 data.

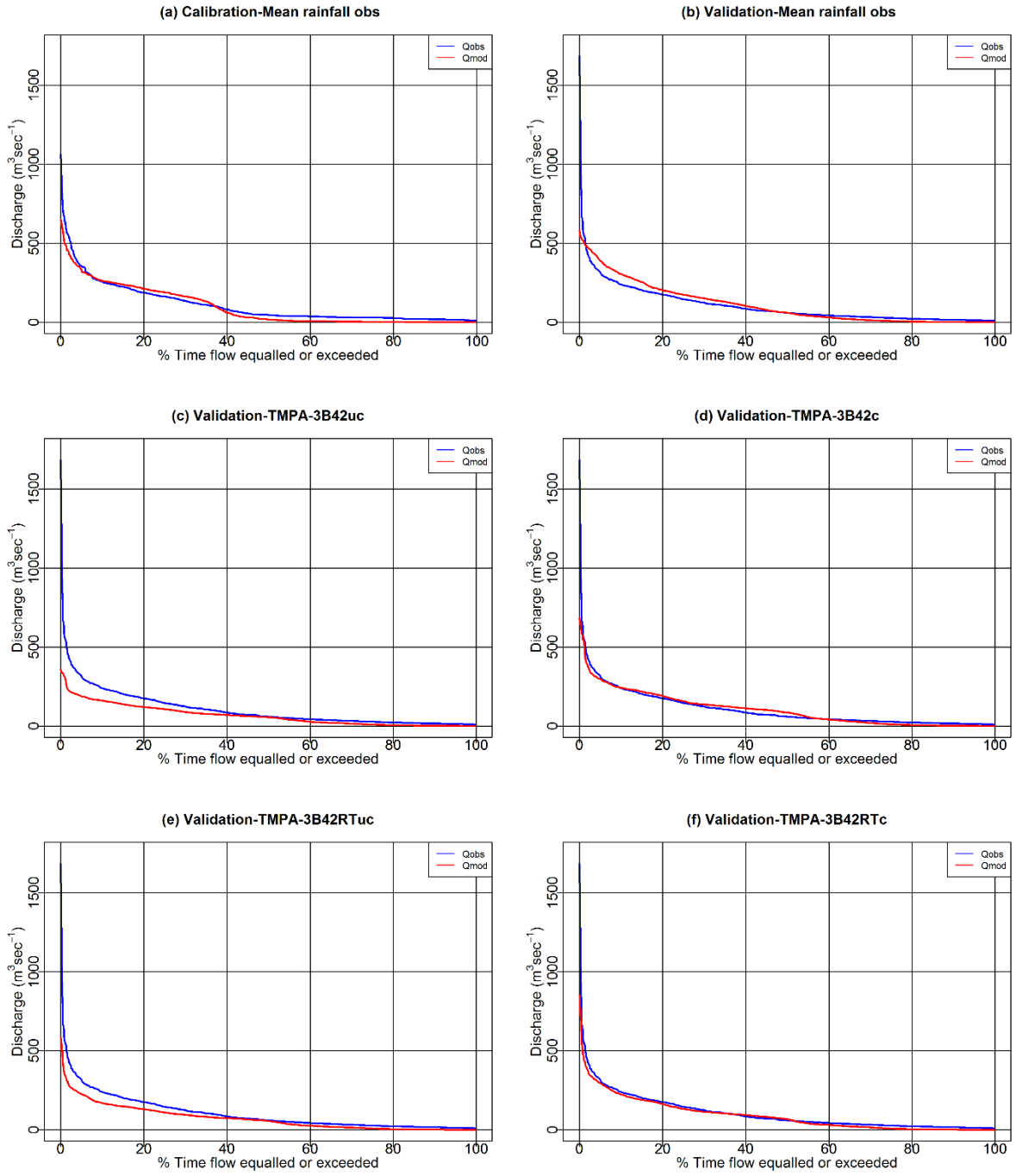

Figure 3. 8. Observed and simulated FDCs for the Lesser Zab catchment. Top panels: (a) Calibration period (2010-2011); (b) Validation period (2012–2014) when the model was driven by the weighted-average gauge-derived rainfall. Middle panels: (c) Validation period when driven by the uncorrected TMPA-3B42 data; (d) Validation period when driven by the corrected TMPA-3B42 data. Bottom panels: (e) Validation period when driven by the uncorrected TMPA-3B42 RT data; (f) Validation period when driven by the corrected TMPA-3B42RT data.

3.3.5 Equifinality

Figure 3.9 shows scatter plots of NSE against MCS-generated parameter values for the calibration period. The blue point indicates the NSE for the calibrated (reference) parameter set (NSE = 0.75). Only parameter combinations yielding NSE > 0.5, are displayed. The graphs clearly demonstrate the frequently reported phenomenon of equifinality (Beven and Binley, 1992; Beven and Freer, 2001; Beven and Alcock, 2012; Brazier et al., 2000; Franks et al., 1997; Beven, 1993) in which reasonable model performance can be achieved using several different combinations of model parameters. Here it occurs, in part, due to the fact that the model is poorly constrained (i.e., measured data are available for only one predicted output variable—stream discharge, with other predicted internal state variables, such as soil water content and groundwater storage, not measured and, hence, not validated). Hence, the "optimal" set of model parameters yields good predictions of the data available but may actually produce poor simulations for unmeasured phenomena such as snow melt and baseflow contributions (i.e., the model may give the "right results for the wrong reasons"). Although it is possible to apply qualitative constraints on parameter combinations to ensure that unmeasured state variable predictions are "sensible" (Kannan et al., 2007), the lack of measured data for these variables mean that both aleatory and epistemic uncertainty are always high. Equifinality also makes evaluating the relative contributions of errors in the individual terms of the water balance equations to the overall model error difficult if not impossible. This is in part, because many of these terms are linked e.g., via a dependence on soil moisture or contain parameters which are calibrated on discharge at the catchment outlet, rather than being determined independently. The results from a local sensitivity analysis are presented in the Figure 3.11 and suggest the following rank order for model sensitivity (high to low $\emptyset > n > z > K_{sat} > f_g > \theta_T, \theta_R, \theta_r, p, R_o, k$. Given the relative insensitivity of the model performance to θ_T, θ_R, θ_r, p, R_o, and k these parameters were fixed to their optimal values and the MCS re-run to generate GLUE uncertainty boundaries on predicted discharge. These are shown in Figure 3.10 for the calibration period (2010–2011).

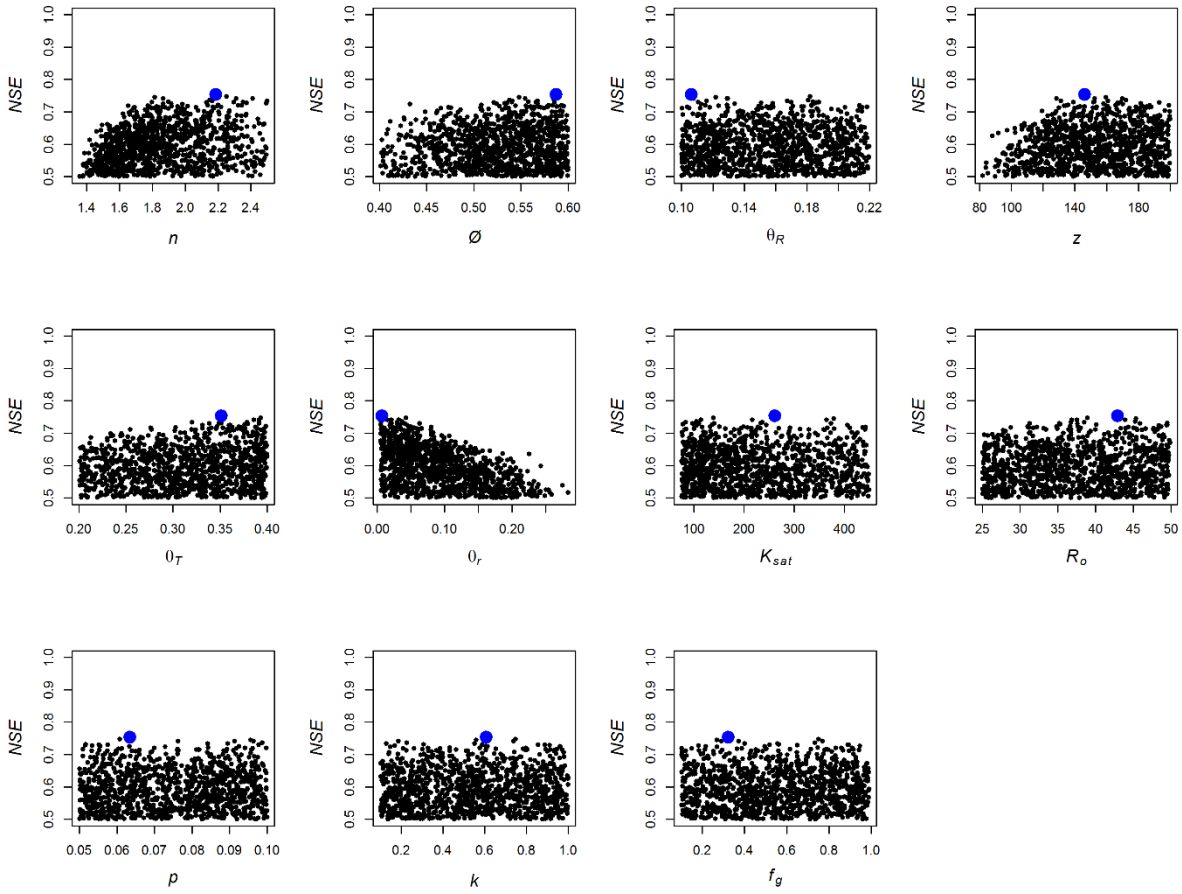

Figure 3. 9. Scatterplots for eleven model parameters versus *NSE* for random parameter combinations yielding *NSE* > 0.5. Blue point shows the highest *NSE* value for the optimised parameter set.

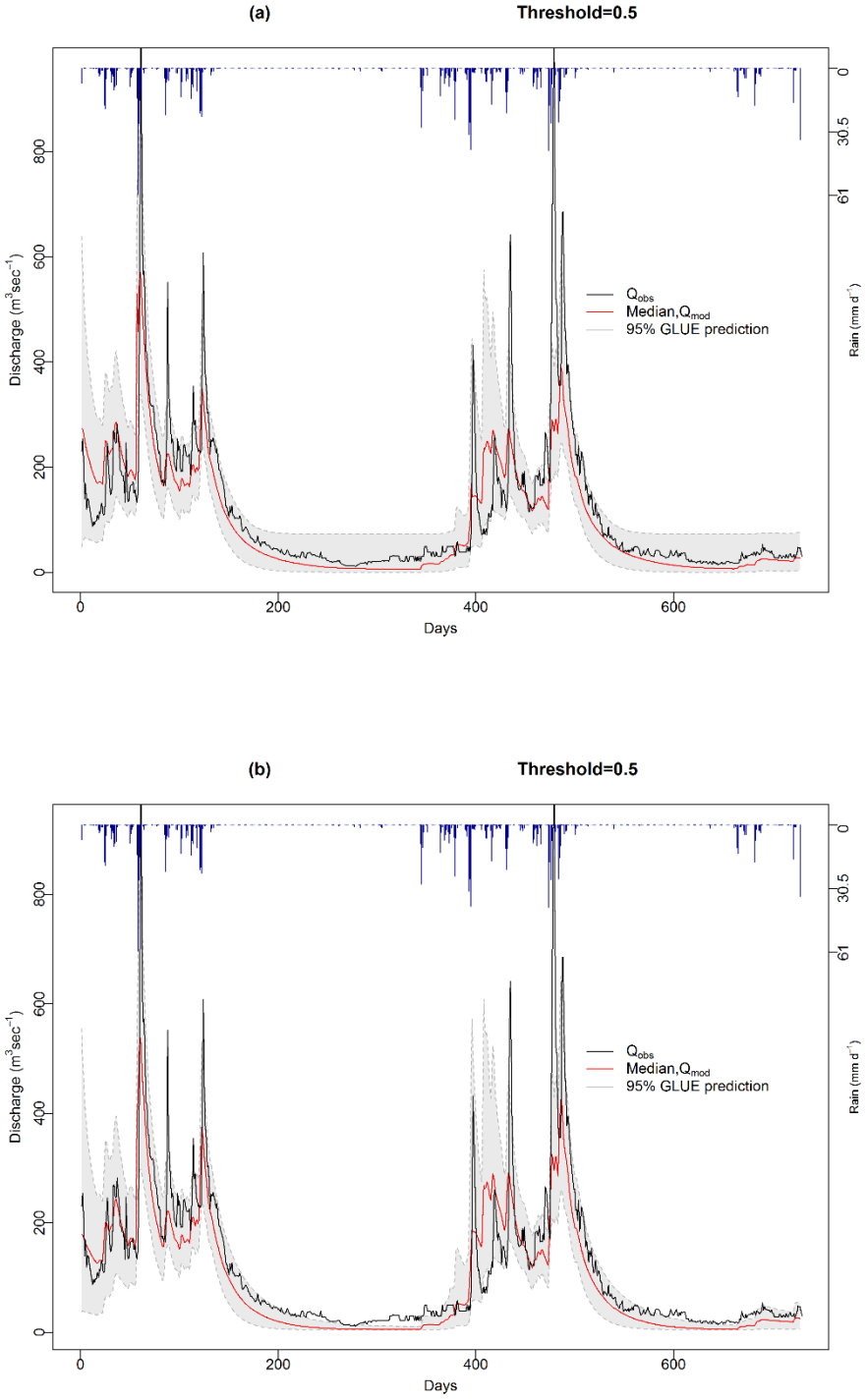

Figure 3. 10. Prediction uncertainty bounds for river discharge in the Lesser Zab River over the calibration period 2010-2011. The black line is the observed discharge; the red line is the median predicted flow for all combinations of parameters yielding *NSE* > 0.5 and the grey area shows the 95% GLUE prediction quantile. (a) All parameters sampled in the MCS; (b) Parameters to which the model was least sensitive (θT, θR, θr, p, Ro and k) fixed at their optima.

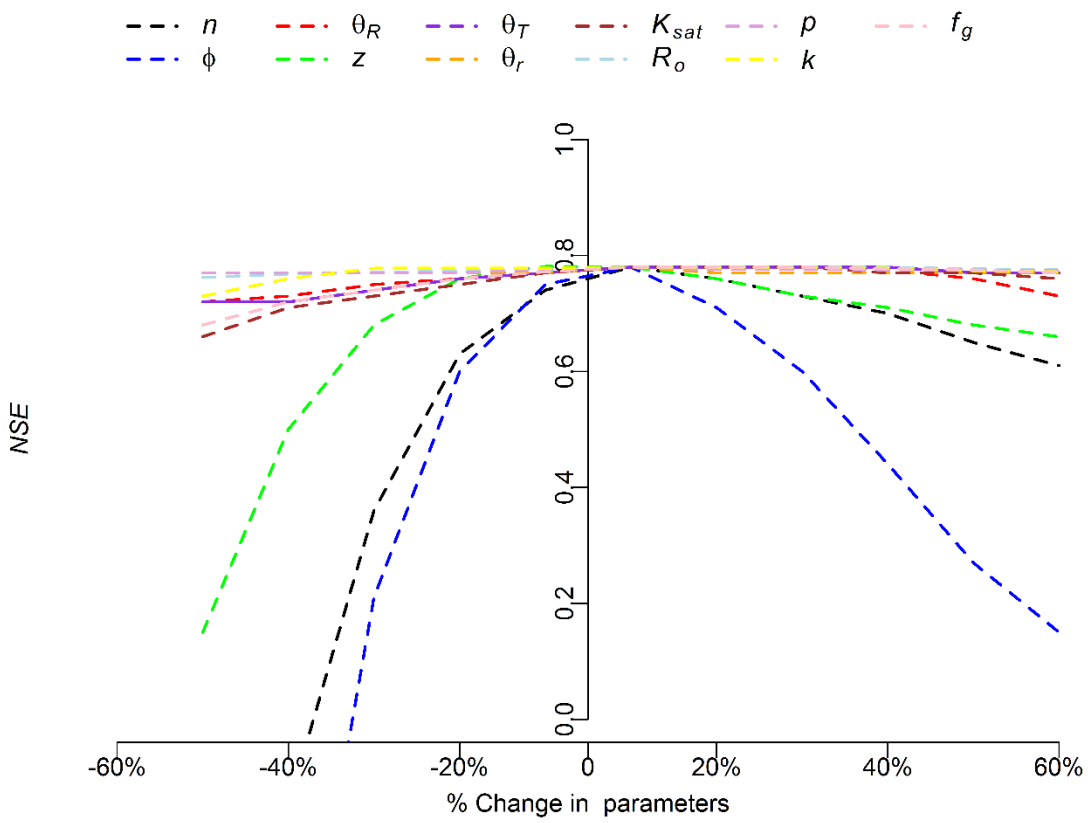

Figure 3. 11. Sensitivity analysis of the LEMSAR model for all parameters using a local sensitivity method for the period 2010-2011.

3.4. Discussion

In this chapterr, a simple rainfall-runoff model which was presented and applied, for the first time, to the Lesser Zab catchment in Iraq using weighted average gauged daily rainfall data and rainfall data derived from remote sensing. The principal aim was to assess the potential value of remotely-sensed rainfall data as a driver for rainfall-runoff modelling in data-scarce semi-arid catchments. Although data availability for the Lesser Zab catchment was actually sufficient for hydrological modelling, this is atypical of most semi-arid regions in the world which often suffer from data scarcity issues related to inadequate resource allocation for instrumentation and monitoring (Wagener et al., 2004). Moreover, even when data exist, they may not be made available for scientific studies without appropriate connections to the data-holding authorities. This study, therefore, provides an excellent opportunity to evaluate model performance and the utility of remotely sensed data under various assumptions of data paucity.

Two daily satellite-derived data products (TMPA-3B42 and 3B42RT) were corrected using mean bias statistics (mean and standard deviation) assuming uniform bias across the whole range of rainfall intensities. Five river discharge simulations were performed, driven by different daily rainfall data sets (gauged data, uncorrected TMPA3B42 data, uncorrected TMPA-3B42RT data, corrected TMPA-3B42 and corrected TMPA-3B42RT data). Both the uncorrected TMPA data products tended to underestimate gauge-derived rainfall. The performance of the TMPA-3B42RT product was poorer than that of the TMPA-3B42 product during rainy days. The 3B42RT also had a higher tendency to predict rainfall on days in which there was no gauge-observed rainfall (hence the higher FAR). In addition, the TMPA-3B42 data generated higher POD values than the 3B42RT data, confirming better performance for predicting rainy days. Generally, the HSS of both products was best for rainfall rates between 5 and 45 mm d^{-1}. Failure to accurately predict events with higher intensities could be related to the low spatial and temporal resolution of the TMPA data products (the time interval between TRMM orbits is too long to capture all rainfall events (Muhammad et al., 2012) and the random, short duration and localized nature of high intensity convective storm events in arid and semi-arid areas which contribute to greater spatial variability for precipitation in these areas compared with humid regions (Pilgrim et al., 1988). This is also an issue for precipitation capture by rain gauges, especially if they are sparsely located (Prabhakara et al., 2002). That said, overall trends are generally captured well.

Aside from the localised nature of convective rainfall, there are many possible explanations for deviations of the TMPA rainfall from the gauge-recorded data, including the influence of topography (e.g., slope, aspect and local relief: Gao and Liu, 2013). In addition, known (and unknown) instrument errors (e.g., the TRMM radar cannot detect rainfall at less than about ~18 dBZ or 0.4 mm/h:(National Space Development Agency of Japan (NASDA), 1999)) will also contribute to deviations. I used area-averaged (Thiessen polygon weighted averaging) precipitation measurements derived from ground observations from four stations over a limited period to correct the TMPA data. These data are associated with considerable uncertainty due to instrument and sampling errors arising from the relatively low spatial density of gauges. In particular, these stations are predominantly located at low elevations (550 to 1300 m ASL) and, hence may under-estimate total precipitation at altitude and total catchment precipitation in general. However, data to verify the extent to which this may have been a major issue or not are currently not available. The uncorrected and corrected TMPA-3B42 data both

underestimated gauged data by −10% and −0.7% respectively. Similarly, the TMPA-3B42RT underestimated gauged data by −10.7% and −1.3 respectively. This finding is in rough agreement with (WMO, 2006) which reported that satellite-derived rainfall could systematically underestimate ground observed rainfall by 30% or more. Collischonn et al. (2008) also showed that relative differences between observed and satellite-derived rainfall data can range from −39% to +25%.

Given the simplicity of the model assumptions and the large and complex nature of the catchment, the performance of the LEMSAR model in the Lesser Zab catchment was surprisingly good. Although model performance was weak in places (e.g., the poor prediction of baseflow and delay in some peak flows Figure 3.10), performance overall was equivalent to or better than that obtained using a similar model in smaller UK catchments (Pullan et al., 2016). The contribution of snow melt and baseflow to river discharge is unknown and the model is poorly constrained with respect to these processes.This contributed to significant equifinality, illustrated by a wide range of "acceptable" parameter combinations. Although a significant part of the catchment (20%) is above 1500 m altitude and, therefore, likely to receive some winter precipitation as snow, the relative contribution of calculated snowmelt to simulated river discharge was generally low, even in the spring melt season (although the absolute volumes were occasionally significant and the snow melt contribution may have been masked by coincidentally high rainfall in this season). However, it would be useful to confirm this prediction by independent studies in high altitude sub-catchments.

All hydrological model runs used weighted average values of daily ET_o calculated from ground-based meteorological observations. No adjustment was made in the model for changes in ET_o with altitude or over snow cover. Instead a weighted average daily ET_o value from the available meteorological stations was used to drive the model. Since ET_o is likely to decrease with altitude, this assumption is likely to lead to an overestimation in mean catchment ET_o. Estimated evapotranspiration and sublimation from snow and frozen soil has generally been reported to be low (Pomeroy and Brun, 2001). For example, Male and Granger (Male and Granger, 1981) estimated daily net evaporation rates of 0.02–0.3 mm d^{-1} in central Saskatchewan. However, in any case, snow cover is predicted to occur in a maximum of 20% of the catchment area and only for three months of the year. Given the lumped nature of the model employed and the other major simplifications assumed, therefore, the impact of this uncertainty is relatively minor.

The representation of the behaviour of the regional groundwater system in the LEMSAR model was simplistic, reflecting high epistemic uncertainty. In fact, model performance was highest overall when ε was fixed at 1 and k was high (resulting in minimal groundwater contribution), suggesting that the aquifer reacts like a single linear reservoir where the groundwater flow is proportional to groundwater storage and water release from the soil store is the principal limit on the timing and magnitude of river discharge. This will, in turn, be controlled by seasonal changes in evapotranspiration and soil moisture content, similar to many humid-temperate catchments. Although the dominant underlying karstic strata in the catchment are volumetrically important, they have rapid hydrological response times (Doummar et al., 2012). We can postulate, therefore, that delays in groundwater flow are short and make little modification to hydrograph shape and magnitude. However, one important issue with this assumption is that low flows in the sustained dry summers experienced in the catchment are poorly predicted. This is clearly important from a water resources management perspective but does not affect the evaluation of the TMPA-3B42/3B42RTdata as a driver for hydrological modelling. Resolving this issue is, therefore, beyond the scope of this study but one solution could be to simply assume an additional fixed baseflow. Finally, although there will be channel network delays in the translation of rainfall to runoff in such a large catchment (>11,000 km^2), these delays are not likely to be important at the daily time step (i.e., network travel times will still be mostly < 24 h—particularly during storm events). Although some modelling uncertainty could be reduced by excluding model-insensitive parameters from the (Li et al., 2009), constraining simulations using measured state variables such as soil water content, snow melt and groundwater behaviour would clearly be more beneficial (Mo and Beven, 2004; Gallart et al., 2007; Beven, 2012).

Observed discharge in the Lesser Zab river was represented reasonably well by the model using in situ gauged rainfall and both TMPA-3B42 and 3B42RT data, particularly when the latter were corrected using a limited set of rain gauge data. Flow simulations using uncorrected TMPA-3B42/3B42RT data generally under-estimated flows for significant periods, with some peaks missed altogether, although seasonal fluctuations were still well captured. It has been reported that TMPA bias tends to increase with rainfall intensity (e.g. Pipunic et al., 2015), suggesting that the bias is multiplicative, not additive. In this study, some rainfall events >40 mm d^{-1} do appear to become more biased after correction (Figure 2b). This means that although our corrections improve rainfall over the most frequent ranges (typically low intensity), they

may fail to improve significantly (or worsen) model performance in lower frequency, higher magnitude events. Application of different bias statistics for different ranges of rainfall intensity could provide a solution to this issue but this has not been explored further here.

The superior accuracy of LEMSAR when driven by corrected, compared to uncorrected, TRMM data mainly reflects the fact that the correction reduced the bias in the TRMM estimates which was translated, in part, into higher predicted flows. These results are consistent with other research (Anders et al., 2006; Collischonn et al., 2008; Kneis et al., 2014) which has indicated that corrected TMPA-3B42 v7 precipitation estimates can provide reasonable model input for the simulation of river discharge. However, previous attempts at correction have used denser rain gauge networks than the network employed here and none have been employed in this region. The TMPA-3B42/3B42RT data were corrected using a limited set of the available rain gauge data in order to evaluate the application of the correction equation to independent data. The agreement between the corrected daily TMPA-3B42/3B42RT data and the daily rain gauge data for Period 2, together with the reasonable performance of LEMSAR when driven by the corrected TMPA data for the whole flow record, suggest that this correction may be generally applicable in this catchment. Nevertheless, it should be noted that the superior performance of the model when driven by both of the corrected satellite data products may be "opportunistic" to some extent—resulting from the fact that flows are slightly over-estimated by the model when calibrated using gauged rainfall whilst gauged rainfall is still slightly under-estimated by the TMPA data.

Furthermore, since the TMPA data provide spatially aggregated rainfall estimates over an area, while rain gauge data are measured at specific point locations, the TMPA data may be useful for modelling catchments where gauge data are sparse. Note that the TRMM data mission has now ended and another platform (Global Precipitation Measurement (GPM) mission is available at http://pmm.nasa.gov/GPM) which supplies similar data to TRMM. The Integrated Multi-satellitE Retrievals for GPM (IMERG) will be much improved in terms of spatial and temporal resolutions (e.g., 0.1 deg and half-hourly: Huffman et al., 2017). The findings of this work should also be broadly applicable to GPM data.

3.5 Summary

Rainfall-runoff modelling is a useful tool for water resources management. This chapter presents a simple daily rainfall-runoff model, based on the water balance equation, which applied to the 11,630 km^2 Lesser Zab catchment in northeast Iraq. The model was forced by either observed daily rain gauge data from four stations in the catchment or satellite-derived rainfall estimates from two TRMM Multi-satellite Precipitation Analysis (TMPA) data products (TMPA-3B42 and 3B42RT) based on the Tropical Rainfall Measuring Mission (TRMM) from 2003 to 2014. As well as using raw TMPA data, we used a bias-correction method to adjust TMPA values based on rain gauge data. The uncorrected TMPA data products underestimated observed mean catchment rainfall by −10.1% and −10.7%. Corrected data also slightly underestimated gauged rainfall by −0.7% and −1.6%, respectively. Nash-Sutcliffe Efficiency (NSE) and Pearson's Correlation Coefficient (r) for the model fit with the observed hydrograph were 0.75 and 0.87, respectively, for a calibration period (2010–2011) using gauged rainfall data. Model validation performance (2012–2014) using ground based ET_o was best (highest NSE = 0.66 and r = 0.81; lowest RMSE = 77 and bias = -2.6) using the corrected 3B42 data product and (poorest NSE = 0.28 and r = 0.59; highest RMSE = 112 and bias = -14.2) when driven by uncorrected 3B42RT data. Uncertainty and equifinality were also explored. The results suggest that TRMM data can be used to drive rainfall-runoff modelling in semi-arid catchments, particularly when corrected using rain gauge data.

In this chapter, the utility of remotely-sensed rainfall data for driving a hydrological model have only evaluated. Next chapter will also explore the effects of using other remotely sensed meteorological data (e.g., surface temperature) to predict ET_o and the potential for simulating hydrological response in this and other catchments completely independently of ground-based observations.

Chapter 4: Predicting river flow in a data-scarce semi-arid catchments using remote sensing estimates of precipitation and evapotranspiration

4.1 Introduction

In chapter 3, the utility of satellite-based precipitation (TMPA) for driving rainfall-runoff model was evaluated. In this chapter, the estimation of daily reference evapotranspiration using remote sensing data ($ET_{o\text{-}RS}$) is carried out and the accuracy of these estimates against ET_o is calculated using ground observations ($ET_{o\text{-}G}$) is quantified. The main purposes of the chapter were (i) to evaluate the accuracy of daily ET_o estimates derived using remote sensing data against ET_o calculated using ground observations based on the PM method as a benchmark (ii) to evaluate the performance of the LEMSAE model when the model was forced just by RS data

4.2 Materials and Methods

4.2.1 Study area

The study area interested in this chapter is (Lesser Zab and Sirwan River catchments) which was described in detail in chapter 2, section 2.1.

4.2.2 In situ data

In situ data used in this chapter was described in (chapter 2, section 2.2).

4.2.3 Remote sensing data

The remote sensing data of interest in this chapter is AIRS products which described in (chapter 2, section 2.3.2)

4. 2.3 AIRSdata

Cloud cover fraction data from AIRS were used to estimate sunshine duration using:

$$DS = H \cdot C_f \quad (4.1)$$

where DS is sunshine duration (hours), C_f is the cloud cover fraction (established from the AIRS/Aqua L3 Daily Standard Physical Retrieval (AIRS + AMSU) 1 degree × 1 degree V006 cloud-cover fraction data (AIRX3STD)) and H is the maximum possible sunshine hours, calculated as (Allen et al., 1998):

$$H = \frac{24}{\pi}\,\omega_s \quad (4.2)$$

where ω_s is the sunset hour angle which is calculated by:

$$\omega_s = \arccos[-\tan(\varphi) - \tan(\delta)] \quad (4.3)$$

in which φ is the latitude and δ is the solar declination (i.e.):

$$\delta = 0.409 \sin\left(\frac{2\pi}{365}\ J - 1.39\right) \quad (4.4)$$

in which J is the Julian day of the year (1 to 365, or 366 in a leap year).

4.2.4 Reanalysis Data

Combination methods such as the Penman-Monteith equation usually requires wind speed measurements at 2 m height above ground (Allen et al., 1998). Daily estimates of wind speed at 10 m height were obtained from MERRA (GMAO: Global Modeling and Assimilation Office, 2008: : http://giovanni.gsfc.nasa.gov/giovanni) at 0.5° x 0.6° spatial resolution adjusted to the standard 2 m height using (Allen et al., 1998);

$$U_2 = U_z \frac{4.87}{\ln(67.8\, z - 5.42)} \quad (4.5)$$

where U_2 is wind speed at 2 m (m s^{-1}) and U_z is wind speed at z m above ground (m s^{-1}).

4.2.5 Reference evapotranspiration (ET_o) estimation methods

ET is commonly estimated indirectly from meteorological data (Allen et al., 1998; Tabari et al., 2011; McMahon et al., 2013) using a variety of different methods (Brutsaert, 1982; Poyen and Ghosh, 2016; Jensen et al., 1990). These methods can be grouped into three categories: (i) those based on energy balance and mass transfer concepts, often referred to as the combination equation or Penman–Monteith (PM) method (Allen et al., 1998); (ii) those based on empirical relationships between ET_o and temperature- (e.g., (Thornthwaite, 1948) and (Hargreaves and Samani, 1985: HS); and (iii) and radiation-based approaches which utilise measured or estimated solar radiation flux density at the surface (e.g., (Jensen and Haise, 1963: JH); (McGuinness and Bordne, 1972: MB); and (Priestley and Taylor, 1972)). The PM method is widely considered to be the most reliable indirect method (Allen et al., 1998; Gong et al., 2006; Pandey et al., 2016). However, its main shortcoming is that it requires a complete weather data set (net radiation flux density, temperature, relative humidity and wind speed) which is not always available for many areas (Tabari and Talaee, 2011). The other methods have fewer meteorological data requirements (Tabari et al., 2011) and are, hence, widely applied—particularly those based solely on temperature. The performance of temperature- and radiation-based methods, relative to the PM method, is often spatially and temporally variable (Sabziparvar et al., 2009; Tabari et al., 2012b). Although the commonly used Thornthwaite approach requires only temperature data, it is not considered here because (i) it cannot be used when Ta < 0 °C; and (ii) it was developed in the mid-latitude continental USA as a climatic-index rather than a method for calculating ET_o. Outside of these region there is significantly more uncertainty about its validity. The HS method is generally agreed to be the best temperature-based approach (WeiB and Menzel, 2008; Tabari, 2009) but has been reported to perform poorly in some semi-arid contexts (Tabari et al., 2012b) where radiation-based methods may be more suitable (Pandey et al., 2016). The JH and MB methods have been successfully applied in humid and arid environments (Oudin et al., 2005; Tabari et al., 2011)

but the main drawback of these equations is underestimation in humid areas (Poyen and Ghosh, 2016) and overestimation in semi-arid areas (Tabari et al., 2011).

Four methods were considered: (1) the Penman–Monteith (PM) equation (Allen et al., 1998) which was used as a benchmark for comparison with the other methods; (2) the (Hargreaves and Samani, 1985: (HS)); (3) the radiation-based method of (Jensen and Haise, 1963: (JH)); and (4) the radiation-based method of (McGuinness and Bordne, 1972: (MB)). All methods require temperature data, the PM also requires RH, wind speed and sunshine hours data. JH and MB also require sunshine data. The equations are as follows.

$$\text{PM: } ET_o = \frac{0.408\Delta(R_n - G) + \gamma \frac{900}{T_a + 273} U_2(e_s - e_a)}{\Delta + \gamma(1 + 0.34U_2)} \tag{4.6}$$

$$\text{HS: } ET_o = 0.0023\ (T_{max} - T_{min})^{0.5}(T_a + 17.8)\frac{R_a}{\lambda} \tag{4.7}$$

$$\text{JH: } ET_o = \frac{0.025(T_a + 3)\ R_s}{\lambda} \tag{4.8}$$

$$\text{MB: } ET_o = \frac{R_s}{\lambda}\ \frac{(T_a + 5)}{68} \tag{4.9}$$

where ET_o is the reference evapotranspiration rate (mm d^{-1}), U_2 is mean daily wind speed at 2 m height (m s^{-1}) (Equation (4.5)), Δ is the slope of the vapour pressure versus temperature curve (kPa °C^{-1}) (Equation (4.10)), R_n is the net radiation flux density at the vegetation surface (MJ m^{-2} d^{-1}) (Equation (4.11)), G is the soil heat flux density (MJ m^{-2} d^{-1})—assumed to be zero because it is very small at the daily time scale (Allen et al., 1998), T_a is mean daily air temperature at 2 m height (°C), T_{min} is minimum air temperature (°C), T_{max} is maximum air temperature (°C), R_s is the solar radiation flux density at the surface (MJ m^{-2} d^{-1}) (Equation (4.13)), R_a is the extraterrestrial radiation (i.e., the theoretical radiation flux density at the top of the atmosphere) [MJ m^{-2} d^{-1}] (Equation (4.14)), e_s is the saturation vapour pressure (kPa) (Equation (4.18)), e_a is the actual vapour pressure (kPa) (Equation (4.19)), $e_s - e_a$ is the

saturation vapour pressure deficit (kPa), λ is the latent heat of vaporization (i.e., 2.45 (MJ kg^{-1})) and γ is the psychrometric constant (kPa $°C^{-1}$) (Equation (4.22)).

Further definitions of variables used in Equations (4.6)–(4.9) are given (Allen et al., 1998) as follows:

$$\Delta = \frac{4096\left[0.6108exp^{\left(\frac{17.27T_a}{T_a+273.3}\right)}\right]}{(T_a+273.3)^2} \tag{4.10}$$

$$R_n = R_{ns} - R_{nl} \tag{4.11}$$

in which R_{ns} is the net shortwave radiation flux density (MJ m^{-2} d^{-1}) (Equation (4.12)) and R_{nl} is the net longwave radiation flux density (MJ m^{-2} d^{-1}) (Equation (4.16)):

$$R_{ns} = (1-\alpha)R_s \tag{4.12}$$

where α is the surface albedo, assumed to be 0.23 for a hypothetical grass sward (Allen et al., 1998).

$$R_s = (a_s + b_s\frac{DS}{H})R_a \tag{4.13}$$

in which DS is the actual duration of sunshine (hours), H is the maximum possible duration of sunshine (hours) and $a_s + b_s$ are regression constants set to 0.25 and 0.5, respectively, as recommend by Allen et al. (Allen et al., 1998).

$$R_a = \frac{24(60)}{\pi}\, G_{sc}\, d_r[\omega_s \sin(\varphi)\sin(\delta) + \cos(\varphi)\cos(\delta)\sin(\omega_s]] \tag{4.14}$$

in which d_r is the inverse of the relative distance between the Earth and the Sun (Equation (4.15)), ω_s is defined by Equation (4.3), φ is the latitude, δ is given in Equation (4.4) and G_{sc} is the solar constant = 0.0820 MJ m^{-1} min^{-1}.

$$d_r = 1 + 0.033 \cos\frac{2\pi}{365}J \tag{4.15}$$

$$R_{nl} = \sigma\left[\frac{(T_{max}+273.3)^4 + (T_{min+}273.3)^4}{2}\right](0.34 - 0.14 * \sqrt{e_a})(1.35\frac{R_s}{R_{so}} - 0.35) \tag{4.16}$$

in which σ is the Stefan–Boltzmann constant ($4.903\ 10^{-9}$ MJ K^{-4} m^{-2} d^{-1}), $(0.34 - 0.14 * \sqrt{e_a})$ expresses the correction for atmospheric humidity, and the cloudiness is expressed by $\left(1.35\frac{R_s}{R_{so}} - 0.35\right)$ (Allen et al., 1998); R_{so} is the clear-sky solar radiation flux density (MJ m^{-2} d^{-1}) which can be used when calibrated values for $a_s + b_s$ are not available (Allen et al., 1998) i.e.,

$$R_{so} = (0.75 + 2 * 10^{-5} * z)R_a \tag{4.17}$$

in which z is the station elevation above sea level (m).

The vapour pressure terms are defined as follows:

$$e_s = (\frac{e^0(T_{max}) + e^0(T_{min})}{2}) \tag{4.18}$$

$$e_a = (\frac{e^0_{min}\frac{RH_{max}}{100} + e^0_{max}\frac{RH_{min}}{100}}{2}) \tag{4.19}$$

where RH_{min} and RH_{max} are minimum and maximum relative humidity (%) and e^0_{min} and e^0_{max} are the saturation vapor pressure at the minimum and maximum air temperatures, respectively (Equations (4.20) and (4.21)):

$$e^0_{min} = 0.6108\ exp(\frac{17.27\ T_{min}}{T_{min} + 273.3}) \tag{4.20}$$

$$e^0_{max} = 0.6108\ exp(\frac{17.27\ T_{max}}{T_{max} + 273.3}) \quad (4.21)$$

The psychrometric constant is defined as:

$$\gamma = \frac{C_p P}{\varepsilon\ \lambda} \quad (4.22)$$

in which C_p is the specific heat capacity at constant pressure; 1.013 10^{-3} (MJ kg^{-1} K^{-1}), ε is the ratio molecular weight of water vapour:dry air (i.e., 0.622); and *P* is the atmospheric pressure (kPa).

4.2.5 Rainfall-runoff model

LEMSAR model applied in this chapter was described in chapter 3.2.4.

4.2.6 Evaluation criteria

Four statistical measures were used to evaluate model performance in validation: *NSE*, *r*, RMSE and percent bias (Equations 3.18- 3.21).

4.3 Results

4.3.1 Comparison between Meteorological Variables Estimated from Remote Sensing with Station Data

Satellite-derived and ground-measured values of mean daily air temperature (T_a), RH, sunshine hours (*DS*) and U_2 are compared in Figure 4.1 for the four stations in the study area. A statistical summary of this comparison is shown in Table 4.1. The R^2 values between the ground-measured and AIRS-derived values of T_a were high ($R^2 > 0.88$) and highly significant for all stations. The RMSE for T_a ranged from 3.2 to 5.1 °C with a tendency of RS to underestimate the ground observations of T_a. For RH, the relationship between satellite-derived and ground-based measurements was also significant for all four stations ($R^2 > 0.3$; $p < 0.05$). For RH the RMSE ranged from 12.5% to 24% with negative bias for all stations. However, there was a

weak but significant relationship for *DS* ($0.15 < R^2 < 0.2$; $p < 0.05$) and the relationship between measured U_2 and MERRA-derived wind speed is even weaker for all stations (Table 4.1). Remotely sensed *DS* and U_2 both had positive bias in all cases, except for wind speed at Dukan (Table 4.1).

Since *ET* is widely known to be driven by turbulent eddies, and is thus sensitive to wind speed, an extra analysis was conducted to evaluate the model sensitivity to the MERRA-wind speed data. ET_o estimates derived using the PM equation for all four stations using U_2 derived from MERRA were compared with PM estimates assuming a constant U_2 value (the mean measured daily value for each station during 2010–2014). The ET_o predictions produced with the constant wind velocity were actually better overall (closer match with PM estimates obtained using ground-measured data in terms of regression equation slope, R^2 and RMSE: see Appendixes, Figures A2 and A3, Table A2, A3 and A4), although (as expected) high *ET* values (>ca 8 mm d^{-1}) which often arise on windy days are not well predicted. This implies that that the PM equation can still be used with RS data provided a reasonable estimate can be made for the mean wind speed for the locations of interest.

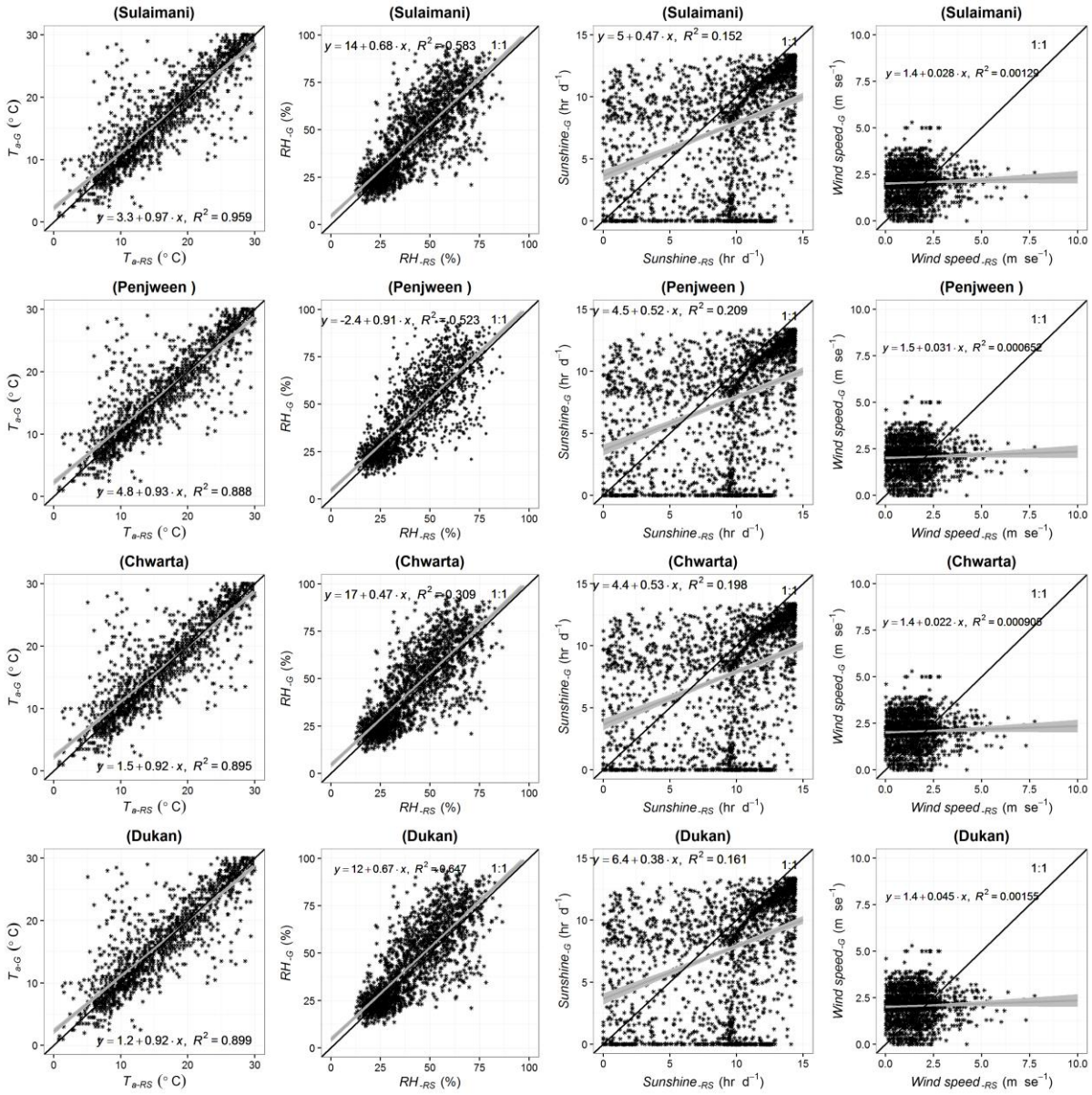

Figure 4. 1. Scatterplots of daily T_a , RH %, DS and U_2 measured at ground-based stations (x-axes) compared with those derived from remote sensing (y-axes) for four different stations. The solid black line indicates the 1:1 relationship. The grey line shows the best-fit regression with 95% confidence interval.

Table 4. 1. Statistical summary of the relationship between daily ground-measured and remotely-sensed values of T_a, RH %, DS *and* U_2 for four different stations during the study period (2010–2014). * Significant at p ≤ 0.05.

Station	Variable	RMSE	BIAS (%)	*r*
Sulaimani	T_a	3.5	−14.2	0.97*
	RH %	12.7	−0.6	0.76*
	DS	4.5	16.1	0.38*
	U_2	1.4	27.8	0.03*
Penjween	T_a	5.1	28.4	0.94*
	RH %	13.8	−13.4	0.72*
	DS	4.3	10.2	0.45*
	U_2	1.7	34.8	0.02
Chwarta	T_a	3.3	−0.1	0.94*
	RH %	24	−26	0.55*
	DS	4.2	9.1	0.44*
	U_2	1.5	24.5	0.03*
Dukan	T_a	3.2	−2.8	0.95*
	RH %	12.5	−7.3	0.80*
	DS	5.1	21.8	0.40*
	U_2	1.4	−47.7	0.03*

4.3.2 Comparison between Daily $ET_{o\text{-}RS}$ and $ET_{o\text{-}G}$

The calculated daily $ET_{o\text{-}G}$ and $ET_{o\text{-}RS}$ estimates are shown in Figure 4.2. In all cases, the black line shows $ET_{o\text{–}G}$. For all stations, there is seasonal agreement between $ET_{o\text{-}G}$ and $ET_{o\text{–}RS}$ for all evapotranspiration methods. Estimated $ET_{o\text{-}G}$ is plotted against $ET_{o\text{–}RS}$ in Figure 4.3, along with the best-fit linear regression and the 1:1 line. Most of the points are scattered around the 1:1 line for the JH and MB methods which always have high R^2 and regression gradients close to unity. However, there is considerable variability in the slope of the ground-derived versus RS-derived regression lines (0.7 to 0.89) and in R^2 (0.64 to 0.9) when using the HS and PM methods—particularly for the Dukan and Sulaimani stations. These stations have relatively low elevations compared with the other two stations, with higher average temperatures (Table 2.1). Average annual ET_o values estimated using the ground and RS data for all methods from 2010 to 2014 are presented in Figure 4.4. The MB method yielded highest average annual values for both $ET_{o\text{-}G}$ and $ET_{o\text{–}RS}$ (1670 mm y^{-1} and 1677 mm y^{-1}, respectively), while the HS method yielded the lowest annual value of $ET_{o\text{–}RS}$ (1198 mm y^{-1}) and the PM method yielded lowest annual values of $ET_{o\text{-}G}$ (1337 mm y^{-1}). The average annual values of $ET_{o\text{–}RS}$ were relatively similar to those of $ET_{o\text{-}G}$, which reflects low bias and hence small cumulative errors.

Goodness-of-fit statistics are presented in Table 4.2. The MB method consistently performed better than other methods (in terms of the similarity of the $ET_{o\text{-}G}$ and $ET_{o\text{-}RS}$ data) for all stations and for all goodness-of-fit criteria, except for the bias at Sulaimani. The greatest differences were observed when the PM and HS methods are compared. The HS method consistently underestimated ground-based *ET* estimates when RS data were used as inputs (i.e., bias was always negative). Pearson correlation coefficients (*r*) between $ET_{o\text{-}G}$ and $ET_{o\text{-}RS}$ were generally high and always highly significant ($p < 0.05$) for all stations.

Table 4. 2. Statistical summary of comparisons between estimated daily reference evapotranspiration using ground-based measurements (ET_o-$_G$) and remote sensing data (ET_o-$_{RS}$) for four different methods at four different stations (Sulaimani, Penjween, Chwarta, and Dukan) over the study period 2010–2014. * Significant at p ≤0.05.

Station	Methods	RMSE (mm d^{-1})	BIAS (%)	*r*
Sulaimani	PM	0.99	2.5	0.80*
	HS	1.26	−17	0.95*
	JH	0.82	−3.2	0.93*
	MB	0.65	−10.5	0.99*
Penjween	PM	1.59	17.7	0.81*
	HS	1	−13	0.94*
	JH	1.46	23.2	0.93*
	MB	0.92	18.2	0.97*
Chwarta	PM	1.26	12.8	0.86*
	HS	0.95	−10	0.92*
	JH	1.19	3.7	0.93*
	MB	0.57	0.3	0.97*
Dukan	PM	1.7	−13	0.81*
	HS	1.1	−19.9	0.94*
	JH	1.56	5.1	0.91*
	MB	0.52	−1.8	0.98*

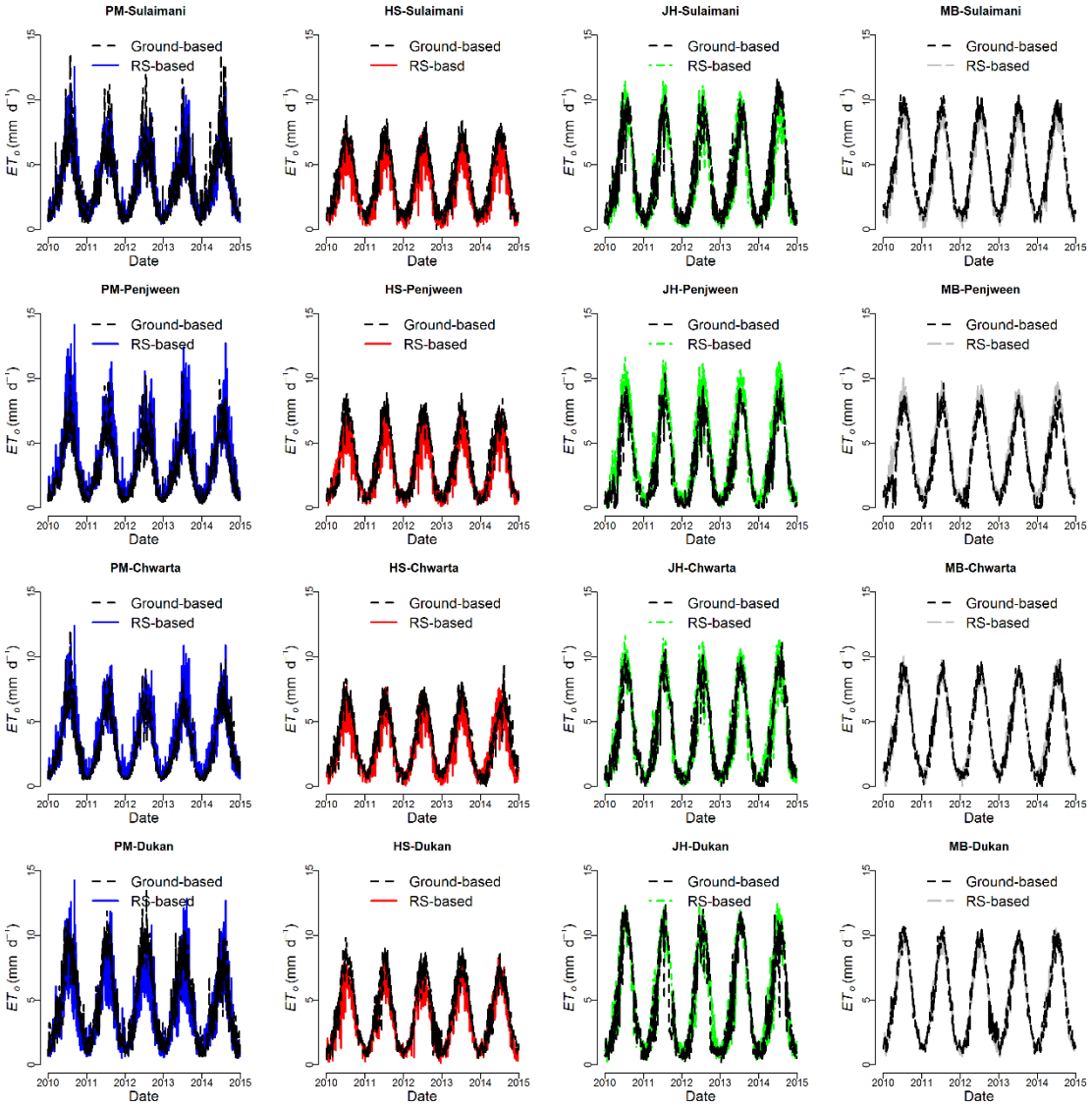

Figure 4. 2. Plot of daily ET_o estimates derived from ground-based measurements (ET_o-$_G$) and remote sensing data (ET_o-$_{RS}$) using four methods from 2010–2014 for Sulaimani, Penjween, Chwarta and Dukan stations. The black line presents the ET_o-$_G$.

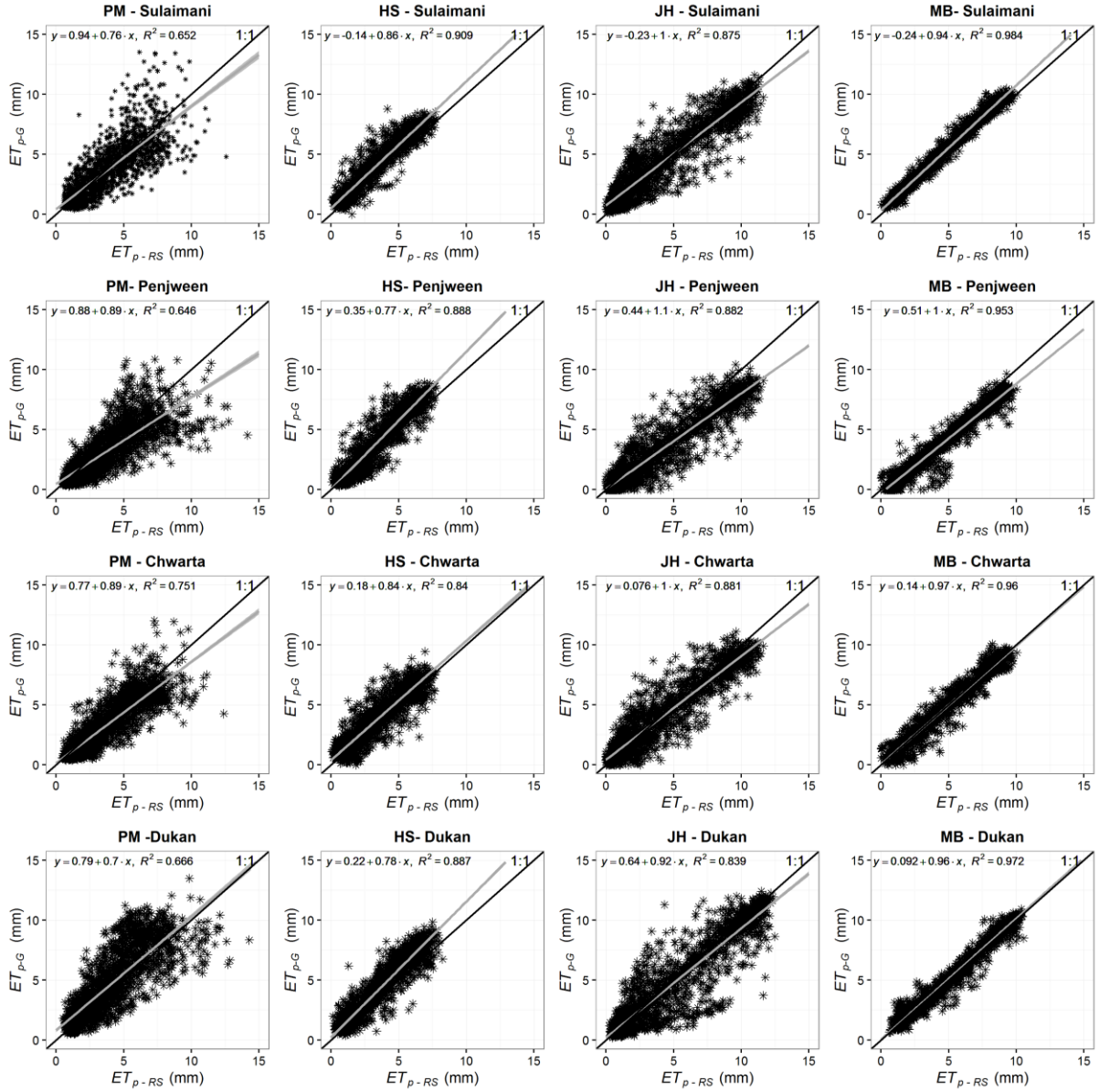

Figure 4. 3. Scatterplots of estimated daily reference evapotranspiration using ground-based measurements (ET_o-$_G$) versus estimated reference evapotranspiration using remote sensing data (ET_o-$_{RS}$) applying four different methods at four different stations (Sulaimani, Penjween, Chwarta, and Dukan). The solid black line indicates the 1:1 relationship. The grey line shows the best-fit regression with 95% confidence interval (equations and R^2 also shown).

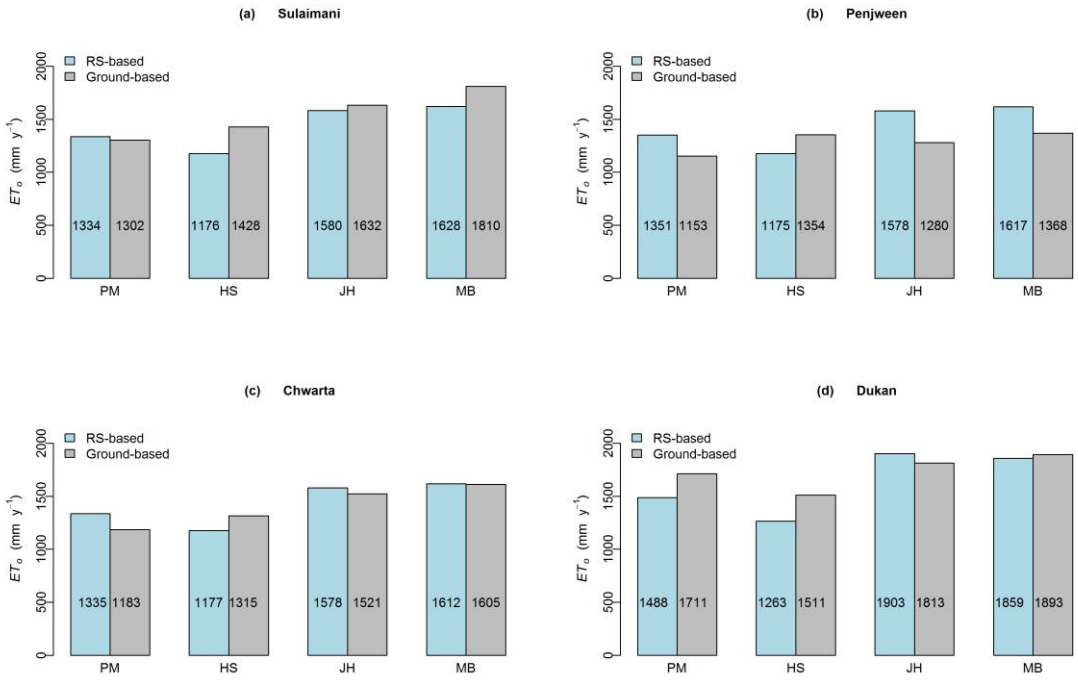

Figure 4. 4. Average annual ET_o estimates derived from ground-based measurements (ET_o-$_G$) and remote sensing data (ET_o-$_{RS}$) using four methods from 2010–2014 for Sulaimani, Penjween, Chwarta and Dukan stations.

4.3.3 Cross-Comparison of the ET_o Methods

In Figure 4.5, different ET_o-$_{RS}$ values calculated using the HS, JH, and MB methods are plotted against benchmark data (i.e., ET_o-$_G$ PM) for all stations. This comparison is based on the assumption that the PM method is most reliable (Allen et al., 2000), and that the ground-based measurements at each station best represent the atmospheric drivers for evapotranspiration (i.e., the ground-based data will best-predict ET_o using the PM method). There was considerable variation in model performance against the benchmark data for different stations. The JH and MB methods had regression slopes in the range between 0.95 and 1.4, with most slopes >1, indicating a slight tendency of these methods to overestimate the benchmark values. However, the slopes for the HS method ranged between 0.63 and 0.82, suggesting a tendency for the HS equation to under-predict *ET* when driven by RS data, particularly at the Dukan station Although the MB method yielded the best coefficient of determination for each station ($0.74 < R^2 < 0.86$), this was not always the best method in terms of proximity to the 1:1 line. At the two stations with higher elevation (Penjween and Chwarta) the HS method was the best

predictor. Table 4.3 summarises the results statistically. This confirms that the HS method tends to underestimate benchmark *ET* ($-9 < \text{bias}\% < -0.6$) and that the other methods tend to overestimate it (bias ranged between 8.6 and 40%). At all stations the HS method had the lowest RMSE (1–1.3 mm d^{-1}). Despite the fact that the JH and MB methods had correlation coefficients which were often better than for the HS method, they had much higher RMSE values (1.8–2.1 mm d^{-1}).

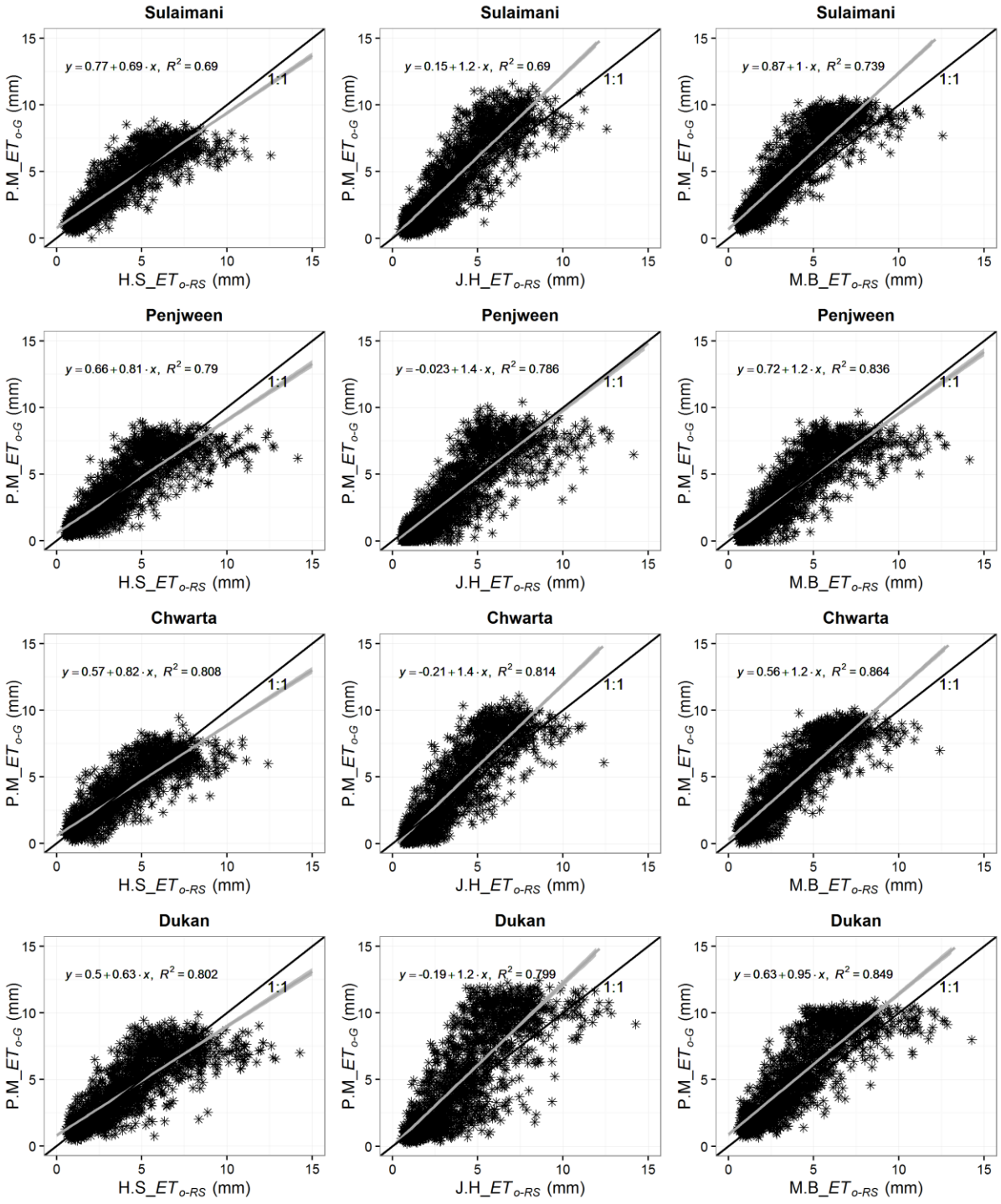

Figure 4. 5. *E*stimated daily reference evapotranspiration using remote sensing data (ET_o-$_{RS}$) for the HS, JH and MB methods against estimated reference evapotranspiration generated using ground-based measurements (ET_o-$_G$) with the PM method (the benchmark model) for four different stations (Sulaimani, Penjween, Chwarta and Dukan). The solid

black line indicates the 1:1 relationship. The grey line shows the best-fit regression with 95% confidence interval (equations and R^2 also shown).

Table 4. 3. Statistical bias, RMSE and Pearson Product Moment Correlation coefficient (*r*) for $ET_{o\text{-}RS}$ values against the benchmark data set $ET_{o\text{-}G}$ (PM) for the different stations over the study period 2010–2014. * Significant at p ≤0.01.

Station	Methods	RMSE (mm d^{-1})	BIAS (%)	*r*
Sulaimani	HS	1.3	−9	0.83*
	JH	2.1	21.4	0.83*
	MB	1.6	24.5	0.85*
Penjween	HS	1	−1.9	0.88*
	JH	2.1	37	0.88*
	MB	1.7	40	0.91*
Chwarta	HS	0.98	−0.6	0.89*
	JH	2	33.3	0.90*
	MB	1.6	37	0.92*
Dukan	HS	1.2	−2.6	0.89*
	JH	1.8	11.2	0.89*
	MB	1.81	8.6	0.92*

4.3.4 Comparing observed and simulated discharge for Lesser Zab and Sirwan River catchments over period 2010-2014.

Observed and simulated discharge for the Lesser Zab and Sirwan River in different periods and driven by different rainfall data-sets and estimated $ET_{o\text{-}RS}$ based on different reference evapotranspiration methods are shown in Figure 4.6. In all cases, the black line shows the observed discharge. In general, the seasonal agreement between observed and simulated discharge is reasonable using corrected TMPA-3B42 / 3B42RT rainfall with all estimated $ET_{o\text{-}RS}$ for both catchments. However, some hydrograph peaks appear to be noticeably under-predicted by the model, particularly when driven by the uncorrected TMPA-3B42 / 3B42RT rainfall data with estimated $ET_{o\text{-}RS}$ according to JH and MB methods. Simulated flows are plotted against measured data in Figure 4.7, along with the best-fit linear regression and the 1:1 line. Most of the points are scattered around the 1:1 line when the model is driven by the area-weighted rain gauge data with estimated $ET_{o\text{-}RS}$ according to PM and HS methods. However,

there is considerable deviation at high flows (e.g. the model underestimates some measured discharge peaks >500 $m^3 s^{-1}$) and for hydrograph recessions (in which predicted flows tend to reduce slightly faster than those observed). This results in a slope for the best-fit regression which is less than unity in the Lesser Zab catchment. This systematic deviation was more pronounced when the model was driven by the uncorrected TMPA-3B42 and TMPA-3BRTuc rainfall data with $ET_{o\text{-}RS}$ using JH and MB methods (Figure 4.7a and c). The slope for the best-fit regression in Sirwan river match the 1:1 line when the LEMSAR driven by corrected TMPA-3B42 and 3B42RT with $ET_{o\text{-}RS}$ HS (Figure 4.7 f and h) compared to the Lesser zab catchment.

Goodness-of-fit statistics are presented in Table 4.4. These statistics reinforce the message derived from the graphs that the model tends to under-estimate the measured river discharge in the validation periods regardless of the rainfall and ET_o data used for the Lesser Zab catchment. While simulated flow tends to over-estimated for Sirwan river catchment. The best NSE value for the validation period was obtained using the corrected TMPA-3B42 with ET_o HS data for the Lesser Zab catchment. As expected, model performance was poorest when it was driven by the uncorrected TMPA-3B42 / 3B42RT with ET_o JH and MB data (lowest NSE, highest BIAS and highest RMSE) in both catchments. Overall, the TMPA-3B42 product has relatively higher performance compare to TMPA-3B42RT with the ET_o HS and PM than ET_o, JH and MB in both catchments.

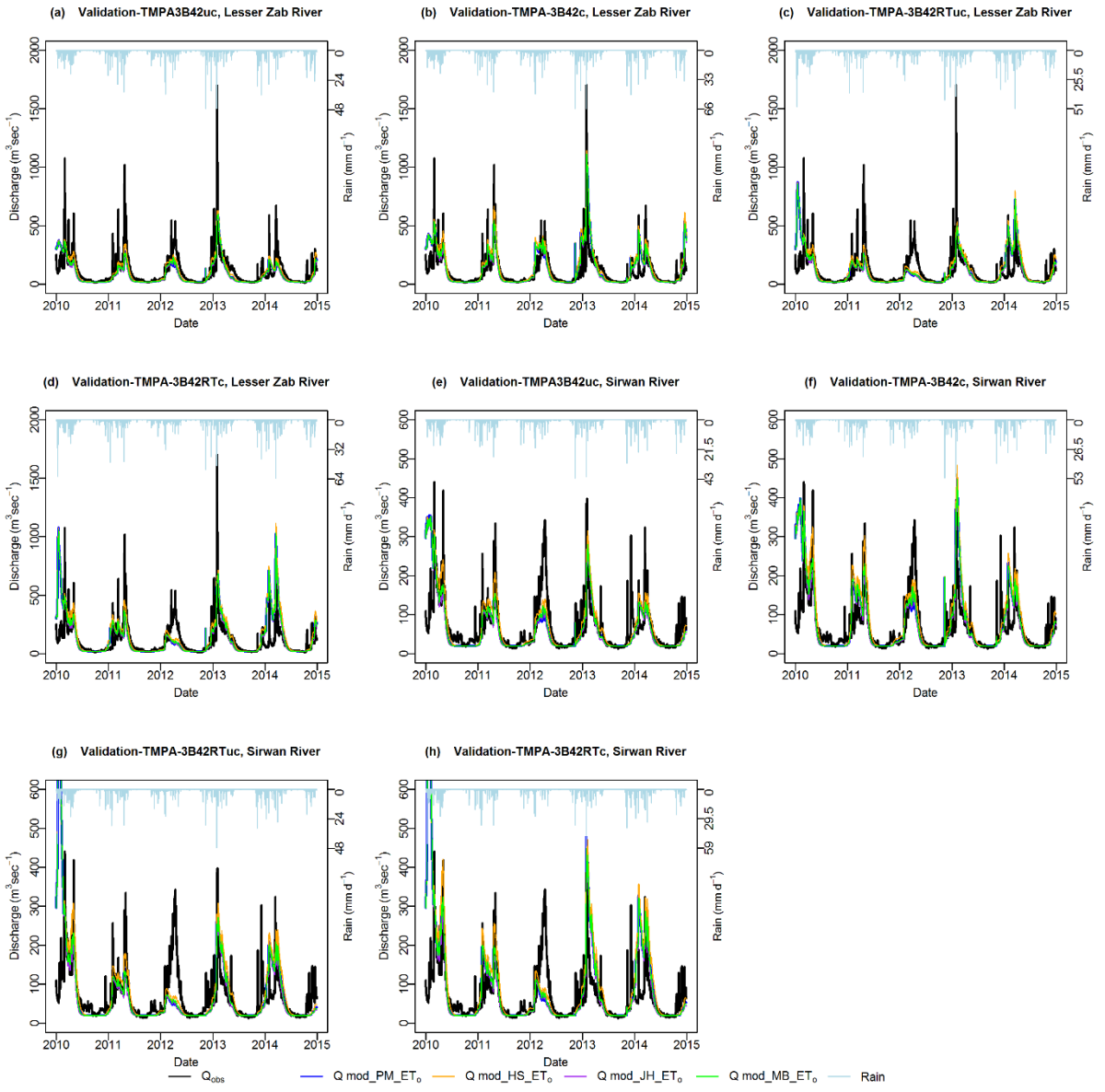

Figure 4. 6. Observed and simulated hydrographs for the Lesser Zab River and Sirwan River above the Dukan and Darbandikhan reservoir. In all cases, hydrological model parameters were calibrated using the gauged rainfall data with $ET_{o\text{-}G}$ (PM) in the Lesser Zab catchment (see section 3.2.5). Validation period (2012-2014) for Lesser Zab when the model was driven by the uncorrected and the corrected TMPA-3B42 rainfall data with different estimated $ET_{o\text{-}RS}$ are shown in (a), (b), (c) and (d). Data for the validation period (2010-2014) for Sirwan catchment are shown in (e), (f), (g) and (h) when the model driven by the uncorrected and the corrected TMPA-3B42 rainfall data with different estimated $ET_{o\text{-}RS}$.

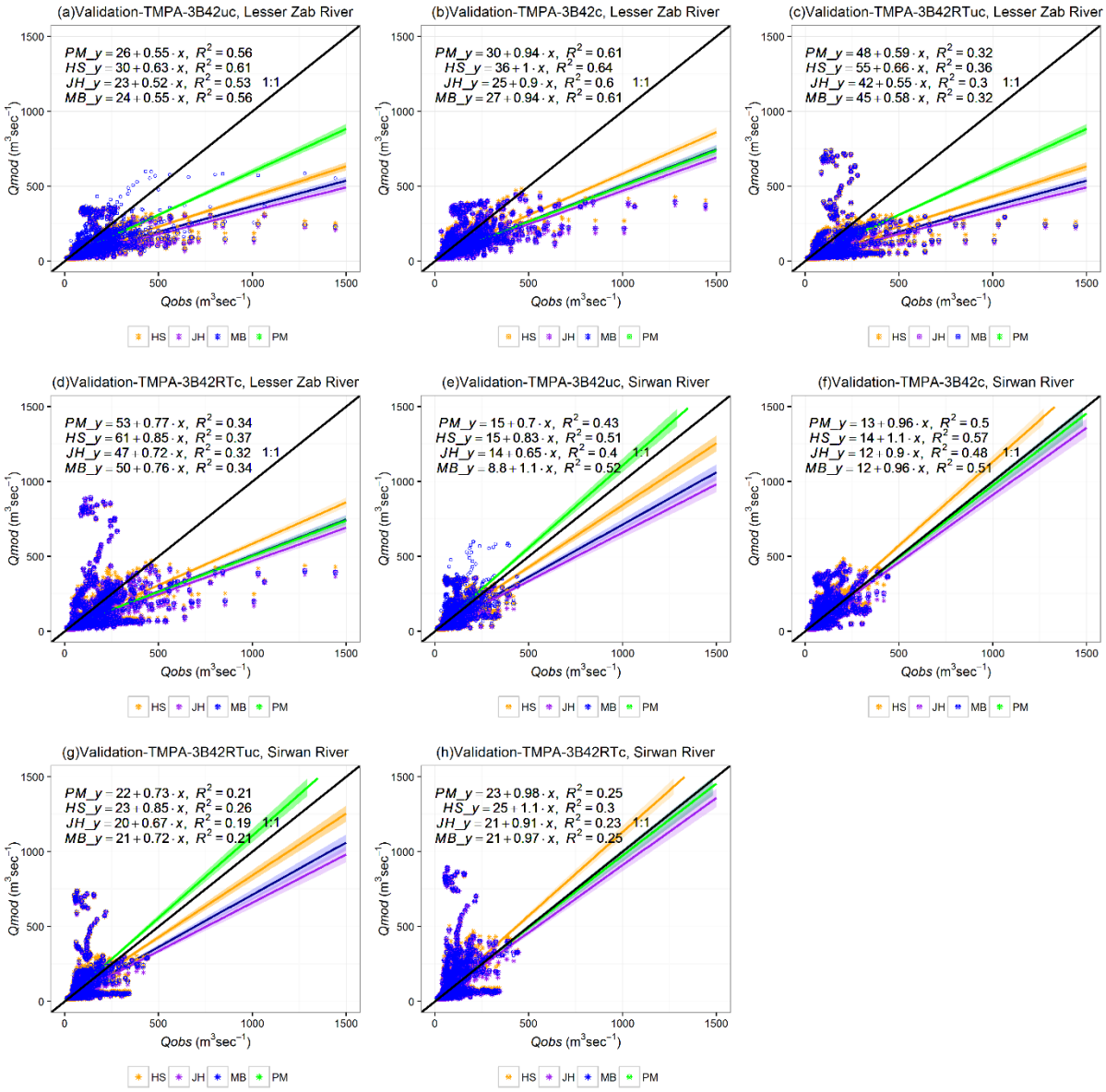

Figure 4. 7. Scatterplots of observed versus simulated discharge for the validation period (2012-2014) for Lesser Zab when the model was driven by the uncorrected and the corrected TMPA-3B42 rainfall data with different estimated $ET_{o\text{-}RS}$ are shown in (a), (b), (c) and (d). Scatterplots for the validation period (2010-2014) for Sirwan River are shown in (e), (f), (g) and (h) when the model was driven by the uncorrected and the corrected TMPA-3B42 rainfall data with different estimated $ET_{o\text{-}RS}$. The solid line indicates the 1:1 relationship. The orange, purple, light blue and green lines show the best fit regression with 95% confidence intervals when the model driven by the uncorrected and the corrected TMPA-3B42 rainfall data with different estimated ET_o (HS, JH, MB and PM) respectively.

Table 4. 4. Summary of goodness of fit criteria for simulated discharge in the Lesser Zab and Sirwan River catchments. * Significant at p ≤0.01. Note that the model was not calibrated for the Sirwan River catchment.

Catchment	Precipitation	ET_o methods	RMSE (m^3 sec^{-1})	BIAS (%)	*r*	*NSE*
Lesser Zab	**TMPA-3B42uc**	PM	92	-21	0.74*	0.41
		HS	84	-10	0.78*	0.44
		JH	96	-28	0.73*	0.42
		MB	92	-23	0.74*	0.41
	TMPA-3B42c	PM	102	20	0.78*	0.52
		HS	99	11	0.80*	0.61
		JH	109	34	0.77*	0.47
		MB	101	17.5	0.78*	0.52
	TMPA-3B42RTuc	PM	127	1.3	0.56*	0.16
		HS	116	15.3	0.58*	0.24
		JH	128	-8	0.55*	0.07
		MB	125	-1.6	0.56*	0.13
	TMPA-3B42RTc	PM	117	-34	0.57*	0.22
		HS	115	-21	0.60*	0.26
		JH	121	-45	0.56*	0.17
		MB	120	-39	0.57*	0.2
Sirwan River	**TMPA-3B42uc**	PM	55	-8	0.65*	0.22
		HS	53	5	0.71*	0.26
		JH	56	-15	0.63*	0.22
		MB	55	-11	0.65*	0.27
	TMPA-3B42c	PM	62	15	0.71*	0.24
		HS	66	32	0.75*	0.31
		JH	60	6.6	0.69*	0.12
		MB	61	13.1	0.71*	0.18
	TMPA3B42RTuc	PM	92	4.3	0.47*	0.18
		HS	91	18.9	0.52*	0.17
		JH	92	-3.1	0.44*	0.19
		MB	92	2.3	046*	0.18
	TMPA-3B42RTc	PM	116	31	0.51*	0.1
		HS	112	21	0.55*	0.14
		JH	118	48	0.48*	0.12
		MB	120	28	0.50*	0.13

4.3.5 Flow duration curves for Lesser Zab and Sirwan River

Flow duration curves (FDC) for both observed and simulated river discharge are shown in Figure 4.8. The match between the curves is generally good, although there is some under-prediction of discharge at high exceedance percentiles (i.e. low flows tend to be under predicted) and some over-prediction of flows in the 5-25 exceedance percentile range. Again, the under-prediction of low flows is due in part to the simple nature of the baseflow model adopted here and its parameterisation. The source of rainfall data and different ET_o used to drive the model had a significant effect on the shape of the FDC. Flows were under predicted over most of the range when the model was driven by the uncorrected TMPA-3B42 and over predicted when the model was driven by the uncorrected 3B42RT data with regardless $ET_{o\text{-}RS}$ data used. Overall, reproduction of the FDC was better when the model was driven by the corrected TMPA-3B42RT data than when it was driven by the TMPA-3B42 with $ET_{o\text{-}RS}$ HS data.

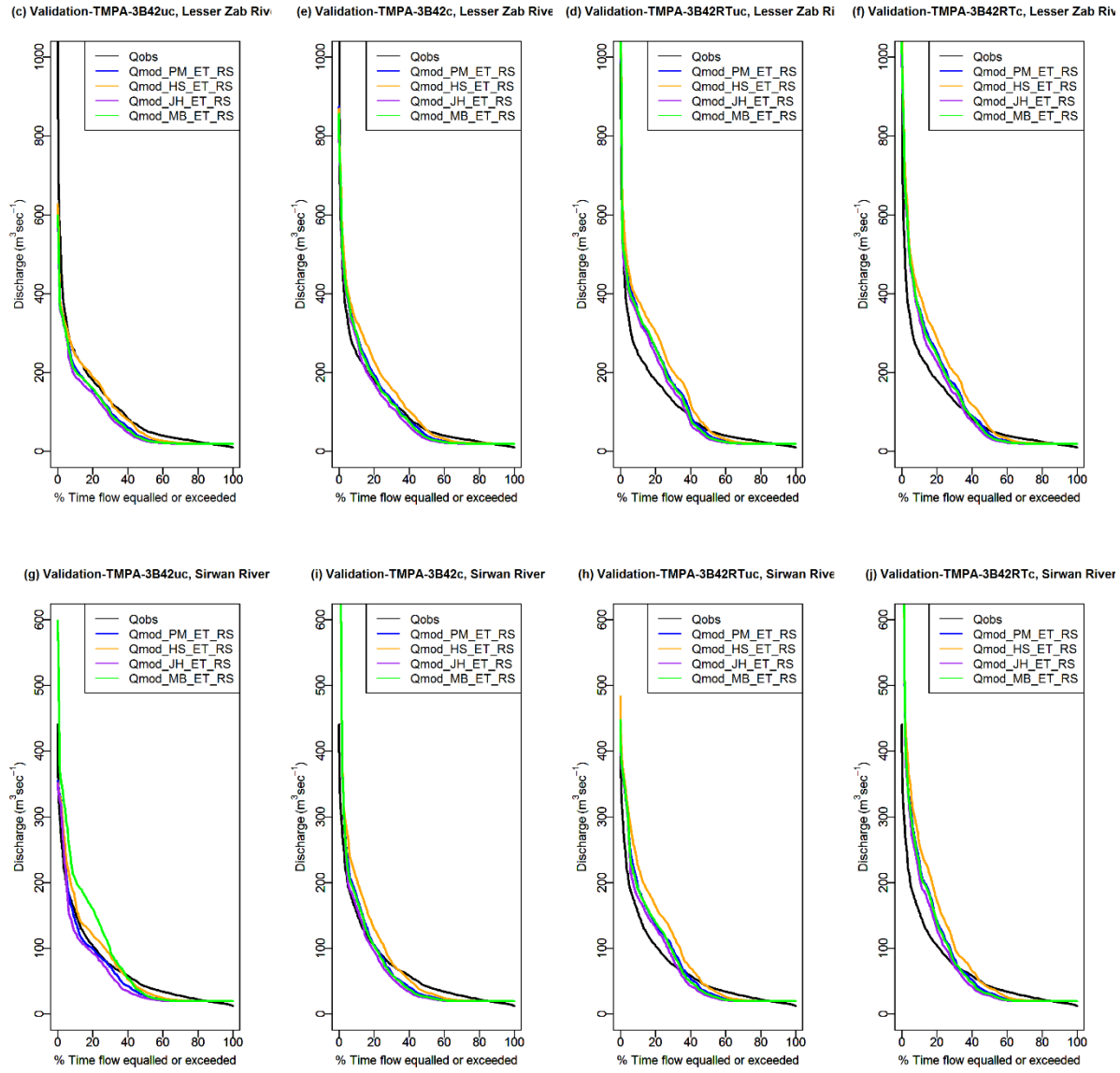

Figure 4. 8. Observed and simulated FDCs for the validation period (2012-2014) for Lesser Zab when the model was driven by the uncorrected and the corrected TMPA-3B42 rainfall data with different estimated ET_o-$_{RS}$ are shown in (a), (b), (c) and (d). FDCs for the validation period (2010-2014) for Sirwan River are shown in (e), (f), (g) and (h) when the model was driven by the uncorrected and the corrected TMPA-3B42 rainfall data with different estimated ET_o-$_{RS}$. The orange, purple, light blue and green lines show FDCs when model driven by the ET_o (HS, JH, MB and PM respectively).

4.4 Discussion

In this chapter, reference evapotranspiration (ET_o) was estimated based on four methods using ground-observed and RS-derived meteorological data (i.e., AIRS and reanalysis wind speed data from MERRA) at four stations in northeastern Iraq. For mean daily air temperature, AIRS and ground-based measurements were very similar for all sampled stations. The positive bias for T_a increased with increasing station altitude. Similarly, for RH the relationship between AIRS and ground-based measurements was strong, albeit with a negative bias, for all stations. Despite the better spatial resolution of the MERRA data compared to AIRS data, this chapter, explicitly, focuses on the value of the RS data and avoid reanalysis products as much as possible. Reanalysis data (which often integrate data from different sources) can be sensitive to observing system changes and there is often some uncertainty due to variations in both the models used and in the analysis techniques employed (Rienecker et al., 2011). Unfortunately, I were not able to avoid using reanalysis products completely and MERRA wind speed data (U_2) was required because to date no RS wind speed data are available. The relationships for *DS* and U_2 were weak for all stations. The effect of differences between RS and ground-based meteorological variables on ET_o rate will depend on the model sensitivity to the variable in question (i.e., if the model is sensitive to an input variable then predictions of *ET* will differ significantly if the RS estimate for that variable differs from the ground-based measurement; conversely, if the model is insensitive to the variable in question then *ET* will be relatively unaffected by errors in the RS estimates). Differences could be due to the different spatial reference frames employed, with meteorological stations recording point measurements and RS platforms observing spatially aggregated variables over large grid cells or pixels. As well as altering *ET* using empirical methods, differences in T_a estimates will also affect other temperature-dependent values such as vapour pressure deficit and Δ.

There was generally reasonable agreement between $ET_{o\text{-}RS}$ and $ET_{o\text{-}G}$ for all the ET_o methods evaluated, based on high R^2 values and regression line slopes close to unity compared with the predictions driven by ground-based measurements. However, there was some variation in model performance for individual stations. Regressions between the bias in input variables (RS versus ground) and the bias in ET_o estimates (calculated using RS versus the benchmark) for all methods are shown in Table A3. Strong and significant relationships were observed between the bias in sunshine duration and the bias in ET_o in the case of the JH and MB methods ($R^2 > 0.95$, $p < 0.05$) for all stations. This is not unexpected, given the dependence of these methods

on solar radiation (and indirectly *DS*) suggesting high sensitivity. Other relationships were insignificant – even for the bias in *ET* from the HS method versus the bias in T_a, possibly because the HS method also depends on the theoretical radiation flux density at the top of the atmosphere. The bias in ET_o-$_{RS}$ for the PM equation was most sensitive to *DS* and wind speed, reflecting the high importance of both radiative and aerodynamic terms in this method (by definition).

The PM model tended to predict lower ET_o than when using ground-based data for the Dukan station, but higher ET_o for the Sulaimani, Penjween and Charta stations. This is mainly due to the sensitivity of the PM method to meteorological input data (i.e. radiation, air temperature, humidity and wind speed: Allen et al., 1998). Thus, the effects of disparities between ground-level measurements and RS estimates can be significant on ET_o calculations especially in windy, warm and or dry conditions (Allen et al., 1998). For instance, T_a derived from RS overestimated ground-based measurements for the Penjween and Chwarta stations in the mountains (1284 and 1128 m ASL, respectively) but underestimated T_a at Dukan, which is located at lower altitude (690 m ASL). These results agree with the results reported by Ferguson and Wood (2010) which showed that the positive bias of near-surface air temperature from AIRS increased with increasing elevation. Similar to T_a, *DS* and U_2 also contributed significantly to the deviation of RS and ground-driven *ET* using the PM method due to high bias and RMSE for the RS-estimates of these variables compared to ground-based measurements.

In the cross-comparison of the ET_o methods (i.e., when the RS-driven models were compared with the benchmark data set), $ET_{o\text{-}RS}$ (HS) slightly underestimated $ET_{o\text{-}G}$ (PM: Table 4). This could be due to: (i) The absence of humidity terms in the HS method (Temesgen et al., 2005; Tabari et al., 2011) in contrast to the PM method in which ET_o is positively correlated with vapour pressure deficit. This is especially important in semi-arid environments were humidity deficits can be high (i.e., when low relative humidity results in a steep gradient in vapour pressure between the surface and the bulk atmosphere). (ii) The fact that temperature-based methods (HS) tend to underestimate ET_o at high wind speeds of >3 m s^{-1} (Allen et al., 2000). In the original PM method, wind speed is included via the aerodynamic resistance term (which is combined with the surface resistance, specific heat capacity and air density in the FAO version shown in Equation (4.6) via the constants 900 and 0.34). (iii) The fact that atmospheric transmissivity (the ratio of the global solar radiation at ground level to that received at the top

of the atmosphere, (Bo et al., 2009; Baigorria et al., 2004)) in semi-arid area tends to differ from other areas due to lower atmospheric moisture content (Bo et al., 2009). A number of other studies (Jensen et al., 1997; Kashyap and Panda, 2001; Yoder et al., 2005; Trajkovic, 2007; Landeras et al., 2008; Tabari and Talaee, 2011) have reported that the HS method can overestimate ET_o in humid environments and under estimate it in semi-arid regions (Tabari, 2009). Although a slight negative bias was also observed here, the HS model yielded lower RMSE values overall compared with the other methods suggesting that it is a reasonable method for estimating ET_o in semi-arid regions similar to our study area (even when driven by RS data). This result is in agreement with López-Urrea et al. (2006), Tabari (2009) and Tabari and Talaee (2011) who concluded that the HS method can be successfully used in semi-arid areas.

The positive bias obtained from comparisons between $ET_{o\text{-}RS}$ calculated using the JH and MB methods and $ET_{o\text{-}G}$ PM is in accordance with both Jensen et al. (Jensen et al., 1990) and Tabari et al. (Tabari et al., 2011) who found that these models tend to overestimate ET_o compared with the PM method, by as much as 30% and 60%, respectively. In this study the JH and MB methods overestimated the benchmark average annual ET_o at all stations (Figure 4.4) by between 9% and 40%. Instead, the average annual ET_o predicted by the HS method was similar to that estimated by the PM method for all stations (e.g., bias ranged between −0.6% and −9%).

This study did not take into account the effects of vegetation factors on the *ET* rate and, instead, focussed on climatic factors. ET_o expresses the evaporation power of the atmosphere at a specific location and time of the year and does not consider land cover characteristics and soil factors (Allen et al., 1998). If required, crop-specific *ETp* can be calculated from ET_o using crop-specific resistance terms in the PM equation or, more generally, using crop coefficients Allen et al. (1998) which account for differences in vegetation canopy characteristics such as leaf area index, canopy height and stomatal resistance. *ETa* can be calculated from *ETp* (or ET_o) if soil moisture content can be estimated, often via a linear reduction in *ETa*:*ETp* between a threshold moisture content and the permanent wilting point.

RS-derived precipitation and ET_o estimates were also combined to force the LEMSAR model in the Lesser Zab and Sirwan River catchments, assuming there is no ground-based meteorological observations. Compared to rainfall, evapotranspiration has little influence on the water balance at a daily time scale. The LEMSAR model had the highest efficiency with

$ET_{o\text{-}RS}$ (HS) compared to the other methods. This is may be because of underestimated of $ET_{o\text{-}RS}$ (HS (section 4.3.3) is balanced by less water lose in the water balance equation used in the LEMSAR model, leading to a good prediction of river discharge. The LEMSAR model performance in the Sirwan river basin was not as good as its performance in the Lesser Zab catchment. This may related to the fact that; using calibrated parameter for Lesser Zab catchment cannot represent characteristics of the Sirwan catchment when streamflow were predicted without calibrating the LEMSAR model to the observed river discharge data of this catchment; hydrological responses between both catchment are different (i.e. the Dukan catchment has fewer more extreme high flow events due to the permeable nature of this catchment than Sirwan catchments).

4.5 Summary

In this chapter, the accuracy of daily ET_o estimates derived from remote sensing ($ET_{o\text{-}RS}$) were assessed and compared with those derived from four ground based stations ($ET_{o\text{-}G}$) in Kurdistan (Iraq) over the study periods (2010-2014). Remote sensing data products used were near surface air temperature, relative humidity and cloud cover fraction from the Atmospheric Infrared Sounder / Advanced Microwave Sounding (AIRS)/ AMSU), and wind speed at 10 m height from MERRA (Modern-Era Retrospective Analysis for Research and Application). Four methods were used to estimate ET_o: Hargreaves - Samani (HS), Jensen - Haise (JH), McGuinness - Bordne (MB) and the FAO Penman Monteith equation (PM). Compared to $ET_{o\text{-}G}$ (PM) as the main benchmark, HS underestimated ET_o by 2%-3% (R^2 = 0.86 to 0.90; RMSE = 0.95 to 1.2 mm d^{-1} at different stations). JH and MB overestimated ET_o by 8% to 40% (R^2= 0.85 to 0.92; RMSE from 1.18 to 2.18 mm d^{-1}). The annual average values of ET_o estimated using RS data and ground-based data were similar reflecting the low bias in daily estimates. They ranged between 1153 and 1893 mm y^{-1} for $ET_{o\text{-}G}$ and between 1176 and 1859 mm y^{-1} for $ET_{o\text{-}RS}$. The overall performance of the LEMSAR is satisfactory as it meets the evaluation criteria in the Lesser Zab catchment. But it performs poorly in the Sirwan catchment. Model validation performance was best (highest NSE and *r*; lowest RMSE and bias) using the corrected 3B42 data product with $ET_{o\text{-}RS}$ HS method and poorest when the model was driven by uncorrected 3B42RT data with $ET_{o\text{-}RS}$ JH and MB methods in both catchments. The results suggest that TRMM data and $ET_{o\text{-}RS}$ can be used to drive rainfall-runoff modelling in data-scarce semi-arid catchments.

Chapter 5: Evaluation of terrestrial water storage variability in northern Iraq using a combination of GRACE, well data and water balance model estimates

Part of this chapter will be submitted as:

Najmaddin, P., Whelan, M. and Balzter, H (2017) Evaluation of water storage variability in northern Iraq using a combination of GRACE, well data and water balance modelling. *Remote Sensing of Environment (2017).*

5.1 Introduction

Water scarcity has long been a major problem across the Middle East (Joodaki et al., 2014) and is likely to increase in future under the combined pressures of climate change and rising demand due to rapid economic development and population growth (Michel et al., 2012). The catchments of many major rivers (e.g. the Tigris and the Euphrates) are shared by more than one country and the construction of dams has significantly contributed to reduced downstream river flows (Abdul Hameed et al., 2010). Groundwater is, therefore, increasingly relied upon for water supply in many areas. It is, therefore, important to understand and quantify spatiotemporal variations in groundwater storage for better water resource planning and management and to reduce unsustainable groundwater exploitation (Konikow and Kendy, 2005) (Stevanovic et al., 2009; Joodaki et al., 2014). This is often challenging due to a paucity of systematic observations at the regional scale (Chenoweth et al., 2011; Kavvas et al., 2011; Voss et al., 2013; Mulder et al., 2015). In chapters 3 and 4 the river discharge was simulated and evaluated based on RS data. In this chapter, GRACE-derived groundwater depletion in northern Iraq are compared and evaluated with observed well water depths and water balance predictions from the LEMSAR calibrated and validated on observed river discharge data.

5.2 Materials and Methods

5.2.1 Study area

The study area of interest in this chapter is Lesser Zab catchment and Hawler well monitoring zone which was described in (chapter 2, section 2.1).

5.2.2 *In situ* data

In situ data (i.e. gauge station and well data) used in this chapter was described in (chapter 2, section 2.2).

5.2.3 Remote sensing data

The remote sensing data of interest in this chapter is GRACE data which described in (chapter 2, section 2.3.4)

The arithmetic mean (*GRACE_TWSA*) calculation

The arithmetic mean (*GRACE_TWSA*) of the three data products (CSR, GFZ and JPL) was taken to minimize the uncertainties associated with the data processing. In addition, TWSA solutions were multiplied by the provided scale factors. Missing data were gap-filled using the na.spline method (R Core Team, 2014). In addition, uncertainty for *GRACE_TWSA* (U_{TWSA}) was calculated (Eq. 5.1) using provided gridded fields of leakage and GRACE measurement errors, which were downloaded as separate files from the NASA data server. Measurement errors are manifested as both random and systematic errors (Wahr et al., 2006). Leakage errors are residual errors after filtering and rescaling (Landerer and Swenson, 2012).

$$U_{TWSA} = \sqrt{(\sigma_m)^2 + (\sigma_l)^2} \tag{5.1}$$

where σ_m is the standard deviation of measurement error:

$$\sigma_m = \sqrt{(\text{variance \_measurment error})/\text{N}} \tag{5.2}$$

and σ_l is the standard deviation of leakage error:

$$\sigma_l = \sqrt{(\text{variance\_ leakage error})/N} \tag{5.3}$$

in which *N* is the number of pixels.

5.2.4 GLDAS data and groundwater storage estimates

Monthly GLDAS water storage prediction were obtained for the study period 2003-2014 from the NASA data server at http://grace.jpl.nasa.gov/data/get-data/land-water-content/. There

were converted to monthly anomalies ($S_{\_GLDAS}$) from the monthly average $\overline{GLDAS}$ for the period 2004-2009 (i.e. $S_{\_GLDAS} = GLDAS_i - \overline{GLDAS}$) where *i* is the month. This was then used to estimate the groundwater contribution to the total water storage anomaly from GRACE. This is facilitated by the fact that GLDAS data have the same spatial and temporal resolution as the GRACE data sets (Rodell et al., 2004). Uncertainty in $S_{\_GLDAS}$ was calculated using.

$$\sigma_g = \sqrt{\frac{\text{variance} - S_{\_GLDAS}}{N}} \tag{5.4}$$

where σ_g is the standard deviation of *GLDAS* data (6.45 mm for the Hawler well monitoring zone and 9.47 mm for the Lesser Zab catchment).

Groundwater residual anomalies (*GRACE*$_{\_GWRA}$) were calculated as the difference between *GRACE*$_{\_TWSA}$ and $S_{\_GLDAS}$ (Figure 5.3). This approach has been evaluated by (Rodell and Famiglietti, 2002; Yeh et al., 2006; Rodell et al., 2009; Voss et al., 2013; Bhanja et al., 2016) and it has been demonstrated that the groundwater component as the residual of the total water can be successfully isolated from the GRACE data using GLDAS data.

Total uncertainties in *GRACE*$_{\_GWRA}$ were calculated using:

$$u_{GWRA} = \sqrt{(\sigma_g)^2} + U_{TWSA} \tag{5.5}$$

where u_{GWRA} is the uncertainty in *GRACE*$_{\_GWRA}$.

5.2.5 Observed groundwater levels and groundwater storage anomalies

In order to validate the *GRACE*$_{\_GWRA}$, regional average groundwater depths were calculated based on raw well depth observations from 65 wells distributed across the Hawler well monitoring zone (Figure 2.1) using kriging (Boisvert and Deutsch, 2011). Average groundwater depth was converted into well level anomalies (i.e. deviations of equivalent water depth relative to the average well level between 2004 and 2009) and then multiplied by the

specific yield (*Sy*) (i.e. the ratio of the volume of water that drains from saturated rock to the total volume of the rock). *Sy* is dimensionless and typically has values in the range 0.01-0.3 (Moore, 2007). A sensitivity analysis of the assumed specific yield is also shown in Figure 5.1 (i.e. $Observed_{\_GWRA}$ calculated with different values of *Sy)*. The specific yield modified the magnitude of the time series of observed groundwater recharge anomaly but not the relative pattern. Hence, the specific yield is assumed arbitrarily to be 0.01 everywhere in the Hawler well monitoring zone and constant with time although, we acknowledge that *Sy* is a substantial source of uncertainty. Additionally, in order to establish the error associated with observed ground water level data the confidence interval (CI) 95% was calculated using:

$$95\%\mathrm{CI} = \overline{M} \pm 1.96 * \mathrm{SE} \tag{5.6}$$

where $\overline{M}$ is the mean value of observations and SE is the standard error of the mean.

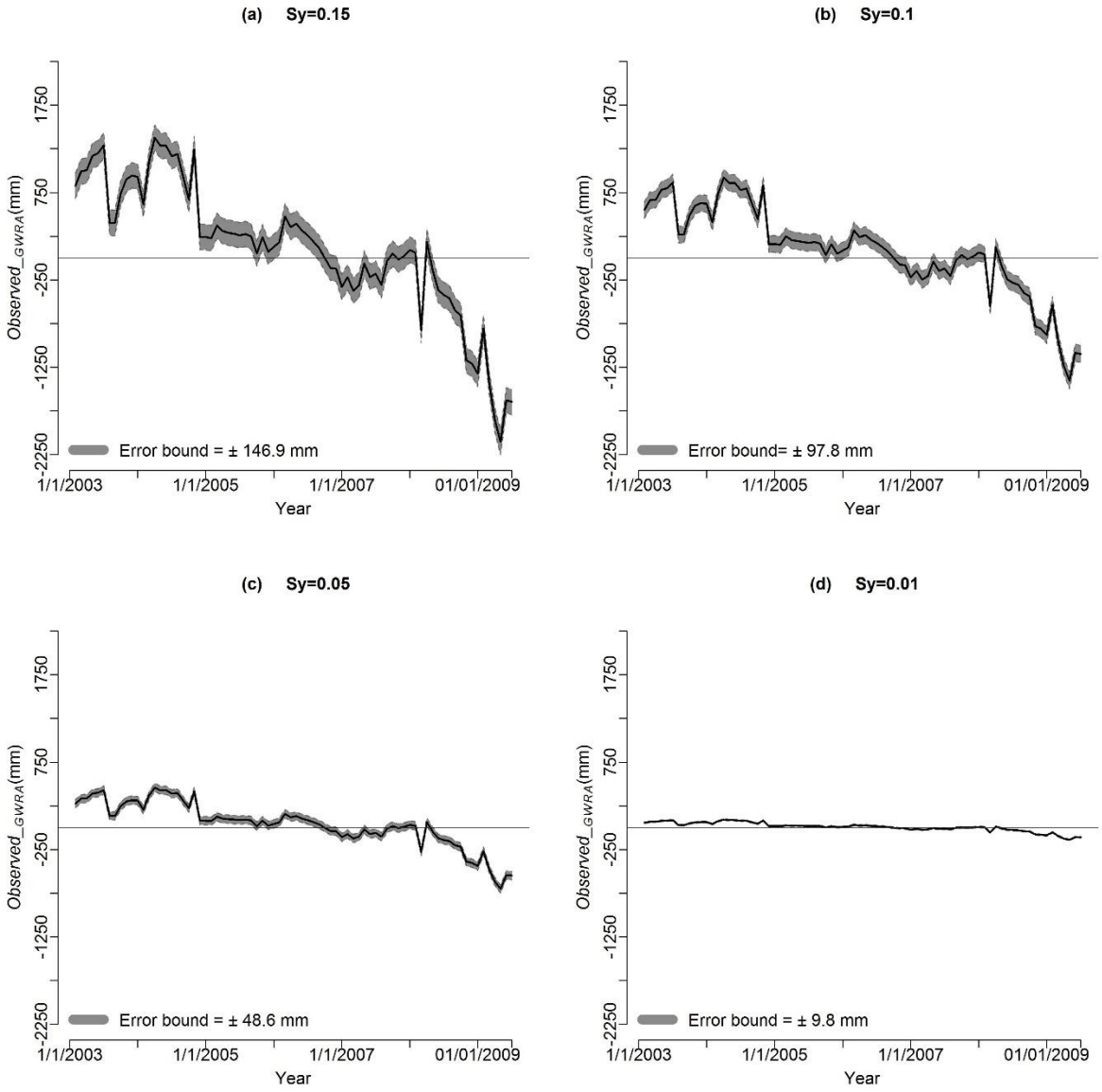

Figure 5. 1. Differences in the average observed groundwater anomaly in the Hawler well monitoring zone, assuming different values of specific yield for the period from 2003 to 2009 (note the different y-axis scales). The dark grey shaded area represents the 95% confidence interval (CI) derived from observed variability in well water depths.

5.2.6 Rainfall-runoff model

LEMSAR model applied in this chapter was described in chapter 3.2.4. It used to calculate the net catchment monthly change in total storage using Eq. 5.7. All terms are calculated on a daily basis using Euler's method of integration with a time step of 0.1.

$$\frac{\Delta S}{month} = \sum_{t=1}^{N=days} P - ET_a - q_b - q_{TF} - q_o - abstraction \qquad (5.7)$$

where ΔS is the total storage change (mm), t is time (d), P is precipitation (mm d^{-1}), ET_a is actual evapotranspiration (mm d^{-1}), q_o is overland flow (mm d^{-1}), q_b is groundwater discharge (mm d^{-1}) and q_{TF} is shallow throughflow (mm d^{-1}).

In order to compare these predictions with GRACE data, the monthly change in total water storage ($GRACE\_{}_{TWSC}$) was derived from $GRACE\_{}_{TWSA}$ using:

$$GRACE_{-TWSC} = GRACE_{-TWSA}(i+1) - GRACE_{-TWSA}\,(i) \qquad (5.8)$$

where *i* is an index for the month.

5.3 Results

5.3.1 GRACE_TWSA and GRACE_GWRA.

Figure 5.2 shows the *GRACE_TWSA* for the Lesser Zab catchment and the Hawler well monitoring zone, along with the trend lines over the monitoring period (2003 – 2014). U_{TWSA} was found to be 32.8 mm for the Hawler well monitoring zone and 69.7mm for the Lesser Zab catchment. Figure 5.3 also shows the *GRACE_TWSA* but, in addition, displays the *GRACE_GWRA* values, calculated as the difference between *GRACE_TWSA* and *S_GLDAS,* in terms of equivalent water heights, for the Lesser Zab catchment and the Hawler well monitoring zone. There is a clear trend in both areas of decreasing total water storage and groundwater storage (*GRACE_TWSA* and *GRACE_GWRA* trends were -33.72 ± 2.52 mm y^{-1} and -31 ± 1.8 mm y^{-1} for the Lesser Zab catchment, respectively and-35.4 ± 2.52 mm y^{-1} and -34 ± 2.04 mm y^{-1} for the Hawler well monitoring zone, respectively). u_{GWRA} was found to be 38.73 mm and 79.17 mm for the Hawler well monitoring zone and Lesser Zab catchment respectively (grey shading).

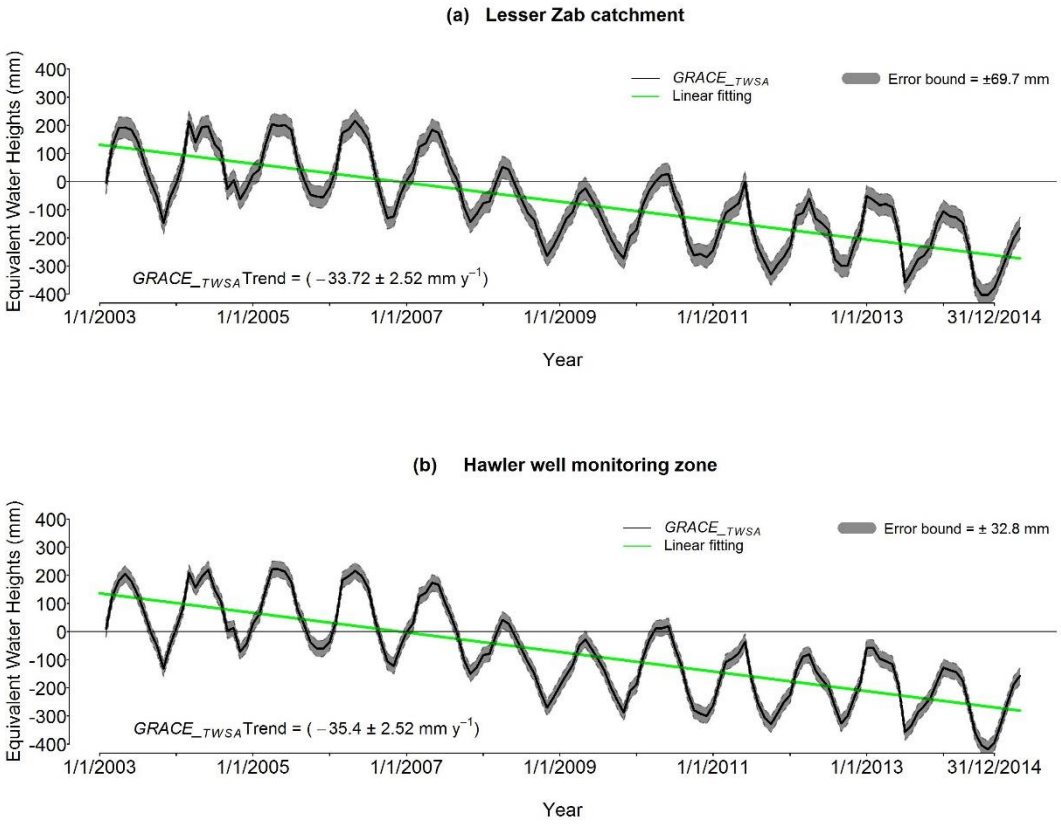

Figure 5. 2. Temporal variability of *GRACE_TWSA*, (a) in the lesser Zab catchment and (b) in the Hawler well monitoring zone from January 2003 to December 2014. The green lines show the linear trends in *GRACE_TWSA* over the whole period. The dark grey shaded area represents the uncertainty error in *GRACE_TWSA* (U_{TWSA}).

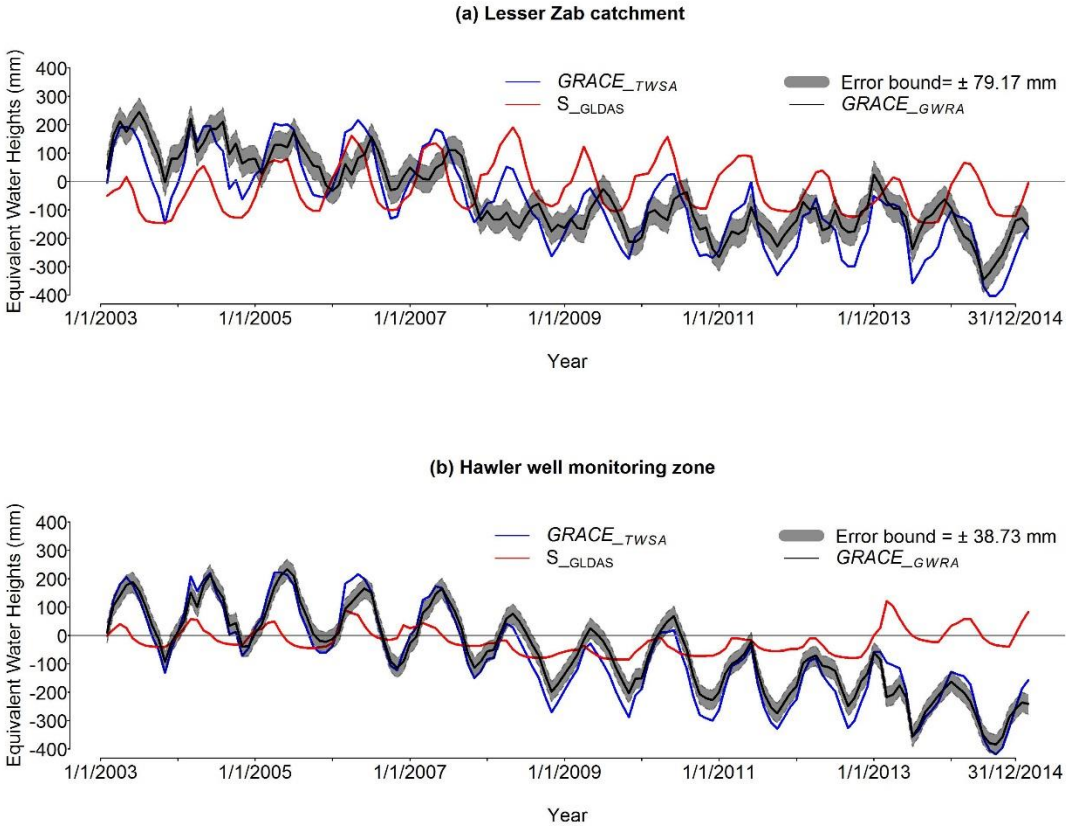

Figure 5. 3. GRACE-total water storage anomalies (GRACE_TWSA), the terrestrial water storage (snow pack and soil) anomaly ($S_{\_GLDAS}$) and GRACE-groundwater residual anomalies (GRACE_GWRA) for the Lesser Zab (a) catchment and the Hawler well monitoring zone (b) over the period 2003-2014. The dark grey shaded area represents the total uncertainties in GRACE_GWRA (u_{GWRA}).

Monthly precipitation and reference evapotranspiration (ET_o) are shown in Figure 5.4 for each zones. This is, to some extent, explained by decreasing rainfall in both areas over the study period (i.e. negative trend of -22 and -9 mm y^{-1}) although the gradient in rainfall and in the net modelled water balance from LEMSAR are not as high as those for groundwater storage estimates derived from GRACE. The seasonality in *GRACE_TWSA*, *GRACE_GWRA* and rainfall are shown in Figure 5.5. *GRACE_TWSA* and *GRACE_GWRA* tend to be higher during winter wet season (October to April) and lowest during the summer (May to September).

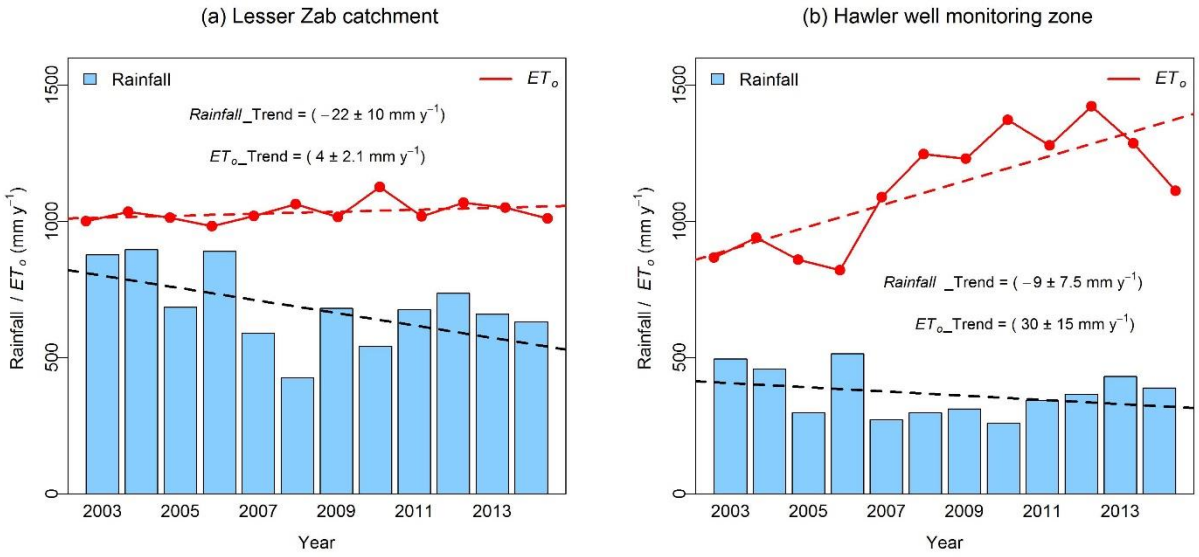

Figure 5. 4. Annual precipitation and reference evapotranspiration for (a) the Lesser Zab catchment and (b) the Hawler well monitoring zone from 2003 to 2014. The dashed red and black lines show linear trends in evapotranspiration and rainfall, respectively.

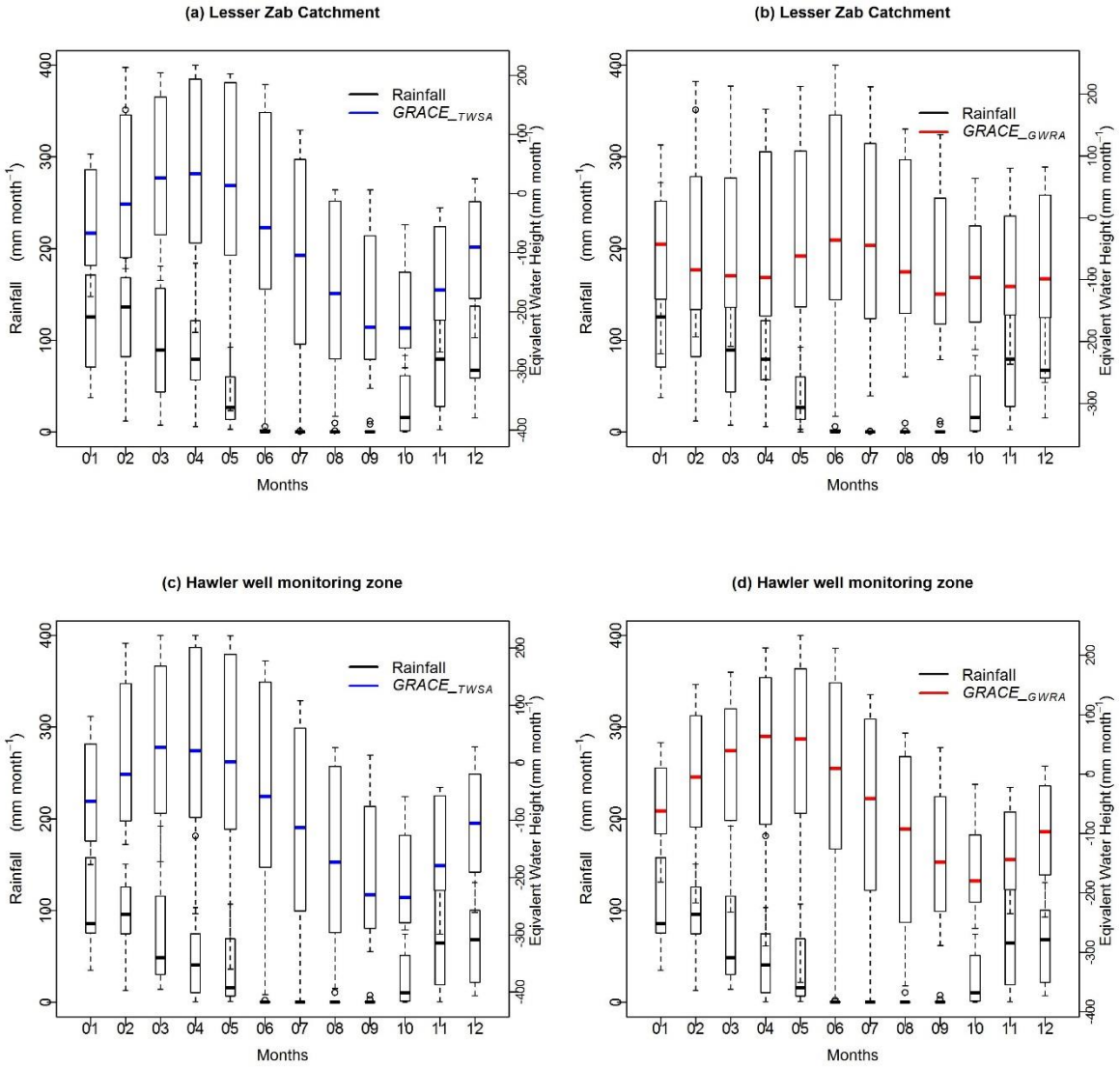

Figure 5. 5. Boxplots of (left) GRACE_$_{TWSA}$, (right) GRACE_$_{GWRA}$ and monthly precipitation for the Lesser Zab catchment (a and b) and the Hawler well monitoring zone (c and d) from 2003 to 2014. The horizontal line within each box represents the median, the box boundaries represent upper and lower quartiles and the dashed whiskers show the maximum and minimum values.

5.3.2 Comparison between Observed_$_{GWRA}$ and GRACE_$_{GWRA}$ in the Hawler well monitoring zone.

Figure 5.6 shows a comparison between *GRACE_$_{GWRA}$* and *Observed_$_{GWRA}$* (assuming *Sy* =0.01). Overall, both variables have a decreasing trend over the period. The *GRACE_$_{GWRA}$* data suggest a total annual groundwater loss of 0.41 km^3 (recharge area = 15553 km^2), over the

study period 2003-2009. The magnitude of observed groundwater loss in the Hawler well monitoring zone depends on the value chosen for *Sy*, so the data shown should be viewed in relative terms. That said, there appears to have been a dramatic decrease in mean observed groundwater level in late 2004 and 2008-2009. The coefficient of determination (R^2) between *GRACE_GWRA* and *Observed_GWRA* was just 0.26 but the slope of the regression was close to 1 when the line was constrained to go through the origin and the RMSE was 92.4 mm y^{-1}. The strong seasonal patterns in *GRACE_GWRA* is also seen in the observed data but is less regular. The gradient in *GRACE_GWRA* with time was slightly steeper than the trend in *Observed_GWRA*.

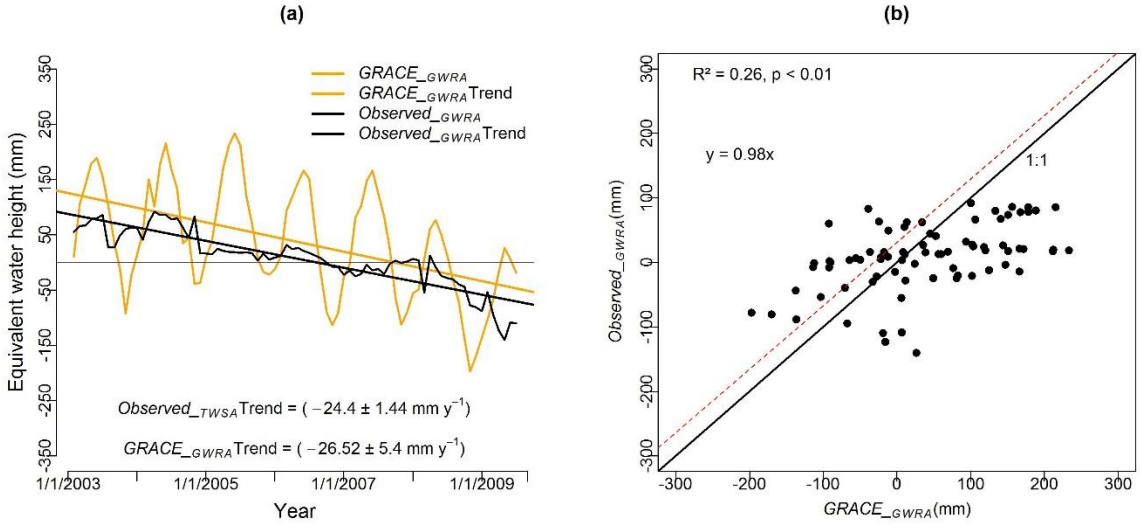

Figure 5. 6. (a) Comparison of GRACE_GWRA and Observed_GWRA for the Hawler well monitoring zone. Linear fits are shown with straight lines. (b) Scatter plot of GRACE_GWRA against Observed_GWRA.

5.3.3 Simulated river discharge in the Lesser Zab catchment

Figure 5.7 shows the simulated and observed river discharge in the Lesser Zab river above the Dukan reservoir. The black line shows the observed river discharge and the green line shows the simulated discharge. Generally, both the magnitude and the seasonal patterns in the observed discharge are well-captured by the model, although there was some deviation at high

flows (hydrograph peaks under-predicted by the model) and baseflow is also under predicted. Goodness-of-fit statistics between simulated and observed river discharge for calibration and validation are presented in (Chapter 3). The daily predicted groundwater flow was significant in low flow periods. Predicted melt-derived flow can be substantial in spring and may contribute to some occasional events and groundwater recharge. Simulated river discharge is plotted against observed data in Figure 5.7 (b), along with the 1:1 line and the best fit linear regression. The slope of the regression equation was close to unity, (0.98) suggesting a good match between modelled and measured discharge, overall. The simulated net-catchment water balance is shown in Table 5.1. Simulated mean river discharge decreased annually by -18 mm y^{-1}. This could be partly explained by an increase in reference evapotranspiration (ET_o) by 6 mm y^{-1}: Table 5.1 over the study period. However, the actual annual evapotranspiration predicted by the model is fairly constant (constrained by soil moisture availability) and the decrease in discharge is most like to be driven by the decrease in rainfall.

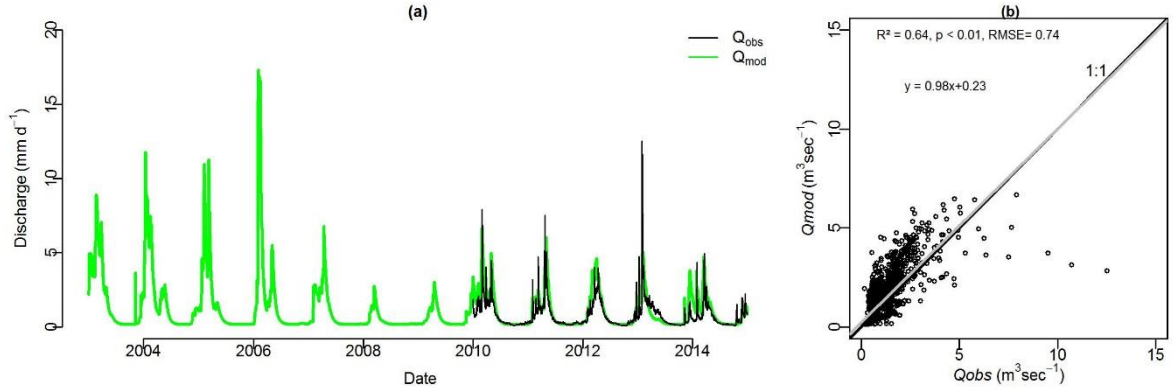

Figure 5. 7. (a) Observed and simulated hydrographs for the Lesser Zab river above the Dukan reservoir. Measured discharge in black (2010 -2014) and simulated in green (2003-2014). (b) Scatter plot of simulated discharge against measured discharge over the period 2010-2014. Linear fit is shown in grey line. The solid line indicates the 1:1 relationship.

Table 5. 1. Annual modelled water balance for the Lesser Zab catchment over the study period 2003-2014.

Date	Precipitation (mm y^{-1})	ET_o (mm y^{-1})	ETa (mm y^{-1})	Simulated discharge (mm y^{-1})	Change in Storgae (mm y^{-1})
2003	878	1267	374	506	-2
2004	897	1317	409	491	-3
2005	685	1288	344	348	-7
2006	890	1246	375	529	-14
2007	590	1297	319	298	-27
2008	426	1356	295	131	0
2009	681	1292	367	306	8
2010	542	1433	276	282	-16
2011	677	1295	359	322	-4
2012	738	1362	380	352	6
2013	660	1338	356	308	-4
2014	633	1285	365	285	-17
Trend (mm y^{-1})	**-19**	**6**	**-2**	**-18**	

5.3.4 Comparison between GRACE and LEMSAR predictions

Comparison between the simulated water balance (Equation 5.7) and total water storage change from GRACE (Equation 5.8) are shown in Figure 5.8. The LEMSAR model was able to capture the changes in total terrestrial water storage estimated by GRACE quite well. The slope for the best-fit regression was 0.75 although the R^2 was low (0.26, $p<0.01$). The relative pattern of water storage was calculated by adding up the change in storage from GRACE and LEMSAR. In each case, the initial storage was set at an arbitrary value of 100 mm. It should be noted that this does not reflect the actual water storage in the system- simply the relative pattern over time in both, so as to facilitate a comparison between GRACE observations and LEMSAR predictions (Figure 5.8c and d). The predicted trend in the relative simulated water balance from LEMSAR was -15 ± 1.44 mm y^{-1} between 2003 and 2014 compared to -33.72 ± 2.52 mm y^{-1} from GRACE. The two graphs differ mainly in the magnitude of winter peaks and

summer troughs with LEMSAR underestimating terrestrial water storage in winter between 2003 and 2007 and over estimating storage in summer between 2008 and 2013. The amplitude of the simulated (LEMSAR) water balance was lower than that for *GRACE_TWSA*. The coefficient of determination between the relative *GRACE_TWSA* and simulated water balance was high (R^2 = 0.69, p< 0.01) but the slope (0.44) was substantially less than unity.

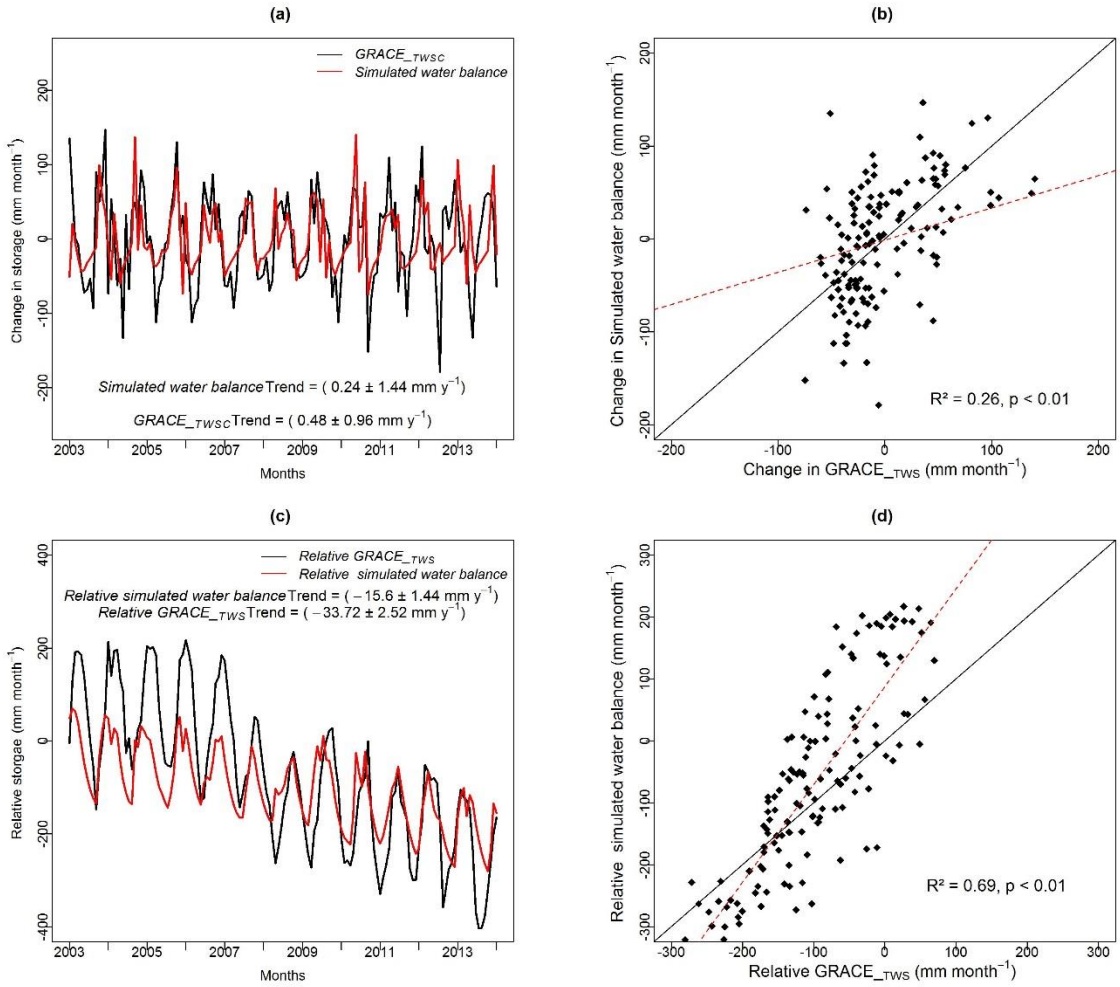

Figure 5. 8. (a) Monthly changes in total water storage estimated from GRACE and simulated by LEMSAR over the period 2003-2014. (b) Scatter plot between GRACE total water storage anomaly change and mass changes predicted by LEMSAR. (c) Comparison between the relative patterns of total water storage from GRACE and LEMSAR. (d) Scatter plot of relative total water storage predicted by LEMSAR (x-axis) and GRACE (y-axis). Linear fits of two variables are shown with the dashed red line. Black line shows 1:1 line.

5.4 Discussion

Other studies have used GRACE data to assess trends in water resources in this region (Voss et al., 2013; Mulder et al., 2015). However, these data have never previously been corroborated by measured data. Here, in this chapter, for the first time, GRACE observations with observed well data in the Northern Iraq have compared. In this chapter, a rainfall-runoff model driven by observed meteorological data and calibrated and validated using observed river discharge observations have also applied. The $GRACE\_{TWSA}$ data suggest that the total water volume stored in the soil, surface waters and groundwater in the region has decreased by approximately 0.55 km^3 each year for the Hawler well monitoring zone and 0.39 km^3 each year for the Lesser Zab catchment over the study period 2003-2014. This loss is alarming because the region was already facing severe water scarcity. Very low precipitation in late 2005 and 2008-2009 probably explains the bulk of the dramatic decreases in $GRACE\_{TWSA}$ signals over this period. Thereafter annual change in the GRACE signal decreases (but does not disappear entirely). Rainfall on the other hand, has been approximately stable since 2009. This suggests that a new (low storage) steady state where the out flow of the system (river discharge, evapotranspiration and enhanced evapotranspiration resulting from irrigation of abstracted water) is in balance with lower recharge values (as suggested by Voss et al. (2013) and Mulder et al. (2015)) may not yet have been established .

There is considerable uncertainty in the $GRACE\_{TWSA}$ values which could be influenced by spatial leakage from neighbouring regions (Bhanja et al., 2016; Rodell and Famiglietti, 2002; Longuevergne et al., 2010; Rateb et al., 2017) although the $GRACE\_{TWSA}$ trend for a larger study area was estimated by Voss, *et al*. (Voss et al., 2013) at 27.2 ± 0.6 mm y^{-1} and Mulder, *et al.* (Mulder et al., 2015) at -39 ±8 mm y^{-1} are comparable to the trends I report here.

The analysis presented here suggests that groundwater depletion is by far the main single contributor to the observed negative $GRACE\_{TWSA}$ trend (i.e. accounting for approximately 70% of the total volume of the water loss in the Lesser Zab catchment and 78% in the Hawler well monitoring zone). Common factors that affect ground water depletion in both areas include; (1) Meteorological drought (i.e. low precipitation combined with high ET_o. Several years of below-normal precipitation (Figure 5.4) have contributed to the decline in ground water levels. Average annual precipitation was low in 2008 and 2010 but it has increased after 2011 (e.g. >700 in 2012). This implies that the observed negative trend in $GRACE\_{TWSA}$ is unlikely to be

related to changes in precipitation alone but may affected by also other factors (2) the dominance of karstified aquifers which have high recharge during wet periods but also fast response through springs which can result in depletion during dry periods (Stevanovic et al., 2009); (3) human activity, such as increases in abstraction to maintain crop yields via increased irrigation. Over-abstraction can lead to decreases in groundwater storage even in the absence of meteorological drought. However, in dry years, abstractions tend to increase as farmers attempt to supplement reduced rainfall with extra irrigation exacerbating the effects of reduced recharge on ground water storage. *In situ* data were used to corroborate this assertion including the documented drilling of 7303 extra wells to exploit groundwater resources according to the well database (Table 2.3). Almost 62% of wells in the Lesser Zab catchment and 60% in the Hawler well monitoring zone are used for irrigation (Figure 5.9), which is common in Arabian countries (Richey et al., 2015). This is likely to have resulted in a rapid increase of groundwater consumption in the study period and may go some way to explain the deviation of modelled water storage calculations (which are only driven by meteorological data) from the GRACE observations and well water levels.

For both areas, results show that the combined contributions of over-abstraction and variation in precipitation exposes the groundwater system to additional stresses. For instance, according to the well database (Table 2.3), approximately 14% of wells in the Hawler well monitoring zone and 28% in the Lesser Zab catchment dried-out completely between 2003 and 2010. Water level is deeper than 100 m > 65% of wells in the Hawler well monitoring zone and 62% in the Lesser Zab catchment (Table 2.3).

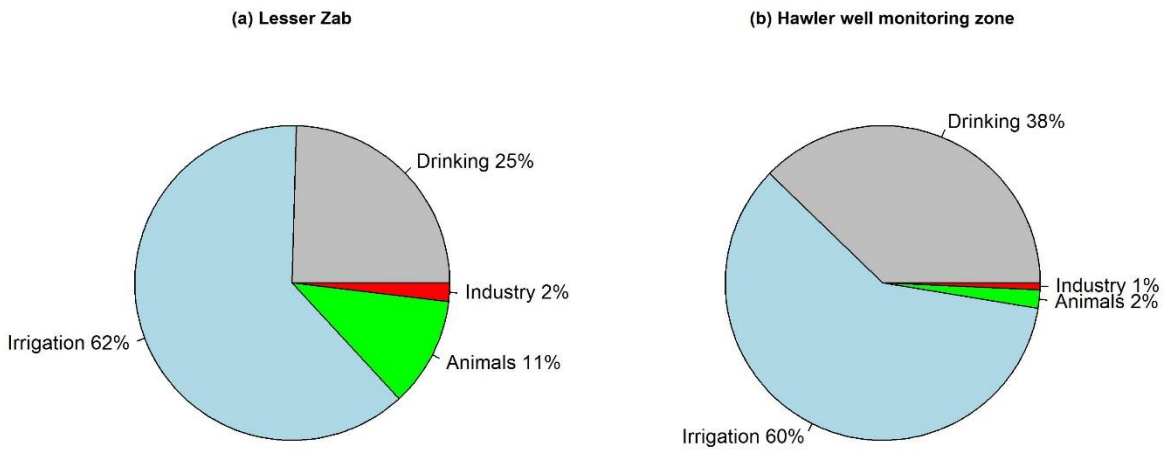

Figure 5. 9. Pie chart of principal usage for existing wells in (a) the Lesser Zab catchment and (b) the Hawler well monitoring zone (Ministry of Agriculture and Water Resources in the Kurdistan Regional Government).

Although the observed and GRACE-based GWS anomalies show strong seasonality in the Hawler well monitoring zone, the gradient of $Observed\_{GWRA}$ was lower than that for the $GRACE\_{GWRA}$. There are several potential explanations for this deviation including the lower spatial resolution of GRACE products (1° x 1°), significant uncertainty in the applied scaling factors (Landerer and Swenson, 2012) and uncertainty (u_{GWRA}) in the $GRACE\_{GWRA}$. There is also significant uncertainty in specific yield assumptions to change observed groundwater levels to EWH.

The good performance of LEMSAR-predicted river discharge (R^2=0.64, p<0.01, slope= 0.98) compared to observed discharge (2010-2014) using measured meteorological data suggests that it can provide good estimates of the water balance (Table 5.1). This is confirmed by reasonable agreement between LEMSAR-derived water balance calculations and total water storage changes from GRACE (Figure 5.8). The seasonal amplitude of storage changes differed in all months ($GRACE\_{TWSC}$ estimates had larger amplitude than the simulated changes in storage) which was manifested as a lower storage loss in LEMSAR compared with $GRACE\_{TWSA}$ in the Lesser Zab catchment. This deviation of LEMSAR total water storage estimates from GRACE

observations support the hypothesis outlined above that meteorological drivers for storage depletion have been exacerbated by other factors. The most obvious additional factor affecting groundwater levels in this region is abstraction, which is believed to have increased in recent years. Once constructed, new wells encourage irrigation in areas where previously irrigation may have been limited, facilitating an unsustainable level of abstraction, even when meteorological drought has passed. It is very difficult to estimate over abstraction. However, if we assume that abstraction is equal to the difference between the storage changes estimated from GRACE and the equivalent LEMSAR outputs (Figure 5.8c), more than 50% of the total water loss may be related to abstraction. Explanation for the difference in yearly mass variations between GRACE and LEMSAR may related to the structure of LEMSAR's groundwater model which has a low storage capacity compared to natural systems and forecasting issues in *GRACE-$_{TWSA}$* itself.

5.5 Summary

Evaluating groundwater resources is crucial for water resources management and policy making. The main goal of this chpter is to explore the capability of the Gravity Recovery and Climate Experiment (GRACE) satellite to quantify multi-annual groundwater trends over the semi-arid land of North Iraq, a region with scarce hydrological and meteorological observations and subject to immense pressures on its limited water resources from urban expansion, agricultural intensification and water demands caused by the significant migration of refugees. The mean of three different GRACE-derived data products for total water storage (*GRACE$_{_TWSA}$*) and monthly soil water content predictions from near-surface hydrological model simulations from the Global Land Data Assimilation System (GLDAS) were used to derive GRACE ground water residual anomalies (*GRACE$_{_GWRA}$*) over the study period 2003 - 2014. These estimates were compared with observation data from 65 wells (*Observed$_{_GWRA}$*). A daily lumped water balance model (the Leicester Model for Semi-Arid Regions: LEMSAR) calibrated on river discharge data in the Lesser Zab catchment was used to calculate the terrestrial water balance independently, using meteorological data from four ground-based stations. Total water storage in the study area decreased significantly over the study period. Trends in *GRACE$_{_TWSA}$* were approximately -33.72 ± 2.52 mm y^{-1} equivalent water height (EWH) for the Lesser Zab catchment and -35.4 ± 2.52 mm y^{-1} for the Hawler well monitoring

zone. Trends in $GRACE_{\_GWRA}$ and $Observed_{\_GWRA}$ were similar and indicate that the well monitoring zone has lost groundwater over the period at an average of -26.52 ± 5.4 and -24.4 ± 1.44 mm y^{-1} respectively. The trend in modelled water storage predicted by LEMSAR was approximately -15 ± 1.44 mm y^{-1} for the Lesser Zab catchment. This suggests that only about half of the decrease in water storage in this region can be explained by meteorological driver. The rest could be due to increased (unsustainable) abstraction from existing and a new wells in the region.

Chapter 6: General Discussion and Conclusions

6.1 Meeting the aim and objectives

Water is an important precious in arid and semi-arid regions where it is often in short supply and, therefore, needs to be managed more carefully. Good management requires a solid understanding of the stocks and flows of water, including consideration of spatial and temporal variability. This understanding can be acquired through the collection and analysis of data and via the construction of conceptual models. Unfortunately, however, the availability of hydrological studies in many semi-arid catchments is poor leading to non-exist ant or inadequate water recourses management strategies. One issue is the common paucity of observations of meteorological variables, water storage (e.g. groundwater level) and river flows, either because of low levels of monitoring investment of the retention of data by government agencies (i.e. data are un available to scientists). Remote sensing offers a number of opportunities for filling data gaps or for substituting ground-based observations entirely. Satellite sensors can now yield estimates of meteorological data (e.g. rainfall temperature, relative humidity and solar radiations flux density) which can be used to drive models of the terrestrial water balance. Satellite data can also be used to estimate terrestrial water storage via systematic changes to the earth's gravitational field. Whilst such data have been available for some time now, their accuracy relative to ground based data) and their utility for hydrological investigations (i.e. for driving hydrological models) remains uncertain. If they can be shown to give reliable estimates of the variables required to calculate (and validate) water fluxes and stores, these methods have tremendous potential for improving systematic water resources management in these water scarce areas. Different algorithms and regression equations of various complexity and theoretical foundations are used to convert raw RS signals into hydrological variables. Such methods are of course, subject to uncertainty which will clearly impact the quality of any simulations using RS data. However, traditional observations are also impacted by uncertainty and measurement errors. Although, RS data can provide a spatial scale that may better correspond to the size of the catchment area (instead of point data). They are hitherto scarcely used in hydrological modelling. This may be related to the lack of ground observation data to verify the RS data.

Given this background, the overall aim of the thesis was to develop a conceptual catchment scale rainfall-runoff model framework using remote sensing data in order to simulate river discharge and groundwater storage variability in a data-scarce semi-arid region. This

framework could then be used to improve present and future water resource management. To achieve this aim the following objectives were accomplished:

1. **To develop a conceptual rainfall-runoff model framework which is parsimonious (i.e. has a low number of easily identifiable parameters) and which can run using a minimum input data set of daily temperature and precipitation.**

The Leicester Model for Semi-Arid Regions (LEMSAR) model (section 3.2.4) has been developed to simulate river discharge at the catchment outlet. LEMSAR attempts to capture the important processes involved in precipitation transfer to river discharge. Briefly, the catchment is conceptualised using three (lumped) moisture stores: (1) a single soil store, characterised by its depth (z), whole profile porosity (ϕ) and by hydraulic parameters which describe the relationship between soil water content and unsaturated hydraulic conductivity; (2) a groundwater store which is augmented by recharge from the soil and depleted by baseflow to the river and (3) a time-variable snowpack. During times of precipitation events soil storage is filled and emptied by drainage described the unit hydraulic gradient (gravity flow) using the g method. LEMSAR model has low data requirements which (daily rainfall and reference evapotranspiration) and a simple conceptual model structure which requires the evaluation of only eleven parameters. The groundwater store model is the weaknesses of the LEMSAR. Currently, a very simple linear storage conceptualisation is employed in LEMSAR with an arbiter choice of initial storage and calibrated parameters. This clearly provides a poor description of low flow in the catchment and also probably misrepresents the contribution of groundwater flow during storm events-due to the karstic nature of the aquifers have. The LEMSAR model was written in R, which allows to inclusion of additional process representations, uncertainty and automatic calibration.

2. **To evaluate the ability of this conceptual model to simulate river discharge at the catchment outlet in a semi-arid catchment.**

In Chapter 3, the LEMSAR model was tested and evaluated in the Lesser Zab catchment in North Iraq. Overall, model performance for predicting discharge was reasonable, particularly given the relatively simplistic assumptions made and the large size of the catchment. This suggests that runoff dynamics in this catchment are principally controlled by the soil moisture

balance and that groundwater dynamics and snow melt make relatively small contributions to the shape and magnitude of the hydrograph (although snow melt is predicted to be significant in spring and baseflow is important in the dry season). However, significant uncertainty exists in the model simulations reported, manifested as equifinality. The aleatory component of this uncertainty could be quantified using GLUE which defines uncertainty bounds on predicted flows (resulting, in part, from poorly constrained calibration) but epistemic uncertainty is unknown and likely to be significant.

3. **To evaluate the utility of satellite-based precipitation data to drive the rainfall-runoff model and to compare the predictions of runoff which are generated with those generated using ground-based meteorological data (i.e. simulating reduced input data availability and quality).**

The utility of satellite-derived rainfall data to force the LEMSAR model were evaluated in Chapter 3. TMPA data products were biased towards an under-estimation of observed rainfall and needed to be corrected. A bias-correction approach was employed, which rescales standard scores (z scores) using the mean and standard deviation of the gauged rainfall data. Overall the TMPA-3B42 data product out-performed the 3B42RT data in terms of the Probability of Detection (POD), the Heidke Skill Score (HSS) and the False Alarm Ratio (FAR) compared with gauged rainfall. Hydrological model performance was also generally better when driven by the corrected 3B42 data than when the 3B42RT data were used. When LEMSAR was driven by corrected TMPA- 3B42c rainfall, predicted runoff in the validation period was as good as or better than that predicted using gauge-derived data. This suggests that the corrected TMPA rainfall data particularly TMPA-3B42 (or equivalent data from GPM) can be used to predict river discharge in this catchment which may be useful for future water resources management.

4. **To estimate reference evapotranspiration (ET_o) from remote sensing (RS) data and to compare these estimates with those generated using ground-based meteorological data (i.e. simulating reduced input data availability and quality).**

Chapter 4 assessed the validity of using daily RS-derived meteorological variables for estimating daily ET_o compared with ET_o from the same models driven by ground-based meteorological variables, for four stations in northeastern Iraq. The results were also compared with a benchmark model (PM) driven by ground-based meteorological observations. The good

agreement (i.e., low RMSE and bias and high r) between AIRS-derived and ground-based data, particularly near-surface air temperature, and the generally good performance of the *ET* models compared to the benchmark data set, suggest that AIRS data can be used as alternatives to conventional meteorological data to estimate daily ET_o with reasonable accuracy. Considering the low density of ground-based stations and the paucity of climatological records in regions such as Iraq, this is encouraging for future hydrological studies and for better-informed water management. The application of the PM method is limited in many semi-arid regions of the world by lack of required weather observations. In such circumstances, simpler models are often used to estimate ET_o. In this case, the RS-driven HS method produced better ET_o estimates (compared to the PM equation as a benchmark) than the other models. This confirms others reports about the performance of the HS model (López-Urrea et al., 2006; Tabari, 2009; Tabari et al., 2011) which should be used where complete weather observation data are lacking and can also can be successfully employed using RS data to yield accurate and useful daily ET_o estimates. Some reanalysis data products already exist which attempt to estimate ET_o using a combination of RS data and ground-based data and numerical models (e.g., MERRA-2). Future work could usefully compare ET_o estimates generated here with those predicted by MERRA-2. RS-derived precipitation and ET_o estimates were also combined to force the LEMSAR model in the Lesser Zab and Sirwan river catchments. Different river discharge simulations were performed, driven by daily uncorrected and corrected TMPA rainfall data sets with different estimated $ET_{o\text{-}RS}$ values. In the Lesser Zab catchment, the LEMSAR model performance was better when it was driven by the corrected TMPA-3B42 data with $ET_{o\text{-}RS}$ (HS) than when 3B42RT was used with $ET_{o\text{-}RS}$ (PM, JH and MB). In the Sirwan river catchment, in which optimized parameter values from the Lesser Zab catchment were used to simulate river discharge, LEMSAR performance was relatively poor. For example, the correlation between simulated river discharge and observed river discharge was low (e.g. NSE < 0.5). This may related to the fact that, although the both catchments are neighbours, the hydrological processes operating are quite different. It also leads weight to the argument that good hydrological model performance can rarely be achieved without catchment-specific calibration (Post and Jakeman, 1999).

5. **To evaluate variations in total terrestrial water storage using a combination of remote sensing data (GRACE), observed well data and rainfall-runoff modelling.**

In Chapter 5, total water storage and groundwater storage variability were evaluated in north-eastern Iraq using a combination of GRACE data, well observation and modelling. The results show that total water storage has been depleted significantly over the period 2003-2014. This trend, in part, reflects prevailing meteorological conditions (e.g. declining rainfall) but this has probably been exacerbated by increased abstraction which may continue into the future, even if rainfall increases. The reasonable correlation between GRACE observations and well levels confirms that GRACE data can be used to monitor the variability of total water storage in the study area. Other studies have used GRACE data to assess trends in water resources in this region such as (Voss et al., 2013; Mulder et al., 2015). However both studies suggested that TWS decreased by 27.2 mm y^{-1} and 39 ± 8 mm y^{-1} respectively between January 2003 and December 2009, unfortunately, these studies were unsupported by ground-based observations of water table levels to verify their results.

Changes in total water storage from LEMSAR were well correlated with GRACE observations but the slope of the decreasing trend predicted by LEMSAR was significantly lower than that implied by both GRACE and well level observations. This could be imply that depletions in groundwater level have been markedly increased by abstractions (which are not taken in to account in LEMSAR). The increase in well numbers documented here suggest that abstraction have significantly increased and that water resources in this region are unlikely to recover unless abstractions are more rigorously managed. Reduction in human dependence on groundwater (e.g. by adopting techniques such as rainwater harvesting (Al-Ansari et al., 2014) and more efficient water use (e.g. drip irrigation (Zakaria et al., 2012) are also urgently required to bridge the supply-demand gap for both domestic and agricultural purposes.

6.2 Conclusions

The research presented in this thesis has focused on developing and testing a new conceptual lumped rainfall-runoff model to simulate river discharge and evaluate ground and surface water storage variability in data scarce semi-arid regions. The LEMSAR model contains only eleven parameters that require calibration and has quick simulation times at daily time-steps. The LEMSAR model uses daily rainfall and reference evapotranspiration (which can be generated using a number of methods, depending on the availability of meteorological data) input to produce a time series of estimated river discharge. The model can be forced by either *in situ* meteorological data or remote sensing data. Overall, remote sensing data (TMPA and $ET_{o\text{-}RS}$) showed reasonable potential for forcing rainfall-runoff models. Simulated discharge was reasonable during calibration periods according to the statistical criteria used in this study (i.e. NSE= 0.75). LEMSAR model validations were also good suggesting satisfactory simulation of daily river flows at the catchment scale (i.e. NSE= 0.66). The trend of GRACE, well level observations and modelling show that total water storage has been depleted significantly. The reasonable correlation between GRACE and well level observation suggest that GRACE data can be used to evaluate total water storage variability in data-scarce semi-arid areas. Specifically, this research explains how RS data can be used to drive hydrological models to simulate streamflow and water storage variability in arid regions when there is a dearth of ground-based observations. The broad-scale approach to modelling presented here may provide valuable information for better policy making and planning to ensure efficient use of water resources in data scarce semi-arid areas.

6.3 Recommendation for future research

Although the application of simple rainfall-runoff models, such as LEMSAR, using RS data has great potential aspects of the model could still be improved. Several future research directions have been revealed through the results in this thesis, in relation to future satellite missions and the development of LEMSAR model including:

- LEMSAR was calibrated based on ground measurements (precipitation and reference evapotranspiration. However, it is important for future work to also re-calibrate LEMSAR with RS data to assess whether its performance is improved or not. This also provide a fairer comparison with model performance during validation using RS data as model inputs. Future work should also be done to evaluate new coming satellite-based rainfall (e.g. the NASA GPM project). TRMM officially ended in 2015, but a recent study by Prakash et al. (2016) highlighted that the recently released Integrated Multi-satellite Retrievals for GPM (IMERG) to detect of rainfall has the same ability as TRMM rainfall data did.
- Obtaining accurate estimates of daily $ET_{o\text{-}RS}$ are still challenging in areas outside of Europe and the USA. Further study is recommended to expand (and, where possible test) the daily $ET_{o\text{-}RS}$ methodology or different ET equations presented in this thesis from catchment scale to global scale.
- The snow melt results presented in Chapter 3 provide a preliminary exploration of the importance of this process for the timing and magnitude of total river discharge. However, the actual contributions of snow melt to river discharge are unknown. Measuring this variable for large remote area using snow surveys is an expensive task. RS is an alternative method, which can detect snow cover area (SCA) and which can then be used as a proxy for snow water equivalent (SWE). Thus, future research is needed to reduce uncertainty on snow melt contributions to the river discharge, especially during the melting period and to validate this prediction by independent studies using some field data in combination with RS data (i.e. MODIS, SCA data).
- Although simulated total stream flow was in broad agreement with the recorded total stream flow, there is still significant uncertainty, particularly at low flows. This may related to existing artificial structures such as irrigation and diversion canals in the study area but no information about the amount water used to irrigate farms is currently available. This clearly influences the accuracy of the model simulation. More

importantly, however, significant uncertainties exist about the nature of groundwater dynamics in this catchment and how best to represent this in the model. Currently, the behaviour of the groundwater model is the weaknesses of the LEMSAR model. One important issue with this groundwater model is that low flows in the sustained dry summers experienced in the catchment are poorly predicted. This is clearly important from a water resources management perspective. Future work is required to improve this aspect of the model.

- The Intergovernmental Panel on Climate Change IPCC (2013) stated that the global temperature is predicted to increase by 1.5 °C by the end of the twenty-first century. Consequently, changes to the climate will be associated with changes in a number of components of the hydrological cycle such as: precipitation patterns, atmospheric water vapour content, soil moisture content, snow cover and snow pack depth, widespread melting of ice and surface water runoff (Bates et al., 2008). As a result annual surface and near- surface runoff, river discharge and water availability are projected to increase in some relatively wet areas (Bates et al. 2008) and projected to suffer a decrease in the arid and semi-arid areas particularly in southern Europe, western Russia, North Africa and the Middle East (Arnell, 2003; Kundzewicz, 2008). It is recommended therefore to evaluate the impact of land use and climate change scenarios in semi-arid regions in terms of changing hydrological processes. Model such as LEMSAR could be used for this purpose-particularly if they can be properly validated for current climatic conditions so that we can have some confidence in their ability to represent processes.
- Further research assessing the transferability of model parameters (Broderick et al., 2016) between contrasting climate conditions and a range of different catchments is recommended to better understand the role of hydroclimatic regime. Future work should also evaluate the impact of uncertainties associated with hydrological modelling (Clark et al., 2016) on water resources management.
- Finally, future work is needed to make the R package for LEMSAR available to the research community. So that it can be more widely used and tested.

Appendixes

Table A. 1. Some soil physical properties for different location in study area (SP% = Saturation Percentage, O.M % = Percent Organic matter, and O.M.C % = Optimum Moisture Content.

ID	Sample Location	Particle size distribution %			Soil texture	Bulk density Mg/m^3	Water content at		Available water %	SP%	O.M %	O.M.C %
		Clay	**Silt**	**Sand**			**-1500 kPa**	**-33kPa**				
1	**Barzinja**	56.093	39.845	4.062	Clay	1.13	24.20	35.55	11.35	60.3	1.740	24.88
2	**Cwarqurna**	15.887	49.073	35.040	Loam	1.43	10.13	19.59	10.72	28.3	1.180	13.04
3	**Dukan**	32.759	49.914	17.328	Silty clay loam	1.36	16.04	26.29	10.25	48.4	2.53	18.34
4	**Chwarta**	46.12	45.26	8.62	Silty clay	16	22.3	33.02	10.72	55	1.4	22.5
5	**Mawat**	29.361	30.484	40.155	Silty clay	1.41	14.85	24.94	10.09	54.6	1.960	15.92
6	**Qalachwalan**	36.713	35.140	28.147	Clay loam	1.3	17.42	27.86	10.44	50.5	1.140	18.53
7	**Qaladza**	57.782	37.838	4.380	Clay	1.2	24.79	36.22	11.43	53.4	2.73	25.27
8	**Sangasar**	50.514	41.534	7.951	Silty clay	1.33	22.25	33.33	11.08	58.6	1.85	23.27
9	**Sarseer**	51.011	41.425	7.564	Silty clay	1.21	22.42	33.53	11.11	57.3	1.53	23.42
10	**Ranya**	50.87	41.79	7.34	Silty clay	1.89	21.2	32.2	11	53.2	1.68	22.21

Figure A. 1. LEMSAR model function code

```
# LEMSAR model function

LEMSAR <- function(param,input){
 par <-param # parameter
 r.obs <- input$r.obs[1:max(input$time.period)]# reading rainfall
 e.obs <- input$pe.obs[1:max(input$time.period)]#reading evapotranspiration
 Qobs<-c(-1, r.obs) # extend time series by one (index t=1 means time 0)
 ## define some empti rooms
 smd_temp <- Qobs * 0
 new_rain <- smd_temp
 drainage <- smd_temp
 new_aet <- smd_temp
 holf <- smd_temp
 olf_new <- smd_temp
 drainage_temp<- smd_temp
 GW_flow<- smd_temp
 sgw<-smd_temp
 qgw_tot<-smd_temp
 gflow<-smd_temp
 thrflow<-smd_temp
 avwatmax <- (par[4]/100)*(par[2]-par[3])*1000 #calculate maximun available water(mm),
 soil_water_deficit<-(par[2]-par[6])*avwatmax #initial saturation deficit(mm)
 tsmd<-(par[2]-par[5])*avwatmax# , threshold SMD when Eta<Etp(mm)
 ###define some constantnt variables
 new_dt<-0.1
 area_catch<-11630# this is a area for the catchment
 conv<-(area_catch*10)/864# convert mm/day to m3 sec-1(24*36)=864
 maxsmd<-avwatmax
 olf_temp = 0
 a<-2
 cPar<-1
 b<-0.5
 m  <- (1 - (cPar / par[1]))
 days <- length(r.obs)
 q <- rep(NA,days)
 sgw<-100
 GW_store<-100
 #####Integration 'integrate over 24 hours with time step new_dt using Euler's method
 for (t in 2:days ){
  nsteps<-1/new_dt
  drain_tot<-0
  qgw_tot<-0
  aet_tot<-0
  gflow_tot <- 0
  thrflow_tot <-0
  pet_temp<- e.obs[t]
  if( r.obs[t]>par[8]){
   holf[t] <- par[9]* (r.obs[t]- par[8])
   new_rain[t] <- r.obs[t]- holf[t]
  } else {
   new_rain[t] <- r.obs[t]
```

```
  }
  sgw[1]<-GW_flow[t-1]

  smd_temp[1] <- soil_water_deficit[t-1]
  rain_temp <- new_rain[t]* new_dt
  # calulate the evaporation
  pet_temp <- pet_temp*new_dt
  olf_temp = 0
  qgw<-0
  for (j in 2:nsteps){
   #cat(smd_temp[j-1])
   if(smd_temp[j-1]<=tsmd){
    new_aet_temp<-pet_temp
   } else {
    aet_pet_ratio<- (1+(tsmd/(avwatmax-tsmd)))-(smd_temp[j-1]/(avwatmax-tsmd))
    new_aet_temp<-pet_temp*aet_pet_ratio
   }
   Se<-(avwatmax-smd_temp[j-1])/avwatmax
   Kr <- (Se^b) * ( ( 1 - ( 1 - Se^(1/m) )^m )^a )
   kunsat<-Kr*param[7]
   drainage_temp<-(kunsat*new_dt)* par[11]
   sgw<-sgw  + new_dt* (drainage_temp - par[10]*sgw)
   qgw<-par[10]*(sgw)
   smd_temp[j]<- smd_temp[j-1] - rain_temp + drainage_temp + new_aet_temp
   if(smd_temp[j]< 0){
    olf_temp<- olf_temp + abs(smd_temp[j])
    smd_temp[j]<-0
   }
   aet_tot<-aet_tot + new_aet_temp
   drain_tot<-drain_tot + drainage_temp
  }
  soil_water_deficit[t]<-smd_temp[nsteps]
  GW_flow[t]<-qgw
  drainage[t]<-drain_tot
  thrflow[t] <-((1-par[11])* drainage[t])
  new_aet[t]<-aet_tot
  olf_new[t] <-olf_temp+ holf[t]
  q[t-1]<-  (olf_new[t]+thrflow[t]+GW_flow[t])* conv  #####    discharge  at the catchment outlet
 }
 return(q)
}
```

```
##############################################################################################
###LEMSAR snow melt model
### Read input data

data<-read.csv("input-data.csv",header=T)

#########################
# DEFAULT SNOW PARAMETERS

snowpar = c(alb=0.75, SRF=0.26, DDF=0.23, Tref=0, min.rain.temp=-0.5, max.snow.temp=1.5)
#DDf dgree day factor
# SRF shortwave radiation factor
############# lapse rate equations to determine  temperature for each zone

DALR<- 0.0065 ####Dry adiabatic lapse rate
Zbase<-500 ########Altitude of station
Za<-1000  # Altitude of defferent zone loaction i
Zb<-1500
Zc<-2000
Zd<-2500
Ze<-3000
Zf<-3500

################################### multiply lapse rate to change in elevation (zonej-zone i) which
zone i =Altitude of station
tza<-DALR*(Za-Zbase)
tzb<-DALR*(Zb-Zbase)
tzc<-DALR*(Zc-Zbase)
tzd<-DALR*(Zd-Zbase)
tze<-DALR*(Ze-Zbase)
tzf<-DALR*(Zf-Zbase)

###################################calculate new temperature based on elevation and Laps rate
Tza= data$T- tza
Tzb= data$T- tzb
Tzc= data$T- tzc
Tzd= data$T- tzd
Tze= data$T- tze
Tzf= data$T- tzf


# DIVISION RAIN/SNOW at base_station
# first guess: all precipitation is rain (frac = rain fraction)
frac  = rep(1, nrow(data))
# if very cold: all snow
frac[data$T < snowpar[5]] = 0
# if cold: partly snow
idx = which(data$T < snowpar[6] & data$T >= snowpar[5])
frac[idx] = (data$T[idx] - snowpar[5]) / (snowpar[6] - snowpar[5])
# compute rain and snow
rain = data$rain* frac
```

```
snowstation = data$rain * (1 - frac)
################
# POTENTIAL MELT
# shortwave radiation factor method
melt_base_station = pmax(0, (snowpar[3] + snowpar[2] * (1-snowpar[1]) * data$RS) * (data$T -
snowpar[4]))
# ACCUMULATION + ACTUAL MELT
# compute snow pack and actual melt
packstation    = c()
packstation[1] = snowstation[1]
# first time step
if(data$T[1]>snowpar[5]){melt_base_station[1] = 0}
# loop over time steps
for(s in 2:nrow(data))
{
 # reduce melt if not enough water in snow pack
 if(melt_base_station[s] > packstation[s-1]) {melt_base_station[s] = packstation[s-1]}
 # compute new snow pack
 packstation[s] = packstation[s-1] + snowstation[s] - melt_base_station[s]
}


# DIVISION RAIN/SNOW at Zone a
# first guess: all precipitation is rain (frac = rain fraction)
frac   = rep(1, nrow(data))
# if very cold: all snow
frac[Tza < snowpar[5]] = 0
# if cold: partly snow
idx = which(Tza < snowpar[6] & Tza >= snowpar[5])
frac[idx] = (Tza[idx] - snowpar[5]) / (snowpar[6] - snowpar[5])
# compute rain and snow
snowZa = data$rain * (1 - frac)
# POTENTIAL MELT
meltZa = pmax(0, (snowpar[3] + snowpar[2] * (1-snowpar[1]) * data$RS) * (Tza - snowpar[4]))
# ACCUMULATION + ACTUAL MELT
############################
# compute snow pack and actual melt
packZa    = c()
packZa[1] = snowZa[1]
# first time step
if(Tza[1]>snowpar[4]){meltZa[1] = 0}
# loop over time steps
for(s in 2:nrow(data))
{
 # reduce melt if not enough water in snow pack
 if(meltZa[s] > packZa[s-1]) {meltZa[s] = packZa[s-1]}

 # compute new snow pack
 packZa[s] = packZa[s-1] + snowZa[s] - meltZa[s]
}
```

```
############ snow melt at Zone b
# DIVISION RAIN/SNOW
####################
# first guess: all precipitation is rain (frac = rain fraction)
frac   = rep(1, nrow(data))
# if very cold: all snow
frac[Tzb < snowpar[5]] = 0
# if cold: partly snow
idx = which(Tzb < snowpar[6] & Tzb >= snowpar[5])
frac[idx] = (Tzb[idx] - snowpar[5]) / (snowpar[6] - snowpar[5])
# compute rain and snow
snowZb = data$rain * (1 - frac)
# POTENTIAL MELT
meltZb = pmax(0, (snowpar[3] + snowpar[2] * (1-snowpar[1]) * data$RS) * (Tzb - snowpar[4]))
# ACCUMULATION + ACTUAL MELT
# compute snow pack and actual melt
packZb    = c()
packZb[1] = snowZb[1]
# first time step
if(Tzb[1]>snowpar[4]){meltZb[1] = 0}
# loop over time steps
for(s in 2:nrow(data))
{
 # reduce melt if not enough water in snow pack
 if(meltZb[s] > packZb[s-1]) {meltZb[s] = packZb[s-1]}

 # compute new snow pack
 packZb[s] = packZb[s-1] + snowZb[s] - meltZb[s]
}


############ snow melt at Zone c
# DIVISION RAIN/SNOW
# first guess: all precipitation is rain (frac = rain fraction)
frac   = rep(1, nrow(data))
# if very cold: all snow
frac[Tzc < snowpar[5]] = 0
# if cold: partly snow
idx = which(Tzc < snowpar[6] & Tzc >= snowpar[5])
frac[idx] = (Tzc[idx] - snowpar[5]) / (snowpar[6] - snowpar[5])
# compute rain and snow
snowZc = data$rain * (1 - frac)
# POTENTIAL MELT
meltZc = pmax(0, (snowpar[3] + snowpar[2] * (1-snowpar[1]) * data$RS) * (Tzc  - snowpar[4]))
# ACCUMULATION + ACTUAL MELT
# compute snow pack and actual melt
packZc    = c()
packZc[1] = snowZc[1]
# first time step
if(Tzc [1]>snowpar[4]){meltZc[1] = 0}
```

```
# loop over time steps
for(s in 2:nrow(data))
{
 # reduce melt if not enough water in snow pack
 if(meltZc[s] > packZc[s-1]) {meltZc[s] = packZc[s-1]}
 # compute new snow pack
 packZc[s] = packZc[s-1] + snowZc[s] - meltZc[s]
}


############ snow melt at Zone d
# DIVISION RAIN/SNOW
# first guess: all precipitation is rain (frac = rain fraction)
frac  = rep(1, nrow(data)
# if very cold: all snow
frac[Tzd < snowpar[5]] = 0
# if cold: partly snow
idx = which(Tzd < snowpar[6] & Tzd >= snowpar[5])
frac[idx] = (Tzd[idx] - snowpar[5]) / (snowpar[6] - snowpar[5])
# compute rain and snow
snowZd = data$rain * (1 - frac)
# POTENTIAL MELT
################
meltZd = pmax(0, (snowpar[3] + snowpar[2] * (1-snowpar[1]) * data$RS) * (Tzd - snowpar[4]))
############################
# ACCUMULATION + ACTUAL MELT
# compute snow pack and actual melt
packZd = c()
packZd[1] = snowZd[1]
# first time step
if(Tzd[1]>snowpar[4]){meltZd[1] = 0}
# loop over time steps
for(s in 2:nrow(f))
{
# reduce melt if not enough water in snow pack
if(meltZd[s] > packZd[s-1]) {meltZd[s] = packZd[s-1]}
# compute new snow pack
packZd[s] = packZd[s-1] + snowZd[s] - meltZd[s]
}


 ############ snow melt at Zone e
 # DIVISION RAIN/SNOW
# first guess: all precipitation is rain (frac = rain fraction)
frac  = rep(1, nrow(data))
# if very cold: all snow
frac[Tze < snowpar[5]] = 0
# if cold: partly snow
idx = which(Tze < snowpar[6] & Tze >= snowpar[5])
frac[idx] = (Tze[idx] - snowpar[5]) / (snowpar[6] - snowpar[5])
# compute rain and snow
```

```
snowZe = data$rain * (1 - frac)
# POTENTIAL MELT
meltZe = pmax(0, (snowpar[3] + snowpar[2] * (1-snowpar[1]) * data$RS) * (Tze - snowpar[4]))
# ACCUMULATION + ACTUAL MELT
# compute snow pack and actual melt
packZe = c()
packZe[1] = snowZe[1]
# first time step
if(Tze[1]>snowpar[4]){meltZe[1] = 0}
# loop over time steps
for(s in 2:nrow(data))
{
# reduce melt if not enough water in snow pack
if(meltZe[s] > packZe[s-1]) {meltZe[s] = packZe[s-1]}
# compute new snow pack
packZe[s] = packZe[s-1] + snowZe[s] - meltZe[s]
 }


############ snow melt at Zone f
# DIVISION RAIN/SNOW
# first guess: all precipitation is rain (frac = rain fraction)
frac  = rep(1, nrow(data))
# if very cold: all snow
frac[Tze < snowpar[5]] = 0
# if cold: partly snow
idx = which(Tzf < snowpar[6] & Tzf >= snowpar[5])
frac[idx] = (Tzf[idx] - snowpar[5]) / (snowpar[6] - snowpar[5])
# compute rain and snow
snowZf = data$rain* (1 - frac)
# POTENTIAL MELT
meltZf = pmax(0, (snowpar[3] + snowpar[2] * (1-snowpar[1]) * f$RS) * (Tzf - snowpar[4]))
# ACCUMULATION + ACTUAL MELT
# compute snow pack and actual melt
packZf = c()
packZf[1] = snowZf[1]
# first time step
if(Tzf[1]>snowpar[4]){meltZf[1] = 0}
# loop over time steps
for(s in 2:nrow(data))
{
# reduce melt if not enough water in snow pack
if(meltZf[s] > packZf[s-1]) {meltZf[s] = packZf[s-1]}

# compute new snow pack
packZf[s] = packZf[s-1] + snowZf[s] - meltZf[s]
}
```

```
###################################define  contribute of each zone into meltting process
Zbase<-0.016
Zaw<-0.21
Zbw<-0.38
Zcw<-0.29
Zdw<-0.08
Zew<-0.02
Zfw<-0.004
################
 M_base<-melt_base_station*Zbase
 Mza<-meltZa*Zaw
Mzb<-meltZb*Zbw
Mzc<-meltZc*Zcw
Mzd<-meltZd*Zdw
Mze<-meltZe*Zew
Mzf<-meltZf*Zfw
Snow_melt<- M_base+ Mza+Mzb+Mzc+ Mzd + Mze + Mzf

# sum rain and Snow#_melt
precipitation =  rain +Snow_melt
P<- precipitation


## read precipitation, eavpotranspiration, Observed discharge and parameter values.
input <- list(r.obs = P ,
              pe.obs = data[,4],
              time.period = c(1,730),
              min.param = c(1,0.4,0.03,50,0.2,0.01,75,5,0.05,0.1,0.1),
              max.param = c(2.5,0.6,0.22,200,0.4,0.3,450,50,0.1,0.99,0.99),
              #par.names = c("n","swc","pwp","sd","twc","iwc","ksat","Ro","Pescra","kgw","k1"))
              par.names = c(expression(paste(italic("n"))),expression(paste(italic(phi))),
                            expression(paste(italic(theta[R]))),expression(paste(italic("z"))),
                            expression(italic(theta[T])),expression(paste(italic(theta[r]))),
                            expression(paste(italic("K"[sat]))),expression(italic("R"[o])),
                            expression(paste(italic("p"))),expression(paste(italic("k"))),
                            expression(paste(italic("f"[g]))), cex=1))

################################################################ Run LEMSAR
source("LEMSAR.R")
MdlName <- "LEMSAR"
nit <- 1
nparam <- length(input$min.param) # number of parameters
# start the loop of the interations
for(ii in 1:nit){
  param <- runif(nparam,input$min.param,input$max.param) # random parameter generation
  # compute the model simulation results
  Qmod <- do.call(MdlName, args = list(param=param,input=input))
}
Qmod <- Qmod[input$time.period[1]:input$time.period[2]]####### LEMSARsimulation output
#############################################################################################
###########
```

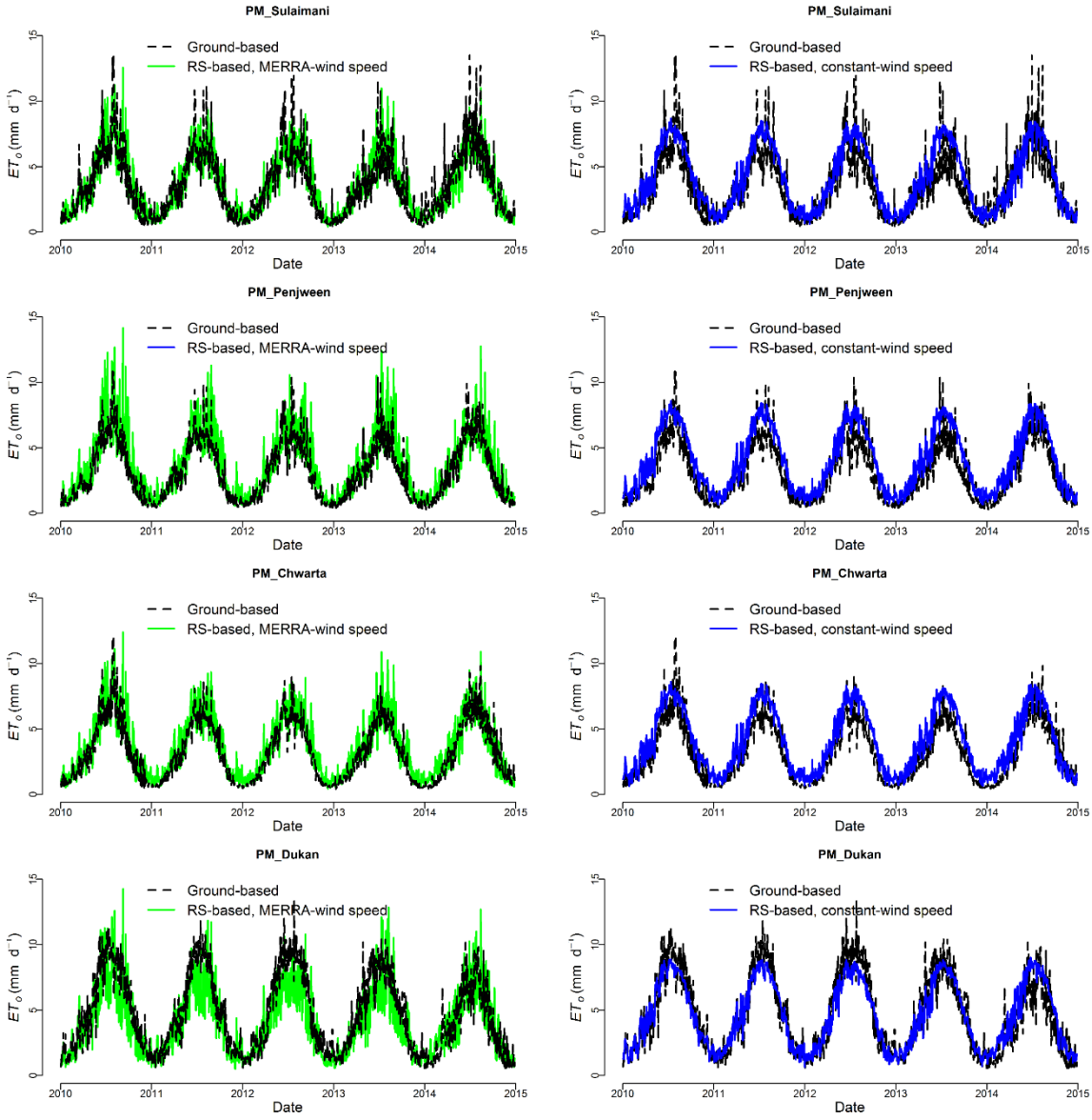

Figure A. 2. Plot of daily ET_o estimates derived from ground-based measurements (ET_o-$_G$) and remote sensing data (ET_o-$_{RS}$) using PM method from 2010 -2014 for Sulaimani, Penjween, Chwarta and Dukan stations. The black line presents the ET_o-$_G$. The blue line presents the ET_o-$_{RS}$ when the PM model driven by constant-wind speed. The green line presents the ET_o-$_{RS}$ when the PM model driven by MERRA-wind speed.

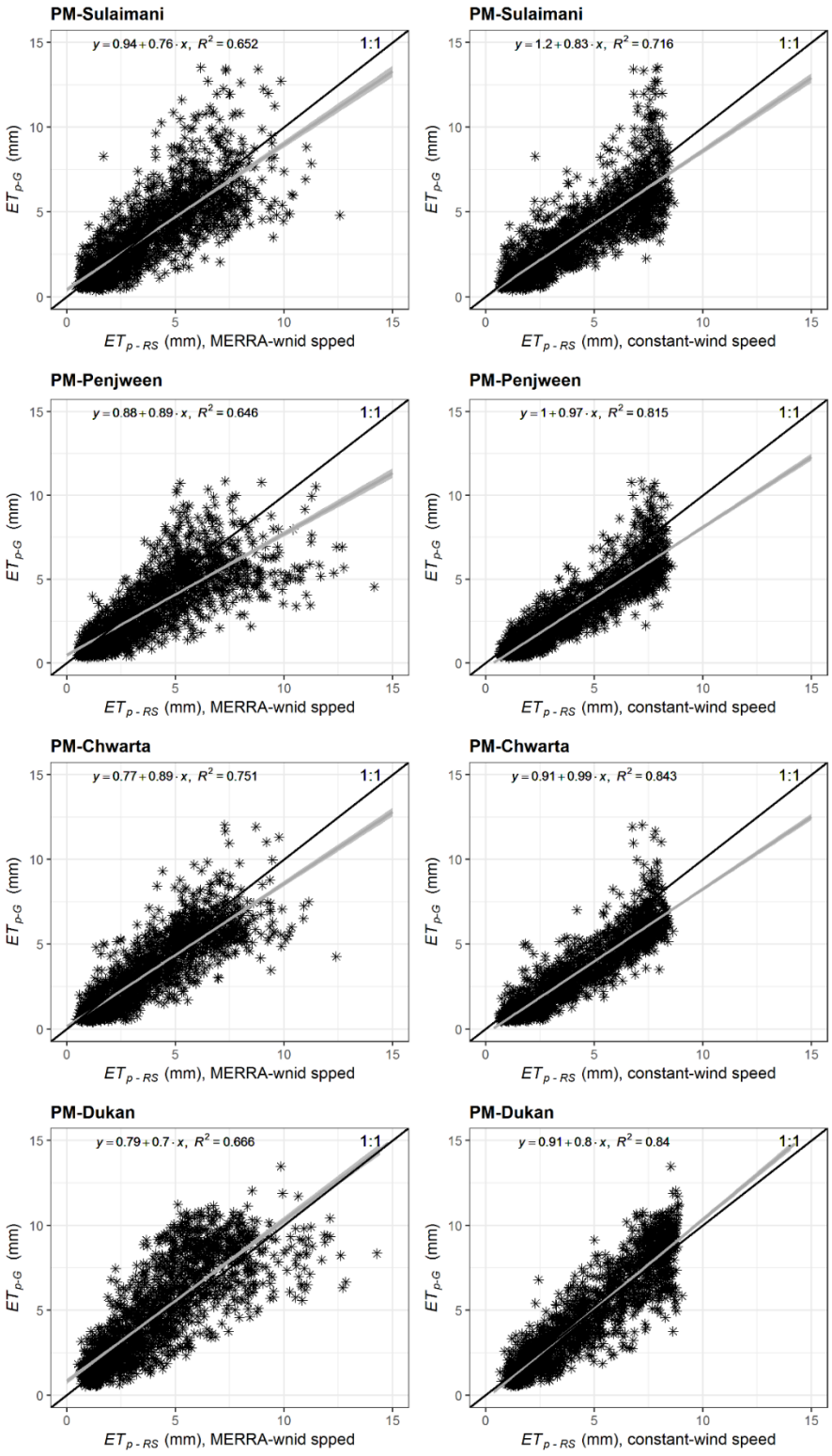

Figure A. 3. Scatterplots of estimated daily reference evapotranspiration using ground-based measurements using PM method (ET_o-$_G$) versus estimated reference evapotranspiration using remote sensing data (ET_o-$_{RS}$) using PM method when the PM was driven by with MERAA-wind speed and constant-wind speed at four different stations (Sulaimani, Penjween, Chwarta, and Dukan). The solid black line indicates the 1:1 relationship. The grey line shows the best-fit regression with 95% confidence interval (equations and R^2 also shown).

Table A. 2. Statistical summary of comparisons between estimated daily reference evapotranspiration using ground-based measurements (ET_o-$_G$) and remote sensing data (ET_o-$_{RS}$) with MERRA-wind speed and constant-wind speed data for PM methods at four different stations (Sulaimani, Penjween, Chwarta, and Dukan) over the study period 2010-2014.

Station	**Variable**	**RMSE**	**BIAS (%)**	***R***
Sulaimani	(MERRA-wind speed)	1.47	2.5	0.8*
	(constant-wind speed)	1.45	15.7	0.85*
Penjween	(MERRA-wind speed)	1.57	17.2	0.8*
	(constant-wind speed)	1.4	30	0.91*
Chwarta	(MERRA-wind speed)	1.23	12.8	0.86*
	(constant-wind speed)	1.2	27	0.92*
Dukan	(MERRA-wind speed)	1.78	-13	0.81*
	(constant-wind speed)	1.1	-1.1	0.492*

Table A. 3. Statistical summary of (BIAS %) between daily ground-measured and remotely-sensed values of T_a , RH %, DS and U_2 and BIAS % summary of estimated daily reference evapotranspiration using remote sensing data (ET_o-$_{RS}$) for four different methods against the benchmark data set (PM method using ground-based measurements: ET_o-$_G$: PM) for four different stations (Sulaimani, Penjween, Chwarta, and Dukan) over the study period 2010-2014. * means significant at p<0.05.

	Bias for *ETo* (%)				Bias for meteorological variables (%)			
Station	PM	HS	JH	MB	T_a	RH	*DS*	U_2
Sulaimani	2.5	-9	21.4	24.5	-14.2	-0.6	27.8	16.1
Penjween	17.7	-1.9	37	40	28.4	-13.4	34.8	10.2
Chwarta	12.8	-0.6	33.3	37	-0.1	-26	24.5	9.1
Dukan	-13	-2.6	11.2	8.6	-2.8	-7.3	-47.7	21.8
Bias for *ETo* vs bias for meteorological variables								
	PM vs T_a	HS vs T_a	JH vs T_a	MB vs T_a				
R^2	0.36	0.35	0.43	0.33				
P- value	0.64	0.65	0.57	0.67				
	PM vs *DS*	JH vs *DS*	MB vs *DS*					
R^2	0.94	0.956	0.969					
P- value	0.06	0.04*	0.031*					
	PM vs RH%							
R^2	0.29							
P- value	0.71							
	PM vs U_2							
R^2	0.81							
P- value	0.19							

Table A. 4. Summary of annual ET_o-$_G$ and ET_o-$_{RS}$ (with MERRA-wind speed and constant-wind speed data) for PM method at four different stations (Sulaimani, Penjween, Chwarta, and Dukan) over the study period 2010-2014.

Station	**variable**	**Year**				
		2010	**2011**	**2012**	***2013***	***2014***
Sulaimani	ET_o-$_G$ mm y^{-1}	1385	1269	1290	1109	1482
	ET_o-$_{RS}$ mm y^{-1} (MERRA-wind speed)	1439	1304	1316	1285	1328
	ET_o-$_{RS}$ mm y^{-1} (constant-wind speed)	1577	1473	1497	1485	1499
Penjween		1183	1150	1154	1054	121
	ET_o-$_{RS}$ mm y^{-1} (MERRA-wind speed)	1474	1329	1305	1321	1323
	ET_o-$_{RS}$ mm y^{-1} (constant-wind speed)	1561	1471	1495	1484	1497
Chwarta	ET_o-$_G$ mm y^{-1}	1274	1133	1144	1091	1275
	ET_o-$_{RS}$ mm y^{-1} (MERRA-wind speed)	1430	1307	1318	1290	1331
	ET_o-$_{RS}$ mm y^{-1} (constant-wind speed)	1560	1472	1496	1484	1498
Dukan	ET_o-$_G$ mm y^{-1}	1864	1767	1848	1706	1372
	ET_o-$_{RS}$ mm y^{-1} (MERRA-wind speed)	1588	1479	1479	1435	1460
	ET_o-$_{RS}$ mm y^{-1} (constant-wind speed)	1762	1678	1675	1674	1677

References

Abbott M, Bathurst J, Cunge J, et al. (1986) An introduction to the European Hydrological System—Systeme Hydrologique Europeen,"SHE", 2: Structure of a physically-based, distributed modelling system. *Journal of Hydrology* 87: 61-77.

Abdul Hameed A, Haider S A and Bahram K M. (2010) Application of water quality index for assessment of Dokan lake ecosystem, Kurdistan region, Iraq. *Journal of Water Resource and Protection* 2: 792-798.

Abdulla F and Al-Badranih L. (2000) Application of a rainfall-runoff model to three catchments in Iraq. *Hydrological Sciences Journal* 45: 13-25.

Abdulla H. (2008) Evaluation of moisture deficit index in dry land in Iraq. *Middle East Journal of Scientific Research* 3: 116-119.

Abo RK and Merkel BJ. (2015) Investigation of the potential surface–groundwater relationship using automated base-flow separation techniques and recession curve analysis in Al Zerba region of Aleppo, Syria. *Arabian Journal of Geosciences* 8: 10543-10563.

Abrahams AD, Parsons AJ and Wainwright J. (1995) Effects of vegetation change on interrill runoff and erosion, Walnut Gulch, southern Arizona. *Geomorphology* 13: 37-48.

Acworth RI, Rau GC, Cuthbert MO, et al. (2016) Long-term spatio-temporal precipitation variability in arid-zone Australia and implications for groundwater recharge. *Hydrogeology Journal* 24: 905-921.

AIRS Science Team/Joao Texeira. (2013) Aqua AIRS Level 3 Daily Standard Physical Retrieval (AIRS+AMSU), version 006. Greenbelt, MD, USA: NASA Goddard Earth Science Data and Information Services Center (GES DISC), Accessed [18/04/2016] 10.5067/AQUA/AIRS/DATA301.

Al-Ansari N, Abdellatif M, Zakaria S, et al. (2014) Future Prospects for Macro Rainwater Harvesting (RWH) Technique in North East Iraq. *Journal of Water Resource and Protection* 6: 403-420.

Al-Ansari N and Knutsson S. (2011) Toward prudent management of water resources in Iraq. *Journal of Advanced Science and Engineering Research* 1: 53-67.

Al-Ansari NA. (2013) Management of Water Resources in Iraq: Perspectives and Prognoses. *Engineering* 05: 667-684.

Al-Turbak AS. (1996) Geomorphoclimatic peak discharge model with a physically based infiltration component. *Journal of Hydrology* 176: 1-12.

Alemayehu T, Griensven Av, Senay GB, et al. (2017) Evapotranspiration Mapping in a Heterogeneous Landscape Using Remote Sensing and Global Weather Datasets: Application to the Mara Basin, East Africa. *Remote Sensing* 9: 390.

Allam MN. (1990) Case study evaluation of geomorphologic rainfall-runoff model, incorporating linear infiltration expression. *Hydrological Processes* 4: 71-84.

Allan CJ and Roulet NT. (1994) Runoff generation in zero-order precambrian shield catchments: The stormflow response of a heterogeneous landscape. *Hydrological Processes* 8: 369-388.

Allan JA. (2001) The Middle East Water Question: Hydro-politics and the Global Economy. London: I. B. Tauris China Despain, 2012. Matt Damon Spills on the Important of Clean Water. *Water ORG*: available from http://www.ecorazzi.com/wp-content/.

Allen , Pereira LS, Raes D, et al. (1998) Crop evapotranspiration - Guidelines for computing crop water requirements. – FAO Irrigation and Drainage Paper 56, FAO, Rome, Italy.

Allen R, Smith M, Pereira L, et al. (2000) Revised FAO Procedures for Calculating Evapotranspiration–Irrigation and Drainage Paper No. 56 with Testing in Idaho. *Bridges*: 1-10.

Allen RG, Pereira LS, Raes D, et al. (1998) Crop evapotranspiration-Guidelines for computing crop water requirements-FAO Irrigation and drainage paper 56. *FAO, Rome*: 1-15.

Ambroise B, Freer J and Beven K. (1996) Application of a generalized TOPMODEL to the small Ringelbach catchment, Vosges, France. *Water Resources Research* 32: 2147-2159.

Amy McNally NASA/GSFC/HSL. (2016) FLDAS Noah Land Surface Model L4 daily 0.1 x 0.1 degree for Southern Africa (GDAS and RFE2) V001. Greenbelt, Maryland, USA, Goddard Earth Sciences Data and Information Services Center (GES DISC) https://disc.gsfc.nasa.gov/datacollection/FLDAS_NOAH01_A_SA_D_001.html.

Anders AM, Gerard HR, Bernard H, et al. (2006) Spatial patterns of precipitation and topography in the Himalaya. In Tectonics, Climate, and Landscape Evolution, S.D. Willett, N. Hovius, M.T. Brandon and D. Fisher (Eds.),. *Geological Society of America Special Paper 398*: 39-53.

Andersen OB, Seneviratne SI, Hinderer J, et al. (2005) GRACE-derived terrestrial water storage depletion associated with the 2003 European heat wave. *Geophysical Research Letters* 32.

Arias-Hidalgo M, Bhattacharya B, Mynett AE, et al. (2013) Experiences in using the TMPA-3B42R satellite data to complement rain gauge measurements in the Ecuadorian coastal foothills. *Hydrology and Earth System Sciences* 17: 2905-2915.

Arnell N. (2003) Effects of IPCC SRES emissions scenarios on river runoff: a global perspective. *Hydrology and Earth System Sciences* 7: 619-641.

Arnold J and Moriasi D. (2012) SWAT: Model use, calibration, and validation. *Transactions of the ASABE* 55: 1491-1508.

Assouline S, Selker JS and Parlange JY. (2007) A simple accurate method to predict time of ponding under variable intensity rainfall. *Water Resources Research* 43: 1-10.

Babu CA, Jayakrishnan PR and Varikoden H. (2016) Characteristics of precipitation pattern in the Arabian Peninsula and its variability associated with ENSO. *Arabian Journal of Geosciences* 9: 1-12.

Baigorria GA, Villegas EB, Trebejo I, et al. (2004) Atmospheric transmissivity: distribution and empirical estimation around the central Andes. *International Journal of Climatology* 24: 1121-1136.

Bakir M and Xingnan Z. (2008) GIS and remote sensing applications for rainwater harvesting in the syrian desert (al-badia). *12th International Water Technology Conference,*. Alexandria, Egypt, 1-10.

Banimahd SA, Khalili D, Kamgar-Haghighi AA, et al. (2015) Evaluation of groundwater potential recharge models considering estimated bare soil evaporation, in a semi-arid foothill region. *Hydrological Sciences Journal* 61: 162-172.

Bates B, Kundzewicz Z, Wu S, et al. (2008) Climate change and water.Technical Paper of the Intergovernmental Panel on Climate Change, IPCC Secretariat, Geneva. 1-210.

Beaumont P, Blake G and Wagstaff JM. (2016) *The Middle East: A Geographical Study Second Edition*: Routledge, Oxford, OX14 4RN, UK.

Bergström S, Carlsson B, Gardelin M, et al. (2001) Climate change impacts on runoff in Sweden assessments by global climate models, dynamical downscaling and hydrological modelling. *CLIMATE RESEARCH* 16: 101-112.

Bergström S and Forsman A. (1973) Development of a conceptual deterministic rainfall-runoff model. *Hydrology Research* 4: 147-170.

Bergström S and Singh V. (1995) Computer models of watershed hydrology. *Water Resources Publications: Colorado, CO, USA*: 443-476.

Betson RP. (1964) What is watershed runoff? *Journal of Geophysical Research* 69: 1541-1552.

Beven K. (1993) Prophecy, reality and uncertainty in distributed hydrological modelling. *Advances in Water Resources* 16: 41-51.

Beven K. (2004) Robert E. Horton's perceptual model of infiltration processes. *Hydrological Processes* 18: 3447-3460.

Beven K. (2010) *Environmental modelling: An uncertain future?*: Routledge, New York, USA.

Beven K and Binley A. (1992) The future of distributed models model calibration and uncertainty prediction. *Hydrological Processes* 6: 279-298.

Beven K and Freer J. (2001) Equifinality, data assimilation, and uncertainty estimation in mechanistic modelling of complex environmental systems using the GLUE methodology. *Journal of Hydrology* 249: 11-29.

Beven KJ. (2012) *Rainfall-runoff modelling: the primer*: John Wiley & Sons.

Beven KJ and Alcock RE. (2012) Modelling everything everywhere: a new approach to decision-making for water management under uncertainty. *Freshwater Biology* 57: 124-132.

Beven KJ and Kirkby MJ. (1979) A physically based, variable contributing area model of basin hydrology / Un modèle à base physique de zone d'appel variable de l'hydrologie du bassin versant. *Hydrological Sciences Bulletin* 24: 43-69.

Bhanja SN, Mukherjee A, Saha D, et al. (2016) Validation of GRACE based groundwater storage anomaly using in-situ groundwater level measurements in India. *Journal of Hydrology* 543: 729-738.

Biondi D, Freni G, Iacobellis V, et al. (2012) Validation of hydrological models: Conceptual basis, methodological approaches and a proposal for a code of practice. *Physics and Chemistry of the Earth, Parts A/B/C* 42-44: 70-76.

Bo H, Yue-Si W and Guang-Ren L. (2009) Properties of Solar Radiation over Chinese Arid and Semi-Arid Areas. *Atmospheric and Oceanic Science Letters* 2: 183-187.

Boisvert JB and Deutsch CV. (2011) Programs for kriging and sequential Gaussian simulation with locally varying anisotropy using non-Euclidean distances. *Computers & Geosciences* 37: 495-510.

Boughton W. (1984) A simple model for estimating the water yield of ungauged catchments. *Civ. Eng. Trans., Inst. Eng. Aus., CE* 26: 83-88.

Bouwer LM, Aerts JCJH, VdC, G.M. , et al. (2004) Evaluating downscaling methods for preparing global circulation model (GCM) data for hydrological impact modelling. *Chapter 2, in Aerts, J.C.J.H. & Droogers, P.(Eds.), Climate Change in Contrasting River Basins: Adaptation Strategies for Water, Food and Environment.* (pp25-47).Wallingford: UK:Cabi Press.

Box G and Jenkins G. (1970) (Time series analysis; forecasting and control. Holden-Day, San Francisco(CA).

Bozkurt D and Sen OL. (2013) Climate change impacts in the Euphrates–Tigris Basin based on different model and scenario simulations. *Journal of Hydrology* 480: 149-161.

Brazier RE, Beven KJ, Freer J, et al. (2000) Equifinality and uncertainty in physically based soil erosion models: application of the GLUE methodology to WEPP–the Water Erosion Prediction Project–for sites in the UK and USA. *Earth Surface Processes and Landforms* 25: 825-845.

Broderick C, Matthews T, Wilby RL, et al. (2016) Transferability of hydrological models and ensemble averaging methods between contrasting climatic periods. *Water Resources Research* 52: 8343-8373.

Brooks RH and Corey AT. (1966) Properties of porous media affecting fluid flow. *Irrigation and Drainage Division* 2: 61-87.

Brutsaert W. (1982) *Evaporation into the atmosphere: theory, history and applications*: Springer Science & Business Media.

Buringh P. (1960) *Soils and Soil Conditions of Iraq. Ministry of Agriculture, Agricultural Research and Projects,Baghdad*.

Burnash RJ, Ferral RL and McGuire RA. (1973) A generalized streamflow simulation system, conceptual modeling for digital computers. 204.

Buytaert W and Beven K. (2011) Models as multiple working hypotheses: hydrological simulation of tropical alpine wetlands. *Hydrological Processes* 25: 1784-1799.

Cai Y, Jin C, Wang A, et al. (2015) Spatio-temporal analysis of the accuracy of tropical multisatellite precipitation analysis 3B42 precipitation data in mid-high latitudes of China. *PLoS One* 10: e0120026.

Campana M and Simpson E. (1984) Groundwater residence times and recharge rates using a discrete-state compartment model and 14 C data. *Journal of Hydrology* 72: 171-185.

Candela L, Elorza FJ, Tamoh K, et al. (2014) Groundwater modelling with limited data sets: the Chari-Logone area (Lake Chad Basin, Chad). *Hydrological Processes* 28: 3714-3727.

Cao C, Weinreb M and Xu H. (2004) Predicting simultaneous nadir overpasses among polar-orbiting meteorological satellites for the intersatellite calibration of radiometers. *Journal of Atmospheric and Oceanic Technology* 21: 537-542.

Casenave A and Valentin C. (1992) A runoff capability classification system based on surface features criteria in semiarid areas of West Africa. *Journal of Hydrology* 130: 231-249.

Castellazzi P, Martel R, Galloway DL, et al. (2016) Assessing Groundwater Depletion and Dynamics Using GRACE and InSAR: Potential and Limitations. *Ground water*: 1-13.

Castillo V, Gomezplaza A and Martinezmena M. (2003) The role of antecedent soil water content in the runoff response of semiarid catchments: a simulation approach. *Journal of Hydrology* 284: 114-130.

Cazorzi F and Dalla Fontana G. (1996) Snowmelt modelling by combining air temperature and a distributed radiation index. *Journal of Hydrology* 181: 169-187.

Cerdà aA, Ibáñezb S and Calvoa A. (1997) Design and operation of a small and portable rainfall simulator for rugged terrain. *Soil Technology* 11: 163-170.

Chahine M. (1992) The hydrological cycle and its influence on climate. *Nature Publishing Group* 359: 373-379.

Chenoweth J, Hadjinicolaou P, Bruggeman A, et al. (2011) Impact of climate change on the water resources of the eastern Mediterranean and Middle East region: Modeled 21st century changes and implications. *Water Resources Research* 47.

Chormanski J and Voorde T. (2008) Improving Distributed Runoff Prediction in Urbanized Catchments with Remote Sensing based Estimates of Imperv. *Sensors* 8: 910-932.

Chow VT, Maidment DR and Mays LW. (1988) *Applied hydrology*.

Clark MP, Wilby RL, Gutmann ED, et al. (2016) Characterizing Uncertainty of the Hydrologic Impacts of Climate Change. *Current Climate Change Reports* 2: 55-64.

Clarke MP. (1973) A review of some mathematical models used in hydrology, with observations on their calibration and use. *Journal of Hydrolgy* 19: 1-19.

Collischonn B, Collischonn W and Tucci CEM. (2008) Daily hydrological modeling in the Amazon basin using TRMM rainfall estimates. *Journal of Hydrology* 360: 207-216.

Crawford NH and Linsley RK. (1966) *Digital Simulation in Hydrology'Stanford Watershed Model 4Rep*, Stanford Univ.39,210 Dept. of Civil Engineering: Stanford, Calif.

Davie T. (2008) *Fundamentals of Hydrology (Routledge Fundamentals of Physical Geography)*: Taylor & Francis.

Dawson CW, Abrahart RJ and See LM. (2007) HydroTest: a web-based toolbox of evaluation metrics for the standardised assessment of hydrological forecasts. *Environmental Modelling & Software* 22: 1034-1052.

Dawson CW and Wilby RL. (2001) Hydrological modelling using artificial neural networks. *Progress in Physical Geography* 25: 80-108.

Dent S, Hanna RB and Wright LT. (2004) Automated Calibration using Optimization Techniques with SWMM RUNOFF. *Journal of Water Management Modeling*.

Dixon SG and Wilby RL. (2015) Forecasting reservoir inflows using remotely sensed precipitation estimates: a pilot study for the River Naryn, Kyrgyzstan. *Hydrological Sciences Journal* 61: 107-122.

Doherty J and Johnston JM. (2003) Methodologies for calibration and predictive analysis of a watershed model1. Wiley Online Library.

Dohnal M, Votrubová J, Sanda M, et al. (2016) Runoff generation mechanism at two distinct headwater catchments-isotopic evidence. *EGU General Assembly Conference Abstracts.* 13583.

Doswell CA, Davies-Jones R and Keller DL. (1990) On summary measures of skill in rare event forecasting based on contingency tables. *Weather and Forecasting* 5: 576-585.

Doummar J, Sauter M and Geyer T. (2012) Simulation of flow processes in a large scale karst system with an integrated catchment model (Mike She) – Identification of relevant parameters influencing spring discharge. *Journal of Hydrology* 426-427: 112-123.

Draper CS, Walker JP, Steinle PJ, et al. (2009) An evaluation of AMSR–E derived soil moisture over Australia. *Remote Sensing of Environment* 113: 703-710.

Dzubakova K. (2010) Rainfall-Runoff Modelling: Its development, classification and possible applications. *Acta Geographica Universitatis Comenianae* 54: 173-181.

Famiglietti JS, Lo M, Ho SL, et al. (2011) Satellites measure recent rates of groundwater depletion in California's Central Valley. *Geophysical Research Letters* 38: 1-4.

FAO. (2011) Country pasture/forage resource profiles. Rome, Italy. Available Online: http://www.fao.org/geonetwork/srv/en/main.home?uuid=ba4526fd-cdbf-4028-a1bd-5a559c4bff38 (accessed on 9 January 2016). Food and Agriculture Organization (FAO).

Feldman A. (2000) Hydrologic Modeling System HEC-HMS: Technical Reference Manual. *Technical Reference Manual*.

Fenicia F, Savenije HH, Matgen P, et al. (2008) Understanding catchment behavior through stepwise model concept improvement. *Water Resources Research* 44: 1-13.

Ferguson CR and Wood EF. (2010) An Evaluation of Satellite Remote Sensing Data Products for Land Surface Hydrology: Atmospheric Infrared Sounder. *Journal of Hydrometeorology* 11: 1234-1262.

Fleming G. (1972) Computer simulation techniques in hydrology. *Computer simulation techniques in hydrology.* Elsevier.

Fontaine T, Cruickshank T, Arnold J, et al. (2002) Development of a snowfall–snowmelt routine for mountainous terrain for the soil water assessment tool (SWAT). *Journal of Hydrology* 262: 209-223.

Food and Agriculture Organization (FAO). (1981) *Arid zone hydrology for agricultural development. Irrig. Drain. Pap.37.,* Rome: FAO.

Franchini M and Pacciani M. (1991) Comparative analysis of several conceptual rainfall-runoff models. *Journal of Hydrology* 122: 161-219.

Franks S, Beven KJ, Quinn P, et al. (1997) On the sensitivity of soil-vegetation-atmosphere transfer (SVAT) schemes: equifinality and the problem of robust calibration. *Agricultural and Forest Meteorology* 86: 63-75.

Frappart F, Ramillien G, Biancamaria S, et al. (2006) Evolution of high-latitude snow mass derived from the GRACE gravimetry mission (2002–2004). *Geophysical Research Letters* 33.

Gallart F, Latron J, Llorens P, et al. (2007) Using internal catchment information to reduce the uncertainty of discharge and baseflow predictions. *Advances in Water Resources* 30: 808-823.

Gan TY, Dlamini EM and Biftu GF. (1997) Effects of model complexity and structure, data quality, and objective functions on hydrologic modeling. *Journal of Hydrology* 192: 81-103.

Gao YC and Liu MF. (2013) Evaluation of high-resolution satellite precipitation products using rain gauge observations over the Tibetan Plateau. *Hydrology and Earth System Sciences* 17: 837-849.

Global Modeling and Assimilation Office. (2008) MERRA 2D IAU Diagnostic, Single Level Meteorology, Time Average 1-hourly (2/3x1/2L1), version 5.2.0, . Goddard Space Flight Center Distributed Active Archive Center (GSFC DAAC) [20/04/2016] 10.5067/B6DQZQLSFDLH,Greenbelt, MD, USA.

Global Modeling and Assimilation Office (GMAO). (2015) MERRA-2 tavgM_2d_flx_Nx: 2d,Monthly mean,Time-Averaged,Single-Level,Assimilation,Surface Flux Diagnostics V5.12.4. Greenbelt, MD, USA, Goddard Earth Sciences Data and Information Services Center (GES DISC), Accessed [30/02/2017] DOI:10.5067/0JRLVL8YV2Y4.

Gong L, Xu C-y, Chen D, et al. (2006) Sensitivity of the Penman–Monteith reference evapotranspiration to key climatic variables in the Changjiang (Yangtze River) basin. *Journal of Hydrology* 329: 620-629.

Goodrich DC, Keefer TO, Unkrich CL, et al. (2008) Long-term precipitation database, Walnut Gulch Experimental Watershed, Arizona, United States. *Water Resources Research* 44: 1-5.

Goodrich DC, Lane LJ, Shillito RM, et al. (1997) Linearity of basin response as a function of scale in a semiarid watershed. *Water Resources Research* 33: 2951-2965.

Gosling SN and Arnell NW. (2013) A global assessment of the impact of climate change on water scarcity. *Climatic Change* 134: 371-385.

Grayson RB, Moore ID and McMahon TA. (1992) Physically based hydrologic modeling: 1. A terrain-based model for investigative purposes. *Water Resources Research* 28: 2639-2658.

Gupta HV, Sorooshian S and Yapo PO. (1998) Toward improved calibration of hydrologic models: Multiple and noncommensurable measures of information. *Water Resources Research* 34: 751-763.

Gutiérrez F, Gutiérrez M and Sancho C. (1998) Geomorphological and sedimentological analysis of a catastrophic flash flood in the Arás drainage basin (Central Pyrenees, Spain). *Geomorphology* 22: 265-283.

Haines A, Finlayson B and McMahon T. (1988) A global classification of river regimes. *Applied Geography* 8: 255-272.

Hargreaves and Samani. (1985) Reference crop evapotranspiration from ambient air temperature. *In Proceedings of the Winter Meeting of the American Society of Agricultural Engineers*, Chicago, IL, Paper No. 85-2517.

Harris A, Rahman S, Hossain F, et al. (2007) Satellite-based Flood Modeling Using TRMM-based Rainfall Products. *Sensors* 7: 3416-3427.

Harris N and Gurnell A. (2000) Classification of river regimes: a context for hydroecology. *Hydrological Processes* 14: 2831-2848.

Hatcher KL and Jones Ja. (2013) Climate and Streamflow Trends in the Columbia River Basin: Evidence for Ecological and Engineering Resilience to Climate Change. *Atmosphere-Ocean* 51: 436-455.

Hendrickx J and Walker G. (1997) *Recharge of phreatic aquifers in (semi-) arid areas*, Rotterdam: AA Balkema.

Hendrickx JMH. (1990) Determination of hydraulic soil properties. In: Anderson MGB, T. P. (ed) *Process studies in hillslope hydrology*. John Wiely & Sons Ltd, 43-92

Herath IK, Ye X, Wang J, et al. (2017) Spatial and temporal variability of reference evapotranspiration and influenced meteorological factors in the Jialing River Basin, China. *Theoretical and Applied Climatology*.

Hernandez M, Miller SN, Goodrich DC, et al. (2000) Modeling runoff response to land cover and rainfall spatial variability in semi-arid watersheds. *Monitoring Ecological Condition in the Western United States.* Springer, 285-298.

Hess T, Harrison P and Counsell C. (2000) WaSim technical manual. HR Wallingford and Cranfield University, UK.

Huffman GJ, Adler RF, MORRISSEY MM, et al. (2001) Global Precipitation at One-Degree Daily Resolution from Multisatellite Observations. *Journal of Hydrometeorology* 2: 36-50.

Huffman GJ, Bolvin DT and Nelkin EJ. (2017) Integrated Multi-satellitE Retrievals for GPM (IMERG) Technical Documentation. *NASA/GSFC* P. 54.

Huffman GJ, Bolvin DT, Nelkin EJ, et al. (2007) The TRMM Multisatellite Precipitation Analysis (TMPA): Quasi-Global, Multiyear, Combined-Sensor Precipitation Estimates at Fine Scales. *Journal of Hydrometeorology* 8: 38-55.

Hughes D. (2008) Modelling semi-arid and arid hydrology and water resources: the southern Africa experience. *Hydrological Modelling in Arid and Semi-Arid Areas*: 29-40.

Hughes DA, Andersson L, Wilk J, et al. (2006) Regional calibration of the Pitman model for the Okavango River. *Journal of Hydrology* 331: 30-42.

Ibraimo N and Munguambe P. (2007) Rainwater Harvesting Technologies for Small Scale Rainfed Agriculture in Arid and Semi-arid Areas. Intergrated Water Resources Mangement For Improved Rural Livelihoods CGIAR Challennge Program on Water and Food, : Department of Rural Engineering, University Eduardo Mondlane.

Immerzeel WW, Rutten MM and Droogers P. (2009) Spatial downscaling of TRMM precipitation using vegetative response on the Iberian Peninsula. *Remote Sensing of Environment* 113: 362-370.

IPCC. (2013) Climate Change 2013: The Physical Science Basis. Contribution of Working Group I to the Fifth Assessment Report of the Intergovernmental Panel on Climate Change [Stocker, T.F., D. Qin, G.-K. Plattner, M. Tignor, S.K. Allen, J. Boschung, A. Nauels, Y. Xia, V. Bex and P.M. Midgley (eds.)]. Cambridge University Press, Cambridge, United Kingdom and New York, NY, USA, 1535 pp.

Issa IE, Al-Ansari NA, Sherwany G, et al. (2014) Expected Future of Water Resources within Tigris-Euphrates Rivers Basin, Iraq. *Journal of Water Resource and Protection* 06: 421-432.

Izady A, Davary K, Alizadeh A, et al. (2014) Groundwater conceptualization and modeling using distributed SWAT-based recharge for the semi-arid agricultural Neishaboor plain, Iran. *Hydrogeology Journal* 23: 47-68.

Jacob T, Wahr J, Pfeffer WT, et al. (2012) Recent contributions of glaciers and ice caps to sea level rise. *Nature* 482: 514-518.

Jain A, Sudheer KP and Srinivasulu S. (2004) Identification of physical processes inherent in artificial neural network rainfall runoff models. *Hydrological Processes* 18: 571-581.

Jakeman A, Littlewood I and Whitehead P. (1990) Computation of the instantaneous unit hydrograph and identifiable component flows with application to two small upland catchments. *Journal of Hydrology* 117: 275-300.

Janssen P and Heuberger P. (1995) Calibration of process-oriented models. *Ecological Modelling* 83: 55-66.

Jensen D, Hargreaves G, Temesgen B, et al. (1997) Computation of ETo under nonideal conditions. *Journal of Irrigation and Drainage Engineering* 123: 394-400.

Jensen ME, Burman RD and Allen RG. (1990) *Evapotranspiration and irrigation water requirements,* New York, USA: ASCE.

Jensen ME and Haise HR. (1963) Estimating evapotranspiration from solar radiation. *Proceedings of the American Society of Civil Engineers, Journal of the Irrigation and Drainage Division* 89: 15-41.

Jiang Y, Liu C, Li X, et al. (2015) Rainfall-runoff modeling, parameter estimation and sensitivity analysis in a semiarid catchment. *Environmental Modelling & Software* 67: 72-88.

Joodaki G, J. Wahr and Swenson. S. (2014) Estimating the human contribution to groundwater depletion in the Middle East, from GRACE data, land surface models, and well observations. *Water Resources* 50,: 2679–2692.

Jung I-W and Chang H. (2011) Assessment of future runoff trends under multiple climate change scenarios in the Willamette River Basin, Oregon, USA. *Hydrological Processes* 25: 258-277.

Kamal HK. (2010) Modification of the time-expanded stratigraphic column of North East Iraq during Cretaceous and Tertiary. *Petroleum Geology of Iraq.* Baghdad, Iraq.

Kannan N, White SM, Worrall F, et al. (2007) Sensitivity analysis and identification of the best evapotranspiration and runoff options for hydrological modelling in SWAT-2000. *Journal of Hydrology* 332: 456-466.

Karnieli AM, Diskin MH and Lane LJ. (1994) CELMOD5—a semi-distributed cell model for conversion of rainfall into runoff in semi-arid watersheds. *Journal of Hydrology* 157: 61-85.

Kashyap P and Panda R. (2001) Evaluation of evapotranspiration estimation methods and development of crop-coefficients for potato crop in a sub-humid region. *Agricultural Water Management* 50: 9-25.

Katara P, Machiwal D, Mittal H, et al. (2013) Estimation of Runoff for Ahar River Catchment in Udaipur District Integrated Remote Sensing and Geographical Information System. *The Institute of Engineers (India), Udaipur local Centre 2013*: 169-175.

Kavvas ML, Chen ZQ, Anderson ML, et al. (2011) A study of water balances over the Tigris–Euphrates watershed. *Physics and Chemistry of the Earth, Parts A/B/C* 36: 197-203.

King C, Lecomte V, Le Bissonnais Y, et al. (2005) Remote-sensing data as an alternative input for the 'STREAM' runoff model. *Catena* 62: 125-135.

Kinzelbach W, Aeschbach W, Alberich C, et al. (2002) A survey of methods for groundwater recharge in arid and semi-arid regions. *Early warning and assessment Report series, UNEP/DEWA/RS* 2.

Kirkby MJ, Irvine BJ, Jones RJA, et al. (2008) The PESERA coarse scale erosion model for Europe. I. - Model rationale and implementation. *European Journal of Soil Science* 59: 1293-1306.

Kneis D, Chatterjee C and Singh R. (2014) Evaluation of TRMM rainfall estimates over a large Indian river basin (Mahanadi). *Hydrology and Earth System Sciences* 18: 2493-2502.

Koeniger P, Gaj M, Beyer M, et al. (2016) Review on soil water isotope-based groundwater recharge estimations. *Hydrological Processes* 30: 2817-2834.

Konikow LF and Kendy E. (2005) Groundwater depletion: A global problem. *Hydrogeology Journal* 13: 317-320.

Kotwicki V. (1987) On the future of rainfall-runoff modelling in arid areas—Lake Eyre case study. *Water for the Future: Hydrology in Perspective.* IAHS Publication, 341-351.

Krásný J, Alsam S and Jassim SZ. (2006) *Hydrogeology, in: Geology of Iraq,* Publishers Dolin, Prague, 1st Edn.

Kundzewicz ZW. (2008) Climate change impacts on the hydrological cycle. *Ecohydrology & Hydrobiology* 8: 195-203.

Kundzewicz ZW, Mata LJ, Arnell NW, et al. (2007) Freshwater resources and their management. . *Climate Change 2007: Impacts, Adaptation and Vulnerability. Contribution of Working Group II to the Fourth Assessment Report of the Intergovernmental Panel on Climate Change.* M.L. Parry, O.F. Canziani, J.P. Palutikof, P.J van der Linden and C.E. hanson, Eds., Cambridge University Press, UK, 173-210.

Kustas WP, Rango A and Uijlenhoet R. (1994) A simple energy budget algorithm for the snowmelt runoff model. *Water Resources Research* 30: 1515-1527.

Landeras G, Ortiz-Barredo A and López JJ. (2008) Comparison of artificial neural network models and empirical and semi-empirical equations for daily reference evapotranspiration estimation in the Basque Country (Northern Spain). *Agricultural Water Management* 95: 553-565.

Landerer FW and Swenson SC. (2012) Accuracy of scaled GRACE terrestrial water storage estimates. *Water Resources Research* 48: 1-11.

Lange J, Greenbaum N, Husary S, et al. (2003) Runoff generation from successive simulated rainfalls on a rocky, semi-arid, Mediterranean hillslope. *Hydrological Processes* 17: 279-296.

Lange NT. (1999) New mathematical approaches in hydrological modeling — an application of artificial neural networks. *Physics and Chemistry of the Earth, Part B: Hydrology, Oceans and Atmosphere* 24: 31-35.

Leavesley G, Lichty R, Troutman B, et al. (1983) Precipitation-runoff modeling system User's manual. Water-Resources Investigation Report 83-4238, 1-214.

Lee YR, Yoo JM, Jeong MJ, et al. (2013) Comparison between MODIS and AIRS/AMSU satellite-derived surface skin temperatures. *Atmospheric Measurement Techniques* 6: 445-455.

Lerner DN, Issar AS and Simmers I. (1990) Groundwater recharge. Aguide to understanding and estimating natural recharge.

Li H, Xu C-Y, Beldring S, et al. (2015) Water Resources Under Climate Change in Himalayan Basins. *Water Resources Management* 30: 843-859.

Li L, Xia J, Xu C-Y, et al. (2009) Analyse the sources of equifinality in hydrological model using GLUE methodology. *Hydroinformatics in Hydrology, Hydrogeology and Water Resources, Proceedings of Symposium JS, Hyderabad, India, pp. 130-138.*

Lillesand T, Kiefer RW and Chipman J. (2014) *Remote sensing and image interpretation*: John Wiley & Sons.

Lombard A, Garcia D, Ramillien G, et al. (2007) Estimation of steric sea level variations from combined GRACE and Jason-1 data. *Earth and Planetary Science Letters* 254: 194-202.

Longuevergne L, Scanlon BR and Wilson CR. (2010) GRACE Hydrological estimates for small basins: Evaluating processing approaches on the High Plains Aquifer, USA. *Water Resources Research* 46: 1-15.

López-Urrea R, Martín dSOF, Fabeiro C, et al. (2006) Testing evapotranspiration equations using lysimeter observations in a semiarid climate. *Agricultural Water Management* 85: 15-26.

Lundin LC, Sten BS, Eriksson E, et al. (1998) Hydrological Models and Modeling.: 129-140.

Male D and Granger R. (1981) Snow surface energy exchange. *Water Resources Research* 17: 609-627.

McCallum AM, Andersen MS, Giambastiani BMS, et al. (2013) River-aquifer interactions in a semi-arid environment stressed by groundwater abstraction. *Hydrological Processes* 27: 1072-1085.

McCollum JR, Gruber A and Ba MB. (2000) Discrepancy between gauges and satellite estimates of rainfall in equatorial Africa. *Journal of Applied Meteorology* 39: 666-679.

McGuinness JL and Bordne EF. (1972) *A comparison of lysimeter-derived potential evapotranspiration with computed values*: Technical Bulletin 1452, Agricultural Research Service, US Department of Agriculture, Washington, DC.

McIntyre N and Al-Qurashi A. (2009) Performance of ten rainfall–runoff models applied to an arid catchment in Oman. *Environmental Modelling & Software* 24: 726-738.

McKinley S and Levine M. (1998) Cubic spline interpolation. *College of the Redwoods* 45: 1049-1060.

McMahon TA, Peel MC, Lowe L, et al. (2013) Estimating actual, potential, reference crop and pan evaporation using standard meteorological data: a pragmatic synthesis. *Hydrology and Earth System Sciences* 17: 1331-1363.

Meier DC and Fiorino ST. (2016) Application of Satellite- and NWP-Derived Wind Profiles to Military Airdrop Operations. *Journal of Applied Meteorology and Climatology* 55: 2197-2209.

Merwade V. (2012) Watershed and Stream Network Delineation using ArcHydro Tools. 1-22.

Michael Jasinski. (2016) NASA/GSFC/HSL, NCA-LDAS Noah-3.3 Land Surface Model L4 Daily 0.125 x 0.125 degree V001. Greenbelt, Maryland, USA, Goddard Earth Sciences Data and Information Services Center (GES DISC). https://disc.sci.gsfc.nasa.gov/uui/datasets/NCALDAS_NOAH0125_D_001/summary.

Michel D, Pandya A, Hasnain SI, et al. (2012) Water Challenges and Cooperative Response in the Middle East and North Africa. *Brookings Insititution, Washington, DC [Available at http://www. brookings. edu/research/papers/2012/11/water-security-middle-east-iwf.]*.

Miller WF. (1991) Density Altitude Maps of Iran and Iraq (No. USAFETAC/PR--91/008). Scott AFB: USAF Environmental Technical Applications Center.

Milman A, Bunclark L, Conway D, et al. (2013) Assessment of institutional capacity to adapt to climate change in transboundary river basins. *Climatic Change* 121: 755-770.

Mo X and Beven K. (2004) Multi-objective parameter conditioning of a three-source wheat canopy model. *Agricultural and Forest Meteorology* 122: 39-63.

Moore R. (2007) The PDM rainfall-runoff model. *Hydrology and Earth System Sciences Discussions* 11: 483-499.

Morel E and Wright C. (1978) *Methods of estimating natural groundwater recharge*: Central Water Planning Unit.

Moriasi DN, Arnold JG, Van Liew MW, et al. (2007) Model evaluation guidelines for systematic quantification of accuracy in watershed simulations. *Transactions of the ASABE* 50: 885-900.

Mourre L, Condom T, Junquas C, et al. (2016) Spatio-temporal assessment of WRF, TRMM and in situ precipitation data in a tropical mountain environment (Cordillera Blanca, Peru). *Hydrology and Earth System Sciences* 20: 125-141.

Mu Q, Jones LA, Kimball JS, et al. (2009) Satellite assessment of land surface evapotranspiration for the pan-Arctic domain. *Water Resources Research* 45.

Mu Q, Zhao M and Running SW. (2011) Brief introduction to MODIS evapotranspiration data set (MOD16).

Muhammad JM, Cheema, Wim G. M, et al. (2012) Local calibration of remotely sensed rainfall from the TRMM satellite for different periods and spatial scales in the Indus Basin. *International Journal of Remote Sensing* 33: 2603-2627.

Mulder G, Olsthoorn TN, Al-Manmi DAMA, et al. (2015) Identifying water mass depletion in northern Iraq observed by GRACE. *Hydrology and Earth System Sciences* 19: 1487-1500.

NASA Jet Propulsion Laboratory (JPL). (2013) NASA Shuttle Radar Topography Mission United States 1 arc second.Version 3. 6ºS, 69ºW. NASA EOSDIS Land Processes DAAC. USGS Earth Resources Observation and Science (EROS) Center, Sioux Falls, South Dakota (https://lpdaac.usgs.gov), accessed April, 12, 2014, at http://dx.doi.org/10.5067/MEaSUREs/SRTM/SRTMUS1.003.

Nash J and Sutcliffe J. (1970) River flow forecasting through conceptual models part I—A discussion of principles. *Journal of Hydrology* 10: 282-290.

National Space Development Agency of Japan (NASDA). (1999) TRMM PR Algorithm Instruction Manual V1.0. Communications Research Laboratory. [Communications Research Laboratory, 4-2-1 Nukui-kitamachi, Koganei-chi, Tokyo 184, Japan], 52.

Návar J. (2017) Fitting rainfall interception models to forest ecosystems of Mexico. *Journal of Hydrology* 548: 458-470.

Nerini D, Zulkafli Z, Wang L-P, et al. (2015) A Comparative Analysis of TRMM–Rain Gauge Data Merging Techniques at the Daily Time Scale for Distributed Rainfall–Runoff Modeling Applications. *Journal of Hydrometeorology* 16: 2153-2168.

New M, Lister D, Hulme M, et al. (2002) A highresolution data set of surface climate over global land areas. *CLIMATE RESEARCH* 21: 1-25.

Nichols MH, Nearing M, Hernandez M, et al. (2016) Monitoring channel head erosion processes in response to an artificially induced abrupt base level change using time-lapse photography. *Geomorphology* 265: 107-116.

Niemela J. (2011) Urban Ecology: Patterns, Processes, and Applications. Oxford [England], : Oxford University Press.

Nikam BR, Kumar P, Garg V, et al. (2014) Comparative evaluation of different potential evapotranspiration estimation approaches. *International Journal of Research in Engineering and Technology* 03: 543-552.

O'Connell P. (1991) A historical perspective. *Recent Advances in the Modeling of Hydrologic Systems.* Springer, 3-30.

Ohana-Levi N, Karnieli A, Egozi R, et al. (2015) Modeling the Effects of Land-Cover Change on Rainfall-Runoff Relationships in a Semiarid, Eastern Mediterranean Watershed. *Advances in Meteorology* 2015: 1-16.

Olivera F, Famiglietti J and Asante K. (2000) Global-scale flow routing using a source-to-sink algorithm. *Water Resources Research* 36: 2197-2207.

Oudin L, Hervieu F, Michel C, et al. (2005) Which potential evapotranspiration input for a lumped rainfall–runoff model? *Journal of Hydrology* 303: 290-306.

Pandey PK, Dabral PP and Pandey V. (2016) Evaluation of reference evapotranspiration methods for the northeastern region of India. *International Soil and Water Conservation Research* 4: 52-63.

Panofsky HA, Brier GW and Best WH. (1958) Some application of statistics to meteorology.

Pearce A, Stewart M and Sklash M. (1986) Storm runoff generation in humid headwater catchments: 1. Where does the water come from? *Water Resources Research* 22: 1263-1272.

Pechlivanidis I and Jackson B. (2011) Catchment scale hydrological modelling: a review of model types, calibration approaches and uncertainty analysis methods in the context of recent developments in technology and applications. *Global NEST* 13: 193-214.

Peng J, Loew A, Chen X, et al. (2016) Comparison of satellite-based evapotranspiration estimates over the Tibetan Plateau. *Hydrology and Earth System Sciences* 20: 3167-3182.

Pilgrim DH, Chapman TG and Doran DG. (1988) Problems of rainfall-runoff modelling in arid and semiarid regions. *Hydrological Sciences Journal* 33: 379-400.

Pipes A and Quick M. (1987) Modelling large scale effects of snow cover. *Large Scale Effects of Seasonal Snow Cover. International Association of Hydrological Sciences Press, Institute of Hydrology, Wallingford, Oxfordshire UK. IAHS Publication*.

Pipunic RC, Ryu D, Costelloe JF, et al. (2015) An evaluation and regional error modeling methodology for near-real-time satellite rainfall data over Australia. *Journal of Geophysical Research: Atmospheres* 120.

Pitman W. (1973) A mathematical model for generating monthly river flow from meteorological data in southern Africa, Rep. 2. Hydrol. Res. Unit, Dep. of Civ. Eng., Univ. of Witwatersrand, Johannesburg, South Africa.

Pomeroy J and Brun E. (2001) Snow ecology: An interdisciplinary examination of snow-covered ecosystems. Cambridge University Press, 45-126.

Post DA and Jakeman AJ. (1999) Predicting the daily streamflow of ungauged catchments in SE Australia by regionalising the parameters of a lumped conceptual rainfall-runoff model. *Ecological Modelling* 123: 91-104.

Poyen EFB and Ghosh AK. (2016) Review on Different Evapotranspiration Empirical Equations. *IJAEMS: Open Access International Journal: Infogain Publication* 2.

Prabhakara C, Iacovazzi JR and Yoo JM. (2002) TRMM precipitation radar and microwave imager observations of convective and stratiform rain over land and their theoretical implications. *Journal of the Meteorological Society of Japan* 80: 1183-1197.

Prakash S, Mitra AK, Pai DS, et al. (2016) From TRMM to GPM: How well can heavy rainfall be detected from space? *Advances in Water Resources* 88: 1-7.

Priestley C and Taylor R. (1972) On the assessment of surface heat flux and evaporation using large-scale parameters. *Monthly weather review* 100: 81-92.

Pullan S, Holman I and Whelan MJ. (2014) Modelling of Pesticide Exposure in Ground and Surface Waters Used for Public Water Supply. *School of Applied Sciences.* Cranfield University, UK.

Pullan SP, Whelan MJ, Rettino J, et al. (2016) Development and application of a catchment scale pesticide fate and transport model for use in drinking water risk assessment. *Sci Total Environ* 563-564: 434-447.

R Core Team. (2014) R: A language and environment for statistical computing. R Foundation for Statistical Computing. Vienna, Austria

Ragab R and Prudhomme C. (2002) Climate Change and Water Resources Management in Arid and Semi-arid Regions: Prospective and Challenges for the 21st Century. *Biosystems Engineering* 81: 3-34.

Rahimi S, Gholami Sefidkouhi MA, Raeini-Sarjaz M, et al. (2014) Estimation of actual evapotranspiration by using MODIS images (a case study: Tajan catchment). *Archives of Agronomy and Soil Science* 61: 695-709.

Rasul A, Balzter H and Smith C. (2016) Diurnal and Seasonal Variation of Surface Urban Cool and Heat Islands in the Semi-Arid City of Erbil, Iraq. *Climate* 4: 42.

Rateb A, Kuo CY, Imani M, et al. (2017) Terrestrial Water Storage in African Hydrological Regimes Derived from GRACE Mission Data: Intercomparison of Spherical Harmonics, Mass Concentration, and Scalar Slepian Methods. *Sensors (Basel)* 17.

Ratto M, Young P, Romanowicz R, et al. (2007) Uncertainty, sensitivity analysis and the role of data based mechanistic modeling in hydrology. *Hydrology and Earth System Sciences Discussions* 11: 1249-1266.

Reaney S. (2008) The use of agent based modelling techniques in hydrology: determining the spatial and temporal origin of channel flow in semi-arid catchments. *Earth Surface Processes and Landforms* 327: 317-327.

Refsgaard JC and Knudsen J. (1996) Operational validation and intercomparison of different types of hydrological models. *Water Resources Research* 32: 2189-2202.

Renard K, Lane L, Simanton J, et al. (1993) Agricultural impacts in an arid environment: Walnut Gulch studies. *Hydrological Science and Technology* 9: 145-190.

Richey AS, Thomas BF, Lo MH, et al. (2015) Quantifying renewable groundwater stress with GRACE. *Water Resour Res* 51: 5217-5238.

Rienecker MM, Suarez MJ, Gelaro R, et al. (2011) MERRA: NASA's Modern-Era Retrospective Analysis for Research and Applications. *Journal of Climate* 24: 3624-3648.

Ries F, Schmidt S, Sauter M, et al. (2016) Runoff generation in a Mediterranean semi-arid landscape: Thresholds, scale, rainfall and catchment characteristics. *EGU General Assembly Conference Abstracts.* 8479.

Rodell M, Chen J, Kato H, et al. (2006) Estimating groundwater storage changes in the Mississippi River basin (USA) using GRACE. *Hydrogeology Journal* 15: 159-166.

Rodell M and Famiglietti J. (2002) The potential for satellite-based monitoring of groundwater storage changes using GRACE: the High Plains aquifer, Central US. *Journal of Hydrology* 263: 245-256.

Rodell M, Houser PR, Jambor U, et al. (2004) The Global Land Data Assimilation System. *Bulletin of the American Meteorological Society* 85: 381-394.

Rodell M, Velicogna I and Famiglietti JS. (2009) Satellite-based estimates of groundwater depletion in India. *Nature* 460: 999-1002.

Rodríguez-Iturbe I and Valdes JB. (1979) The geomorphologic structure of hydrologic response. *Water Resources Research* 15: 1409-1420.

Rojas-Serna C, Lebecherel L, Perrin C, et al. (2016) How should a rainfall-runoff model be parameterized in an almost ungauged catchment? A methodology tested on 609 catchments. *Water Resources Research*.

Rushton K and Ward C. (1979) The estimation of groundwater recharge. *Journal of Hydrology* 41: 345-361.

Saad ZJ and Jeremy CG. (2006) *geology of Iraq*, Prague and Moravian Museum, Brno: Dolin.

Sabziparvar A-A, Tabari H, Aeini A, et al. (2009) Evaluation of Class A Pan Coefficient Models for Estimation of Reference Crop Evapotranspiration in Cold Semi-Arid and Warm Arid Climates. *Water Resources Management* 24: 909-920.

Santillan J, Makinano M and Paringit E. (2011) Integrated Landsat Image Analysis and Hydrologic Modeling to Detect Impacts of 25-Year Land-Cover Change on Surface Runoff in a Philippine Watershed. *Remote Sensing* 3: 1067-1087.

Sarhadi A, Burn DH, Johnson F, et al. (2016) Water resources climate change projections using supervised nonlinear and multivariate soft computing techniques. *Journal of Hydrology* 536: 119-132.

Savenije HG. (2004) The importance of interception and why we should delete the term evapotranspiration from our vocabulary. *Hydrological Processes* 18: 1507-1511.

Sawunyama T and Hughes DA. (2008) Application of Satellite-Derived Rainfall Estimates to ExtendWater Resource Simulation Modelling in South Africa. *(Pretoria: Water Research Commission)* 34: 1-9.

Scanlon B, Keese K and Flint A. (2006) Global synthesis of groundwater recharge in semiarid and arid regions. *Hydrological Processes* 20: 3335-3370.

Scanlon BR, Longuevergne L and Long D. (2012) Ground referencing GRACE satellite estimates of groundwater storage changes in the California Central Valley, USA. *Water Resources Research* 48.

Seibert J. (1999) Conceptual runoff models-fiction or representation of reality? : Acta Univ. Ups., Comprehensive Summaries of Uppsala Dissertations from the Faculty of Science and Technology 436. 52pp. Uppsala. ISBN 91-554-4402-4, 52.

Seo DJ, Breidenbach JP and Johnson ER. (1999) Real-time estimation of mean field bias in radar rainfall data. *Journal of Hydrology* 223: 131-147.

Shadeed S, Shaheen H and Jayyousi A. (2007) GIS-based KW-GIUH hydrological model of semiarid catchments: the case of Faria Catchment, Palestine. *Arabian Journal for Science and Engineering* 32: 3.

Sharma M and Hughes M. (1985) Groundwater recharge estimation using chloride, deuterium and oxygen-18 profiles in the deep coastal sands of Western Australia. *Journal of Hydrology* 81: 93-109.

Shaw EM. (1994) *Hydrology in practice*: Chapman & Hall London ; New York.

Shepherd A, Gill KM and Rood SB. (2010) Climate change and future flows of Rocky Mountain rivers: converging forecasts from empirical trend projection and down-scaled global circulation modelling. *Hydrological Processes* 24: 3864-3877.

Simmers I. (1988) *Estimation of natural groundwater recharge*: Springer Netherlands.

Simpson J, Kummerow C, Tao WK, et al. (1996) On the Tropical Rainfall Measuring Mission (TRMM). *Meteorology and Atmospheric Physics* 60: 19-36.

Šimůnek J and De Vos J. (1999) Inverse optimization, calibration and validation of simulation models at the field scale. *Modelling of Transport Process in Soils at Various Scales in Time and Space*: 431-445.

Singh VP. (1995) *Computer models of watershed hydrology*: Water Resources Publications, Highlands Ranch.

Sivapalan M and Viney N. (1994) Large scale catchment modelling to predict the effects of land use and climate. *Water(Australia)* 21: 33-37.

Solomatine D and Wagener T. (2011) Hydrological Modeling. In Peter Wilderer (ed.) Treatise on Water Science, . *Oxford: Academic Press* 2: 435-457.

Stevanovic Z, Iurkiewicz A and Maran A. (2009) New insights into karst and caves of Northwestern Zagros (Northern Iraq). *Acta carsologica* 38.

Stevanovic Z and Markovic M. (2004) Hydrogeology of Northern Iraq (vol 1), Climate, Hydrology, Geomorphology, Geology. *Spec. Ed. TCES, FAO, Rome*.

Strugnell N, Lucht W and Schaaf C. (2001) A global albedo data set derived from AVHRR data for use in climate simulations. *Geophysical Research Letters* 28: 191-194.

Swenson S, Chambers D and Wahr J. (2008) Estimating geocenter variations from a combination of GRACE and ocean model output. *Journal of Geophysical Research* 113: 1-12.

Swenson S and Wahr J. (2002) Methods for inferring regional surface-mass anomalies from Gravity Recovery and Climate Experiment (GRACE) measurements of time-variable gravity. *Journal of Geophysical Research: Solid Earth* 107: ETG 3-1-ETG 3-13.

Syed TH, Famiglietti JS, Chen J, et al. (2005) Total basin discharge for the Amazon and Mississippi River basins from GRACE and a land-atmosphere water balance. *Geophysical Research Letters* 32.

Tabari H. (2009) Evaluation of Reference Crop Evapotranspiration Equations in Various Climates. *Water Resources Management* 24: 2311-2337.

Tabari H, Aeini A, Talaee PH, et al. (2012a) Spatial distribution and temporal variation of reference evapotranspiration in arid and semi-arid regions of Iran. *Hydrological Processes* 26: 500-512.

Tabari H, Grismer ME and Trajkovic S. (2011) Comparative analysis of 31 reference evapotranspiration methods under humid conditions. *Irrigation Science* 31: 107-117.

Tabari H, Kisi O, Ezani A, et al. (2012b) SVM, ANFIS, regression and climate based models for reference evapotranspiration modeling using limited climatic data in a semi-arid highland environment. *Journal of Hydrology* 444-445: 78-89.

Tabari H and Talaee PH. (2011) Local Calibration of the Hargreaves and Priestley-Taylor Equations for Estimating Reference Evapotranspiration in Arid and Cold Climates of Iran Based on the Penman-Monteith Model. *Journal of Hydrologic Engineering* 16: 837-845.

Tada T and Beven KJ. (2012) Hydrological model calibration using a short period of observations. *Hydrological Processes* 26: 883-892.

Tapley BD, Bettadpur S, Ries JC, et al. (2004) GRACE measurements of mass variability in the Earth system. *Science* 305: 503-505.

Tarnavsky E, Mulligan M, Ouessar M, et al. (2013) Dynamic Hydrological Modeling in Drylands with TRMM Based Rainfall. *Remote Sensing* 5: 6691-6716.

Tartaglione N. (2010) Relationship between precipitation forecast errors and skill scores of dichotomous forecasts. *Weather and Forecasting* 25: 355-365.

Temesgen B, Eching S, Davidoff B, et al. (2005) Comparison of some reference evapotranspiration equations for California. *Journal of Irrigation and Drainage Engineering* 131: 73-84.

Thornthwaite CW. (1948) An approach toward a rational classification of climate. *Geographical review* 38: 55-94.

Tiwari VM, Wahr J and Swenson S. (2009) Dwindling groundwater resources in northern India, from satellite gravity observations. *Geophysical Research Letters* 36: 1-5.

Todini E. (1988) Rainfall-runoff modeling—Past, present and future. *Journal of Hydrology* 100: 341-352.

Todini E. (1996) The ARNO rainfall—runoff model. *Journal of Hydrology* 175: 339-382.

Trajkovic S. (2007) Hargreaves versus Penman-Monteith under humid conditions. *Journal of Irrigation and Drainage Engineering* 133: 38-42.

Tregoning P, McClusky S, Van Dijk A, et al. (2012) Assessment of GRACE satellites for groundwater estimation in Australia. *National Water Commission, Canberra* 82.

Unver I. (1997) Southeastern Anatolia Project (GAP). *Water Resources Development* 13: 453-483.

van Genuchten MT. (1980) A closed-form equation for predicting the hydraulic conductivity of unsaturated soils. *Soil science society of America journal* 44: 892-898.

van Meerveld IH, Prasad Ghimire C, Zwartendijk BW, et al. (2016) Land cover effects on thresholds for surface runoff generation in Eastern Madagascar. *EGU General Assembly Conference Abstracts.* 15072.

Vezzoli R. (2013) Using a weather generator to simulate daily precipitation scenarios from seasonal weather forecasts. *Centro Euro-Mediterraneo*: 1-9.

Vogel RM and Kroll CN. (1996) Estimation of baseflow recession constants. *Water Resources Management* 10: 303-320.

Voss Ka, Famiglietti JS, Lo M, et al. (2013) Groundwater depletion in the Middle East from GRACE with implications for transboundary water management in the Tigris-Euphrates-Western Iran region. *Water Resources Research* 49: 904-914.

Wagener T, Boyle DP, Lees MJ, et al. (2001) A framework for development and application of hydrological models. *Hydrology and Earth System Sciences* 5: 13-26.

Wagener T, Howard S W and Hoshin V G. (2004) *Rainfall-runoff Modelling in gauged and ungauged cathments,* Imperial College Press, 57 Shelton Street, Covent Garden, London WC2H 9HE: World Scientific Publishing Co. Pte. Ltd.

Wagener T, McIntyre N, Lees MJ, et al. (2003) Towards reduced uncertainty in conceptual rainfall-runoff modelling: dynamic identifiability analysis. *Hydrological Processes* 17: 455-476.

Wahr J, Molenaar M and Bryan F. (1998) Time variability of the Earth's gravity field: Hydrological and oceanic effects and their possible detection using GRACE. *Journal of Geophysical Research* 103: 30205.

Wahr J, Swenson S and Velicogna I. (2006) Accuracy of GRACE mass estimates. *Geophysical Research Letters* 33.

Wallace D and Lane L. (1976) Geomorphic thresholds and their influence on surface runoff from small semiarid watersheds. *Hydrology and Water Resources in Arizona and the Southwest.* Arizona-Nevada Academy of Science.

WeiB M and Menzel L. (2008) A global comparison of four potential evapotranspiration equations and their relevance to stream flow modelling in semi-arid environments. *Advances in Geosciences* 18: 15-23.

Weyman DR. (1975) *Runoff processes and streamflow modelling*: Oxford University Press.

Wheater H, Ballard BW and Jolley T. (1997) An integrated model of arid zone water resources: evaluation of rainfall-runoff simulation performances. Sustainability of Water Resources under Increasing Uncertainly. *Proc. Rabat Symp. S.*

Wheater H, Jakeman A and Beven K. (1993) Progress and directions in rainfall-runoff modelling. In Jakeman A.J.,Beck M. B., and McAleer M.J., editors. *Modelling Change in Environmental Systems.* Chichester,UK: John Wiley & Sons, 101-132.

Wheater H, Sorooshian S and Sharma KD. (2007) *Hydrological modelling in arid and semi-arid areas*: Cambridge University Press.

Wheater HS. (2002) Progress in and prospects for fluvial flood modelling. *Philosophical transactions. Series A, Mathematical, physical, and engineering sciences* 360: 1409-1431.

Whelan MJ and Gandolfi C. (2002) Modelling of spatial controls on denitrification at the landscape scale. *Hydrological Processes* 16: 1437-1450.

White S, García-Ruiz JM, Martí C, et al. (1997) The 1996 Biescas campsite disaster in the Central Spanish Pyrenees, and its temporal and spatial context. *Hydrological Processes* 11: 1797-1812.

Wilby RL, Clifford NJ, De Luca P, et al. (2017) The 'dirty dozen' of freshwater science: detecting then reconciling hydrological data biases and errors. *Wiley Interdisciplinary Reviews: Water* 4: e1209.

Wilby RL and Dawson CW. (2013) The Statistical DownScaling Model: insights from one decade of application. *International Journal of Climatology* 33: 1707-1719.

Wilby RL, Dawson CW, Murphy C, et al. (2014) The Statistical DownScaling Model-Decision Centric (SDSM-DC): conceptual basis and applications. *Clim Res* 61: 259-276.

Wilby RL and Yu D. (2013) Rainfall and temperature estimation for a data sparse region. *Hydrology and Earth System Sciences* 17: 3937-3955.

WMO. (2006) Guide to meteorological instruments and methods of observation and information dissemination. *In Seventh Edition (Geneva: Secretariat of the World Meteorological Organization).*

WMO. (2007) Guide to the Global Observing System, World Meteorological Organization (WMO-No. 488). In: Third (ed). Geneva, Switzerland.

Xie Z, Huete A, Ma X, et al. (2016) Landsat and GRACE observations of arid wetland dynamics in a dryland river system under multi-decadal hydroclimatic extremes. *Journal of Hydrology* 543: 818-831.

Yair A and Lavee H. (1976) Runoff generative process and runoff yield from arid talus mantled slopes. *Earth Surface Processes* 1: 235-247.

Yair A and Lavee H. (1985) Runoff generation in arid and semi-arid zones. *Hydrological forecasting/edited by MG Anderson and TP Burt*.

Ye W, Bates B, Viney N, et al. (1997) Performance of conceptual rainfall-runoff models in low-yielding ephemeral catchments. *Water Resources Research* 33: 153-166.

Yeh PJF, Swenson SC, Famiglietti JS, et al. (2006) Remote sensing of groundwater storage changes in Illinois using the Gravity Recovery and Climate Experiment (GRACE). *Water Resources Research* 42: 1-7.

Yoder R, Odhiambo L and Wright W. (2005) Evaluation of methods for estimating daily reference crop evapotranspiration at a site in the humid southeast United States. *Applied Engineering in Agriculture* 21: 197-202.

Young P. (1998) Data-based mechanistic modelling of environmental, ecological, economic and engineering systems. *Environmental Modelling & Software* 13: 105-122.

Young P. (2001) Data-based mechanistic modelling of environmental systems. *IFAC Workshop on Environmental Systems, First Plenary Session Keynote Paper, Yokohama, Japan*.

Young P. (2003) Top-down and data-based mechanistic modelling of rainfall-flow dynamics at the catchment scale. *Hydrological Processes* 17: 2195-2217.

Young PC, Jakeman AJ and Post DA. (1997) Recent advances in the data-based modelling and analysis of hydrological systems. *Water Science and Technology* 36: 99-116.

Zaitchik BF, Evans JP and Smith RB. (2007) Regional Impact of an Elevated Heat Source: The Zagros Plateau of Iran. *Journal of Climate* 20: 4133-4146.

Zaitchik BF, Rodell M and Olivera F. (2010) Evaluation of the Global Land Data Assimilation System using global river discharge data and a source-to-sink routing scheme. *Water Resources Research* 46.

Zakaria S, Al-Ansari NA, Knutsson S, et al. (2012) Rain water harvesting and supplemental irrigation at Northern Sinjar Mountain, Iraq. *Journal of Purity, Utility …* 1: 121-141.

Zakaria S, Mustafa YT, Mohammed DA, et al. (2013) Estimation of annual harvested runoff at Sulaymaniyah Governorate, Kurdistan region of Iraq. *Natural Science* 05: 1272-1283.

Zelinka I. (2004) SOMA—self-organizing migrating algorithm. *New optimization techniques in engineering.* Springer, Berlin Heidelberg, 167-217.

Zhang YQ, Chiew FHS, Zhang L, et al. (2008) Estimating catchment evaporation and runoff using MODIS leaf area index and the Penman-Monteith equation. *Water Resources Research* 44: 1-15.

Zhao L, Xia J, Xu C-y, et al. (2013) Evapotranspiration estimation methods in hydrological models. *Journal of Geographical Sciences* 23: 359-369.

Zhu Q, Jiang H, Peng C, et al. (2012) Effects of future climate change, CO2 enrichment, and vegetation structure variation on hydrological processes in China. *Global and Planetary Change* 80-81: 123-135.

Zubieta R, Getirana A, Espinoza JC, et al. (2015) Impacts of satellite-based precipitation datasets on rainfall–runoff modeling of the Western Amazon basin of Peru and Ecuador. *Journal of Hydrology* 528: 599-612.

Zubieta R, Saavedra M, Silva Y, et al. (2016) Spatial analysis and temporal trends of daily precipitation concentration in the Mantaro River basin: central Andes of Peru. *Stochastic Environmental Research and Risk Assessment*: 1-14.

Zulkafli Z, Buytaert W, Onof C, et al. (2014) A comparative performance analysis of TRMM 3B42 (TMPA) versions 6 and 7 for hydrological applications over Andean–Amazon River basins. *Journal of Hydrometeorology* 15: 581-592.